

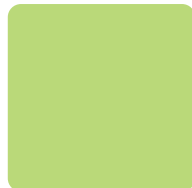


Warsaw University of Technology

Faculty of Power
and Aeronautical Engineering



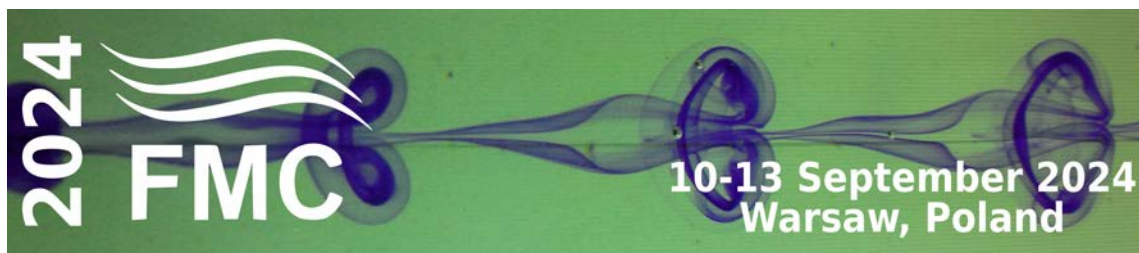
XXVI FLUID MECHANICS CONFERENCE



10-13 September 2024 - Warsaw, Poland

BOOK OF ABSTRACTS

Editors: S. Gepner, S. Kubacki, T. Waclawczyk



All contributed abstract papers in this volume were reviewed by anonymous referees from FMC2024 International Scientific Committee prior to publication.

ISBN: 978-83-943935-1-9

ISBN 978-83-943935-1-9



CONTENTS

PREFACE	7
HONORARY PATRONAGE AND SUPPORT	8
SPONSORS	9
XXVI FMC 2024 INTERNATIONAL SCIENTIFIC COMMITTEE	10
ORGANIZING COMMITTEE	11
PLENARY LECTURES	12
Krzysztof J. Fidkowski: Output-Based Discretization Error Control in Turbulent Flow Simulations	13
Jerzy M. Floryan: On the Structured Convection	15
Genta Kawahara: Ultimate states of turbulent thermal convection and shear flow	17
Luis Pablo Ruiz-Calavera: Some aerodynamic challenges of the future sustainable commercial aircraft	20
Spencer Sherwin: Advancing spectral/hp element high fidelity simulation of incompressible and compressible flows	22
Daniele Simoni: The role of experiments and data reduction techniques in the tuning of different transition models	24
AERODYNAMICS AND HYDRODYNAMICS	26
M. Piotrowicz, A. Joseph, P. Flaszynski, M. Kurowski, P. Doerffer: Investigations of Reynolds number effect on Mach number distribution on compressor stator profile	27
F. Wasilczuk, K. Pietrzycka, R. Szewczuk, P. Flaszynski: Effect of yaw angle on wind turbine power generation and velocity in the wake	29
V. Uruba, P. Prochazka, D. Duda: On Streamwise Vorticity Dynamics in Circular Cylinder Wake	31
K. Urbanowicz, C. Di Nucci, B. K. Sharma, K. Ashok, S. Krajewski: Validation of Yamaguchi-Ichikawa water hammer model	33
K. Rusin, W. Wróblewski, E. H. Malekshah, M. Pahlavanzadeh, S. Rulik: Velocity profile correction in the analytical model of flow between disks of Tesla turbine	35
M. Pisula, M. Poćwierz: Assessment of Wind Conditions in Urban Spaces: A Case Study of Warsaw Downtown	37
O. Szulc, P. Flaszynski, T. Suresh: Aerodynamic and aeroacoustic analysis of a model UAV propeller	39
K. Kubryński: Aerodynamic Multipoint Aircraft Design Including Aeroelastic Wing Deformation	41
A. Drózd, V. Sokolenko, W. Elsner: Analysis of turbulent flow separation control method using wall corrugation under different flow history	43
J. Wiśniewski, J. Szumbariski: Creation and verification of a large Vertical Axis Wind Turbine airfoil class	45
COMBUSTION AND REACTIVE FLOWS	47
A. Wawrzak, A. Tyliszczak: Investigation of steam-diluted hydrogen combustion in a counter-current nozzle configuration using LES	48
A. Mardani, K. C. Kim: Swirl Effect Assessment on NO_x Formation for CH₄/H₂/NH₃ Flame under MILD Condition	50

J. A. M. Méndez, B. Dorneanu, H. Schmidt, H. Arellano-García: Revisiting homogeneous modeling with volume averaging theory: structured catalysts for steam reforming and CO₂ methanation	52
K. Wawrzak, A. Wawrzak, A. Bogusławski, A. Tyliczszak: A high-order LES of a flow in complex geometry	54
J. Piechna, M. Szudarek, A. Piechna: Numerical modelling of a rotary shock wave compression heat engine with a rotating detonation wave combustion chamber	56
S. Telyma, O. Oliynyk: Some theoretical problems of creation the mathematic model of joint treatment of wastewaters with organic contaminants and nitrogen compounds by method of biofiltration	58
COMPUTATIONAL FLUID DYNAMICS	60
A. Kajzer: Isotropy of numerical errors in the context of implicit large eddy simulation	61
J. Fabisiak, S. Gepner: Quantification of laminar mixing efficiency using ‘strange eigenmodes’ approach	63
P. Radomski, D. Kreft, P. Ziółkowski, I. Mukha, J. Zieliński, D. Mikielwicz: Heat transfer of laser-illuminated gold nanorod platforms distributed in a flow germicidal chamber	65
M. Marek: Numerical modelling of gas flow in random packed bed with a helical flow deflector	67
S. Koval, N. Dimitrieva: Numerical simulation of two-phase flow in OpenFOAM software	69
S. Motoki, G. Kawahara: Dissimilar heat transfer enhancement in pipe flow with deep axial grooves	71
T. Bodnar: Numerical evaluation of mass diffusive compressible fluids flows models	73
A. Couvez, S. Gyuran, N. Leterrier, P. Omnes, E. Saikali: Code coupling for the Tube Support Plate clogging in steam generators	75
P. Niegodajew: Numerical investigation of Air Flow within a Human Nasal Cavity	77
V. Oliynik, T. Batutina: Semiempirical model of the acoustics of a supersonic jet upon collision with a perpendicular wall	79
J. Malet, R. Ploix, E. Géhin: Step-by-step CFD validation of turbulent particle transport and deposition in industrial bends	81
J. Gałecki, J. Szumbariski: High performance least-squares spectral/hp element method solvers for fluid dynamics problems	83
B. Kopiczak, K. Karbowski, K. Nering, Z. Malecha, R. Chrzan, J. Gawlik, A. Sucherska, J. Szaleniec, J. Karbowski: Application of CFD airflows to aid nasal obstruction diagnosis	85
I. Gorban: Application of the model of trapped vortices to the control of flow around a bridge pear	87
N. Yurchenko, P. Vynogradskyy, R. Pavlovskyy: Improvement of the aerodynamic performance using the developed method of energy-efficient flow control	89
EXPERIMENTAL METHODS	91
P. Korczyk., T. Kurniawan, S. Błoński, B. Kupikowska-Stobba: Integrated Approaches in Microfluidic Design for Enhanced Droplet Manipulation and Biological Insights	92
K. Bukowski, Ł. Klotz: Influence of micro- and mesoscale on the permeability characteristics of 3D printed porous objects	94
D. Duda, V. Yanovych, V. Uruba: PIV measurement of model nuclear fuel rod bundle	96
T. Kowalewski: Experimental Challenges of Nano and Microfluidics	98

M. Kiwan, E. Younes, C. Castelain, T. Burghilea: Mapping the efficiency of a novel rotating arc-wall inline mixer	99
FLOW CONTROL AND OPTIMIZATION	101
L. Caban, A. Wawrzak, A. Tyliczszak, D. Thévenin: LES of flow dynamics downstream of new type bluff bodies	102
P. Kamiński, Y. Li, K. Wawrzak, A. Tyliczszak, B. Noack: Machine learning-supported CFD optimization of heat transfer in a pipe with a corrugated wall shape	104
Z. Drafsh, M. Nili-Ahmadabadi, M. Y. Ha: Airfoil design in separated ultra-low Reynolds flows using a shear stress-based inverse design method	106
M. Rutkowski, Ł. Łaniewski-Wołk: Box-spline parametrisation of motion kinematics in aerodynamic optimisation of flapping motion	108
MULTIPHASE FLOWS AND COMPLEX FLUIDS	110
A. Michel, B. Rosa, A. Ababaei: Collision efficiency of cloud droplets considering electrostatic and hydrodynamic interactions	111
T. Waławczyk: Enhancing numerical resolution of statistical phase-field method	113
N. Kizilova: Interaction of liquid droplets with micro-structured and nanostructured surfaces	115
A. Bose, D.J. Borman, T.N. Hunter, J.T. Spencer, C.J. Cunliffe: Impact of pipe inclination on fill height for partially filled pipes used in a custom slurry transport rig	117
M. Klamka, T. Bobinski: Droplet surfing on a boundary layer - origin of droplet shape oscillation	119
M. Arogeti, A. Vinod, M. Tadmor: Forces acting on a pendant drop on a small pillar	121
M. Rajek, J. Pozorski: Particle clustering and velocity statistics in large-eddy simulations of isotropic turbulence	123
B. Bakhtar Khan, S.K. Tahmida, A.B. Vir: Estimation of droplet size using pressure oscillation-based approach in microfluidics by simulations	124
S. Shabani, M. Majkut, S. Dykas, K. Smółka: Utilizing a pressure-based CFD solver for modelling wet steam flow in low-pressure turbine stages: a predictive approach to assessing flow losses	126
D. Asendrych: Numerical simulation of the oil-water flow in a horizontal pipe in a stratified flow regime	128
M. Jaszczur, P. Marczak, R. Hanus, A. Golijanek-Jędrzejczyk, A. Andruszkiewicz, M. Zych: Liquid-gas flow modelling in horizontal pipe	130
M. Dzikowski, P. Szymczak: Time-resolved imaging of reactive transport instability during multiphase flow in porous media	132
SPONSOR'S SESSION	134
K. Dörner: Dantec Dynamics systems in Macro and Micro Experimental Fluid Dynamics ..	135
TURBULENCE AND TRANSITION	137
M. Waławczyk, J. L. Nowak, J. C. Vassilicos, S. Król, S. P. Malinowski: Turbulent cascades in the Atmospheric Boundary Layers	138
S.P. Malinowski, M. Waławczyk, J. Nowak, S. Król, R. Grosz: Atmospheric turbulence: anisotropic, nonstationary and intermittent. What can we do?	140
K. Bukowski, K. Gumowski, Ł. Klotz: Influence of porous material on the flow behind backward-facing step - experimental study	142

P. Baj, P. Czubak, B. Załęcki, A. Czaplińska: Replicating environmental flows with an active grid	144
E. Tuliszką-Sznitko: A shear flow in counter-rotating Taylor-Couette configuration	146
P. Prusiński, S. Kubacki: Large Eddy Simulation of turbulent flow at the entrance to an annular pipe section	148
S. Król, M., S. Malinowski: Anisotropic turbulence in marine cumulus clouds	150
S. Gepner, G. Kawahara: Tracking invariant solutions of the Navier-Stokes within spectral element framework	152
K. Dylewicz, V. Theofilis: Global instabilities on ROTEX-T cone-flare model in hypersonic flow at high altitude cruise conditions	154
J. Michna, K. Rogowski: URANS numerical analysis of turbulence intensity influence on laminar separation bubble in the case of the NACA0018 airfoil	156
YOUNG RESEARCHERS PROF. J.W. ELSNER'S COMPETITION	158
P. Jędrejko, J.-I. Yano, M. Waławczyk: Turbulent Coherent Structures in Thermal Vortex Rings	159
P. Kamiński, A. Tyliczszak: Control of turbulent boundary layer separation using a sinusoidal-type wavy-wall	161
B. Kaźmierski, Ł. Kapusta: Impact of flashing conditions on impinging-jet sprays	163
R. Ploix, J. Malet, E. Gehin: Numerical investigation of local aerosol deposition in a real scale T-junction of a ventilation network	165
M. Romańczyk, A. Drózdź, W. Elsner: Evaluation of hot-wire measurement accuracy in turbulent boundary layers under strong adverse pressure gradient conditions	167
T. Suresh, O. Szulc, P. Flaszynski: Aeroacoustic analysis of propeller rotor noise using the porous FW-H acoustic analogy	169
D. Żyła, T. Bobinski: Rectangular waveguide cavities as cloaks for cylindrical obstacles	171
POSTERS	173
K. Balcerzak, B. Potęga: Preliminary wind tunnel testing of a racing motorcycle using a scale model	174
R. Gnatowska, K. Gumowski, P. Niegodajew, K. Gajewska: Fluid Dynamics of Flow around Various Cylinders Geometries	176
P. Marczak, M. Jaszczur: Multiphase flow analysis in horizontal pipe - numerical issues	178
A. Merdjani, N. Kizilova: Experimental analysis of fractal distributors	180
K. Michałowski, S. Gepner: Extending Channelflow: Incorporating Temperature Effects in Poiseuille and Couette Flows	182
A. Muhsen, N. Kizilova, B. H. Attiya: Fractal-Type Structures for Heat Exchangers: A CFD Investigation of Tube Geometry Influence	184
S. B. Naqvi, M. Matyka: Numerical Investigation of Gas Injection into the Crossflow for High Reynolds Number	186
J. Nzotungishaka, M. Waławczyk and J.-I. Yano: Time dependence of similarity functions in the atmospheric boundary layer	188
B. Olszański: Surrogate model of missile's flight control surface aerodynamics	190
A. Osiaacz, Ł. Kotyński, F. Uilhoorn, T. Bleschke, M. Kwestarz, M. Chaczykowski: Composition tracking of CO₂-rich streams in large-scale pipeline networks under steady-state conditions	192
T. Polski, M. Żyto, M. Płatek Ł. Rybakowski, M. Bartoszek, G. Spruch, R. Szulejko, E. Podlevski: Optimisation of the design of Formula SAE car aerodynamics	194

Preface

Dear Esteemed Colleagues and Members of the Scientific Community,

It is with great pleasure that we welcome you to the XXVI Fluid Mechanics Conference, a key regional event dedicated to the experimental, theoretical, and numerical research challenges in fluid mechanics. Your participation highlights our community's shared commitment to advancing knowledge in this vital field. This year's conference holds special significance as it marks the 50th anniversary of a series that began in 1974.

As we gather in Warsaw, a city rich in history and scientific achievement, we eagerly anticipate a vibrant exchange of ideas to further our understanding and application of fluid mechanics. This conference will showcase the latest advancements and foster discussions crucial to addressing the complex challenges in fluid mechanics. We are confident that your contributions will enrich this event and inspire new avenues of research and collaboration.

We sincerely thank all participants, speakers, and organizers who have made this conference possible. Your engagement and expertise are what will make this event a success. We hope your time here will be intellectually stimulating and professionally rewarding. Welcome to Warsaw, and welcome to the XXVI Fluid Mechanics Conference - an event that has shaped our field for half a century.

On behalf of the XXVI Fluid Mechanics Conference Committees,

Jacek Szumbariski

Co-financed by the Ministry of Education and Science of the Republic of Poland on the basis of the agreement no. KONF/SP/0407/2023/01 of 01 09 2023, entitled "Support for the organization of the international conference XXVI Fluid Mechanics Conference 2024" carried out as part of the "Excellent Science II Program", Funding of MEiN PLN 118 910.00, Project value PLN 418 010,00.



Ministry of Education and Science
Republic of Poland



Ministerstwo
Edukacji i Nauki

Projekt finansowany ze środków budżetu państwa, przyznanych przez Ministra Edukacji i Nauki w ramach Programu „Doskonała Nauka II”

Honorary Patronage



ERCOFTAC

European Research Community On
Flow, Turbulence And Combustion



**Polskie Towarzystwo Mechaniki
Teoretycznej i Stosowanej**



Rector of the Warsaw University of Technology

Sponsors



XXVI FMC 2024 International Scientific Committee

Chairman: Prof. Jacek Pozorski	The Szewalski Institute of Fluid-Flow Machinery Polish Academy of Sciences, Gdansk, Poland
Prof. Janusz Badur	The Szewalski Institute of Fluid-Flow Machinery Polish Academy of Sciences, Gdansk, Poland
Prof. Ali Beskok	Southern Methodist University, USA
Prof. Tomas Bodnar	CTU Praha, Czech Republic
Prof. Andrzej Bogusławski	Częstochowa University of Technology, Poland
Prof. Piotr Doerffer	The Szewalski Institute of Fluid-Flow Machinery Polish Academy of Sciences, Gdansk, Poland
Prof. Witold Elsner	Częstochowa University of Technology, Poland
Prof. Maria Ekiel-Jezewska	Institute of Fundamental Technological Research Polish Academy of Science, Poland
Prof. Krzysztof Fidkowski	University of Michigan, USA
Prof. Jerzy Maciej Floryan	University of Western Ontario, Kanada
Prof. Andrzej Herczyński	Boston College, USA
Prof. Genta Kawahara	Osaka University, Japonia
Prof. Tomasz Kowalewski	Institute of Fundamental Technological Research Polish Academy of Sciences, Warsaw, Poland
Prof. Sławomir Kubacki	Warsaw University of Technology, Poland
Prof. Anna Kucaba-Piętal	Rzeszow University of Technology, Poland
Prof. Henryk Kudela	Wrocław University of Technology, Poland
Prof. Lech Łobocki	Warsaw University of Technology, Poland
Prof. Marek Morzyński	Poznań University of Technology, Poland
Prof. Spencer Sherwin	Imperial College London, UK
Prof. Alfredo Soldati	TU Wien, Austria
Prof. Janusz Szmyd	The AGH University of Krakow
Prof. Jacek Szumbariski	Warsaw University of Technology, Poland
Prof. Andrzej Teodorczyk	Warsaw University of Technology, Poland
Prof. Krzysztof Tesch	Gdansk University of Technology, Poland
Prof. Ewa Tuliszcza-Sznitko	Poznań University of Technology, Poland
Prof. Artur Tyliszczak	Częstochowa University of Technology, Poland
Prof. Markus Uhlmann	KIT Karlsruhe, Germany
Prof. Włodzimierz Wróblewski	Silesian University of Technology, Gliwice, Poland
Prof. Luc Vervisch	INSA Rouen, France

Organizing Committee

Jacek Szumbariski	Conference Chair
Sławomir Kubacki	Conference Vice-Chair
Tomasz Waclawczyk	Secretary
Paweł Baj	Secretary
Stanisław Gepner	Technical Secretary
Tomasz Bobiński	Technical Secretary

Members of the Organising Committee

Magdalena Majewska
Marta Poćwierz
Michał Remer
Michał Klamka
Zbigniew Rarata

Volunteers helping during FMC2024

Bartosz Olszański
Bartosz Potęga
Mariusz Rutkowski
Jan Wiśniewski

Plenary Lectures

Krzysztof J. Fidkowski, Prof.

University of Michigan, Michigan, USA



Krzysztof J. Fidkowski is a Professor of Aerospace Engineering at the University of Michigan. He earned his S.B. in Physics and S.B., S.M, and Ph.D. degrees in Aeronautics and Astronautics from MIT. His doctoral thesis was in computational fluid dynamics and investigated the applicability of high-order discontinuous finite-element methods to aerodynamics simulations over complex geometries. Before joining the University of Michigan in 2008 as an assistant professor, he was a post-doctoral associate at the Aerospace Computational Design Laboratory at MIT, where he worked on projection-based reduced models. At the University of Michigan, Professor Fidkowski teaches aerodynamics, numerical methods, and computational fluid dynamics. He has received young investigator awards from the Department of Energy and the Air Force Office of Scientific Research. He previously served as chair of the CFD Subcommittee of the AIAA Fluid Dynamics Technical Committee, organised fluids and CFD tracks at multiple AIAA conferences, and is an AIAA Associate Fellow. His primary research field is in algorithmic development for computational fluid dynamics, specifically in the use of adjoint methods for numerical error estimation, mesh adaptation, and uncertainty quantification. In recent work, Professor Fidkowski has studied reduced models of high-order dynamical systems, optimisation under uncertainty, machine learning for error estimation and mesh adaptation, panel methods for low-speed aerodynamics, and dynamic closure models for turbulent flows.

Output-Based Discretization Error Control in Turbulent Flow Simulations

K J Fidkowski¹

¹ The University of Michigan, Department of Aerospace Engineering, Ann Arbor, Michigan,
USA

E-mail: kfid@umich.edu

Advances in computational power have enabled scale-resolving simulations of turbulent flow, yet the high cost of these simulations prohibits their use in a multi-query setting, such as design optimization. In addition, discretization errors resulting from under-resolved spatial and temporal domains often go unchecked, as a posteriori error estimates do not easily extend to such simulations due to their chaotic nature. As evidenced by recent workshops on high-fidelity discretizations, these errors can significantly impact numerical solutions and prevent the use of such simulations for predictive analysis. We discuss two solutions to this challenge of robust turbulent-flow computation. The first is a mesh adaptation procedure based on the entropy adjoint, which is stable and inexpensive to compute, and which minimizes spurious entropy production in unsteady simulations. The second is a data-driven approach for calculating adjoints by correcting a lower-fidelity model, such as Reynolds-averaged Navier-Stokes (RANS). The corrected RANS equations yield a steady adjoint solution that can be used with unsteady residuals to define an output-based indicator for adaptation. Results for several prototypical aerodynamic problems demonstrate the utility of the proposed methods for estimating and reducing discretization errors.

J.M. Floryan, Prof.

Western University, London, Ontario, Canada.



J.M. Floryan is a Professor at the Western University, London, Ontario, Canada. He received his Ph.D. in 1980 from Virginia Tech and did postdoctoral work in 1981 at Northwestern University. He was a visiting professor at the City University of Hong Kong, Stuttgart University, Darmstadt Technical University, National University of Singapore, and Beijing Institute of Technology. He was a visiting researcher at DLR Gottingen, National Aerospace Laboratory Tokyo, CERT-ONERA in Toulouse, and Los Alamos National Laboratory. Dr. Floryan's primary professional interests are developing flow management strategies relying on passive and active actuation patterns (roughness, suction, heating, and vibration). He served as President of the Canadian Society for Mechanical Engineering (CSME) and the Canadian Congress of Applied Mechanics (CAN-CAM). Dr. Floryan is a Fellow of the American Physical Society (APS), the American Society of Mechanical Engineers (ASME), the CSME, the Canadian Aerospace and Space Institute (CASI), the Engineering Institute of Canada (EIC), and the Japanese Society for the Promotion of Science (JSPS), as well as being a NATO Research Fellow (France) and a Science and Technology Agency Fellow (Japan). An AIAA Associate Fellow, he was the winner of the Robert W. Angus Medal (CSME), the Canadian Pacific Railway Engineering Medal (EIC), the McCurdy Award (CASI), the Humboldt Research Prize, Erskine Fellow (New Zealand), and Lady Davis Fellow (Technion). He is the Canadian representative to IUTAM.

XXVI FLUID MECHANICS CONFERENCE
Warszawa, 10-13 September 2024

On the Structured Convection

J M Floryan¹

¹ The University of Western Ontario, Department of Mechanical and Materials Engineering,
London, Ontario, Canada

E-mail: floryan@uwo.ca

Natural convection driven by heating patterns is known as structured convection. It gives rise to fascinating new physics. It has been determined so far that it can reduce pressure losses in conduits, intensify mixing, be used to extract energy from the flow (energy harvesting), give rise to thermal drift and nonlinear thermal streaming, can be used for propulsion, used for horizontal pumping (horizontal chimney effect), can be used to create streaks and rolls in shear layers, and can dominate local contamination transport. Patterns of thermal waves offer further exciting applications, from pumping in conduits to wind generation. Combining heating and topography patterns activates the pattern interaction effect, whose strength changes significantly with minor changes in both patterns' relative positions, similar to initial conditions in a chaotic system. The spatial parametric resonance drives such flows' stability, which can give rise to many flow structures, including solitons. Heating patterns frequently occur in nature, e.g., the surface topography (building pattern) and thermally relevant features of this topography, like color variations (color patterns of roofs, streets, and parks) in the urban environment (heat island effect). Similar conditions are encountered in rural environments where local circulation can be driven by different heating rates of forests and lakes and can be modified by terrain topography. Recent progress in the analysis of structured convection will be discussed.

Genta Kawahara, Prof.

Osaka University, Osaka, Japan



Prof. Genta Kawahara received his B.S., M.S. and Ph.D. degrees from Osaka University. He was a visiting scholar at Center for Turbulence Research, NASA Ames Research Center/Stanford University before being appointed to an associate professor at Kyoto University in 2001 and a professor at Osaka University in 2005. Currently, he is an associate editor of *Journal of Fluid Mechanics* and an editor-in-chief of *Fluid Dynamics Research*. His research interests are in turbulence, subcritical transition to turbulence, simple invariant solutions to the Navier-Stokes equation and turbulent heat transfer.

Ultimate states of turbulent thermal convection and shear flow

Genta Kawahara¹

¹Osaka University, Graduate School of Engineering Science, 1-3 Machikaneyama, Toyonaka, Osaka 560-8531, Japan

E-mail: genta.kawahara.es@osaka-u.ac.jp

Abstract. Turbulent heat transfer is reviewed for thermal convection (or shear flow) between horizontal (or parallel) permeable walls. It is shown that wall permeability can lead to the so-called ultimate state in which a wall heat flux is independent of thermal diffusivity or kinematic viscosity. In the ultimate state of thermal convection (or shear flow) between permeable walls, large-scale thermal plumes (or spanwise rolls) are induced even in the vicinity of the walls. These large-scale thermal and flow structures fully extend in the fluid layers, yielding the ultimate heat transfer.

Keywords: Turbulence, Thermal Convection, Wall-Bounded Shear Flow, Heat Transfer

If there is a difference in temperature between bulk fluid and a wall surface in wall-bounded turbulent flows, heat will be transferred between the fluid and the wall. Such heat transfer is dominated by thermal conduction on the wall where turbulent heat flux is null, although it highly depends on turbulence characteristics. In this talk, turbulent heat transfer in wall-bounded thermal convection and shear flow is discussed with emphasis on the so-called ultimate state in which a wall heat flux is independent of thermal diffusivity, i.e. conduction anomaly (or anomalous thermal dissipation), while energy dissipation is independent of kinematic viscosity, i.e. the Taylor dissipation law implying the inertial energy dissipation or anomalous energy dissipation.

In the first part of this talk, the classical scaling widely observed in turbulent Rayleigh-Bénard convection is reviewed to differentiate the ultimate state from the classical state. Feasibility of the ultimate heat transfer is then explored numerically [1]. Wall permeability, which can be implemented on a porous wall, is introduced in Rayleigh-Bénard convection. It is found that in thermal convection between the horizontal permeable walls, the ultimate heat transfer can be achieved at high Rayleigh numbers. We discuss the reason why the wall permeability can lead to the ultimate scaling in wall-bounded convective turbulence. In the ultimate state large-scale thermal plumes are induced by buoyancy in the close vicinity of the walls, yielding intense transpiration velocity. The ultimate heat transfer is attributed to such large-scale significant fluid motion.

In the second part, we further pursue the ultimate heat transfer numerically in turbulent channel flow by introducing the wall permeability [2]. The ultimate heat transfer can be accomplished even in shear flow between the parallel permeable walls at high Reynolds numbers. In the ultimate state large-scale spanwise rolls appear from the Kelvin-Helmholtz instability [3], significantly enhancing near-wall heat transfer without flow separation. The large-scale turbulence structures with similarly strong velocity and temperature fluctuations bring about the ultimate heat transfer.

In the last part, it is demonstrated that the ultimate heat transfer can be achieved in realistic configurations by numerical simulation and experiment of turbulent thermal convection between horizontal porous walls. At low Rayleigh numbers, vertical (wall-normal) fluid motion is not excited in the near-wall region despite wall permeability, so that the classical state can be observed. At high Rayleigh numbers, however, large-scale thermal plumes appear even near the walls from convective instabilities of near-wall thermal conduction layers to intensify the vertical heat flux, leading to the ultimate state. In between these two distinct scaling ranges of the Rayleigh number, we have found super-ultimate behaviour represented by the heat flux significantly exceeding that in the ultimate state. This super-ultimate scaling is considered to be a consequence of full excitation of large-scale thermal plumes comparable with those in the ultimate state at the high Rayleigh numbers and of less energy dissipation in the flow through porous walls than in the ultimate state at the high Rayleigh numbers.

Acknowledgements

This is the author's joint work with Dr S. Motoki, Dr M. Shimizu, Mr K. Kawano, Mr K. Tsugawa, Mr A. Shirai and Mr F. Meng.

References

- [1] Kawano K, Motoki S, Shimizu M and Kawahara G 2021 *J. Fluid Mech.* **914** A13
- [2] Motoki S, Tsugawa K, Shimizu M and Kawahara G 2022 *J. Fluid Mech.* **931** R3
- [3] Jiménez J, Uhlmann M, Pinelli A and Kawahara G 2001 *J. Fluid Mech.* **442** p 89

Luis Pablo Ruiz-Calavera, Prof.

Airbus & Universidad Politécnica de Madrid



Prof Luis Pablo Ruiz-Calavera is currently the Executive Expertise Leader for Aerodynamics at Airbus and the Associated Professor at Universidad Politécnica de Madrid. He received his PhD in Aerodynamics from Universidad Politécnica de Madrid. Since 1984 he has held several positions, including Researcher at Instituto Nacional de Técnica Aeroespacial, HO Aerodynamics at Airbus Military and Vice-president HO Flight Physics at Airbus Defence and Space. Within these roles, he has participated in and successfully lead many aerospace research and development projects.

Some aerodynamic challenges of the future sustainable commercial aircraft

L P Ruiz-Calavera^{1,2}

¹ Airbus Defence & Space, Flight Physics CoC, Getafe, Spain

² Universidad Politécnica de Madrid, Department of Aircraft and Space Vehicles, Madrid, Spain

E-mail: luis.ruiz.calavera@upm.es

The Aviation Industry has committed to net-zero carbon emissions in global civil operation by 2050. To achieve this goal the next generation of commercial aircraft will need to incorporate new technologies to significantly increase the aerodynamic efficiency and to make use of new types of power plants and energy sources. This will result in the need to evolve the aircraft configuration and to bring to a robust operational standard technologies that have so far not been routinely used on large airlines. Industry is actively exploring these concepts while developing the technology bricks that would enable them. This talk will review some of these technologies in the aerodynamics field and will present Airbus' view on the still existing gaps that need to be matured before they find practical implementation in the future sustainable commercial aircraft.

Spencer Sherwin, Prof.

Imperial College London, London, UK



Professor Spencer Sherwin is Head of Department and Professor of Computational Fluid Mechanics in the Department of Aeronautics at Imperial College London. Currently, he is an associate editor of Journal of Fluid Mechanics. He received his MSE and PhD from the Department of Mechanical and Aerospace Engineering Department at Princeton University. Prior to this he received his BEng from the Department of Aeronautics at Imperial College London. Professor Sherwin leads an active research group specializing in the development and application of parallel high order spectral/hp element methods (Nektar++) for flow around complex geometries with a particular emphasis on vortical and bluff body flows and biomedical modelling of the cardiovascular system. He has been closely involved in industrial application of these methods through partnerships with McLaren Racing, Airbus and Rolls Royce. Currently Professor Sherwin is Principal Investigator on the EPSRC funded Platform for Research in Simulation Methods.

Advancing spectral/hp element high fidelity simulation of incompressible and compressible flows

Spencer Sherwin¹

¹ Department of Aeronautics, Imperial College London, UK

E-mail: s.sherwin@imperial.ac.uk

Keywords: Computational Fluid Dynamics, Spectral/hp element methods, High order methods, Compressible Flow, Incompressible Flow

1. Introduction

Advanced high order methods using Spectral/hp element discretization [1] including Galerkin, Discontinuous Galerkin (DG) and Flux Reconstruction (FR) formulations are gaining notable interest in both the academic and industrial sectors. The compact nature of the approach is not only attractive from the perspective of implementation on modern computational hardware but also provides a consistent geometric and spatially localized accuracy unlike many high order finite volume methods. These features make the methodology attractive in complex geometry flows involving transitional and turbulent boundary layers demanding a high level of accuracy for high end engineering applications that commonly arise in the automotive and aeronautical sectors.

In this presentation, we will present our current work on developing and advancing spectral/hp element incompressible and compressible flow solvers for industry relevant, high-fidelity applications [2]. The demands of handling “industrial strength” complex geometries at high Reynolds numbers presents a number of challenges both in terms high order mesh generation [2], stabilization of marginally resolved flows [3,4] and maintaining computational efficiency. In this presentation we will highlight our on-going efforts to address all these challenges and demonstrate the suitability of the approach for a number of representative examples.

References

- [1] Karniadakis G and Sherwin S 2005 *Spectral/hp element methods for computational fluid dynamics* Oxford University Press
- [2] Mengaldo G, Moxey D, Turner M, Moura RC, Jassim A, Taylor M, Peiro J, Sherwin S, 2021, *Industry-Relevant Implicit Large-Eddy Simulation of a High-Performance Road Car via Spectral/hp Element Methods*, SIAM Review, 63, p 723-755
- [3] Moura RC, Aman M, Peiró J, Sherwin SJ, 2019, *Spatial eigenanalysis of spectral/hp continuous Galerkin schemes and their stabilisation via DG-mimicking spectral vanishing viscosity for high Reynolds number flows*, Journal of Computational Physics, p 109112-109112,
- [4] Moura R, Cassinelli A, da Silva AFC, Burman E, Sherwin S, 2021, *Gradient jump penalty stabilisation of spectral/hp element discretisation for under-resolved turbulence simulations*, Computer Methods in Applied Mechanics and Engineering, 388, p 1-29

Daniele Simoni, Prof.

University of Genova



Prof. Daniele Simoni is the Head of the Aerodynamics and Turbomachinery Laboratory of the University of Genova. He graduated in Mechanical Engineering at the University of Genova with honours (09/2005). He received his PhD in Fluid Machinery from the University of Genova in 2009. He became Full Professor at the University of Genova in 2020. Since 2023 he is Coordinator of the Ph. D course in “Machine and Systems Engineering for Energy, Environment and Transport”. Prof. Daniele Simoni developed expertise in the design of open and closed loop wind tunnels, and in the design of turbomachinery and aero-engine components. He is expert on the application and data analysis of advanced measuring techniques for the investigation of time-dependent unsteady and distorted flow fields developing into turbomachinery components, such as laser Doppler Velocimetry, Time Resolved Particle Image Velocimetry, Fast Response Aerodynamics Pressure Probes (FRAPP), as well as hot-wire and hot-film anemometers. He developed acquisition and post-processing techniques for data reduction and identification of reduced order model by means of Proper Orthogonal Decomposition (POD), Dynamic Mode Decomposition (DMD) and wavelet techniques.

The role of experiments and data reduction techniques in the tuning of different transition models

D Simoni¹

¹ University of Genova, Department of Mechanical, Energy, Management and Transport Engineering, Genova, Italy

E-mail: daniele.simoni@unige.it

The Reynolds averaged Navier Stokes-based CFD solvers require closure strategies for the estimation of the Reynolds stress tensor, providing an eddy viscosity affecting the momentum transfer processes of the mean flow. Different turbulence and transition schemes have been developed in the past, especially for prediction of transitional boundary layer flows, relying on different assumptions and ability to predict transitional and turbulent flows of various applications. However, irrespective of the specific kind of numerical scheme considered, such model strategies necessarily require empiricisms to properly set the key terms appearing in the set of transport equations, definitively adopted to provide an accurate estimation of the eddy viscosity.

In the present work, an experimental data base spanning a large Design of Experiments devoted to tuning of possibly different transition closure schemes will be described in detail. This large database has been acquired in the last years in the Laboratory of Aerodynamics and Turbomachinery of the University of Genova. It includes more than 90 combinations of the most influencing parameters affecting transition, like the flow Reynolds number, the adverse pressure gradient and the free-stream turbulence intensity. Time-Resolved Particle Image Velocimetry (TR-PIV) has been used to characterize the response of the boundary layer transition process to variation of the inflow parameters. Data have successively been further reduced to provide closure elements required by different transition models. The spot production rate source term appearing in the $\gamma - Re_\theta$ model, the energy transfer rate appearing in the Laminar Kinetic Energy (LKE) transition model and the apparent viscosities characterizing the Pope's tensorial expansion are a few examples that will be discussed in detail during this presentation. The focus will be also paid to the reduction techniques and machine learning algorithms used to identify parsimonious models able to maximize their generalizability. Additional examples involving schemes for parallelized codes will be also discussed.

Aerodynamics and Hydrodynamics

Investigations of Reynolds number effect on Mach number distribution on compressor stator profile

M Piotrowicz¹, A Joseph¹, P Flaszynski¹, M Kurowski¹ and P Doerffer¹

¹Institute of Fluid-Flow Machinery, Polish Academy of Sciences, ul. Fiszera 14, 80-231 Gdansk, Poland

E-mail: mpiotrowicz@imp.gda.pl

Abstract. The paper focuses on the effect of Reynolds number (7.3×10^5 , 5.0×10^5 , 2.3×10^5) on Mach number distribution, shock wave position and boundary layer development on the suction side of the compressor stator profile. SBLI effects are investigated numerically and experimentally. Therefore, a rectilinear three-profile test section has been designed based on linear cascade configuration. Numerical results are compared with wall pressure measurements, oil flow visualization from experimental campaign.

Keywords: Aerodynamics, Transonic flows, Internal flows, Reynolds number, Shock-wave boundary layer interaction, Compressor.

1. Introduction

The development of advanced engine technology is required to solve emission control and maximize efficiency in response to present environmental challenges. This involves the ongoing research of higher stage pressure ratios and lower weights for fans and compressors [1]. These advancements can result in complex flow structures characterized by separation and vortices [2], along with adverse pressure gradients derived from SBLI (Shock Wave Boundary Layer Interaction). Notably, to reduce drag caused by skin friction, especially at higher altitudes, efforts have been focused on maintaining laminar boundary layers upstream of shocks. While laminar boundary layers have an advantage at low Reynolds numbers, they are susceptible to separation in adverse pressure gradients, potentially leading to increased internal flow turbulence and total pressure losses.

The Reynolds number effect on Mach number distribution on a stator profile has been carried out numerically and experimentally. Therefore a rectilinear three-profile test section has been designed based on the linear cascade configuration for the transonic wind-tunnel facility of IMPPAN as shown in Figure 1. The cascade geometry was defined by project partner Rolls-Royce Deutschland. One of the main design challenges of the test section was to reproduce the similar flow structure as in cascade simulations.

2. Numerical results

The numerical simulations were carried out on the representative test section model using the FINE/Turbo Cadence code. The two-equation nonlinear eddy viscosity turbulence model of the EARSM (Explicit Algebraic Reynolds Stress Model) with the transition model was chosen for predicting SBLI effects on the suction side of the stator profile. With Numeca/Cadence IGG, the

structured grid for the computation was created. There are 128 blocks in the test section mesh domain, each with 47×10^6 cells. The main focus of this research is the flow structure comparison at the chosen Reynolds number (7.3×10^5 , 5.0×10^5 , 2.3×10^5) within the transonic stator blade passage. The inflow Mach number has been defined as 0.9 for all three cases. The impact of the Reynolds number on the distribution of Mach number, the position of shock waves, secondary flow structures, distribution of wall shear stress on the suction side, as well as boundary layer separation at selected traverses, have been compared.

The Reynolds number was defined for the airfoil chord $c = 0.05$ m and flow conditions upstream of the airfoils. The Reynolds number is reduced by reduction of total pressure downstream of the control valve located upstream of the test section. The inlet Mach number is adjusted by the control valve downstream of the test section and static pressure modification. However, it should be noted that this is not possible to set the Reynolds number precisely, but Reynolds number is an effect of reduced total pressure (reduced density) upstream of the test section.

The numerical predictions from the chosen turbulence model have been compared with experimental data. The isentropic Mach number distribution has been estimated based on the static pressure measurements from the pressure taps located on the suction side of the lower and middle profile and the pressure side of the upper and middle profile. The inflow Mach number has been estimated using pressure taps located at the upper and lower walls. To visualize the separation bubble and corner flow effects the oil flow visualization has been performed on the suction side of the middle profile and is compared with numerical predictions using streamlines closer to the surface.

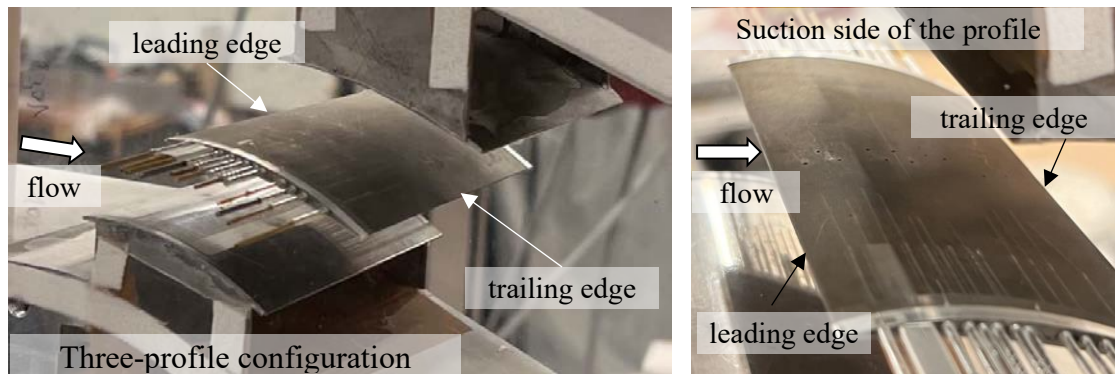


Figure 1. Designed test section for IMP-PAN transonic wind-tunnel facility.

Acknowledgements

This project has received funding from the European Union Horizon 2020 research and innovation programme under the Marie Skłodowska-Curie grant agreement 860909 **TEAMAero** (Towards Effective Flow Control and Mitigation of Shock Effects in Aeronautical Applications). Numerical simulations were performed in the Computational Centre of **TASK** (Trojmiejska Akademicka Siec Komputerowa).

References

- [1] J. Foret *et al.*, “Experimental Aerodynamic and Aeroelastic Investigation of a Highly-Loaded 1.5-Stage Transonic Compressor with Tandem Stator,” *14th Eur. Conf. Turbomach. Fluid Dyn. Thermodyn. ETC 2021*, 2021, doi: 10.3390/ijtp6030021.
- [2] J. Hu, R. Wang, R. Li, and P. Wu, “Effects of slot jet and its improved approach in a high-load compressor cascade,” *Exp. Fluids*, vol. 58, no. 11, pp. 1–13, 2017, doi: 10.1007/s00348-017-2437-4.

Effect of yaw angle on wind turbine power generation and velocity in the wake

F Wasilczuk¹, K Pietrzycka², R Szewczuk², P Flaszynski¹

¹Institute of Fluid-Flow Machinery, Polish Academy of Sciences, Fiszerza 14, 80-231 Gdansk, Poland

²Gdańsk University of Technology, Narutowicza 11/12, 80-233 Gdansk, Poland

E-mail: fwasilczuk@imp.gda.pl

Abstract. A technology called „wake steering” is being developed to increase the productivity of wind turbine clusters. Wake steering turns the upstream turbine of the cluster in such a way, that the wake of this turbine goes around turbines downstream. Even though the power production from the upstream turbine drops, there is power gain in the downstream turbines. This technology was investigated using methods with varying fidelity. Low-fidelity FLORIS code was used to study the impact of wake steering on the wake of the entire wind farm. In turn, the flow structure of the wake was investigated with the use of higher fidelity RANS models in Star CCM+, with two wind turbines modeled using the actuator disc model.

Keywords: Aerodynamics, Computational Fluid Dynamics, Wind Energy, Wake steering

1. Introduction

Thanks to its wide availability and sustainability, wind energy is one of the most rapidly developing alternative energy sources. When more than one wind turbine is installed in a cluster, wake effects have a dominating impact on the productivity of downstream turbines. Traditionally, the turbines within the wind farm are controlled in a manner, where each turbine maximizes its own production by adjusting yaw position so that the rotor plane is perpendicular to the wind. Such an approach does not consider the wake effects and power production of neighboring wind turbines, which can be significant.

Wake steering is a technique, where the rotor of the upstream turbine is turned away from the wind to deflect the wake [1]. For certain conditions, the wake can miss the downstream turbine, for others only part of the wake can interact with the downstream turbine. However, it is important to note that the effectiveness of wake steering relies in a major way on the wind conditions, in particular wind direction, so to use it effectively an algorithm prescribing the yaw angle deflection depending on the wind direction and speed has to be proposed.

The impact of wake steering on power production and wake has been studied over recent years using methods of different fidelity. Wake steering can be modeled in low-fidelity, fast engineering tools [2]. Such tools allow for fast calculation of optimal yaw angle for large arrays, due to their simplicity and low computational requirements. On the other hand, more advanced models, like RANS or LES [3] can be used to study the flow structure of the deflected wake. Such models can utilize Actuator Disc (ADM)

and Actuator Line (ALM) models of the rotor, to limit the resources necessary for simulation. However, with computational power available nowadays, the simulation time for turbine clusters poses a challenge to the investigation of large clusters for a wide array of conditions. Wake steering proved effective in field tests, using real turbines [2].

2. Methods definition

The wake structure was investigated using a two-turbine RANS model, created using STARCCM+ code. Reference wind turbine NREL 5MW was used for the analysis. The unstructured, hexahedral grid had up to 1.1 million elements. The model was validated using the results from LES simulations [3]. Power generated by each turbine was recorded for variable yaw angles and a wide array of boundary conditions. In addition, the wake flow structure was analyzed.

FLORIS python library, which allows for a calculation of wakes in wind farm clusters was used to determine the possible reduction of wind farm wake using wake steering. The model was validated with data from two sources – one is power measurements in a farm experiencing wind farm wake [4] and another is power measurements for a small cluster of turbines utilizing wake steering [2]. The wake and deflection models were selected based on the validation and comparisons. A model of two generic farms was created and the impact of the wake steering application to the upstream farm on the power generation of both farms was investigated.

3. Results

RANS simulations have shown that in fact the total power output for a two-turbine array increases when wake steering is utilized. Fig. 1 shows the power generated by each turbine and total power, normalized using the power for individual turbine without yaw. The wake of a turbine with yaw deflects (Fig 2) and changes shape from round to kidney-like.

Using the optimal yaw angle for the upstream farm causes a power increase for both farms. The increase depends on wind speed and direction. For the configuration that generates the most losses, wake steering increased the power of the upstream farm by over 21% and for the downstream farm by 12-19%. This shows that the wake steering impact is largest within the farm, but has some influence on the wake of the wind farm. For configurations with less wake losses, the effect of steering was lower.

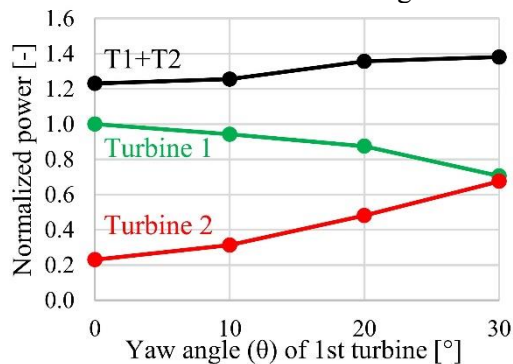


Figure 1. Power of two-turbine array depending on yaw angle of upstream turbine.

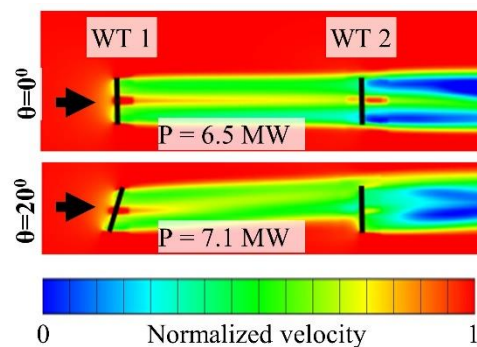


Figure 2. Velocity at the hub height for configuration with and without wake steering.

References

- [1] Meyers, J. *et al.* (2022) Wind farm flow control: prospects and challenges, *Wind Energ. Sci.*, 7
- [2] Howland M. F., Lele S. K., and Dabiri J. O. (2019) Wind farm power optimization through wake steering, *Proceedings of the National Academy of Sciences*, Vol. 116 (29)
- [3] Nakhchi, *et al.*, A novel hybrid control strategy of wind turbine wakes in tandem configuration to improve power production, *Energ Convers Manage*, Vol. 260 (115575), 2022, <https://doi.org/10.1016/j.enconman.2022.115575>.
- [4] Nygaard and Hansen (2016) Wake effect between two neighbouring wind farms, *J. Phys.: Conf. Ser.* 753 032020

On Streamwise Vorticity Dynamics in Circular Cylinder Wake

V Uruba^{1,2}, P Prochazka² and D Duda¹

¹ Power System Engineering Department, Faculty of Mechanical Engineering, University of West Bohemia in Pilsen, Czech Republic

² Department of Fluid Dynamics, Institute of Thermomechanics, Czech Academy of Sciences, Prague, Czech Republic

E-mail: uruba@fst.zcu.cz

Abstract. The streamwise vortices are detected experimentally in the wake behind a circular cylinder in Reynolds number 5 thousand on the top of Kármán vortex street dynamics. The stereo time-resolved PIV method has been used. The wake is moving periodically in spanwise direction due to Kármán vortex street dynamics, consisting of vortices oriented in the cylinder axis direction. Both dynamical structures in the wake, the streamwise velocity component deficit and the streamwise vorticity concentration, are moving periodically in transversal direction with the same frequency, the vorticity concentration is shifted by a quarter of period before the velocity deficit in the shedding process. The streamwise vorticity is the most intense in the wake position in dead points.

Keywords: Experimental Fluid Mechanics, Wake, Dynamics, 3D Topology, Turbulence

1. Introduction

The wake behind circular cylinder is one of the canonical cases, which is characterized by excessive number of applications and extreme attention of researchers during the whole history of fluid mechanics. Despite application of all available methods both mathematical and experimental, there are still some aspects unclear, namely those connected with turbulence appearance resulting in extremely complex 3D dynamical behavior.

The preliminary study on this subject has been already published in [1]. In the presented paper deeper analysis is to be shown. A wake could be considered as the zone with streamwise velocity deficit, as shown in [2]. The presence of streamwise vortices is recognized and studied.

2. Experimental setup

As a typical case, the circular cylinder with diameter $d = 15$ mm and the low-turbulence incoming velocity $U_e = 5$ m/s have been chosen. The Reynolds number was thus around 5 thousand.

The measurement has been carried out using time-resolved stereo PIV technique with frequency 2 kHz in the measurement plane perpendicular to the incoming flow and parallel to the cylinder axis $3.83 d$ behind it. The Safex generator of particles in the form of micron oil droplets was used. The data were acquired and post-processed using the Dynamic Studio and Tecplot software.

3. Results and discussion

As an example, there is Fig. 1 with instantaneous streamwise velocity component distribution on left and streamwise vorticity component on right. In vorticity graph, the vector-lines are added.

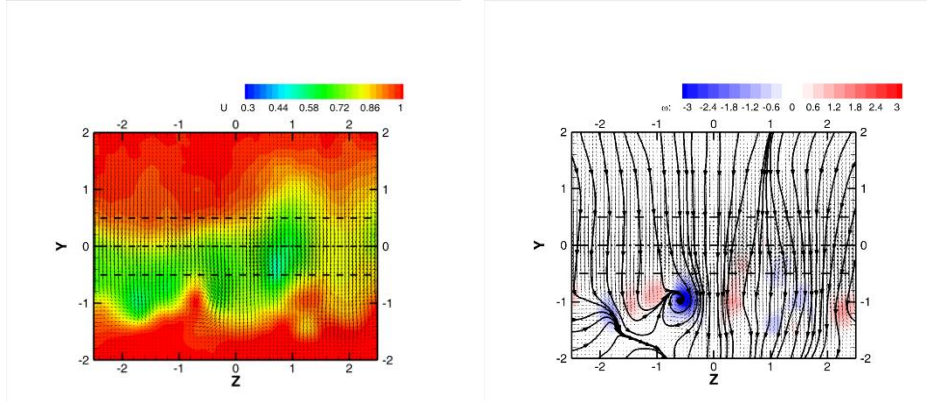


Figure 1. Wake structure for symmetrical phase, wake is moving downwards.

In Fig. 1, both y and z axes are perpendicular to the incoming flow (x direction) the z axis is identical with the cylinder axis. The cylinder silhouette is shown as a dashed line, distances are in multiples of the cylinder diameter d . Fig. 1 shows the situation, when the velocity deficit is located around cylinder axis (left). However, the vorticity is located close to the lower cylinder contour (red positive and blue negative vorticity).

Both structures, streamwise velocity component deficit and streamwise vorticity concentration, are moving periodically in transversal direction y with the same frequency. However, the vorticity concentration is shifted by a quarter of period before the velocity deficit in the shedding process.

4. Conclusions

The dynamical aspects accompanying the Kármán vortex street of a fully turbulent wake behind a circular cylinder in cross-flow were studied experimentally using time resolved stereo PIV method. The results of the study show clearly, that despite the fact of presence 2D body geometry, the flow in the turbulent wake is always 3D, at least its dynamical part.

Typical dynamical patterns topology will be presented in the full paper. The wake is dominated by streamwise vortices appearing in distinct locations and phases of the quasi-periodical vortex shedding process randomly. Both dynamical structures in the wake, the streamwise velocity component deficit and the streamwise vorticity concentration, are moving periodically in transversal direction with the same frequency, the vorticity concentration is shifted by a quarter of period before the velocity deficit in the shedding process.

Acknowledgements

This publication was supported by the Institute of Thermomechanics, v.v.i. and the project of University of West Bohemia in Pilsen SGS-2022-023.

References

- [1] Uruba V, Procházka P. Experimental Investigation of 3D Dynamical Effects in a Wake behind Circular Cylinder, 2022, Conference on Power System Engineering 2022
- [2] Duda D, Uruba V and Yanovych V. Wake Width: Discussion of Several Methods How to Estimate It by Using Measured Experimental Data, 2021, Energies, 14, 15: 4712

Validation of Yamaguchi-Ichikawa water hammer model

K Urbanowicz¹, C Di Nucci², BK Sharma³, K. Ashok⁴ and S Krajewski¹

¹ West Pomeranian University of Technology in Szczecin, Faculty of Mechanical Engineering and Mechatronics, Al. Piastów 17, 70-310 Szczecin, Poland

² Civil Construction-Architectural and Environmental Engineering Department (DICEAA), University of L'Aquila, L'Aquila, Italy

³ Department of Mathematics, Birla Institute of Technology and Science Pilani, Pilani, Rajasthan, India

⁴ Advanced Computational Facility, School of Mechanical Engineering, Vellore Institute of Technology, Vellore, India

E-mail: kamil.urbanowicz@zut.edu.pl

Abstract. This study comprehensively analyzes the Yamaguchi-Ichikawa (YI) model for water hammer phenomena in hydraulic systems, alongside recent theoretical studies and experiments. While promising initially, comparative investigations reveal limitations in the YI model's alignment with experimental data, particularly regarding initial conditions and pulsation periodicity. These shortcomings, including the absence of a phase shift, may hinder its applicability in complex pressure systems with multiple wave reflections. This research contributes to refining analytical models for hydraulic phenomena to enhance predictive accuracy and suggesting avenues for future investigations to bridge theoretical frameworks with experimental observations.

Keywords: Hydromechanics, Water hammer, analytical solution, transient pipe flow

1. Introduction

Structural damages in hydraulic systems, particularly due to cyclic transient states causing impulsive pressure increases known as water hammer, pose significant risks. These phenomena, encompassing both high and low pressures, induce fatigue loads on conduit materials and damage hydraulic components, often costly to repair. Despite the simplicity of some hydraulic systems, analytical solutions in the time domain remain scarce, with early approaches neglecting friction effects. Recent advancements [1,2,3] have addressed this, but limitations persist, especially in accurately modeling water hammer across varying water hammer numbers $Wh=(vL)/(cR^2)$ (where v – kinematic liquid viscosity, L – pipe total length, c – pressure wave speed and R – inner pipe radius). This study focuses on analyzing the Yamaguchi-Ichikawa (YI) model [4], proposed for very viscous Newtonian fluid flows, to address existing gaps in analytical modeling and enhance understanding of water hammer phenomena, crucial for hydraulic system safety and efficiency.

2. Analytical models of water hammer

Attention was paid on the analysis of the Yamaguchi-Ichikawa analytical model (YI). In conference paper a shortened derivation of this equation is present, as well as the necessary initial and boundary conditions assumed. Additionally, final formulas describing other analytical models (AM) will be presented [3]: the quasi-steady Rich model (R), the unsteady Muto-Takahashi model (MT), and the Mei-Jing model (MJ).

3. Comparisons of analytical model

Comparison section consists three subsections, in which the results are compared as follows: a) YI with experimental results YI; b) obtained with the help of analytical solutions YI, R, MJ, MT with

experimental results of Adamkowski-Lewandowski (AL) [5] and Urbanowicz et al. [6], as well as numerical results (using the method of characteristics, MOC); c) numerical MOC with analytical results YI,R,MJ, MT in the range of high values of the water hammer number Wh .

3.1. Comparisons to Yamaguchi-Ichikawa experimental results

The fit of initially performed comparison appears to be not just good but very satisfying (Fig. 1). Only in one test, a discrepancy was noted compared to what was visible in the original YI manuscript [4]. The above prompted a desire to conduct further research.

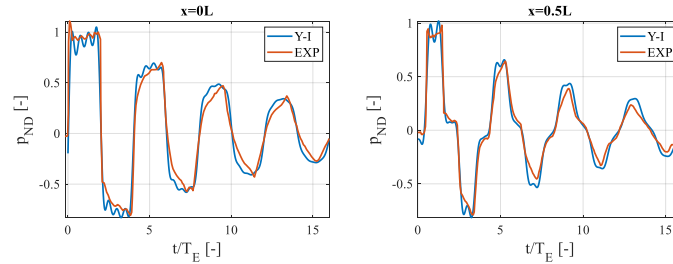


Figure 1. Experimental EXP results compared to YI model ($Wh=0.0087$).

3.2. Comparisons to other experimental results

The next comparisons were carried out in reference to scientifically validated experimental studies. On first 3 pressure amplitudes, the difference between models YI and MT and MJ is not easily noticeable (Fig. 2), while on subsequent amplitudes, due to the increasing phase shift (appearance of wave dispersion), the differences are much more pronounced. Quasi-steady model R perform poorly.

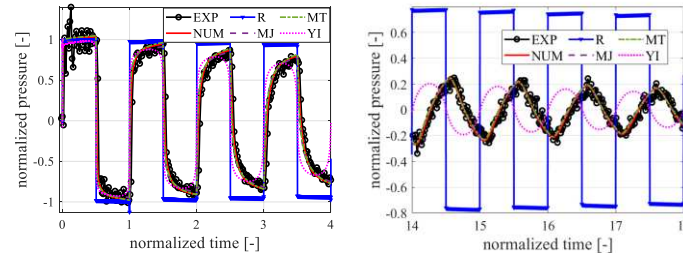


Figure 2. Comparison to Adamkowski and Lewandowski experimental results ($Wh=0.0011$).

3.3. Comparisons of analytical model in large Wh number domain

In this subsection, analytical results from AM are compared solely to numerical results to assess their compliance across a spectrum of flow changes. The YI model closely replicates pressure profiles akin to the quasi-steady R model, resulting in divergent analytical outcomes from those obtained with the unsteady model in the method of characteristics (MOC).

4. Conclusions

The comparative studies of the YI model revealed limitations: lack of agreement at $t=0$ and periodic pulsation identical with the quasi-steady R model. These deficiencies hinder its applicability in modeling complex pressure systems. Despite drawbacks, the YI model offers advantages, notably minimal series term consideration for modeling highly viscous Newtonian fluid flows. The observed mathematical similarity with other models suggests a common structure for a complete analytical model.

References

- [1] Mei C C and Jing H 2018 *European Journal of Mechanics - B/Fluids* **69** 62
- [2] García-García F J and Alvariño P F 2022 *J. Fluid Mech.* **951** A4
- [3] Urbanowicz K et al. 2023 *Journal of Sound and Vibration* **562** 117848
- [4] Yamaguchi K and Ichikawa T 1972 *Bulletin of the JSME* **15** 1197
- [5] Adamkowski A and Lewandowski M 2006 *ASME J. Fluids Eng.* **128(11)** 1351
- [6] Urbanowicz K et al. 2021 *Engineering Failure Analysis* **128** 105607

Velocity profile correction in the analytical model of flow between disks of Tesla turbine

K Rusin¹, W Wróblewski¹, E Hasani Malekshah¹, M Pahlavanzadeh¹, S Rulik¹

¹Silesian University of Technology, Faculty of Energy and Environmental Engineering, ul. Konarskiego 18, 44-100 Gliwice, Poland

E-mail: krzysztof.rusin@polsl.pl

Abstract. The paper concerns the analytical model of a flow in a rotor of Tesla turbine with consideration of nozzle-rotor interaction. The model solves 2D equations but also considers the shape of the velocity profile. Sudden enlargement loss and nozzle efficiency are also accounted for. The model yields the radial distributions of pressure, velocity components, and temperature. The turbine performance is estimated.

Keywords: Flow Machinery, Analytical Model, Tesla turbine

1. Introduction

Global energy trends, especially phasing out fossil fuels and shifting towards renewable energy sources, necessitate the development of energy technologies adapted to new conditions. Expanders, a critical component of many energy systems, have to be adjusted to the new demands arising from the application of unconventional working media. Resistance to erosion, ability to work with multiphase fluid, and rapid start-up are among the most important features. Tesla turbine fulfils these requirements and, therefore, seems to be a suitable candidate for an expander in distributed systems based on renewable energy sources.

The investigations presented herein pertain to an analytical model of flow in a Tesla turbine rotor that also accounts for the losses in the nozzle apparatus.

2. Analytical model

The analytical model is based on the works [1,2,3]. The governing equations are momentum, mass and energy conservation laws in simplified forms that account for 2-D laminar, compressible and axially symmetrical flow. The model considers the shape of the velocity profiles when the velocity components are substituted by the product of the average values and the velocity profile terms ($E_1 - E_{10}$). For this reason, the equations solve for axially averaged quantities:

$$\frac{\partial \bar{w}_r}{\partial r} = - \left(\bar{w}_r \left(E_9 + \frac{1}{r} \right) + \frac{\bar{w}_r}{p} \frac{\partial p}{\partial r} \right) \quad \text{Eq.(1)}$$

$$\frac{\partial \bar{w}_\theta}{\partial r} = \frac{\nu E_3 \bar{w}_\theta - \bar{w}_r \bar{w}_\theta E_{10} - \frac{E_1 \bar{w}_r \bar{w}_\theta}{r} - 2\omega E_2 \bar{w}_r}{\bar{w}_r E_1} \quad \text{Eq.(2)}$$

$$\frac{\partial p}{\partial r} = \frac{\bar{w}_r^2 \left(E_8 + \frac{E_4}{R} \right) - \bar{w}_r (E_4 E_9 + \nu E_7) - \frac{E_6}{r} \bar{w}_\theta^2 - 2E_5 \omega \bar{w}_\theta - \frac{\omega r B}{2}}{\frac{E_4 \bar{w}_r^2}{p} - \frac{R_g T B}{p^2}} \quad \text{Eq.(3)}$$

3. Results

Figure 1 presents radial distributions of the averaged tangential velocity and static pressure in the Tesla turbine rotor obtained from the analytical code. Calculations were carried out for a total pressure of 300kPa, total temperature equal to 300K, rotational speed of 17500 rpm, gap size equal to 0.75mm and inlet and outlet radii equal to 0.08m and 0.04m, respectively. Air is a working medium. It is shown that the tangential velocity at the inlet is equal to 183 m/s and is gradually increasing with decreasing radius to achieve 296 m/s at the outlet. The expansion in the rotor starts from 170kPa. The details of the thermodynamic processes are shown in Figure 2 on Belpaire’s chart. The expansion in the nozzles starts in point 0. The isentropic expansion in the nozzle would end at point 1s, but the real process ends at point 1n. After expansion in nozzle, air undergoes sudden expansion in enlargement when it enters the radial tip clearance before admission to the rotor. This process contributes to losses, therefore, expansion in the rotor starts from point 1. Line 1-2 is the expansion in the rotor.

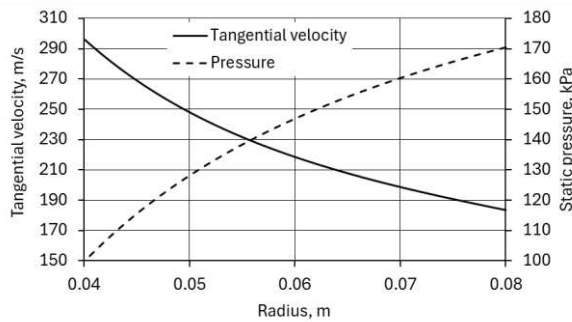


Figure 1. Radial distributions of tangential velocity and static pressure in Tesla turbine rotor

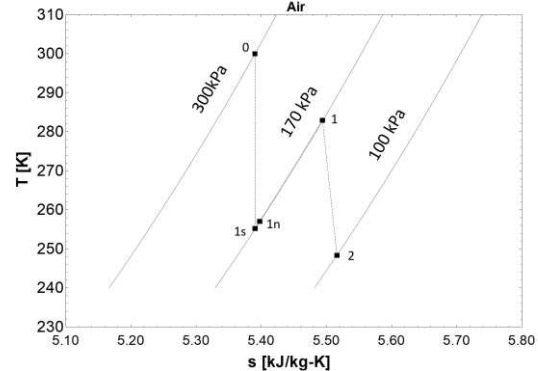


Figure 2. Thermodynamic processes in Tesla turbine on Belpaire’s chart

The power defined by Euler’s equation for turbomachinery totalled 106.99W and the isentropic efficiency related to the total-to-static enthalpy drop was equal to 6.85%. As can be seen, one of the major reasons for low efficiency is the interaction between the stator and the rotor, so this problem has to be addressed to improve Tesla turbine efficiency.

Acknowledgements

The presented research was conducted within the UMO-2019/35/B/ST8/01871 research project “The enhancement of momentum transfer efficiency in the flow between rotating discs”, financed by the Polish National Science Centre

References

- [1] Manfrida G, Pacini L, Talluri L, 2017, *Energy Proc*, **129** 1055-1062
- [2] Talluri L, Fiaschi D, Neri G, Ciappi L, 2018, *Applied Energy*, **226** 300-319
- [3] Rusin K, Hasani Malekshah E, Wróblewski W, Rulik S, 2022 *Proc. ASME Turbo Expo GT 2022-83879*

Assessment of Wind Conditions in Urban Spaces: A Case Study of Warsaw Downtown

M Pisula¹ and M Poćwierz²

^{1,2} Warsaw University of Technology, Faculty of Power and Aeronautical Engineering,
ul. Nowowiejska 24, 00-665 Warszawa, Poland

¹E-mail: maciej.pisula.dokt@pw.edu.pl

²E-mail: marta.pocwierz@pw.edu.pl

Abstract. This paper deals with experimental and numerical studies of airflow in a dense urban area with varying heights. Experimental methods include oil visualization and sand erosion techniques in a wind tunnel, while numerical simulations use ANSYS Fluent software with the k-e realizable turbulence model. The results show potential contaminant accumulation zones and assess the impact of a hypothetical high-rise building on flow intensification in adjacent streets.

Keywords: *Aerodynamics, Computational Fluid Dynamics, Air Pollution, Wind Tunnel*

1. Introduction

Since the 1970s, there has been a significant increase in efforts to integrate aerodynamic research with architectural and urban planning [1], [2], as reflected in the literature on wind conditions around buildings and in urban areas [3]. These studies clearly show a strong correlation between airflow patterns and the spatial configuration of buildings, including the size, shape and relative positioning of individual structures. In this context, the authors carried out an analysis of wind conditions in an area of diverse, densely built development in the heart of Warsaw, near Złota Street. The analysis included the introduction of a hypothetical high-rise building among the existing structures, proposed by an architect. The aim of the experiment was to identify potential pollution accumulation zones within the dense urban fabric and to investigate the impact of the introduction of a tall building on the ventilation conditions in its vicinity.

2. The subject of the research

The study area covers a section of the centre of Warsaw and is marked on the map with a red circle (Fig. 1a). The radius of the circle is about 300m. The conceptual location of the high-rise building is shown in blue. The model of the area with buildings for wind tunnel testing was made at a scale of 1:700.



Figure 1. Study area

3. Research methods

The area including the buildings was studied in a wind tunnel and a numerical analysis of the airflow between the structures was carried out. Two qualitative methods were used in the tunnel experiments: oil visualization and sand erosion. These methods are complementary and their results effectively reflect airflow directions and velocity changes. Example results of visualization and sand erosion are shown in Figure 2.

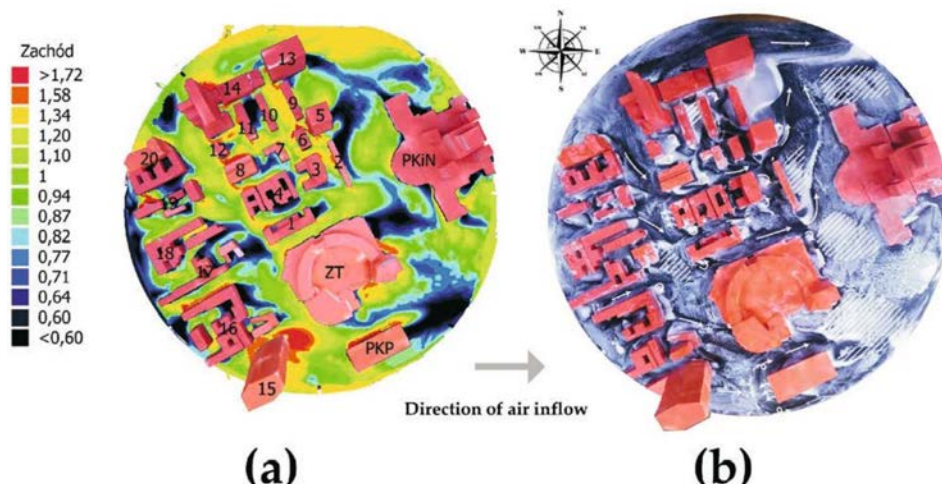


Figure 2. West wind - the distribution of α , created on the basis of sand erosion (a), oil visualization results (b).

The ANSYS Fluent software was used for the numerical simulation of the air flow in the presented built-up area. Following the guidelines given in the article [3], the RANS model, a pressure-based solver, and the SIMPLE algorithm based on the segregated method were selected. A second order upwind method was used to discretise the momentum equations, kinetic energy and turbulence dissipation. In addition, the k- ϵ realisable turbulence model was used. The standard wall function approach was used to calculate the flow parameters near obstacles. The velocity profile was implemented in the software using a custom written function in C language.

4. Conclusions

In summary, this study focused on the analysis of wind conditions in a specific urban area characterised by dense and varied development. The introduction of a tall building into this area was examined in terms of its impact on the ventilation of neighbouring streets. The study showed that for most of the wind directions analysed, the presence of the concept building led to turbulence and increased velocity gradients in its immediate vicinity. Despite the increased airflow in its vicinity, there was no noticeable improvement in ventilation between neighbouring buildings or only a marginal improvement for some wind directions. The results showed that dense urban development, even at different building heights, reduces wind permeability, resulting in poor ventilation and negatively affecting the urban microclimate and energy efficiency of buildings. As urban densification is planned, it is necessary to develop spatial planning rules for the geometry of buildings and the distances between them, in order to strike a balance between the intensity of development and the possibilities for proper ventilation of the surrounding space.

5. References

- [1] Liu CH., Ng CT., Wong, C., 2015 *Journal of Hazardous Materials*. 296, 9-16
- [2] Krauthaim, M., Pasel, R., Pfeiffer, S., Schultz-Granberg, J., 2014. *City and wind. Climate as an Architectural Instrument*. DOM publishers, Berlin
- [3] Blocken, B., Stathopoulos, T., van Beeck, J., 2016, *Building and Environment*. 100, 50-81

Aerodynamic and aeroacoustic analysis of a model UAV propeller

O Szulc¹, P Flaszyński¹ and T Suresh¹

¹ Institute of Fluid-Flow Machinery, Fiszerza 14, 80-231 Gdańsk, Poland

E-mail: Oskar.Szulc@imp.gda.pl

Abstract. The paper summarizes development and validation of an in-house aeroacoustic solver and its application to propellers of Unmanned Aerial Vehicles (UAVs).

Keywords: Aerodynamics, Aeroacoustics, CFD, FW-H analogy

1. Introduction

The paper summarizes the development of an in-house aeroacoustic solver [1] and its application to harmonic and broadband noise predictions for propellers of Unmanned Aerial Vehicles (UAVs). It is based on Farassat's formulation 1A of the solution to Ffowcs-Williams-Hawkings (FW-H) acoustic analogy. Initially, the validation process is presented for elementary rotating and fluctuating momentum sources (forces) with available analytical solutions. Next, the model of the two-bladed propeller of Delft University of Technology [2] is simulated with block-structured flow solver FLOWer (RANS and DES turbulence models) operating with the tip Mach number of 0.23 (tripped). The predicted rotor aerodynamic performance is compared against the experimental data for a wide range of advance ratios. Finally, the predicted surface pressure fluctuations are used to model the propeller noise signature for hover conditions.

2. Elementary rotating and fluctuating momentum sources (forces)

An existing FW-H solver, intended for analysis of helicopter rotor monopole (thickness) and dipole (loading) acoustic radiation, is extended not only to take into account the steady loading but also the surface pressure oscillations induced by the flow. An example validation for an elementary point source of momentum (force) rotating in space and fluctuating in time is presented in Figure 1 for time (LHS) and frequency (RHS) domains. The source strength and motion are compatible with the conditions at the tip of the investigated propeller blade. The comparison of FW-H predictions with the analytical solutions (in-plane) is acceptable.

3. CFD and acoustic analysis of the TUD propeller

Two-bladed (0.15 m radius) propeller (LHS of Figure 2) is simulated in axial flight for advance ratios J between 0 and 0.8 using FLOWer solver (2nd order finite volume scheme with artificial dissipation) and structured grid (172 blocks and $95.6 \cdot 10^6$ volumes). Steady solutions to RANS equations using Strain Adaptive Linear Spalart-Allmaras (SALSA) turbulence model provide satisfactory estimate of the thrust c_t and torque c_q coefficients (middle and RHS of Figure 2).

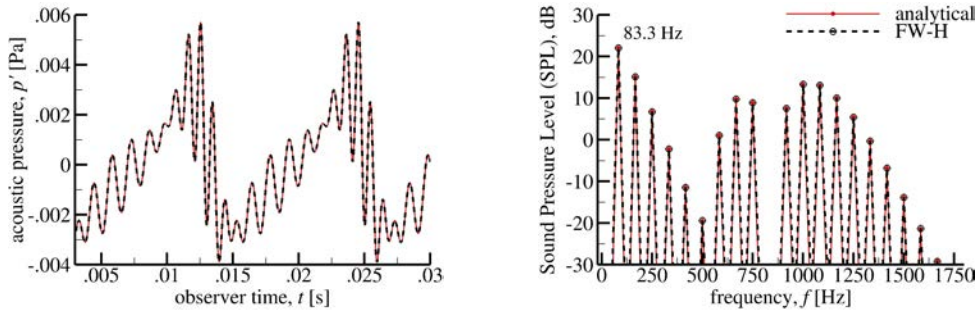


Figure 1. In-plane acoustic signal of rotating and fluctuating point source of momentum (force).

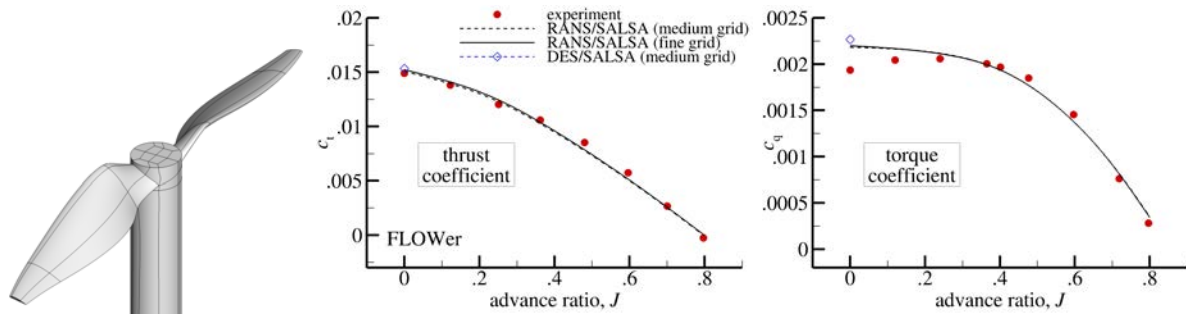


Figure 2. Propeller geometry (left) and rotor thrust c_t and torque c_q coefficients (right).

Due to the inability of RANS modeling to capture flow unsteadiness for investigated conditions, the Detached Eddy Simulation (DES) approach is attempted (subgrid model of SALSA). FLOWer solver (SLAU2 upwind scheme of 4th order in space and BDF2OPT Optimized Second Order Backward Difference Scheme in time) and a structured grid of medium density ($12.0 \cdot 10^6$ volumes) and time-step equivalent to 0.25° of rotation (1440 time-steps per revolution) provide surface pressure fluctuations due to massive separation (LHS of Figure 3).

Surface pressure data was collected for 2.5 revolutions (3600 files) in hover and fed for subsequent FW-H analysis with results presented in Figure 3 (middle and RHS) for an in-plane microphone location (distance of 1.2 m). The acoustic pressure signal resembles the elementary solution depicted in Figure 1. Moreover, the harmonic and broadband contents of the propeller signature are present and satisfactorily correlate with measurements conducted at TUD.

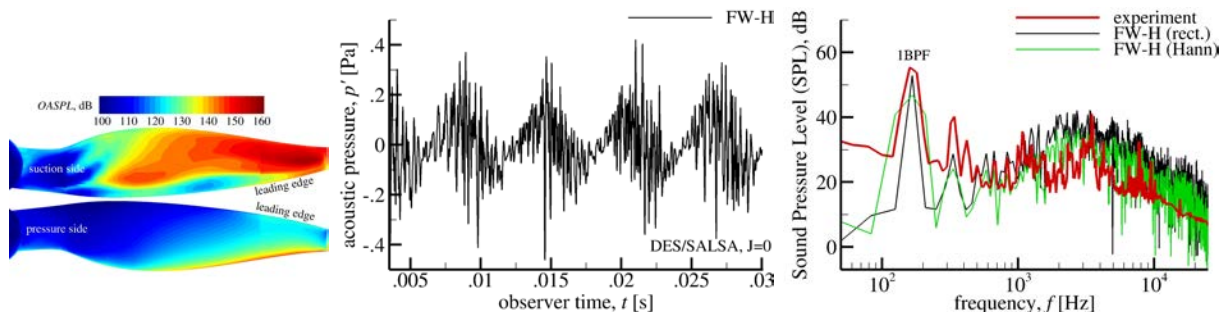


Figure 3. Surface pressure fluctuations (left) and predicted in-plane acoustic signal (right).

References

[1] Suresh T, Szulc O and Flaszynski P 2022 *Arch. Mech.* **74** 2-3 10.24423/aom.3999
 [2] Casalino D, Grande E, Romani G, Ragni D, Avallone F 2021 *Aerosp. Sci. Technol.* **113** 106707

Aerodynamic Multipoint Aircraft Design Including Aeroelastic Wing Deformation

K Kubryński¹

¹ Warsaw University of Technology, Faculty of Power and Aeronautical Engineering,
ul. Nowowiejska 24, 00-665 Warszawa, Poland

E-mail: kkubryn@pw.edu.pl

Abstract. The paper describes the panel method that allows multipoint aerodynamic design of three-dimensional aircraft configuration including aeroelastic wing deformation. The wing deformation is determined iteratively based on the beam method and the current load distribution. The method allows the determination of an required undeformed aircraft geometry that after deformation minimizes deviations from the design pressure distributions, minimizes the induced drag, and enforces the required values of lift and longitudinal moment coefficient (longitudinal trim conditions).

Keywords: Aerodynamics, Aerodynamic design, Aeroelasticity, Optimization

1. Introduction

The deformation of the aircraft or glider wing geometry induced by aerodynamic loading in flight can reach quite extreme values, and as a result, it can have significant impact on performance and flight characteristics. It can also have a significant impact on structure loads, and as a result, airworthiness authority requires taking into account wing deformation in the resulting aerodynamic loads. A good example of such a problem is the in-flight deformation of the Concordia glider wing, illustrated below.



Figure 1. In-flight wing deformation of “Concordia” sailplane.

Both torsional and flexural deformation can prove significant, albeit in slightly different aspects. Torsional deformation leads to changes in local angles of attack along the wing span, consequently altering the distribution of load as well as pressure distributions and boundary layer development. This ultimately results in changes in lift and induced drag values. It also causes departure of the aerodynamic profiles' working conditions at wing sections from the design conditions, i.e., from the

assumed values of angles of attack and lift coefficients. This may lead, for example, to exiting the airfoil laminar low drag bucket and causing drag rise. Flexural deformation of the wing primarily induces changes in aerodynamic derivatives associated with the aircraft dynamic stability, which may lead to Dutch roll instability or request of larger vertical fin. The problem is particularly important for high-performance gliders and unmanned aerial vehicles intended for long-duration flights. This is due to their very high aspect ratios and the tendency to reduce wing thickness to minimize drag.

One way to address this problem is by shaping the wing with tailored stiffness properties, resulting in a different wing deformation compared to classical structural designs and isotropic materials. Examples of such an approach could be the X-29 aircraft and the HIMAT research project. However, such a solution has limited effectiveness when dealing with large variations in flight conditions and significant effects of controls and speed flaps on wing loads and deformations - a typical issue in the design of high-performance gliders.

A promising solution to these problems seems to be the consideration of wing deformation (on load and pressure distributions) during the aerodynamic design, thus eliminating the influence of deformation on aerodynamic ground. It should be expected that to reconstruct pressure distributions from optimized two-dimensional airfoils (and thereby boundary layers and aerodynamic characteristics) on a deforming wing under various flight conditions, the geometry of the designed wing sections will deviate from the geometry of the original profiles. Full reconstruction of pressure distributions in such cases will undoubtedly not be possible. However, critical from the perspective of aerodynamic properties are essentially pressure distributions on the lower surface at high speeds and on the upper surface at low flight speeds – and thus, this is the problem to be addressed.

The KK-AERO software package [1], based on the panel method, has been adapted for aerodynamic analysis and design considering aeroelastic wing deformations. As a result, it is possible to achieve satisfactory design outcomes (enforcing required pressure distributions and boundary layer development under various flight conditions, as well as minimizing induced drag and trim drag), but also to account for the influence of deformations on the aircraft's dynamic stability and piloting characteristics at a fairly early stage of the design process. The following illustrations (Fig. 2) depict an example of multipoint design (for $CL = 0.3-0.7$ and corresponding velocities). The difference in wing twist between low and high speeds exceeds 3 degrees. Wing deformation is shown for one of the design points, along with the achieved and required pressure distributions in one of cross-sections of the deformed wing. The original undeformed wing section is also marked. As can be seen, both the section geometry and twist angle differ, yet an acceptable level of the desired pressure distributions and aerodynamic properties has been achieved.

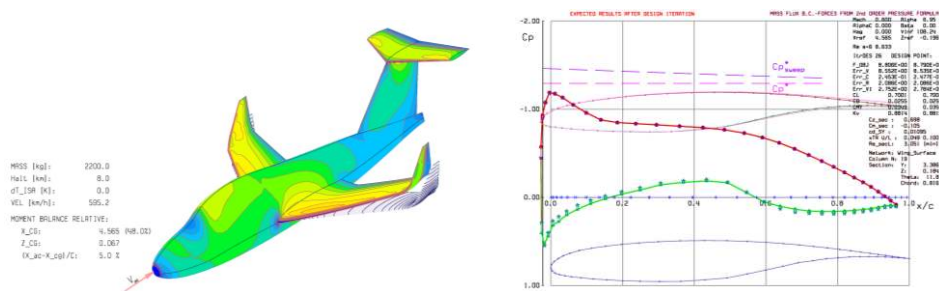


Figure 2. Geometry of the deformed wing and corresponding sectional pressure distribution.

References

- [1] Kubrynski K. 1999, “Subsonic Aerodynamic Design Via Optimization” Recent Development of Aerodynamic Design Methodologies – Inverse Design and Optimization, Ed. K.Fuji, G.S.Dulikravich, Notes on Numerical Fluid Mechanics, Vol. 68, Vieweg.

Analysis of turbulent flow separation control method using wall corrugation under different flow history

A Drózdź¹, V Sokolenko¹, and W Elsner¹

¹ Czestochowa University of Technology, Department of Thermal Machinery, Aleja Armii Krajowej 21, 42-200 Czestochowa, Poland

E-mail: artur.drozdz@pcz.pl

Abstract. The paper discusses the impact of pressure gradient history effect on the effectiveness of a passive flow control method utilizing a wavy wall in the streamwise direction. The sensitivity analysis of flow history is crucial for the potential adaptation of the fixed wavy wall under unstable conditions on the airfoil surface. The same fixed wavy wall geometry was used for different flow histories, guaranteeing the maximum increase of wall shear stress downstream of the wavy wall for strong pressure gradients. The analysis was performed for a turbulent boundary layer at a constant friction Reynolds number $Re_\tau = 4000$ to evaluate the method's effectiveness under variable flow history conditions. The results showed that the method reduces its efficiency by only about 50% under different pressure gradient distributions.

Keywords: Experimental Fluid Mechanics, Turbulent Boundary Layer, Flow Separation Control

1. Introduction

The flow separation at high Reynolds number occurs earlier, and the separation bubble is noticeably larger on rough surface compared to the flat plate (Wu and Piomelli 2018[1]). Recently discovered amplitude modulation has provided a better understanding of the momentum transport that occurs from the outer to the inner part of the turbulent boundary layer (TBL) and its subsequent effect on skin friction (Drózdź et al. 2023 [2], Drózdź et al. 2021 [3]). At sufficiently high Reynolds numbers, Drózdź et al. 2021 [3] demonstrate that a streamwise waviness with carefully selected amplitude and period (see Figure 1), can effectively enhance the amplitude modulation effect and thus substantial increase in skin friction under an adverse pressure gradient (APG). In the present study the extensive analysis was carried out to determine the corrugation-induced effect for different streamwise pressure gradient flow history. The sensitivity analysis of flow history is crucial for the potential adaptation of the fixed wavy wall over unstable conditions on the airfoil surface.

2. Methodology and Experimental setup

The experiment was carried out in a wind tunnel, where a TBL was developing along a 5035mm long flat plate that allowed the friction Reynolds number of $Re_\tau \approx \delta^+ \approx 4000$ (where δ is the boundary layer thickness) corresponds to $Re_x \approx 8 \cdot 10^7$ (see Figure 1a). Different flow histories, that is, different distributions of pressure coefficient $C_p = 1 - (U_e/U_{e0})^2$ (where

indexes e and 0 corresponds to edge of TBL and inlet plane, respectively) were obtained by applying different suction conditions on the perforated upper wall in the measuring section of the wind tunnel. The sealed off perforation corresponds to weak APG, perforation area 370 mm to moderate APG and perforation area 500 mm to strong APG (conditions used in Drózdź et al. 2021 [3]). For these three different APG conditions the hot-wire velocity profiles obtained at three location downstream the wavy wall where compared to those at the flat plate. The wall shear stress $\tau_w = \mu dU/dx$ was obtained using the method introduced by Niegodajew et al. 2019 [4], which was verified against oil-film method for flat plate (Niegodajew et al. (2019) [4] and downstream wavy wall (Appendix in Drózdź et al. 2021 [3]).

3. Results and discussion

In Figure 1b the average increase of τ_w were shown for analysed in function of $\delta_0 dC_p/d_{max}$ found in each C_p distribution. The maximum increase of 10.5%, in respect to τ_w at the inlet, occurs at $\delta_0 dC_p/d_{max} = 0.042$, which corresponds to the flow case analysed in Drózdź et al [3]. The wavy wall geometry performs well also for weaker APGs, while the effectiveness decay until $\delta_0 dC_p/d_{max} = 0.042$. The results demonstrate that the method can be used directly as a passive flow control method, stabilising the TBL on the wing section for a specific pressure gradient range.

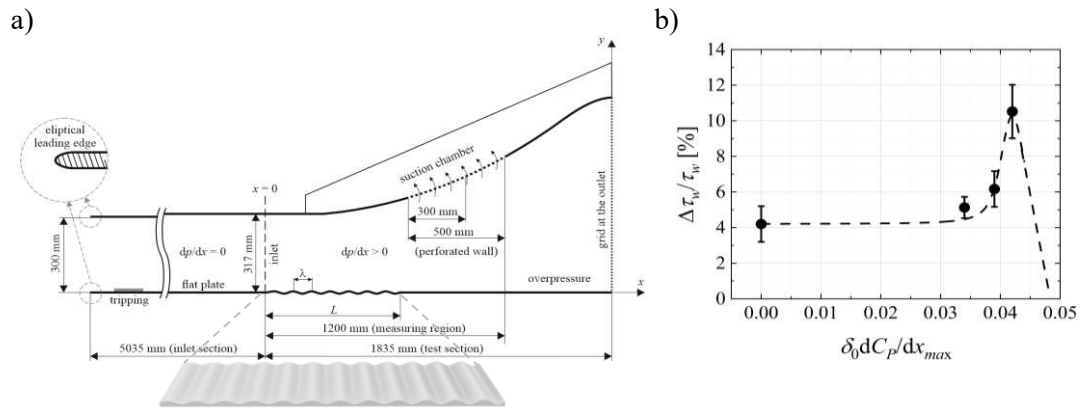


Figure 1. Test section and geometry of the wavy wall at Czestochowa University of Technology (a). Percentage difference of wall shear stress $\Delta\tau_w/\tau_{w0}$ at different $\delta_0 dC_p/dx_{max}$ (b).

Acknowledgements

The investigation was supported by the Polish National Science Centre under grant no. UMO-2020/39/B/ST8/01449.

References

- [1] Wu, W., & Piomelli, U. (2018). *Journal of Fluid Mechanics*, **841**
- [2] Drózdź A., Niegodajew P., Romańczyk M., Elsner W. (2023) *Exp. Thermal and Fluid Science* **145**
- [3] Drózdź A., Niegodajew P., Romańczyk M., Sokolenko V., Elsner W. (2021) *Exp. Thermal and Fluid Science*, **121**
- [4] Niegodajew P., Drózdź A., Elsner W. (2019) *International Journal of Heat and Fluid Flow* **79**

Creation and verification of a large Vertical Axis Wind Turbine airfoil class

J Wiśniewski¹ and J Szumbariski¹

¹ Warsaw University of Technology, The Faculty of Power and Engineering, Division of Aerodynamics, ul. Nowowiejska 24, 00-665 Warszawa, Poland

E-mail: jan.wisniewski@pw.edu.pl

Abstract. The text describes a new class of airfoils for use in industrial scale Vertical Axis Wind Turbines (VAWTs). Based on the concept of VAWT flow curvature and the most widely accepted class of airfoils for large VAWTs a new class of dual-convex airfoils has been created and tested computationally. Members of the class offer increased production capabilities than standard symmetrical NACA airfoils – for an 18% thickness, m2115, a member of the class, offers an additional 2.62% growth in power extracted from the wind for an optimal production scenario.

Keywords: Computational Fluid Dynamics, Aerodynamics, VAWT, Vertical Axis Wind Turbine, Aerodynamic Optimization, Airfoils.

1. Introduction

Based on experimental aerodynamic characteristics, symmetrical NACA profiles are typically treated as most prospective in terms of the highest achievable aerodynamic efficiencies for large vertical axis wind turbines (VAWTs) and therefore have been used extensively for large VAWT projects. However, along with other effects, VAWT blades do not move linearly as in wind tunnel tests but circularly at a speed several times that of the wind. Therefore, it has been postulated [1] that symmetrical airfoils rotating around an axis do not have the aerodynamic performance of symmetrical airfoils moving linearly - but seem to "bend" the airflow as if they were asymmetrical. This effect, known as flow curvature, causes symmetrical four-digit NACA profiles to not behave optimally, as expected based on classic quasi-statistical computation models.

2. Basis for research

Vertical Axis Wind Turbines have several distinct differences compared to their horizontal counterparts (HAWTs). Firstly, the achievable efficiencies for large VAWTs are beyond those of large HAWTs within simulations conducted with both quasi-static and CFD methods – with possible efficiencies achievable for very large VAWT installations potentially beyond the limit set for HAWTs within Betz's law. Secondly, for efficient, sleek turbine blades there is a strong lever effect at the bottom of the turbine shaft, leading historically to either a need for greater material use, increased beyond economic feasibility as compared to HAWTs, or a very short turbine life-cycle. This is due to the fact, that for classical VAWTs the variation of angle of attack during each revolution causes the torque to be transmitted as variable loading at the generator [2]. Large material savings, and therefore increased

economic viability, have been made possible with the use of load-reducing VAWT builds [3], creating a much greater use for appropriate airfoils, adequate for working in a range of conditions within large Reynolds numbers. Creating such airfoils is currently done either through flow curvature correction factors, or evolutionary methods, typically set to achieve maximum torque – optimized for a single set of working conditions [4]. The authors’ method instead used the preexisting knowledge of reliable designs and factors influencing utility of airfoils for large VAWT use to create an entire, mathematically formulated, class of airfoils, based on the four-digit NACA series – with improved production. The theoretical airfoil class design has been verified with over 1000 of multi-parameter optimized large VAWT CFD cases. The smooth, dual-convex build of all profiles within the class, in addition to increased torque within the range of production conditions, as compared to symmetrical NACA counterparts with the same thickness, is a good initial indicator of industrial reliability within adequate thickness values.

$$y_t = 5tc \left[0.2969 \sqrt{\frac{x}{c}} - 0.1260 \left(\frac{x}{c}\right) - 0.3516 \left(\frac{x}{c}\right)^2 + 0.2843 \left(\frac{x}{c}\right)^3 - 0.1015 \left(\frac{x}{c}\right)^4 \right] \quad (1)$$

, where t – thickness, c – chord, x – x coordinate value, y_t – y coordinate value for given thickness t.

Each of the modified airfoils discussed in this chapter is constructed of two symmetrical four-digit NACA halves. The airfoil name starts from the letter “m” as marking of a modified NACA profile. The zeros from the two first digits of the airfoils are omitted and the final two digits from both symmetrical NACA profiles are given, first for the lower/inner half, afterwards for the upper/outer half. In this naming sense a profile constructed out of two symmetrical NACA airfoil halves, the inner one from a NACA0018 profile and the outer one from a NACA0012 profile would be referred to as m1812.

Therefore, the any airfoil within the series can be plotted using two different-thickness curves for adequate halves of a symmetrical four digit NACA profile.

3. Constraints

Due to the rotary character of the movement, in order to achieve increased torque within operational parameters, the outer half of the profile should be plotted with a lower thickness than the inner one. The optimal thickness difference is dependent on the TSR of the turbine.

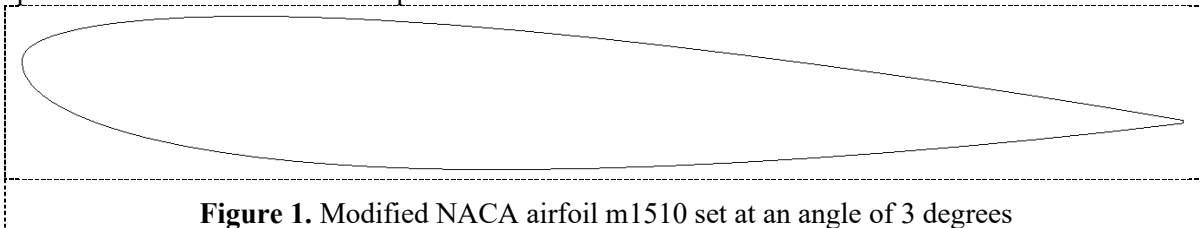


Figure 1. Modified NACA airfoil m1510 set at an angle of 3 degrees

The optimal scenario for a 22.5m wide 3-wing rotor was achieved for the m1510 profile set within the turbine at an attachment angle of positive 3 degrees. For the same conditions an optimal thickness of a symmetrical four-digit NACA profile was 13%. A symmetrical profile with a 12.5% thickness was further from the optimum. The power gain from substituting the optimal NACA0013 airfoil with the m1510 airfoil equals 0.63% for optimal rotation speed and attachment angle parameters. For thicker airfoils this increase in a system’s aerodynamic capacity to generate power grows. For industrial use, mostly greater thickness airfoils are used. Within airfoils with an 18% thickness, the optimal m2115 offers 2.62% more power than the standard NACA0018 airfoil.

References

- [1] Akimoto H et al., *Proc. of Int. Conf. on Offshore Mechanics and Arctic Engineering*, 2013
- [2] Galinos C et al., *Energy Procedia 00 (2016) 000–000*, 2016
- [3] Wisniewski J et al., *Wind Energy Science*, 6, 287–294, 2021
- [4] Carrigan T J et al., *International Scholarly Research Notices, Article ID 528418*, 2012

Combustion and Reactive Flows

Investigation of steam-diluted hydrogen combustion in a counter-current nozzle configuration using LES

A Wawrzak¹ and A Tyliszczak¹

¹ Czestochowa University of Technology, Faculty of Mechanical Engineering and Computer Science, al. Armii Krajowej 21, 42-201 Czestochowa, Poland

E-mail: agnieszka.wawrzak@pcz.pl

Abstract. The study concerns a co-axial counter-current jet configuration conceptualized as a wet hydrogen/air injector. Such an injector system induces a flow pattern beneficial for triggering global instability near a nozzle lip. Using high-fidelity LES, we explore how global instability and steam addition alter the flame dynamics through adjustments in the strength of the counter-current flow or dilution levels. In particular, we present regimes for lifted flames to mitigate hydrogen corrosion risk and enhance combustion efficiency.

Keywords: Computational Fluid Dynamics, Global Instability, Hydrogen, Wet Combustion

1. Introduction

Control of the combustion process by steam injection finds applications in ultra-wet gas turbines where it affects the flame dynamics both through alteration of chemical reactions and purely hydrodynamically by changing the density of injected fuel/oxidizer. The steam dilution increases the specific heat capacity of a mixture, lowering possible temperature peaks [1]. Therefore, it offers a promising option for improving efficiency, reducing NO_x emissions, and facilitating the combustion of hydrogen and hydrogen-rich fuels. A crucial aspect in the advancement of wet combustion systems is the design of the injector component, which must withstand exposure to significant amounts of steam while ensuring operational stability. Another formidable challenge arises in hydrogen-fueled combustion chambers due to the risk of hydrogen corrosion and high combustion temperature leading to thermal stress in the injection nozzles.

In the present study, a co-axial nozzle is considered as the wet hydrogen/air injector. Such a nozzle produces a counter-current flow in the vicinity of its lips, which is beneficial for triggering global instability. The global instability phenomenon along with the steam addition exhibit the potential to change the flame position from the attached to the lifted one either by changing the strength of the counterflow [3] or dilution level [2]. Performing high-fidelity large eddy simulations (LES) we study the impact of both factors. In particular, we are interested in determining the inlet conditions resulting in a lifted flame as in this case the risk of above mentioned problems (corrosion, high nozzle temperature) is largely eliminated.

2. Modeling

We consider a counter-current injection system in which a central jet nozzle ($D = 0.002$ m) supplying a fuel (hydrogen blended with nitrogen) is surrounded by a co-axial nozzle ($D_{suc} =$

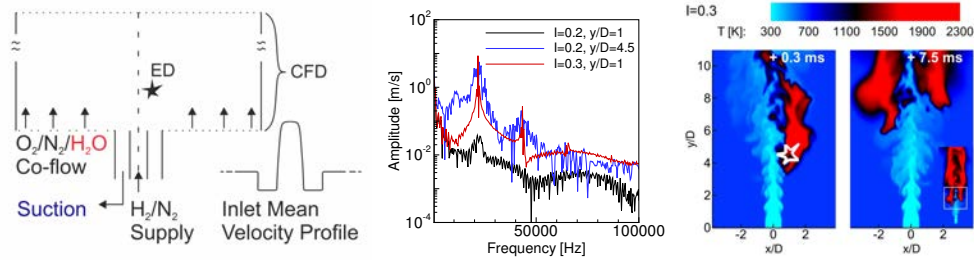


Figure 1. Injector setup (left), axial velocity spectra (middle), and temperature fields (right).

2D = 0.004 m) sucking the fluid. Outside of the annulus section, a stream of oxidizer (humidified air) is providing. The analyzed counter-current configuration is presented schematically in Fig. 1.

The composition and temperature of the fuel and oxidizer are adjusted to obtain a density ratio of $S = \rho_j / \rho_{cf} > 1$ (ρ - density of the jet/co-flow), which is far above the critical one ($S \approx 0.7$) for which global instability may occur spontaneously [4]. Thus, this phenomenon can appear only due to a significantly strong counter-current flow. The suction strength is controlled through the velocity ratio $I = -U_{suc} / U_j = 0 - 0.3$ (U - velocity of the suctioned gases/injected fuel). The flame is initiated by a spark introduced into the flow through the energy deposition model. The jet, suction, and co-flow are modeled by assuming the instantaneous velocity profile at the inlet of a rectangular domain in terms of mean and fluctuating components. A high-order compact difference LES code SAILOR [5] is used to perform the computations.

3. Results

Two different flow regimes can be observed depending on the suction strength, while maintaining a constant air humidity level. For $I = 0.2$, the flow pattern features Kelvin-Helmholtz instability with toroidal vortices formed at $y/D = 4.5$. When the suction is increased to $I = 0.3$, robust coherent structures appear immediately above the inlet plane, confirmed by the amplitude peak in the velocity spectra computed at $y/D = 1$ (see Fig. 1). These structures break down within a short axial distance ($y/D < 5$), releasing a large amount of oxidizer, thereby facilitating mixing. In the flow region where the vortices break up, the flame is initiated.

In Fig. 1, we demonstrate an ignition scenario for $I = 0.3$ in which the flame kernel expands quickly (0.3 ms) and coherent structures prevent the flame propagation towards the nozzle. As a result, the lifted flame stabilizes at $y/D \approx 7$. Similar ignition scenarios are possible for convectively unstable flow due to Kelvin-Helmholtz vortices or steam dilution. This work addresses the impact of H₂O mass fraction in the oxidizer stream for both flow regimes. We propose a novel injector system suitable for wet combustion techniques and provide advice concerning the amount of steam necessary for flame lifting.

Acknowledgments

This work was supported by the National Science Center (Grant No. 2022/47/D/ST8/01902). The simulations were carried out in the Poznan Supercomputing Center Network.

References

- [1] Krueger O, Terhaar S, Paschereit CO and Duwig C 2012 *J. Eng. Gas Turbine. Power* **41** 9705–9717.
- [2] Rosiak A and Tyliczszak A 2016 *Int. J. Hydrog. Energy* **22** 9705–9717.
- [3] Wawrzak A et al. 2023 *Int. J. Heat Mass Transf.* **213** 124260.
- [4] Jendoubi S and Strykowski PJ 1994 *Phys. Fluids* **6** 3000–3009.
- [5] Tyliczszak A 2016 *Comput. Fluids* **127** 131–145.

Swirl Effect Assessment on NO_x Formation for CH₄/H₂/NH₃ Flame under MILD Condition

A Mardani^{1,3} and KC Kim^{2,3}

¹Department of Aerospace Engineering, Sharif University of Technology, Tehran, Iran

²School of Mechanical Engineering, Pusan National University, Busan, Republic of Korea

³Eco-friendly Smart Ship Parts Technology Innovation Center, Pusan National University, Busan, Republic of Korea

E-mail: amardani@pusan.ac.kr

Abstract. In this work, the replacement of hydrogen with ammonia in a laboratory Moderate or Intense Low-Oxygen Dilution (MILD) burner is being investigated by incorporating air swirling to study NO_x formation in the flow field. Numerical predictions suggest that swirl enhances the reactivity of nitrogen-containing reactions, but the sensitivity to swirl varies depending on the ammonia inlet content. Results indicate the possibility of greater dilution and increased flexibility in controlling NO_x formation.

Keywords: Combustion, MILD, Ammonia, Methane, Hydrogen, NO_x.

1. Introduction

Ammonia is a carbon-free fuel with three hydrogen atoms and is a practical solution for transitioning to hydrogen usage burners. Pure ammonia has both advantages and disadvantages as a fuel such as combustion NO_x emissions, low burning velocity, and slow chemical kinetics. Ammonia combustion characteristics could be improved by blending it with more reactive fuels, such as methane and hydrogen. To address NO_x formation in ammonia combustion, the MILD combustion regime is recommended [1]. Additionally, the swirl concept, by increasing local residence time and enhancing mixing, may help establish the MILD combustion regime. Flow expansion after discharging the swirler port could create a low-velocity region along the burner axis and even flow reversal. This work aims to numerically study the effect of swirling hot diluted air in addition to replacing the hydrogen content of a laboratory MILD burner with ammonia.

2. Numerical Model and Discussion

The 2D-axisymmetric computational domain of the JHC burner [2] is considered after a grid study. Ansys-Fluent RANS solver is used along with the detailed chemical mechanism of GRI2.11, a modified K-ε turbulence model, and the Eddy Dissipation Concept combustion model (EDC). Kinetic theory is applied for transport properties, while the Simple algorithm utilizing a control-volume method and QUICK scheme is employed to simulate the CH₄/(H₂/NH₃) jet flame in a 1300 K hot oxidizer composition with 9% O₂ (mass). The H₂ portion of the fuel stream is reduced by replacing H₂ with NH₃ in varying mass proportions of

18%, 15%, and 10%. Additionally, the airflow inlet is designed to discharge tangentially with a swirl number of 0.8

2.1. Results and discussion.

Figure 1a shows the comparison of predictions with measurements [2] for chemical species and temperature radial fields at a height of 30 mm from the fuel nozzle. The chemical and heat fields are predicted relatively well. In Figure 1b, the flow field is depicted. Hot diluted air penetrates the shear layer where OH is concentrated, and heat release occurs limitedly due to dilution effects and NO produced in this region. The MILD region, as defined by Cavaliere et al [3], is depicted, where the combustion temperature increase is lower than the inlet autoignition temperature. This area is selected as the field of interest for this work. Comparing the OH contours of the air swirl cases with the cases without swirl refer to that the OH expands radially and towards the upstream, indicating a less lifted and radially expanded reaction zones (not shown here due to lack of space). In Figure 1c, the variations

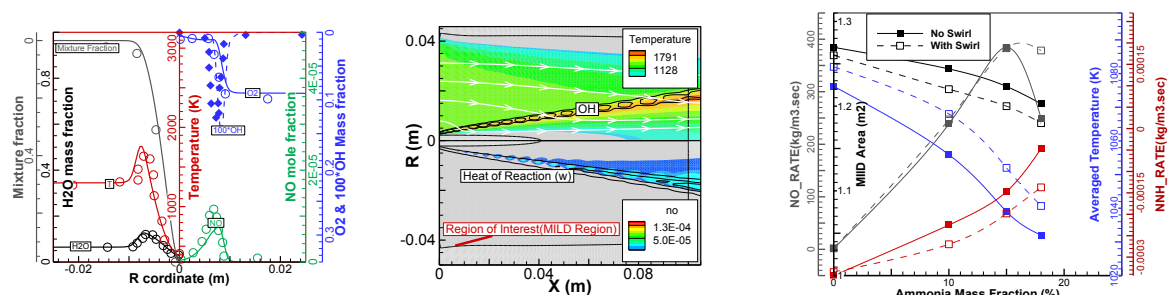


Figure 1a) Comparison of prediction and measurement (left) b) flow field (middle) c) comparison of swirl with non-swirl case by NH₃ variation (right)

in the MILD area indicate that the swirl flow has reduced this area while increasing the temperature. The higher temperature levels have led to an increase in nitrogen chemistry reactivity. The cumulative production of NO and NO₂ has increased due to swirl induction, while NNH consumption has increased and N₂O consumption has decreased. This suggests that swirl enhances the NO_x formation pathways, but in DeNO_x pathways, only the NNH pathway is enhanced, and the NO pathway for NO conversion to N₂ is suppressed. This behavior is consistent for ammonia concentrations ranging from 0 to 15%, but for 18% NH₃, the sensitivity of predictions to swirl is heightened, and the reactivity variation caused by adding swirl to the air flow is significantly affected. The net reaction rate of HCN demonstrates an increasing then decreasing trend with increasing ammonia fuel content. This means that a small amount of ammonia in the fuel could boost NO_x formation through prompt routes, but at higher ammonia concentrations, this effect is not observed, possibly due to the lower reactivity of ammonia.

Miscellaneous points

- (i) Swirl provides more residence time and enhances reactions.
- (ii) Following the first point, more dilution is possible using swirl in MILD combustion.
- (iii) For ammonia, disadvantages could be overcome by the swirl concept.
- (iv) Reacting fuel response to swirl at low and high ammonia content is different

Acknowledgements

This work was supported by Brain Pool Program and RLRC project through the National Research Foundation of Korea (NRF) funded by Ministry of Science and ICT (RS-2023-00283774, No. 2020R1A5A8018822)

References

- [1] Elbaz A., et al., Fuel Comm. 10 (2022), 100053.
- [2] Dally B.B., et al., Proc. Combust. Inst. 29 (1) (2002) 1147–1154.
- [3] Cavaliere A., de Joannon M., Prog. Energy Combust. Sci. 30 (4) (2004) 329–366.

Revisiting homogeneous modeling with volume averaging theory: structured catalysts for steam reforming and CO₂ methanation

J A Medina Méndez^{1,*}, B Dorneanu², H Schmidt¹ and H Arellano-García²

^{1,2} BTU Cottbus-Senftenberg, ¹Chair of Numerical Fluid and Gas Dynamics, ² Chair of Process and Plant Technology. Siemens-Halske-Ring 15a, 03046 Cottbus, Germany

E-mail: * medinjua@b-tu.de

Abstract. We discuss the fluid mechanics modeling of structured catalysts for use on steam reforming (SR) and carbon dioxide (CO₂) methanation (MT). Results of the study should allow better informed modeling decisions. As an example, we do not find significant differences among the choice of available gas or homogeneous surface kinetics models. For homogeneous models, we verify assumptions that prioritize appropriate modeling of thermodynamic dispersion tensors over the modeling of hydrodynamic dispersion (drag).

Keywords: Combustion, reactive flows, porous flows, homogeneous modeling, structured catalysts, steam reforming, CO₂ methanation.

1. Context of the research

Utilizing hydrogen (H₂) as an alternative fuel can contribute to industrial decarbonization. A large part of H₂ production is achieved via SR of natural gas, a relatively high efficiency process (80 – 85%, [1]). When compared to natural gas (methane CH₄), H₂ has a lower energy density (≈ 11 MJ/m³ versus ≈ 36 MJ/m³). This poses technical storage and transport challenges, especially in terms of existing infrastructure. To alleviate the shortcoming, one may produce CH₄ from H₂ (during excess H₂ production) for transport, storage or utilization (CO₂-MT). Both SR and MT processes require catalysts, given their hindered kinetics at typical operating conditions [2]. Advancements in structured catalysts are crucial for enhancing efficiency and scalability in industrial applications [3]. Studies have extensively explored reactive flows over catalyst surfaces, covering chemical kinetics analysis [4], as well as porosity and dispersion analysis for porous media flow simulations [5]. The focus of this contribution is on modeling strategies favouring the use of homogeneous models, due to the complexities of large scale H₂ production, either related to turbulence, or complex porous structures. Both situations may hinder the application of otherwise more reliable direct numerical simulations (DNS).

2. Modeling strategies and most relevant results

2.1. Zero-dimensional (0-D) homogeneous modeling

We formulate a 0-D homogeneous modeling strategy to assess the influence of simplified gas chemical kinetics versus detailed surface chemistry. Figure 1a) illustrates the 0-D model results for CO₂ conversion in a MT process under conditions similar to [3]. The choice between available gas or detailed surface chemistry has a minimal impact on the MT modeling outcome. Figure 1b) shows the 0-D model results for temperature-dependent concentrations obtained from the SR process simulated by [6]. As seen, 0-D models deliver reasonable results.

2.2. Three-dimensional (3-D) modeling

We also formulate a 3-D homogeneous model employing volume averaging theory (VAT). To compare the results of the 3-D homogeneous model, we conduct 3-D inhomogeneous simulations (implicit large eddy simulations with a deliberate choice of no sub-grid stress modeling). Figure 2a) shows the model results for H₂ concentration and velocity field magnitude for the selected SR process in 2.1. Figure 2b) shows a cross-sectional view of the detailed simulation results. The results and key implications will be discussed and analyzed in detail in the full paper.

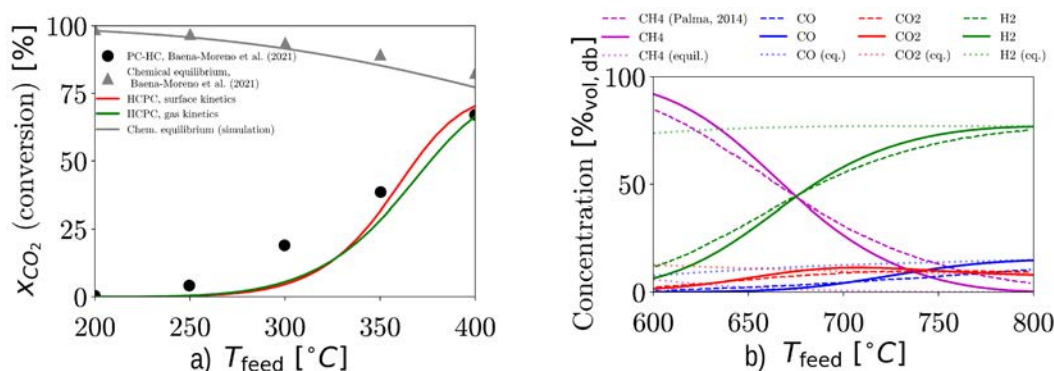


Figure 1. a) CO₂ conversion in a MT process and b) concentration in a SR process (0-D model)

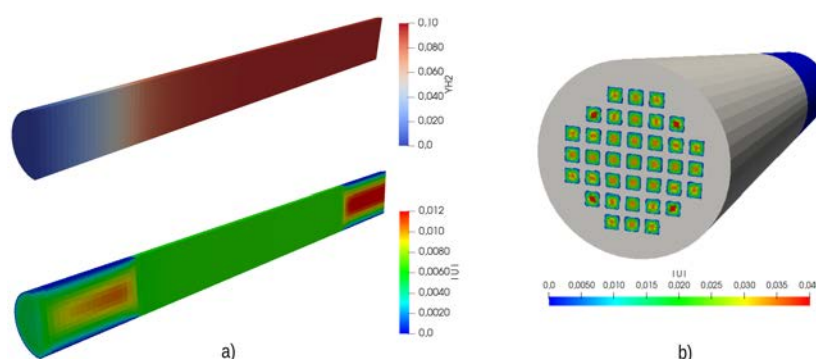


Figure 2. 3-D model for SR process as in [6]

References

- [1] Chaubey R et al 2013 *Renewable Sustainable Energy Rev.* **23** 443-462.
- [2] Schlereth D 2015, PhD Thesis, Technische Universität München.
- [3] Baena-Moreno F M et al 2021 *ACS Sustainable Chem. Eng.* **9**(24) 8198-8206.
- [4] Schmider D et al 2021 *Ind. Eng. Chem. Res.* **60** 5792-5805.
- [5] Wood B D et al 2020 *Annu. Rev. Fluid Mech.* **52** 171-203.
- [6] Palma V et al 2014 *Fuel* **138** 80-90.

A high-order LES of a flow in complex geometry

K Wawrzak¹, A Wawrzak¹, A. Bogusawski¹, A Tyliczszak¹

¹ Czestochowa University of Technology, Faculty of Mechanical Engineering and Computer Science, al. Armii Krajowej 21, 42-201 Czestochowa, Poland

E-mail: karol.wawrzak@pcz.pl

Abstract. Modeling combustion systems is challenging for numerical studies due to their complex geometry. The high-order compact differential approximation works for chambers, but injection systems are beyond its capabilities. The solution to this problem is a two-step approach using ANSYS Fluent and a high-order compact difference algorithm. Results align well with experiment, offering insights into the dynamics of a dual swirl H₂-air coaxial burner.

Keywords: Computational Fluid Dynamics, LES, Dual swirl burner, Compact differencing

1. Introduction

High-order discretization methods play an indispensable role in Direct Numerical Simulation (DNS) and Large Eddy Simulation (LES) studies, particularly when aiming for in-depth and detailed analyses of fluid flow problems. Compact differences (CD) offers advantages in terms of accuracy and efficiency. However, they cannot be compared with the flexibility of finite volume or finite element-based methods when implementing them for complex geometries.

Among the numerous Computational Fluid Dynamics (CFD) problems, modeling combustion systems poses a challenge to the research community. Typically, the combustion chamber is nearly rectangular box that can be modeled successfully applying high-order CD approximation in combination with the immersed boundary approach. The problematic part is the injection system, where the radially inclined pipes and/or internal swirlers are often embedded. Such geometries are too complex to be modeled by applying the immersed boundary method. Thus, the analysis of the flow in the injection system using the high-order CD methods is not feasible.

A two-step procedure has been proposed to overcome the above-mentioned limitation. It relies on combined simulations performed in the first stage using the ANSYS Fluent software to model the flow in a complex domain of the injection system, and then, in the second stage using the high-order SAILOR code [1] for modeling the flow in a combustion chamber. In the first stage, the results of the simulations are extracted from a plane connecting the injection system and the combustion chamber. The velocity components are recorded and then treated as time-varying boundary conditions imposed at the inlet to the combustion chamber.

2. HYLON burner

In this study, we consider the HYdrogen LOW NOx injector (HYLON) [2], which aims to stabilize pure H₂-air swirled flames. Figure 1 illustrates the schematic of the HYLON burner, comprising two coaxial swirling ducts. The annular channel provides the air with an external

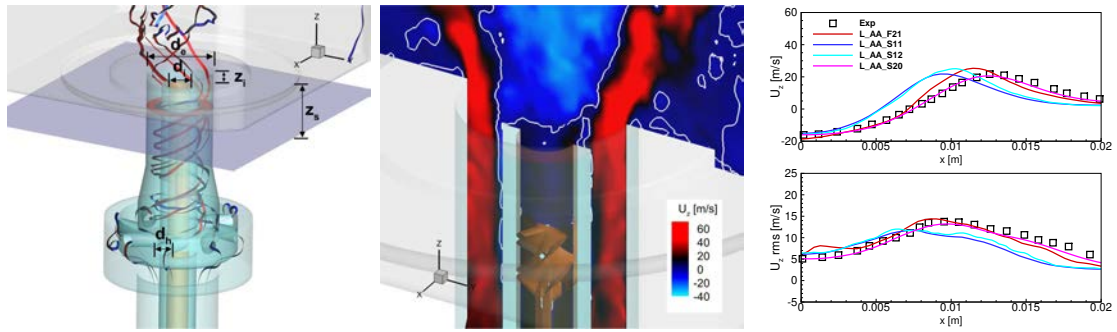


Figure 1. HYLON burner (left), contours of axial velocity in the central cross-section (middle) and radial profiles of mean and RMS axial velocity at location $z = 15$ mm (right).

diameter of $d_e = 18$ mm. An eight-vane cylindrical swirler ($d_h = 4$ mm) is integrated into the external passage. The inner injector delivers hydrogen through a tube of $d_i = 6$ mm diameter, incorporating an axial helicoidal swirler. The coaxial burner includes a recess ($z_i = 4$ mm) between the hydrogen injector's lip and the burner backplane, enhancing reactants mixing before combustion. The injector supplies a square combustion chamber. The velocity data, including axial, radial, and tangential components, for the inlet velocity condition in SAILOR, are collected at surfaces with a recess of $z_s = 10$ mm.

3. Results

In the present work, numerical simulations are conducted for the operating conditions corresponding to aerodynamically stabilized flame shifted from of the injector lip (referred to as flame L). During these simulations, hydrogen is substituted with air (non-reactive scenario AA), and its mass flow rate in the pilot stream is controlled to maintain the original momentum flux ratio between the internal and external ducts. The flow field in HYLON burner is visualized by the Fig. 1, which demonstrates the axial velocity contours along with iso-lines of $U_z=0$. These results were obtained from LES calculations with the ANSYS Fluent (case L_AA_F21). The overall flow dynamics is well reproduced taking into account the width and the position of the recirculation zones. The comparison between experimental data [2] and numerical predictions at $z = 15$ mm confirm the correctness of the two-stage computational procedure. Regarding the Fluent calculations (case L_AA_F21) they adeptly capture the velocity field. LES conducted with the SAILOR code exhibit notable agreement with experimental data, particularly when a variant of the code based on the cylindrical coordinate system is applied (L_AA_S20). The results obtained using the Cartesian mesh (L_AA_S11 - base mesh, L_AA_S12 - dense mesh) suggest a slight suppression of the swirl effect independently of the mesh resolution. Nevertheless, the levels of the axial velocity peaks agree reasonably well.

Acknowledgments

This work was supported by the HESTIA project no. 101056865 (Horizon Europe). The computations were carried out using PCSS infrastructure.

References

- [1] Tyliczszak A 2014 *J. Comput. Phys.* **276** 438–467.
- [2] Aniello A et al. 2023 *Combust. Flame* **249** 112595.

Numerical modelling of a rotary shock wave compression heat engine with a rotating detonation wave combustion chamber

J Piechna¹, M Szudarek², A Piechna²

¹ Warsaw University of Technology, Faculty of Power and Aeronautical Engineering, ul. Nowowiejska 24, 00-665 Warszawa, Poland

² Warsaw University of Technology, Faculty of Mechatronics, ul. Andrzeja Boboli 8, 02-525 Warszawa, Poland

E-mail: janusz.piechna@pw.edu.pl

Abstract. Although the concept of a moving detonation wave engine emerged as early as the 1960s, it is only in the last two decades that research into its possible realization has gained momentum. To date, there are several challenges to overcome in terms of the physics of the phenomenon and implementation. The purpose of this work was a preliminary numerical analysis of the operating range of a rotary shock wave compression heat engine with a rotating detonation wave combustion chamber. The numerical analyses focused on shockwave-generated compression for different air mass flow rates, mixing air with hydrogen, maintaining stable rotating detonation, preventing flame backflow into the fuel supply channels and energy recovery.

Keywords: Computational Fluid Dynamics, Flow Machinery, Combustion

1. Introduction

Shockwave compression is a technique that has been used for many years in supersonic flying objects in the form of i.a. ramjet engines. The idea of applying this method in rotary engines is conceptually simple but poses a number of technical difficulties. The requirement of supersonic speeds at the device inlet translates into high rotational speeds and large centrifugal forces. A number of prototype designs have been developed that demonstrate the potential of the technology but also highlight the existing problems [1].

In recent years, patents for a supersonic heat engine have been filed [2, 3], where a rotating detonation wave is used as an additional compression stage. The rotating detonation works in a thermodynamic cycle similar to Fickett-Jacobs' and takes place in a combustion chamber that rotates with the main rotor. This type of engine has a practical realization. A prototype engine developed by a Japanese team [4] achieved an increase in rotational speed for a short period of time, during which a stable rotating detonation occurred.

The advantages of the shock wave compression engine are: its structural simplicity (low number of moving parts), relatively high efficiency, high power density and the possibility of being

powered by hydrogen. At the same time, control of the generated shock wave, high temperatures and high inertial forces acting on engine components are the main challenges.

2. Numerical studies

The purpose of this work was a preliminary numerical analysis of the operating range of a rotary shock wave compression heat engine with a rotating detonation wave combustion chamber. Numerical simulations were performed for an engine in a radial configuration. Figure 1 presents shockwaves in the compressor part and the rotating detonation in the combustion chamber.

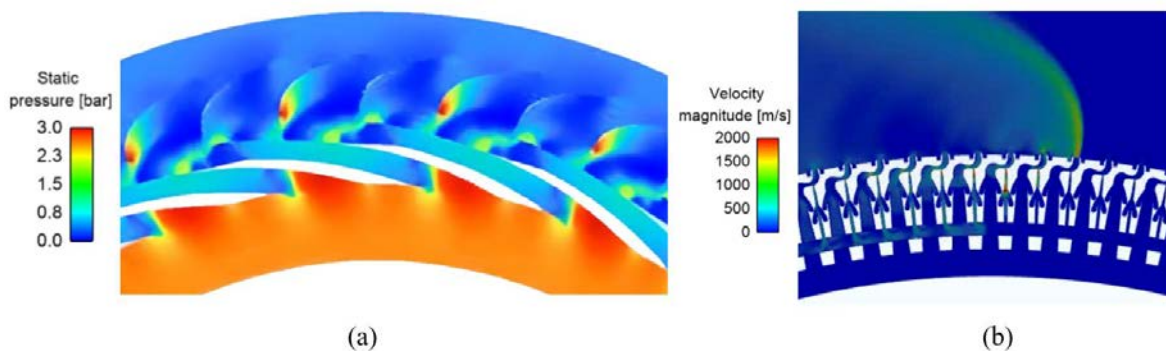


Figure 1. (a) Shockwaves in the compressor for pressure ratio equal to 3; (b) rotating detonation wave in the combustion chamber.

The numerical analyses focused on such aspects as

- (i) shockwave-generated compression for different air mass flow rates
- (ii) mixing of air with hydrogen
- (iii) maintaining stable rotating detonation
- (iv) preventing flame backflow into the fuel supply channels
- (v) energy recovery

References

- [1] Piechna J. A Review of Shock Wave Compression Rotary Engine Projects, Investigations and Prospects. *Energies*. 2022 Dec 10;15(24):9353.
- [2] Piechna, J.; Laube, T.; Piechna, A. Rotary Supersonic Heat Engine with Rotating Detonation Wave Combustion Chamber. PL Patent 238,627, 13 September 2021.
- [3] Piechna, J.; Laube, T.; Kindracki, J.; Piechna, A. Rotational Supersonic Heat Engine with Rotating Detonation Wave Combustion Chamber with Improved Efficiency. PL Patent 238,626, 13 September 2021.
- [4] Higashi, J.; Nakagami, S.; Matsuoka, K.; Kasahara, J.; Matsuo, A.; Funaki, I.; Moriai, H. Experimental Study of the Disk-Shaped Rotating Detonation Turbine Engine. In *Proceedings of the 55th AIAA Aerospace Sciences Meeting*, Grapevine, TX, USA, 9–13 January 2017; American Institute of Aeronautics and Astronautics: Grapevine, TX, USA, 2017.

Some theoretical problems of creation the mathematic model of joint treatment of wastewaters with organic contaminants and nitrogen compounds by method of biofiltration

S Telyma and O Oliynyk

Institute of Hydromechanics of National Academy of Sciences of Ukraine. str. M.Kapnist,
8/4,03057, Kyiv, Ukraine

E-mail: sertelyma@gmail.com

Abstract. The some problems of creation and realization of the mathematic models of joint treatment the organic contaminants (OC) and ammonium nitrogen compounds (N) in the bioreactors-aerotanks with fixed biocenosis as a biofilm in their volume and questions of heterogeneous structure of biofilm from different bacteria and substantiation of removing OC and N in taking into account on the oxygen regime in biofilm are considered. In this case removing of the contaminants occurs separately in two stages and at first the organic pollutants are extracted without nitrification and then the nitrification process takes place. So for joint removing of wastewaters the flooded filters are proposed with using the biofilm models which describe the processes of biooxidation different contaminants by different microorganisms in the biofilm

Keywords: bioreactor, biofilm, biocenosis, biofiltration, model, diffusion, mass transfer, organic contamination, nitrogen, wastewaters treatment

It is known that the biofiltration methods of wastewaters treatment from organic pollutions and nitrogen compounds which are based on the using of the biofilms with the high concentration of the biomass fixed on the filter loading material has become widespread in the last years [1,2,3]. Practically all wastewaters contain both organic contaminants (OC) and ammonium nitrogen ($\text{NH}_4\text{-N}$) so the processes of ammonium removal (nitrification) compete with the oxidation of organic matter since they are oxidized by various microorganisms namely heterotrophic and autotrophic ones respectively. Therefore the removing of the specified contaminants mainly occurs separately in two stages, namely: first- organic pollutants are extracted without nitrification and in the second stage the nitrification process is optimized. The use of flooded filters makes it most expedient to organize the combined extraction of hazardous substances in the volume of the filter and based on the use of biofilm models which describe the processes of biooxidation of various contaminants by various microorganisms in the biofilm. In both cases for the growth and vital activity of microorganisms it is necessary to ensure an uninterrupted supply of oxygen (DO) in the required amount.

In the liquid volume OC, N and DO are transported by the filtration flow. A thin laminar boundary layer (liquid film) is formed near the surface of the loading particles where the mass transfer of the

specified components to the surface of the biofilm occurs. Transport (transfer) of OC, N and DO in the biofilm is controlled by molecular diffusion and is assumed that it do not occur on the surface of the biofilm.

When building a general mathematical model it is necessary to justify and take into account on a number of existing features and processes that occur during the joint extraction of OC and N on submerged filters using biofilms which have as a rule the complex heterogeneous structure. At this the efficiency of removal of OC and N in flooded filters is related to the formation of fixed biomass (biofilm) on the surface of the loading material with a high concentration of bacteria per unit volume of the filter. According to [1] the composition of the latter includes polysaccharides, proteins, free nuclide acids and water and it is mainly a glue that holds the biofilm in place. In general the inactive biofilm part makes up to 40-45%. At the same time the structure of the biofilm changes in its thickness and in the height of the filter and in a general models it is necessary to pay it in attention.

As an example for dynamic modeling and determination of biofilm parameters the following well-known equation may be used which takes into account on the processes of growth, detachment and adhesion [1,2]:

$$\frac{d\delta}{dt} = U_F(\delta) - U_{de} + U_{at} \quad (1)$$

where $\delta, U_F(\delta), U_{de}, U_{at}$ - thickness of biofilm, speed of growth, separation and adhesion.

Using of presented above model allowed to obtain some results of the dynamics of biofilm growth in the conditions of competition between various microorganisms and the location of individual components in the biofilm in particular EPS [1]. The change in internal porosity in the biofilm during of modeling was taken into account on by using the effective diffusion coefficient of dissolved components. The implementation of the proposed model has shown that it well describes important aspects of biofilm formation processes. More complex models of biofiltration and the problems connected with heterogeneous structure of biofilm and taking into account on the oxygen regime and different factors and parameters are presented in detail in our works[3,4].

In presented above brief survey the problems of creation and realization of the mathematic models of joint treatment of the organic contaminants (OC) and ammonium nitrogen compounds (N) in the bioreactors-aerotanks with fixed biocenosis as a biofilm in their volume are considered. The necessity of creation the models of biofiltration of joint wastewater treatment in bioreactors contained simultaneously organic contaminants and nitrogen compounds are shown and substantiated. The great attention should be taken on the subsequent development and improvement of models that allows to modeling the processes of wastewaters treatment taking into account on the heterogeneity of the biofilms and transient regime biofiltration along the its thickness and influence of the different parameters on the technology of biotreatment in bioreactors.

REFERENCES

- [1] Gujer W 2010 *Nitrification and me- A subjective review* Water Res. 44 p1-19
- [2] Kelareva D Kravchuk A&Oliynyk O 2012 *Modeling of the joint removing of the organic contaminations and nitrogen at the wastewater treatment by biofiltration* Dopov.Nac.acad.nauk Ukr. 5 p179-183 (in Ukrainian)
- [3] Oliynyk O Telyma S Kalugin Yu & Oliynyk E 2022 *Modeling and calculations of parameters of joint treatment of organic contaminations (OC) and nitrogen (N) compounds in bioreactors with using of the fixed biocenosis (biofilm)* Ecological safety and natural resources 3 p82-96 (in Ukrainian)
- [4] Oliynyk O Telyma S Kalugin Yu & Oliynyk E 2023 *Theoretical analysis of the processes of the simultaneous wastewater treatment from the organic contaminants and nitrogen compounds using of the biofilm models* Dopov.Nac.acad (in Ukrainian)

Computational Fluid Dynamics

Isotropy of numerical errors in the context of implicit large eddy simulation

A Kajzer¹

¹ Institute of Fluid-Flow Machinery,
Polish Academy of Sciences, ul. Fizyka 14, 80-231 Gdańsk, Poland

E-mail: akajzer@imp.gda.pl

Abstract. Implicit large eddy simulation of pseudo-incompressible flow is considered. The mass and momentum conservation equations are solved at low Mach number applying the finite volume method. A variety of numerical methods is studied with respect to proper resolution of flow structures. We propose an efficient low-diffusive methodology which, thanks to the isotropy of numerical errors, avoids the known problem of spurious vortices creation on coarse meshes.

Keywords: Computational Fluid Dynamics, Turbulence, Implicit LES, low Mach number flows

1. Introduction

The large eddy simulation (LES) consists in spatial filtering of the numerical solution of the governing equations and the structures that can not be resolved on the mesh used in the simulation are “removed” from the solution but their dissipative effect is modelled (usually by local, artificial increase of viscosity, as done in the well-known Smagorinsky LES model). The implicit LES (ILES) approach [1] utilises the fact that the numerical diffusion introduced by suitable discretisation techniques acts similarly as the physically-sound viscous term.

Incompressible flows are usually modelled assuming infinite speed of sound. This leads to a simpler eigenstructure of the governing equations (all eigenvalues of similar order of magnitude) but simultaneously introduces the elliptic character of the model which requires the solution of large linear systems of equations during the simulation. An alternative is to assume a finite speed of sound and keep the Mach number sufficiently low to treat flow as incompressible; in this case the equations are of hyperbolic-parabolic type which is simpler in algorithmic handling and more efficiently parallelisable. However, in the modelling of low-Mach flows a problem of large disparity of the speed of sound and the convective velocity scale appears. Discretisation schemes which allow to avoid significant spurious oscillations (dispersive errors) introduce numerical diffusion which depends on the signal speeds and therefore undesired strong diffusion may locally appear. Ways to mitigate this problem mainly use approximate Riemann solvers which recognize the detailed wave structure of the model equations, modify the eigenvalues and utilise high order spatial discretisation schemes. We show that for a successful ILES of the low Mach number flows not only the reduction of numerical diffusion but also its isotropy is required. Presented findings also apply to the fully compressible flow model (however, the flows involving discontinuities would require further investigation).

2. Flow model, numerical methods and chosen results

The governing equations of the model we use are:

$$\partial_t \rho = -\nabla \cdot (\rho \mathbf{u}), \quad (1)$$

$$\partial_t (\rho \mathbf{u}) = -\nabla \cdot (\rho \mathbf{u} \otimes \mathbf{u} + p \mathbf{I} - \boldsymbol{\tau}), \quad (2)$$

where ρ is the density, \mathbf{u} is the velocity vector and p is the pressure; $\boldsymbol{\tau}$ is the viscous stress tensor and \mathbf{I} is the unit tensor. The pressure is computed using the isothermal equation of state $p = \rho c_s^2$ with c_s being the speed of sound. During the solution we set c_s adaptively to the flow conditions, i.e. $c_s(t) = U_{\max}(t)/\text{Ma}$ where U_{\max} is the maximal flow speed at given time instant t and Ma is the assumed Mach number (lower than 0.1). This reduces the stiffness of the model and saves one from the necessity of knowing the maximal flow speed a priori (alike in truly incompressible model) but the density variations are artificial in this case (the pressure is correct) [2]. For the discretisation of the hyperbolic part of the model we have tested known Riemann solvers [?]: Rusanov, Lax-Wendroff and HLL(C)-type ones. To compute the Riemann states we used MUSCL type schemes (possibly with slope limiters), multidimensional limited schemes and 5th-order monotonic interpolation (MP5). To assess the different numerical set-ups we performed simulations of the so-called doubly periodic shear layer (DPSL) at Reynolds number of 10^4 . When applied in a usual dimension-by-dimension (DBD) manner, all the schemes lead to creation of spurious vortices in underresolved simulations unless a highly diffusive Riemann solver is applied. Results (not shown here) strongly suggest that the isotropy of the numerical diffusion has to be assured. Interpolation and finite difference schemes with isotropic truncation errors have been introduced in [4]. When isotropic interpolation is applied for the DBD-MUSCL extrapolated states then physically-sound solutions are obtained with a low diffusive HLLC Riemann solver even with additional low-Mach corrections, as shown in Fig. 1. Current investigation involves 3D turbulent flows and is promising.

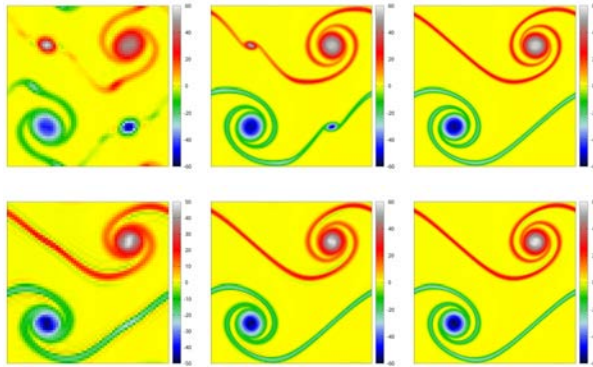


Figure 1. The DPSL simulation at dimensionless time equal 1. Vorticity fields obtained using HLLC scheme with low Mach correction at grids of 64×64 , 128×128 and 192×192 (left to right panels). The results obtained with MP5 scheme using conventional DBD stencils (top row) and 3rd-order MUSCL using isotropic stencils (bottom row) are shown.

References

- [1] Aspden A, Nikiforakis N, Dalziel S and Bell J 2008 *Comm. App. Math. Comp. Sci.* **3** 1 103-126.
- [2] Kajzer A and Pozorski J 2022 *Comp. Math. App.* **121** 18-29.
- [3] Drikakis D and Rider W 2005 *High-Resolution Methods for Incompressible and Low-Speed Flows* (Berlin: Springer-Verlag).
- [4] Shukla R Giri P 2014 *J. Comp. Phys.* **276** 252-290.

Quantification of laminar mixing efficiency using 'strange eigenmodes' approach

J Fabisiak¹ and S Gepner¹

¹ Warsaw University of Technology, Faculty of Power and Aeronautical Engineering, ul.
Nowowiejska 24, 00-665 Warszawa, Poland

E-mail: jakub.fabisiak.dokt@pw.edu.pl

Abstract. We consider laminar mixing in a duct with longitudinal grooves, where decay of the selected mixing metric becomes exponential, suggesting a form close to the eigenfunction of the Advection-Diffusion (AD) operator. Patterns of the scalar remain time-invariant, with amplitude decaying exponentially. The slowest decaying mode can lead to the upper bound of the mixing rate. An algorithm for obtaining such eigenmodes and the mixing upper bound is presented.

Keywords: Computational Fluid Dynamics, Laminar Mixing, Strange Eigenmode

1. Introduction

In our previous work, we investigated low Reynolds number ($Re \approx \mathcal{O}(100)$) flow destabilization resulting from the application of longitudinal (lines of constant elevation run parallel to the flow direction) wall corrugation [1]. The resulting flow, while still laminar, results in the kinematics capable of producing chaotic advection and consequently improving the mixing efficiency. We evaluated mixing rates resulting from the application of perturbations in the unstable flow by tracking the decay of selected mixing measures (either the variance or the negative index Sobolev norm) of the concentration of a scalar quantity. Irrespective of the applied measure, scalar distribution initially undergoes a short (around five periods of instability wave oscillations) transient decay, followed by an exponential decrease. Following [2], this exponential time variation suggests that the concentration of the scalar field locks onto an eigenfunction of the AD operator, the so-called 'strange eigenmode'.

The concept of 'strange eigenmodes' was first observed and described in [2] and has been studied both numerically [3] but also experimentally [4]. It describes the persistent state attained in mixing a scalar field with stirring resulting from the action of a periodic velocity field. In this state, time-invariant spatial patterns are achieved by the mixed scalar field. As the spatial pattern conserves its shape in time, the amplitude of the distribution decays exponentially. This type of evolution can be interpreted as related to the eigenmode of the AD operator, while the corresponding eigenvalue is associated with the exponential decay rate.

2. Problem statement and approach

In the cases we considered, we calculated the mixing efficiency as the decay of variance and mix-norm (based on the negative index Sobolev norm). An exponential decay (Fig. 1) is observed for each case past the initial transient phase. The associated form of the 'strange eigenmode' is

shown in Fig. 2. We presume that the norms' exponential decay rate is strictly related to the eigenvalue of the slowest decaying, dominant 'strange eigenmode'.

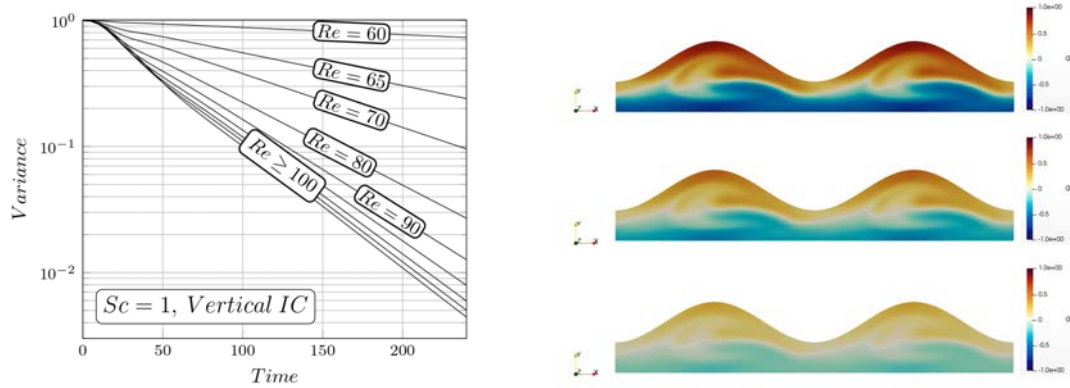


Figure 1: (left) Variance of concentration, straight lines in logarithmic scale suggest exponential decay. (right) Channel cross-section is colored with scalar distribution after 5, 12, and 20 periods of the perturbation.

Following [3] we write the AD problem as $\frac{\partial \theta}{\partial t} = L(\theta)$, where $L = -\mathbf{u} \cdot \nabla + \frac{1}{ReSc} \nabla^2$ is the AD operator, with \mathbf{u} the flow velocity field. Considering the action of the AD operator, we can decompose an arbitrary initial scalar distribution into modes, each with a corresponding decay rate. As homogenization progresses, the fast decaying modes become attenuated and do not manifest in the asymptotic-in-time process. Consequently, the homogenization rate quickly becomes dependent on the least attenuated mode of the AD operator. This mode should be associated with the upper bound of the available mixing efficiency.

This work outlines a numerical algorithm to efficiently perform the operation of finding such dominant modes for given kinematics and diffusivity. The approach is based on the similarity between the application of the AD operator to a standard eigenproblem. I.e. we utilize an algorithm similar to the well-known power method by continuously applying the AD to the given scalar concentration distribution. Multiple applications and renormalizations of the AD operator should allow for the determination of the dominant mode together with the corresponding eigenvalue thus yielding the upper-bound of the homogenization process.

3. Conclusions

We present that the longitudinal channel instability we studied earlier [1] results in the formation of strange eigenmodes when considered as velocity in the scalar AD process. We propose a numerical algorithm that utilizes a power-method approach to perform the effective computation of the slowest decaying mode and consequently determine the upper-bound of available mixing rate. The relation between the previously studied mix-norms' decay rate and the obtained eigenvalues is analyzed and discussed.

References

- [1] Gepner S W, Yadav N and Szumbariski J 2020 Secondary flows in a longitudinally grooved channel and enhancement of diffusive transport. *International Journal of Heat and Mass Transfer* **153**(June): 119523.
- [2] Pierrehumbert R T 1994 Tracer microstructure in the large-eddy dominated regime. *Chaos, Solitons & Fractals* **4**(6): 1091-1110, Special Issue: Chaos Applied to Fluid Mixing.
- [3] Singh M K, Speetjens M F M and Anderson P D 2009 Eigenmode analysis of scalar transport in distributive mixing. *Physics of Fluids* **21**(9): 093601/1-17.
- [4] Rothstein D, Henry E and Gollub Jerry P 1999 Persistent patterns in transient chaotic fluid mixing. *Nature* **401**(6755): 770-772.

Heat transfer of laser-illuminated gold nanorod platforms distributed in a flow germicidal chamber

Piotr Radomski¹, Dominik Kreft¹, Paweł Ziółkowski¹, Iuliia Mukha^{2,3},
Jacek Zieliński⁴ and Dariusz Mikielewicz¹

¹Gdansk University of Technology, Faculty of Mechanical Engineering and Ship Technology, ul. Gabriela Narutowicza 11/12, 80-233 Gdańsk, Poland

²Chuiko Institute of Surface Chemistry, National Academy of Science of Ukraine, ul. General Naumov 17, 03164 Kyiv, Ukraine

³National Center for Tumor Diseases (NCT/UCC), ul. Fiedlerstrasse 23, 01307 Dresden, Germany

⁴Medical University of Gdańsk, ul. Dębinki 1, 80-211 Gdańsk, Poland

E-mail: piotr.radomski@pg.edu.pl

Abstract. The purpose of this work is to examine heat transfer in a glass-aluminum germicidal chamber which was prepared and equipped with platforms containing 15-15-88-nm gold nanorod arrays illuminated by infrared lasers. To verify the highest effectiveness of heating, the platforms are distributed in three different positions, at the top, bottom and inside the chamber. The intensification of heat transfer processes is crucial to overheat germs of tumors which are immune to strong chemical compounds.

Keywords: Computational Fluid Dynamics, heat transfer, gold nanorods, thermal inactivation

1. Introduction

Overheating is a more-and-more popular technique for these applications where strongly-protective viruses or vast and extensive tumors can be easily inactivated by thermal irreversible metabolism modifications. The problem is stated for the effective heating of the system from its interior, close to the destination, so as to accelerate and to diminish the noninvasiveness of the process.

Additionally, computational fluid dynamics (CFD) is a method which allow to predict the temperature distributions in selected systems to prepare satisfying experiments, e.g. using particle image velocimetry (PIV) apparatus or thermal cameras, and to compare results with the benchmark geometry. Therefore, this is indicated to investigate temperature distributions and to verify where the gold nanorod platforms should be dislocated to intensify the heat transport processes.

2. Methodology

The 1,5-x-2,5-cm water-filled germicidal chamber, as a working geometry, was prepared to provide easy flow and to manipulate with the inlet velocity. Each platform consists of two 10.2-0.1mm round cover glasses, which are separated by a 15-15-88-nm gold nanorods array.

Subsequently, the glasses are either glued to the chamber's walls or settled at aluminum nobs, located in the middle of the chamber. The nanorods are heated by a one-watt 980-nm laser with the 8-mm beam diameter, and the heat generation rate is here described as a source term from authors' works [1-2]. The flow is delivered by a moving hinge, located at the bottom.

Steady-state temperature distributions data are obtained by solving mass, momentum and energy balance equations at the SIMPLE algorithm and second-order upwind schemes. Results are extrapolated on three grids following the Richardson and Roacher methods.

3. Results

Figures 1 demonstrate CFD temperature distribution results in the considered chamber for the platforms dislocated, respectively from left side, at the bottom, at the top and in the middle of the chamber. Top images presents the results under the $\vec{v}_o = 1.0 \text{ cm}\cdot\text{s}^{-1}$ velocity inlet flow whereas bottom part reveals the results with no flow.

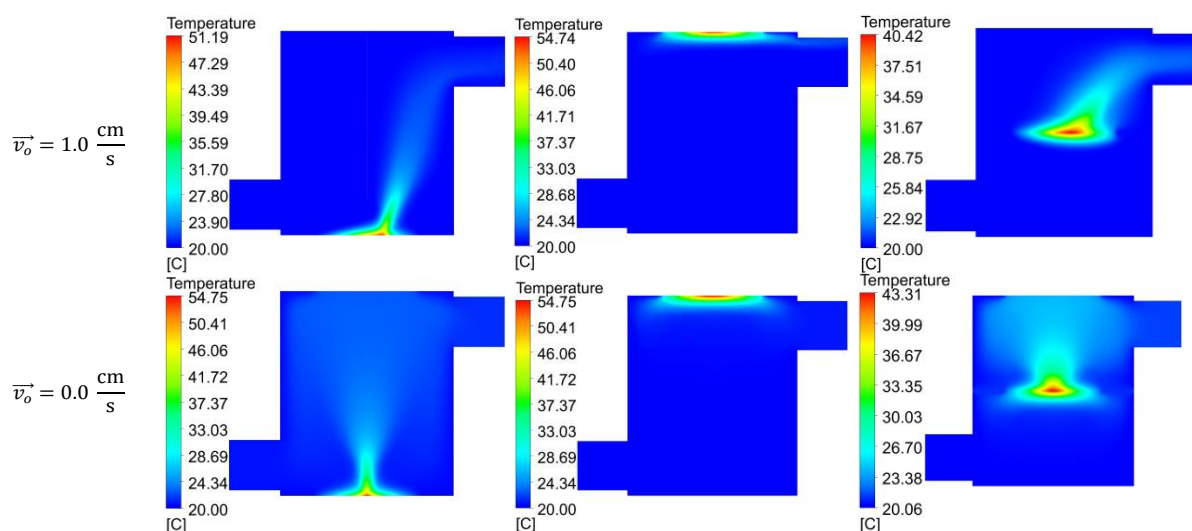


Figure 1. Steady-state temperature contours for platforms distributed in exemplary positions

4. Conclusions

Illumination of the gold nanorod platforms located at the walls implies the highest temperature increase, whereas the interior position contributes to the better heat transportation during fluid flow, even at relative low-power sources. Appropriate combination of these positions would provide the efficient and functional germ and tumors inactivation, which is indicated to be studied extensively.

Acknowledgements

This research of Gdańsk University of Technology was partially supported by National Science Centre in Poland under the project no UMO-2021/43/D/ST8/02504 and 'Excellence Initiative – Research University' Gdańsk Tech no. DEC-13/1/2022/IDUB/II.1a/Au. Computations were carried out using the computers of Centre of Informatics Tricity Academic Supercomputer & Network (CI TASK) in Gdansk.

References

- [1] Zaccagnini F et al. 2023 *J. Mat. Chem. B* **11** 29 p 6823
- [2] Radomski P et al. 2023 *Acta Mechanica et Automatica* **17** 4 p 540

Numerical modelling of gas flow in random packed bed with a helical flow deflector

M Marek

Częstochowa University of Technology, Faculty of Mechanical Engineering and Computer Science, Department of Thermal Machinery, al. Armii Krajowej 21, 42-200 Częstochowa, Poland

E-mail: maciej.marek@pcz.pl

Abstract. Random packed beds are often employed in chemical reactors as a means to increase the contact surface between reactants or a catalyst. The present work proposes a helical flow deflector placed within the bed and numerical simulations are performed to analyse the influence of the deflector on the residence time distribution (RTD) in the reactor and the pressure drop. The geometry of the packed bed is obtained in a separate numerical simulation with sequential deposition of ring-like equilateral particles. The flow equations are solved on a structured grid and the immersed boundary method accounts for the complex geometry of the random packing, cylindrical walls of the reactor and the flow deflector. The increase of the residence time leads to increase of the pressure drop along the reactor and the relation between them is studied as a function of the rise per revolution of the helical surface.

Keywords: Computational Fluid Dynamics, Immersed Boundary Method, Random Packed Bed, Residence Time Distribution

1. Introduction

The efficiency of the reaction depends on the contact surface between the reactants, which may be increased by employment of a random packing of particles of various types within a reactor. Due to complexity of the packed bed geometry the streamlines of the flow tend to be highly tortuous but, still, the flow paths averaged over the meso-scale (comparable to the size of the bed particles) are nearly parallel to the walls of the reactor.

In order to increase the time spent by the fluid in the reactor the flow paths must be curved at much larger scales. In the present work, a flow deflector is proposed in the form of a helical surface introduced within the random packing. On the one hand, the deflector increases the residence time (RT) of the fluid (gaseous in the present study). On the other hand, the pressure drop Δp also is higher together with the power needed to drive the flow through the reactor. The numerical model verified and validated in many previous studies (see e.g. [1, 2, 3, 4]) is used to examine the relation between the geometrical parameters of the flow deflector (namely the rise per revolution – λ) and the residence time – $RT = f_1(\lambda/D_c)$ – as well as respective relation for the pressure drop – $\Delta p = f_2(\lambda/D_c)$ (where D_c is the reactor diameter).

2. Methods

The geometry of the random packing is obtained with the numerical method described in [2, 3]. Ring-like particles are dropped sequentially into a cylindrical container and move due to gravity and reaction forces until the state of equilibrium is reached (Fig. 1a). After that the helical flow deflector (Fig. 1b) is introduced into the packing, crossing through the particles (more realistic model with generation of the packing with the deflector already present in the container and acting like a solid wall will be considered in future studies).

The incompressible Navier-Stokes equations are solved on a structured grid with second order accuracy in space and time. Application of this solver to flow in such a complex geometry is possible due implementation of the immersed boundary method (IBM) and the direct forcing approach [5]. The details of the algorithm are described in [3]. The residence time distribution (RTD) is calculated through passive advection of a scalar, marker field – a step impulse of the field is placed above the packed bed, transported through the reactor and measured close to the outlet.

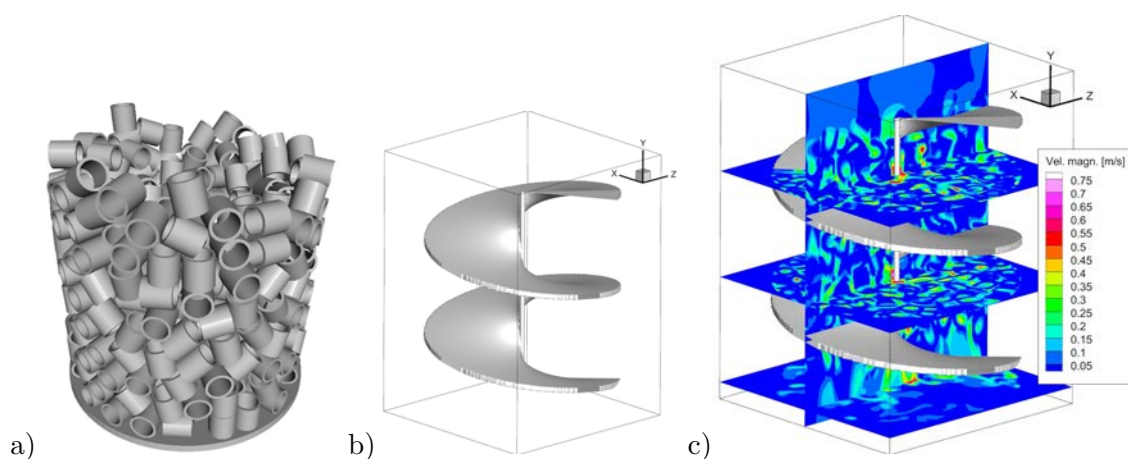


Figure 1. Sample numerically generated random packed bed of rings (a), helical flow deflector (b) and flow velocity magnitude inside the reactor (c).

3. Sample results

The simulation results concerning the velocity magnitude of the single-phase flow within the reactor in the steady state are shown in Fig. 1c (flow entering through the upper plane in the downwards direction). The model provides full information about the velocity field both outside and inside the random packing and pressure profiles along the axis of the reactor (averaged over the normal cross-section). As the parameters of the flow deflector may be easily changed and no re-meshing is required, the functions $RT = f_1(\lambda/D_c)$ and $\Delta p = f_2(\lambda/D_c)$ can be obtained straightforwardly.

Acknowledgments

The work was supported by the statutory research funds Nr BS/PB-1-100-301/2024/P .

References

- [1] Marek M 2019 *Chem. Eng. Sci.* **197** 296-305
- [2] Marek M 2013 *Chem. Proc. Eng.* **34** (3) 347-359
- [3] Marek M 2017 *Chem. Eng. Sci.* **161** 382-393
- [4] Niegodajew P and Marek M 2016 *Powder Technology* **297** 193-20
- [5] Mittal R and Iaccarino G 2005 *Annu. Rev. Fluid. Mech.* **37** 239-261

Numerical simulation of two-phase flow in OpenFOAM software

S Koval¹ and N Dimitrieva¹

¹ Institute of Hydromechanics of National Academy of Sciences of Ukraine, str. Marii Kapnist
8/4, 03057 Kyiv, Ukraine

E-mail: Dimitrieva@nas.gov.ua

Abstract. The non-stationary 3D problem of the flow of a gas bubbles in a liquid was studied. Mathematical modeling is based on the Volume of Fluid method. Numerical modeling was performed using open source software OpenFOAM, SALOME, ParaView. Calculations were carried out for various regimes of two-phase flows. Of interest is the formation of one stable gas cavity in a liquid flow. Qualitative agreement with experimental data was obtained for this application. Airlift of small bubbles in a vertical pipe has also been studied.

Keywords: Computational Fluid Dynamics, Two-phase Flows, Volume of Fluid (VOF), OpenFOAM, SALOME, ParaView.

1. Introduction

One of the difficult problems in computational fluid dynamics is the accurate modeling of two-phase flows. There are many approaches to mathematical modeling. But this is currently an active area of research that is to some extent impaired by the lack of a common modeling framework [1].

The purpose of this research is to develop a technique for numerical calculation of the non-stationary problem of blowing gas into a liquid flow. Of scientific and practical interest is the analysis of geometric and dynamic parameters affecting the formation and development of gas bubbles, their size, shape and stability.

2. Mathematical modeling

The two-phase medium is considered as a single effective fluid. The system of governing equations consists of the Navier-Stokes equation, continuity, phase transport, energy conservation, and equations of state for liquid and gas

$$\frac{\partial (\rho_{eff} \vec{U})}{\partial t} + \vec{U} \vec{\nabla} (\rho_{eff} \vec{U}) = -\vec{\nabla} p_{total} - \vec{g} \vec{h} (\vec{\nabla} \rho_{eff}) + \vec{\nabla} (\tau_{ij}) + \sigma \kappa (\vec{\nabla} \alpha), \quad (1)$$

$$\frac{\partial \rho_{eff}}{\partial t} + \vec{\nabla} (\rho_{eff} \vec{U}) = 0, \quad (2)$$

$$\frac{\partial \alpha}{\partial t} + \vec{\nabla} \cdot (\alpha \vec{U}) = S_{\alpha}^c, \quad (3)$$

$$\frac{\partial (\rho_{\text{eff}} T)}{\partial t} + \vec{\nabla} \cdot (\rho_{\text{eff}} \vec{U} T) = \vec{\nabla} \cdot (k_{\text{eff}} \vec{\nabla} T) + S_T^c. \quad (4)$$

Here \vec{U} is velocity, p_{total} is total pressure, $\alpha(\vec{x}; t)$ is indicator function *VOF* which means volume fraction of water in cell, σ is surface tension coefficient, \vec{g} is gravity, κ is phase fraction curvature, the source terms on the right hand sides of 3₃ and 4₄ are, due to the individual phases compressibility combined with the fact that 4₄ represents the balance of the specific total energy e_{total} defined as:

$$e_{\text{total}} = c_{\text{veff}} T + \frac{|\vec{U}|^2}{2}. \quad (5)$$

Effective physical parameters such as thermal conductivity coefficient k_{eff} , dynamic viscosity coefficient μ_{eff} , density ρ_{eff} and specific heat capacity c_{veff} are determined by using "weighted average rule" [1]. The equations of state for the air and water phases are used by the ideal gas model and the Boussinesq approximation, respectively:

$$\rho_g = \frac{p M_g}{R T}, \quad (6)$$

$$\rho_l = \rho_{l0} [1 - \beta (T - T_0)], \quad (7)$$

where R is universal gas constant, M_g is molar weigh of air, β is volume expansion coefficient, ρ_{l0} is water density at temperature T_0 .

3. Computations

The numerical solution of the equations set (1-4) was performed using the finite volume method in the open source software OpenFoam. The selection of the computational domain was carried out taking into account their individual scales. Both the open mesh generator SALOME and some utilities inside OpenFOAM were used [2, 3]. The calculation results were presented in the open software ParaView. Particularly interesting is the surface of the indicator function, α , which visualizes the phase interface zone. In Figure 1 you can see visualization of two-phase flow in both small bubble mode and cavity mode.

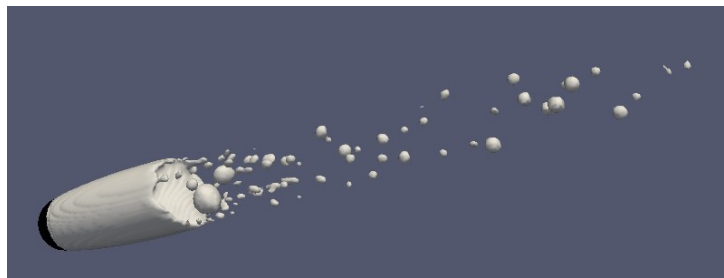


Figure 1. Visualization of two-phase flow.

References

- [1] Scheuflera H and Roenbyb J 2021 *J. Comp. Phys.* **383** 1.
- [2] Dimitrieva N F 2021 *In Proc. Topical Problems of Fluid Mechanics 2021*, ed T Bodnár, T Neustupa and D Šimurda (Prague) p 32.
- [3] Koval S O and Dimitrieva N F 2023 *In Proc. Topical Problems of Fluid Mechanics 2023*, ed D Šimurda and T Bodnár (Prague) p 88.

Dissimilar heat transfer enhancement in pipe flow with deep axial grooves

S Motoki¹ and G Kawahara¹

¹ Osaka University, Graduate School of Engineering Science, 1-3 Machikaneyama, Toyonaka,
Osaka 560-8531, Japan

E-mail: motoki.shingo.es@osaka-u.ac.jp

Abstract. Direct numerical simulations have been performed for convective heat transfer in a pipe flow with deep axial grooves. The temperature is supposed to be a passive scalar. The Prandtl number is set to unity, and similar boundary conditions are imposed on the velocity and the temperature fields. We have found that large-scale radial undulations appear in the shear flow. The large-scale structures exhibit travelling-wave-like patterns in the streamwise direction, leading to dissimilar heat transfer enhancement.

Keywords: Computational Fluid Dynamics, Interdisciplinary Areas in Heat and Fluid Flow, Turbulence, Pipe Flow, Flow Control

1. Introduction

Efficient control of convective heat transfer is one of the major issues in many energy systems. The nature of flow significantly affects heat and momentum transfer, thus leading to remarkable differences in the efficiency of engineering thermo-fluid systems. Turbulent flow provides much higher heat transfer than laminar flow, but generally results in higher friction loss due to the similarity between heat and momentum transfer [1]. It is well known that the introduction of surface roughness on a wall can break the similarity, however, rough surfaces typically lead to ‘bad’ dissimilarity, where heat transfer is not enhanced relatively to momentum transfer [2, 3]. Recently, on the other hand, it has become clear that wall transpiration generates large-scale flow structures in turbulent flows, yielding dissimilar heat transfer enhancement [4, 5]. This suggests that suitable modification of wall conditions can effectively enhance convective heat transfer in shear flows. In this study, we investigate heat and momentum transfer in a pipe flow with deep axial (streamwise) grooves and report that the introduction of grooves has a significant effect on flow instability and turbulence structures, achieving to dissimilar heat transfer enhancement.

2. Numerical simulations

We consider the flow in a straight circular pipe of radius a with axial grooves as shown in figure 1(a). The cylindrical polar coordinate system (r, θ, z) is introduced with the z -axis taken on the pipe centerline, r the radial coordinate, and θ the angular coordinate. The axially uniform grooves are regularly mounted in the θ -direction. The distance from the pipe centre to the bottom of the grooves is represented by A , and θ_s and θ_f are the angles of the solid and fluid parts, respectively. The governing equations are the Navier–Stokes equation for incompressible

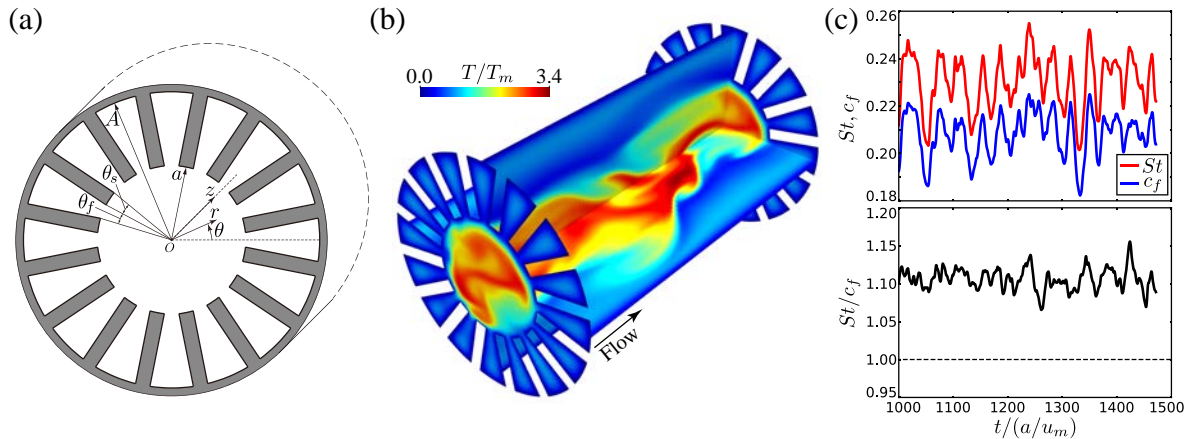


Figure 1. (a) Configuration of the pipe flow with grooves. (b) Instantaneous temperature on the planes $\theta = 0, \pi/2$ and $z/a = 0, 2\pi$, (c) Time evolution of St , c_f and St/c_f at $Re_m = 392$.

flows and the energy equation, with time-independent and spatially uniform driving force $f\mathbf{e}_z$ per unit mass and internal heat source q per unit mass, where \mathbf{e}_z is a unit vector in the z -direction. The isothermal, no-slip and impermeable conditions are imposed on the solid wall surface, and the velocity and temperature fields are supposed to be periodic in the z -direction with the period L . The Prandtl number is set to unity. The governing equations have been numerically solved using the open-source spectral/hp element code Nektar++ [6]. The direct numerical simulations have been performed employing the 2-D spectral element method based on Lagrange polynomials in the (r, θ) plane combined with the 1-D Fourier spectral method in the z -direction. The 2-D unstructured quadrangular mesh is generated by Gmsh. Time advancement is performed with the aid of the third-order implicit-explicit (IMEX) scheme.

In this paper, we present results obtained for the deep grooves of comparable depth with a , i.e., $A = 2a$, $\theta_s = \theta_f = \pi/8$, and $L = 2\pi a$. The Reynolds number, based on the radius a and the mean axial velocity u_m averaged over the whole fluid region, is $Re_m = u_m a / \nu \approx 392$, where ν is the kinematic viscosity. We use 640 elements, polynomials of order 7, and 64 Fourier modes.

As Re_m increases, the flow exhibits streamwise travelling-wave-like patterns and becomes turbulent eventually. Figure 1(b) shows the instantaneous temperature distribution in the turbulent state. We can observe large-scale radial undulations which transfer the hot fluid in the central region into the groove while the cold fluid in the groove to the centre. Figure 1(c) shows the Stanton number $St = aq / (c_p u_m T_m)$, the friction coefficient $c_f = af / u_m^2$, and St/c_f as a function of the time $t / (a / u_m)$, where T_m is the mean temperature averaged over the whole fluid region and c_p is the specific heat at constant pressure. The dissimilar heat transfer enhancement can be attributed to the large-scale radial fluid motions over the grooves.

Acknowledgments

This work was supported by JST PRESTO Grant Number JPMJPR23OC, and JSPS KAKENHI Grant Number 22K14180.

References

- [1] Chilton T H and Colburn A P 1934 *Ind. Engng Chem.* **26** 1183–1187.
- [2] Webb R L, Eckert E R G and Goldstein R J 1971 *Intl J. Heat Mass Transfer* **14** 601–617.
- [3] MacDonald M, Hutchins N and Chung D 2019 *Phys. Rev. Fluids* **4** 071501(R).
- [4] Motoki S, Tsugawa K, Shimizu M and Kawahara G 2022 *J. Fluid Mech.* **931** R3.
- [5] Kuwata Y 2022 *J. Fluid Mech.* **952** A21.
- [6] Cantwell C D et al. 2015 *Comput. Phys. Commun.* **192** 205–219.

Numerical evaluation of mass diffusive compressible fluids flows models

T. Bodnár^{1,2}

¹ Faculty of Mechanical Engineering, Czech Technical University in Prague,
Karlovo náměstí 13, 121 35 Prague 2, Czech Republic.

² Institute of Mathematics, Czech Academy of Sciences,
Žitná 25, 115 67 Prague 1, Czech Republic.

E-mail: Tomas.Bodnar@fs.cvut.cz

Abstract. This contribution presents first numerical tests of some recently published alternative model describing the flow of a viscous compressible fluid. Models are solved by high resolution compact finite difference scheme with strong stability preserving Runge-Kutta time stepping. Two simple computational test cases are presented, based on the double-periodic shear layer and the Kelvin-Helmholtz instability. The obtained time-dependent flow fields are showing pronounced shear and vorticity layers being resolved by the standard as well as by the new mass-diffusive modified models. The preliminary results show that the new model might be an alternative to the well established classical models.

Keywords: Compressible fluid, Navier-Stokes-Fourier system, mass diffusive, compact finite difference scheme, explicit Runge-Kutta scheme

1. Introduction

The aim of this paper is to present the initial results of a computational study based on the mass-diffusive compressible fluids flows model following the works of Svärd [1] extended by Kajzer & Pozorski in [2]. The model results are mutually compared for two test cases, documenting the agreement and comparative advantages of the newly formulated models.

2. Mathematical model

The full system of *Navier-Stokes-Fourier (NSF)* equations describing the flow of a compressible heat conducting fluid was reformulated by Svärd [1] who replaced it by a *modified Navier-Stokes-Fourier (M-NSF)* system, having similar form, but different right-hand sides.

$$\partial_t \rho + \nabla \cdot (\rho \mathbf{v}) = \nabla \cdot (\nu \nabla \rho) \quad (1)$$

$$\partial_t (\rho \mathbf{v}) + \nabla \cdot (\rho \mathbf{v} \otimes \mathbf{v} + p \mathbb{I}) = \nabla \cdot (\nu \nabla (\rho \mathbf{v})) \quad (2)$$

$$\partial_t E + \nabla \cdot ((E + p) \mathbf{v}) = \nabla \cdot (\nu \nabla E) \quad (3)$$

The diffusion coefficient $\nu = \mu/\rho$ has now the same value in all the considered equations of the modified *M-NSF* system.

3. Numerical Simulations

The test cases were chosen to represent low velocity (low Mach number) flows, with important solution gradients, evolving in time. The compact finite-difference approximation [3], [4] of spatial derivatives was adopted, together with high-order compact filters for stabilizing the purely central (upwinding free) scheme [5]. The temporal discretisation was carried out using explicit Runge-Kutta multistage scheme in the Strong Stability Preserving (*SSP*) form proposed in [6]. The numerical tests cases include the Kelvin-Helmholtz instability and double periodic shear layer among others.

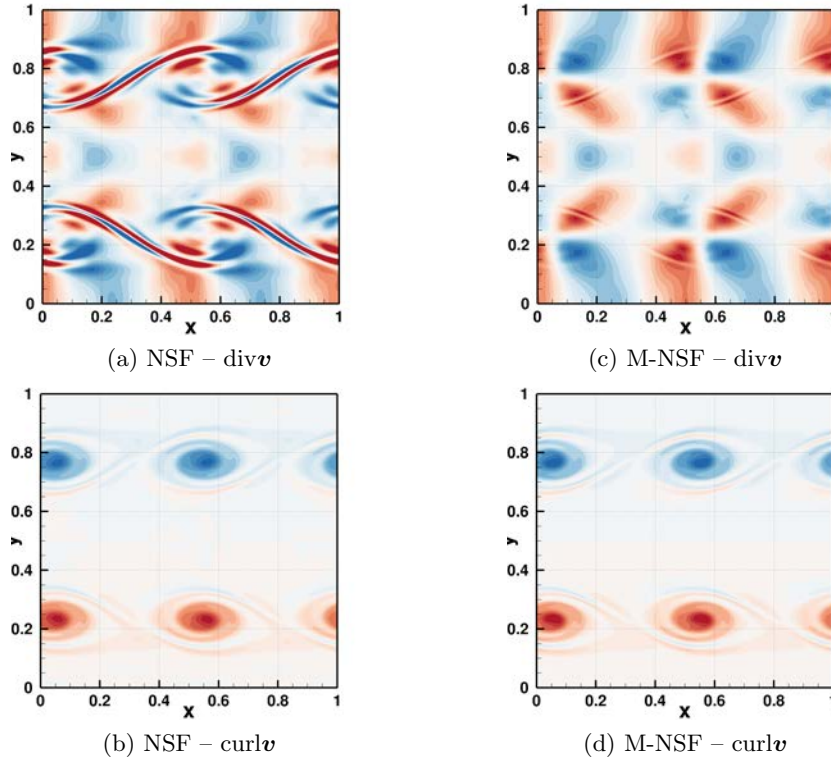


Figure 1: Divergence and curl of the velocity field at $T = 3.0$ for the Kelvin-Helmholtz Instability.

4. Conclusion

The numerical simulations have demonstrated the very good to excellent agreement between the solutions of the classical *Navier-Stokes-Fourier (NSF)* and the newly developed *modified Navier-Stokes-Fourier (M-NSF)* system. There are however some open questions to be answered, namely related to the non-symmetrical stress tensor in the modified system. The conditions under which the new system is a good approximation of the original one need to be discussed in detail.

Acknowledgments

The financial support for the present work was provided by the Czech Science Foundation under the grant No. *GA22-01591S* and partly by the Czech Academy of Sciences under the *Praemium Academiae of Š. Nečasová* and RVO:67985840.

References

- [1] Svärd M 2018 *Physica A* **506** 350–375
- [2] Kajzer A and Pozorski J 2022 *Computers and Mathematics with Applications* **121** 18–29
- [3] Gaitonde D, Shang J and Young J 1999 *International Journal for Numerical Methods in Engineering* **45** 1849–1869
- [4] Visbal M and Gaitonde D 2002 *Journal of Computational Physics* **181** 155–185
- [5] Bodnár T, Beneš L, Fraunié P and Kozel K 2012 *Applied Mathematics and Computation* **219** 3336–3353
- [6] Shu C 1988 *SIAM Journal of Scientific & Statistical and Computing* **9** 1073–1084

Code coupling for the Tube Support Plate clogging in steam generators

A Couvez¹, S Gyuran¹, N Leterrier¹, P Omnes¹ and E Saikali¹

¹ Commissariat à l'énergie atomique et aux énergies alternatives (CEA), 91191 Gif-sur-Yvette cedex, France

E-mail: antonin.couvez@cea.fr

Abstract. The overall background of this research is the design of a numerical platform for the secondary circuit of a nuclear power plant, with a focus on the modelling of effects combining thermal-hydraulics and chemistry. This study aims at taking into account the impact of a precipitate or deposit in the thermal-hydraulic code TrioCFD[1] from an accurate chemical modelling. The presence of the precipitate is modelled in TrioCFD by a friction term and a turbulence contribution in the momentum equation, as well as by a thermal effect in the energy equation.

Keywords: Computational Fluid Dynamics, Chemical Transport, Multi-physics Coupling, Steam Generators, TSP Clogging.

1. Introduction

There is a growing interest among industrial partners for Digital Twins (DTs), in particular for nuclear power plants. Creating a digital twin for the secondary circuit requires a strong thermal-hydraulic and chemical coupling in order to deal with corrosion, clogging and fouling. Since reactive transport calculations cannot predict accurately the interfaces that appear between precipitates and flow, the chemical deposit is treated like a porous media in the thermal-hydraulic calculation. We show how we take this issue into account through specific developments undertaken in TrioCFD. The thermal-hydraulic calculation after the transition zone between the porous media and the fluid is our main focus and we present numerical results illustrating the effects of the precipitate.

2. Clogging in steam generators

The Tube Support Plate (TSP) clogging is driven by thermochemistry, transport and deposition/erosion effects and creates a feedback on the thermal-hydraulic problem. We begin our study with a single phase-flow of water in two dimensions. The thermal-hydraulic code is TrioCFD and, for the present test, the chemical problem is calculated by SCORPIO [2] with a single chemical equation that models precipitation. The RANS equations are used for the turbulent flow ($Re = 10^5$) with a $k-\epsilon$ model. SCORPIO and TrioCFD are based on the TRUST platform [3]; this platform allows us to use the ICoCo API [3] and the MEDCoupling [3] library for data exchange and supervising the two codes.

2.1. Problem description and meshes

Under boiling condition, potential contributing factors to clogging of TSP are the centrifugal settling, the gravitational settling, the flashing in low pressure zone and the impact on the bottom surface [4]. For performance reasons, the mesh for the chemical part is much coarser than the underlying fluid mesh.

The reactive transport code is given the temperature and velocity fields. It calculates the porosity field, which is in turn sent to the thermal-hydraulic code. The chemical reactions are assumed to be neither endo- nor exothermic.

3. Governing equations and numerical approach

In the thermal-hydraulic solver, the presence of the solid precipitate is described by a porosity field defined as a volume fraction in each mesh cell. In TrioCFD, the momentum equation is discretized at the faces σ of the mesh and incorporates a friction term S_f approached on the face σ between two cells Ω_1 and Ω_2 by the following formula:

$$S_f \approx -\rho\beta_\sigma(1-\beta_\sigma)\frac{l(\sigma)}{A(\Omega_1)+A(\Omega_2)}C_f\|\vec{V}_\sigma\|\vec{V}_\sigma, \quad (1)$$

where β_σ is a face interpolation of the cell-based porosity field, ρ is the density of the fluid, $l(\sigma)$ is the length of the face, $A(\Omega_i)$ is the area of Ω_i , while C_f is the friction coefficient given by a correlation used for porous media and \vec{V}_σ is the velocity at the face.

The thermal contribution linked to the porous media is described in TrioCFD by the following additional heat flux:

$$q_e = \left[\frac{1}{\lambda_m \left(\frac{\beta}{\lambda_e} + \frac{1-\beta}{\lambda_m} \right)} - 1 \right] \times \frac{(1-\beta)\lambda_e}{\beta} \times \nabla T, \quad (2)$$

where T is the temperature, λ_e the thermal conductivity of the fluid and λ_m the thermal conductivity of the deposit.

4. Results

First results obtained on the velocity field with these news contributions are available on Figure 1. We clearly observe the impact of the deposit produced by the chemical calculation. The last part of this study will describe the term used to take into account the influence of the deposit on the turbulence term.

References

- [1] Angeli P, Bieder U and Fauchet G. **Overview of the TrioCFD code: main features, V&V procedures and typical applications to nuclear engineering.** *Proc. of 16th International Topical Meeting on Nuclear Reactor Thermohydraulics*, 2015
- [2] Leterrier N. <https://trio CFD.cea.fr/Pages/Presentation/SCORPIO.aspx>
- [3] Saikali E, Ledac P, Bruneton A, Khizar A, Bourcier C, Bernard-Michel G, Adam E, Houssin-Agbomson D. **Numerical modeling of a moderate hydrogen leakage in a typical two-vented fuel cell configuration.** *Int. Conf. Hydrogen Safety*, 2021
- [4] Rummens H, Rogers J and Turner C. **The thermal hydraulics of tube support fouling in nuclear steam generators.** *Nuc. Tech.*, 2004

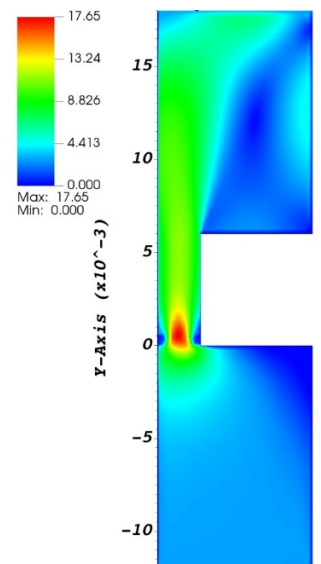


Figure 1. Thermal-hydraulic results with velocity fields.

Numerical investigation of Air Flow Within a Human Nasal Cavity

P Niegodajew¹

¹Czestochowa University of Technology, Department of Thermal Machinery,
Armii Krajowej 21, Czestochowa, 42-200, Poland

E-mail: pawel.niegodajew@pcz.pl

Abstract. This work explores the flow inside a human nasal cavity with the goal to determine such breathing cycle conditions that ensure maximising the airflow within the olfactory region. The reason for doing so is that this process is critical for the optimum delivery of drugs through a nasal spray.

Keywords: Computational Fluid Dynamics, Human Upper Airways, Olfactory Cleft.

1. Introduction

Spray inhalation has become a popular way to treat respiratory ailments like congestion or allergies, and has become an alternative to oral and injection methods of delivering drugs for many diseases. However, the efficiency of the nasal drug delivery equals only (10 – 20%) [1] and according to the review paper of Ronald *et al.* [2] the rest of the drug load can cause a serious side effects for the patient. The efficiency of such products is measured as the amount of particles that deposit on the highly vascular mucous walls. Further computational analysis can be helpful to find a way to increase the efficiency of injected sprays and to determine the optimal amount of injected ration drug to minimize the negative side effects for the human and the present study is a step forward towards improving this process.

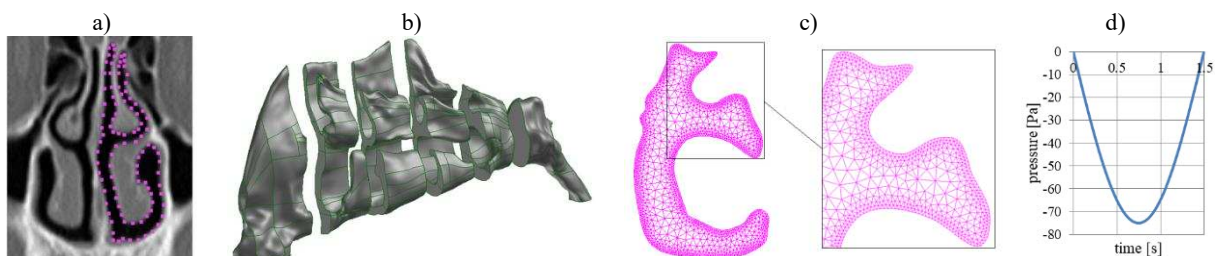


Figure 1. Computed tomography scan of nasal cavity (a), final geometry with exposed cross-sections (b), computational mesh for a selected cross-section (c) and the pressure distribution used as the pressure outlet boundary condition (d).

2. Methods

Forty eight computed tomography scans were used to truly reconstruct each part of the nose geometry (Fig. 1a). Note that for the purpose of the present study only a half of the nasal cavity was considered (see the fully reconstructed geometry with exposed cross-sections in Fig. 1b). The mesh size with 1.5 million tetrahedron cells (Fig. 1c) was used in the computations. Pressure inlet and pressure outlet were assumed as the boundary conditions and the air flow was enforced by employing the pressure distribution (typical for a single inspiration cycle) adopted from Ref. [3] (Fig. 1d). The numerical simulations were conducted in ANSYS FLUENT software with the finite volume discretization method. The flow was assumed to be laminar since the Reynolds number $Re < 2300$ in the most of the domain.

3. Results

To assess the flow behaviour locally, ten streamlines were released from two particular lines I and IV marked with red colour in Fig. 2a illustrating the inlet boundary. The results obtained under the time moment $t = 0.75$ s (see Fig. 1d), i.e. for the highest underpressure (so the greatest values of velocity are expected to occur locally), are presented in Figs 2b and 2c. The results show that when the streamlines are released from line I (Fig. 2b) most of the flow enters the olfactory region which is crucial for a proper drug delivery within the spray inspiration. On the other hand, when the streamlines are released from line IV, the flow occupies the lower part of the nasal cavity which is undesired scenario since all the injected medicine would not reach the destination region.

This simple analysis indicates how just selection of the location of the flow injection can contribute to the potential medicine distribution inside the nasal cavity. Note that, the results presented herein are just a tiny portion of much more insightful analysis of the flow behaviour that will be presented in an extended version of the paper.

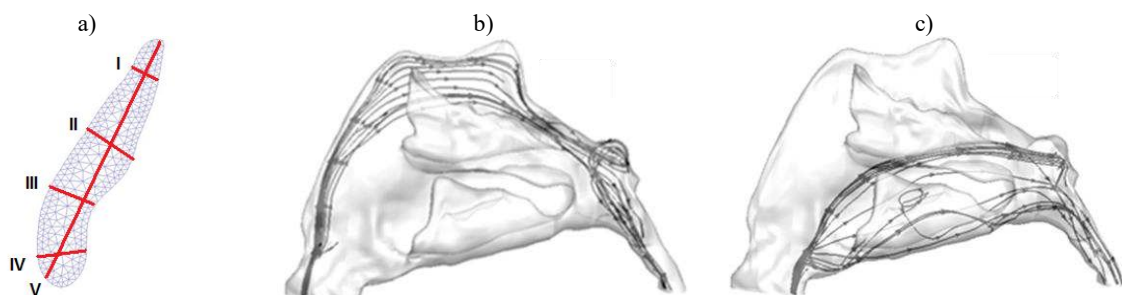


Figure 2. Inlet boundary with marked lines' locations (a), visualisation of streamlines released from line I (b) and line IV (c).

Acknowledgements

The research was supported by the statutory founding Nr BS/PB-1-100-301/2024/P .

References

- [1] Cheng Y S, Holmes T D, Gao, J, Guilmette R A, Li S, Surakitbanharn Y and Rowlings C 2001 *J. Aerosol Med.* 14(2):267-280.
- [2] Roland N J, Bhalla R K and Earis J 2004 *Chest* 126: 213-219.
- [3] Lee J H, Na Y, Kim S K, Chung S K 2010 *Respiratory Physiology & Neurobiology* 172: 136–146

When the jet collides with an obstacle, a sudden change in the nature of turbulence results in a significant increase in the emitted sound level. For example, the rocket noise approaches its maximum on the starting section of the flight with the intense interaction of the flow with elements of starting facilities. This leads to the reconfiguration of turbulent acoustic sources, but none of the existing semi-empirical methodologies offer clear recommendations for its description [2, 3]. Moreover, some studies suggest to set the special acoustic source responsible for the direct flow-obstacle interaction [4].

We propose a straightforward approach to the localization of gas-dynamic sound sources in a supersonic jet impinging on a normal wall using only the acoustic properties of the free jet.

2. Methodology

According to the theory of sound generation by supersonic flows, about 0.5% of the total jet's kinetic energy is converted into acoustic form [5]. The radiating part of the rocket jet extends for five lengths s_L of its laminar core, starting from the nozzle exit cross-section [2].

Experimentally determined self-similar functions relate the characteristics of the sound emitted by point sources to the jet's macroscopic parameters, such as thrust N , flow velocity v_e , and Mach number M_e at the nozzle exit having a diameter d_e . The acoustic power is distributed along the flow axis for a normalized source location s_n/s_L [2, 6]. The frequency spectrum depends on the longitudinal Strouhal Number $St_n = fs_n/v_e$ that relates the position s_n of the source with the frequency f [2]. The circumferential Strouhal Number $St_d = fd_e/v_e$ controls the directivity pattern with the main lobe in the direction of $(50 \dots 60)^\circ$ to the flow [2, 3].

Choose the arbitrary observation point P beyond the jet. Let r_n and θ_n be its distance from the n th source, and the angle between the flow and r_n (see Figure 1). Then the acoustic load at the observation point is given by the sum of contributions from all uncorrelated sources with the allowance for geometric correction for the divergence of spherical waves [2].

Let H be the distance from the nozzle to the perpendicular wall. Then for the impinging supersonic jet, all the "distant" acoustic sources with $s_{n'} > H$ should be projected to a single point of intersection of its axis and the wall, $\bar{r}_{n'} = \min(r_{n'}, H)$. Moreover, set $\bar{\theta}_{n'} = \theta_{n'} - 90^\circ$ due to reversal of the flow along the surface. Also note that the acoustic reflection from the wall is expressed in the doubling of the intensity of the acoustic sources projected to the center of the flow-surface interaction.

3. Discussion and Conclusions

- (i) According to the numerical results, the interaction of a supersonic jet with an obstacle close to nozzle exit ($H \leq d_e$) leads to the one-order increase of the acoustic loads in comparison with noise from the free jet. The level of exceeding acoustic loads rapidly decreases with H and may be neglected for $H > s_L$. These results correlate with known experimental data [4].
- (ii) The proposed approach may be readily extended to an arbitrary angle of inclination of the plate $0^\circ < \alpha \leq 90^\circ$. The obtained estimates of acoustic loads may be overestimated due to We omitting the effects of the jet flow around the surface.

References

- [1] Nonomura T Goto Y and Fujii K 2011 *Int. J. Aeroacoust.*, B **10** 4 401.
- [2] Eldred K 1971 *Acoustic loads generated by the propulsion system* (Washington: NASA) 49 p.
- [3] Plotkin K, Sutherland L and Vu B 2009 *Proc. 15th AIAA/CEAS Aeroacoust. Conf. (Miami)* (Washington: AIAA) 11 p.
- [4] Koudriavtsev 2000 *InterNoise 2000 (Nice)* (Paris: SFA) 6 p.
- [5] Ffowcs Williams J 1963 *Phil. Trans. Roy. Soc. Lond.* B **A255** 1061 p 469.
- [6] Gee K 2021 *J. Acoust. Soc. Am.* B **149** 4 p 2159.

Step-by-step CFD validation of turbulent particle transport and deposition in industrial bends

J. Malet¹, R. Ploix^{1,2}, E. Gehin²

¹ Institut de Radioprotection et de Sûreté Nucléaire (IRSN), PSN-RES/SCA/LEMAC, F-91400 Saclay, France

² CERTES . UPEC, University Paris Est, Créteil, France

E-mail: jeanne.malet@irsn.fr

Abstract. Numerical tools are necessary to assess particle transport in ventilation ducts, a topic of many interests for sanitary, safety and security reasons. The objective of this study is to evaluate CFD modelling in industrial rectangular bend ducts. Sensitivity studies are performed at small-scale and the resulting observations are applied at large industrial scale focusing on deposition in bends for which experimental data are obtained on a large-scale facility especially developed for this purpose.

Keywords: Computational Fluid Dynamics, Particle, Aerosol, Deposition, Duct Flow, Ventilation Ducts, Experimental Fluid Mechanics, Multi-phase Flows, Turbulence

1. Introduction

Indoor air as well as many industrial applications imply the use of ventilation networks in which particle transport is a subject of interests for sanitary, safety and security reasons. Numerical tools are necessary to evaluate the aerosol transport and deposition under such industrial channel flows and these ones must be easy to use for applied engineering. One way to produce such numerical tools is to perform parametric CFD calculations to obtain database or develop simple correlations. However, particle transport and deposition modelled by CFD especially in bends exhibit a large range of variation and questions [1]. The objective of this study is to evaluate CFD modelling of particle transport and deposition in large scale bends of different shapes.

2. Experimental facility and measurement techniques

The experimental facility is a 60 m length channel of rectangular cross section with many different singularities such as horizontal and vertical bends of different shapes, reductions of different shapes and T-junctions [2]. The main channel is 400×600 mm² and the smaller one of 200×300 mm² both of galvanized steel, which makes, to our knowledge, one of the largest scale for such studies compared to previous ones [3]. This facility works under aspiration with an air conditioning station: the air is filtered; humidity is condensed, and the air is reheated to ensure a desire temperature. A honeycomb is located downstream the air conditioning section. Reynolds bulk numbers Re_b are about 10^5 , Reynolds numbers based on the friction velocity Re_τ are about 9000. Aerosol is generated by a specific vibrating ceramic system that allows to

produce almost monodisperse NaCl particles between 2 and 6 μm diameter ($\sigma_g = 1.4$). The aerosol is marked with a fluorescent tracer to allow its detection on walls. High frequency hot wires (Dantec HFHW) up to $y^+ = 5$ and PIV (LaVision) at large scale (50 cm window) have been used to characterize the flow. Particle size distribution is measured continuously with an APS (TSI). The bulk aerosol is measured by sampling on filter and a specific protocol has been developed for the measurement of aerosol deposited mass on local 100 cm^2 zone, without any subtract on the duct surface [4][1]. Data reduction is avoided to compare deposited mass without further modelling that might bring uncertainties (friction velocity, bulk concentration). Deposition is performed between thirty minutes and two hours. Specific attention is given to the boundary conditions derived from experiments. The size distribution is controlled during the whole steady-state and the flowrate, temperature and humidity are sampled at 1 Hz. The channel walls are insulated with 5 cm layer material. The presentation will describe the experimental facilities and validation.

3. Numerical study and preliminary validations

The use of an industrial scale experiment and a commercial software (Ansys Fluent v. 2022 R1) led to several questions on the code-experiment validation. Before considering the results on the large-scale duct, parametric sensitivity studies are performed at a small-scale test [5]. Since the goal here is to model bends and T-junctions flows, adverse pressure gradients make the use of wall laws inadequate. The wall mesh is thus refined to $y^+ = 1$ in most of the domain with up to 20 layers below $y^+ = 30$ and at least 4 nodes up to $y^+ = 5$. For the particle modelling, for the same reason, no wall functions are used since they are not accurate in such flows. A lagrangian stochastic particle tracking (one-way coupling) is performed considering no bouncing on walls. SIMPLE scheme is used with Green-Gauss Node-Based discretization and second order discretization. Neither customized wall-correction nor Eddy Interaction Model modifications [6] are used and Best Practice Guidelines recommended by Fluent [7] are applied.

A sensitivity study to the bulk mesh density, the type of mesh (tetra/hexa), the turbulence model (SST-k- ω and RSM based on epsilon), and the lagrangian stochastic model is performed on the small-case test and will be detailed in the presentation, illustrating the importance of these parameters to get accurate results. Calculations on the large-scale facility are then performed on the same basis of modelling choices. A flow analysis based on mean variables down to second order moments of the wall shear stresses is presented in a companion paper [8].

4. Code-experiment comparison and discussion

Focus is mainly given to the bend flows. Experimental results of streamwise velocity and particle mean concentration horizontal profiles upstream and downstream of a horizontal bend are presented. Aerosol mass deposited on local surfaces are also measured. These measurements are performed for three various bend shapes (smooth to sharp 90° angle) and are analysed using the numerical data. Aerosol deposition is mainly observed on the bend horizontal walls whereas side walls deposition is about 10 to 100 times lower.

References

- [1] Abbasi S., A. Mehdizadeh, 2024, International Journal of Multiphase Flow **174**, 104754
- [2] Malet J., *et al.* 2022, Building and Environement, **222**, 109223
- [3] Sippola M. R., W. W. Nazaroff, 2004 *Aerosol Science and Technology*, **38** 9
- [4] Costa D., J. Malet, E. Géhin 2022 *Meas. Sci. Technol.* **33** 9
- [5] Pui D. Y., H. F. Romay-Novas, B. Y. Liu., 1987, *Aerosol Science and Technology* **7:3** 301
- [6] Jubaer H., *et al.*, 2024, *J. Aerosol Sci.* , **175** 106262
- [7] Menter F.R., *et al.*, 2021, BPG: RANS Turbulence Modeling in Ansys CFD, Ansys Germany GmbH
- [8] Ploix P., J. Malet, E. Gehin, 2024 *Proc. XXVI Fluid Mechnaics Conference*, (Warszaw, Poland)

High performance least-squares spectral/hp element method solvers for fluid dynamics problems

J. Gałecki^{1,2}, J. Szumbariski¹

¹ Warsaw University of Technology, Faculty of Power and Aeronautical Engineering

² University of Warsaw, Interdisciplinary Centre for Mathematical and Computational Modelling

E-mail: jakub.galecki.dokt@pw.edu.pl

Abstract. The least-squares finite element method poses an attractive alternative to the classical Galerkin-type FEM. The present work explores its computational and numerical aspects, most notably the selection of the optimal operator evaluation strategy. Issues related to implementations on modern supercomputers are further investigated.

Keywords: Computational Fluid Dynamics, Least-Squares Finite Element Method, High Performance Computing

1. Introduction

Since its inception in the 1990s, the least-squares spectral/hp element method (LSSEM) has been successfully employed in CFD applications [1]. It offers a number of benefits, including the symmetric and positive definite nature of the resulting algebraic systems (even for non-self-adjoint problems), the ease of application to multiphysics problems, and the lack of compatibility constraints on the bases used to discretize the pressure and velocity fields (LBB condition). The existing body of research is aimed at developing formulations for more complex physics, as well as new numerical schemes to address some of the method's shortcomings [2]. The present work focuses on the computational aspects of LSSEM, aiming to bring it to parity with Galerkin-type methods in this regard.

2. Operator evaluation strategies

Finite element operators can be evaluated using one of the following techniques: (a) the global matrix approach, where the (sparse) operator is precomputed and explicitly stored in memory, (b) the local matrix approach, where the action of the operator is evaluated only at the element level, and (c) the sum-factorization approach, which further exploits the tensor product structure of the basis and quadrature rules to reduce the algorithmic complexity of the operation and allows the computation to be expressed as a series of matrix-matrix products. The optimal choice depends on the element order p and, in the case of operators arising in CFD using Galerkin-type methods, has been extensively studied [4]. LSSEM formulations typically involve multiple degrees of freedom per node and higher quadrature orders. A key example is the advection-diffusion equation recast to the first order form, which is the cornerstone of splitting schemes for the incompressible Navier-Stokes equations [3]:

$$\left\{ \begin{array}{l} \frac{\partial \phi}{\partial t} + (\mathbf{u} \cdot \nabla) \phi - \frac{1}{Pe} \nabla \cdot \mathbf{q} = f \\ \nabla \phi - \mathbf{q} = \mathbf{0} \\ \nabla \times \mathbf{q} = \mathbf{0} \end{array} \right.$$

It can be seen that the evaluation of the LSSEM three-dimensional advection-diffusion operator is approximately an order of magnitude more expensive than its Galerkin counterpart. In fact, for higher values of p , the matrices required for the local matrix and sum-factorization approaches become so large that they cannot fit in the private (typically L2) cache of a modern CPU core. The present work investigates a new, seemingly counterintuitive parallelization paradigm, wherein the operator evaluation for a single element is handled by multiple threads. This approach stems from the parallelization algorithms employed in high-performance matrix-matrix multiplication implementations [5]. Further batching techniques are also considered for the transitional regime where the relevant matrices do not fit into the private cache, but are not quite big enough to occupy a meaningful fraction of the shared (typically L3) cache. The proposed approaches are tested on several CPU architectures with varying amounts of cache.

3. Results

The aforementioned LSSEM operator evaluation strategies were implemented within the L3STER framework [7]. Interestingly, the intermediate range of p for which the local matrix approach is optimal is significantly broader in the case of LSSEM than Galerkin-type SEM. Comparisons in this regard are made with the benchmarks of Fischer [6]. It can be seen that all strategies must be supported by an LSSEM solver in order to accommodate values of p which may be used in practice. Furthermore, the proposed intra-element parallelism proves to be a viable strategy for higher p , which bears strongly upon the need for a hybrid MPI and thread parallel architecture of LSSEM codes. Finally, examples of applications are shown to demonstrate the viability and scalability of the proposed approach.

Acknowledgments

This research was carried out with the support of the Interdisciplinary Centre for Mathematical and Computational Modelling, University of Warsaw (ICM UW), under computational allocation g93-1616.

References

- [1] Jiang, B. (1998). *The Least-Squares Finite Element Method*. Springer Berlin Heidelberg.
- [2] Vallalaa, V. P. P., Sadr, R., & Reddy, J. N. N. (2014). Higher order spectral/hp finite element models of the Navier–Stokes equations. *International Journal of Computational Fluid Dynamics*, 28(1–2), 16–30.
- [3] Pontaza, J. P. (2007). A new consistent splitting scheme for incompressible Navier–Stokes flows: A least-squares spectral element implementation. *Journal of Computational Physics*, 225(2), 1590–1602.
- [4] Cantwell, C. D., Sherwin, S. J., Kirby, R. M., & Kelly, P. H. J. (2011). From h to p Efficiently: Selecting the Optimal Spectral/hp Discretisation in Three Dimensions. *Mathematical Modelling of Natural Phenomena*, 6(3), 84–96.
- [5] Marker, B., van Zee, F. G., Goto, K., Quintana-Ortí, G., & van de Geijn, R. A. (2007). Toward Scalable Matrix Multiply on Multithreaded Architectures. In *Lecture Notes in Computer Science: Vol. 4641 LNCS* (pp. 748–757). Springer Verlag.
- [6] Fischer, P., Min, M., Rathnayake, T., Dutta, S., Kolev, T., Dobrev, V., Camier, J.-S., Kronbichler, M., Warburton, T., Świrydowicz, K., & Brown, J. (2020). Scalability of high-performance PDE solvers. *The International Journal of High Performance Computing Applications*, 34(5), 562–586.
- [7] <https://github.com/kubagalecki/L3STER>

Application of CFD airflows to aid nasal obstruction diagnosis

B Kopiczak¹, K Karbowski¹, K Nering¹, Z Malecha², R Chrzan³, J Gawlik⁴, A Sucherska⁴, J Szaleniec⁴ and J Karbowski⁵

¹ Cracow University of Technology, Faculty of Mechanical Engineering, Cracow, Poland

² Wrocław University of Technology, Faculty of Mechanical and Power Engineering, Wrocław, Poland

³ Jagiellonian University Medical College, Chair of Radiology, Cracow, Poland

⁴ Jagiellonian University Medical College, Department of Otolaryngology, Cracow, Poland

⁵ AGH University of Science and Technology, Faculty of Computer Science, Cracow, Poland

E-mail: bartosz.kopiczak@pk.edu.pl

Abstract This paper describes the results of experimental and numerical studies of airflow through the nasal cavities. The flow geometry obtained from the CT scan is used to produce a 3D printout for the experimental measurements and the numerical models used in the CFD analyses. The effect of the segmentation level on the numerical results is presented. Experimental verification of the numerical flows is performed.

Keywords: CFD, Bio-flows, reverse engineering, virtual rhinomanometry,

1. Introduction

Correct and effective airflow identification is crucially important in otolaryngology diagnostics. Anterior rhinomanometry (RMM) is a typical method of identifying airflow in the nasal cavities. The rapid growth of Computer-Aided Design (CAD) and Reverse Engineering (RE) methods enables the construction of virtual models of anatomical structures based on Computed Tomography (CT) imagery. These models can be used to simulate airflows in Computational Fluid Dynamics (CFD). Thus, it is possible to conduct a numerical analysis of airflow through the nasal cavities. The concept of this procedure we have called Virtual Rhinomanometry (V-RMM) [1, 2] - figure 1.

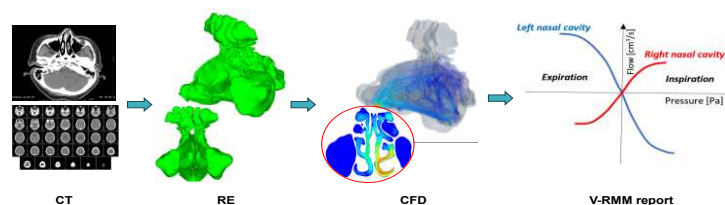


Figure 1. Concept of the virtual rhinomanometry

2. Flow simulation methodology

The basis for the preparation of the three-dimensional airflow space of the nasal cavities is a CT scan performed on patients exhibiting breathing difficulties due to a deviated nasal septum. Detailed 3D nasal model preparation and smoothing procedure in 3D Slicer software is presented.

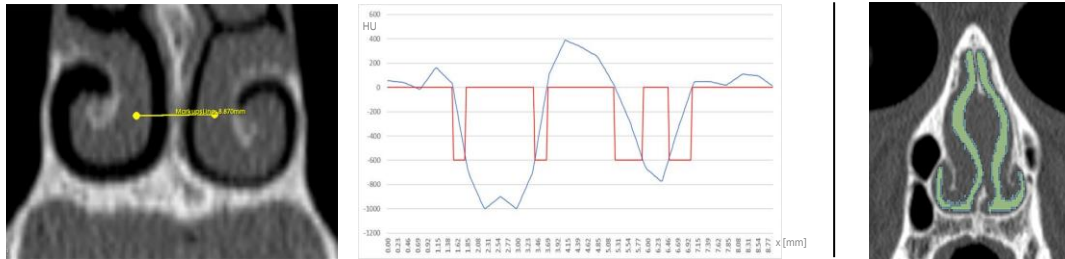


Figure 2. Hounsfield Units profile through the nasal cavities along the markup line designated in the CT view on the left; isolated air space marked with a coloured mask for different segmentation thresholds of -50HU(green) and -600HU (blue-green) respectively on the right

Airflow through the nasal cavity is simulated using OpenFOAM CFD software. The computational mesh is generated based on the image from a CT scan using the snappyHexMesh tool which is part of the OpenFOAM framework. Comparatively, for the selected segmentation level of -200HU, a CFD model is prepared using the ANSYS FLUENT. CFD results have been verified by reference measurements performed on the 3D-printed DLP model of nasal cavities.

3. CFD and experimental results

The RMM and CFD comparison of example patient is shown in figure 3. The rhinomanometry report is presented as charts of airflow versus pressure difference, separately for the left and right nasal cavities. In quadrant I of the diagram is the right nasal cavity inspiration, in quadrant II – left nasal cavity expiration; in quadrant III – right nasal cavity expiration and in quadrant IV – left nasal cavity inspiration.

CFD simulation can be used for the prediction of airflow asymmetry. The CT image segmentation threshold plays an important role in the preparation of the virtual 3D models of nasal cavities and airflow calculation results.

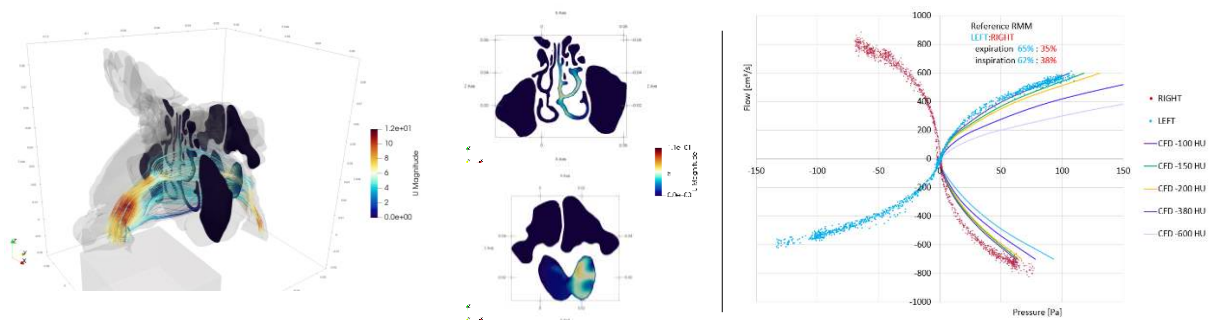


Figure 3. Visualisation of CFD airflow through the left nasal passage on left; comparison of RMM and CFD simulation results for variable segmentation threshold on right.

References

- [1] Karbowski K, Kopiczak B, Chrzan R, Gawlik J, Szaleniec J 2023 *Accuracy of virtual rhinomanometry*, *Polish Journal of Medical Physics and Engineering*, vol 29, Issue 1
- [2] Chrzan R, Szaleniec J, Karbowski K, Kopiczak B, Gawlik J, Tomik J, Popiela T 2023 *Virtual rhinomanometry based on computed tomography of the paranasal sinuses in patients with nasal septum deviation – a pilot study*, *Otolaryngol Pol*, 77 (1), p 1-5

Application of the model of trapped vortices to the control of flow around a bridge pier

I. Gorban¹

¹ Institute of Hydromechanics of the National Academy of Sciences of Ukraine,
ul. Mariyi Kapnist 8/4, 03057 Kyiv, Ukraine

E-mail: ivgorban@gmail.com

Abstract. Control of flow around a rectangular prism, which relies on the use of two attached frontal plates, is proposed. It is aimed at creating a new flow topology with a stable critical point. A reduced order model of a standing vortex is applied to calculate optimal geometric parameters of the control device. The feasibility of this scheme is confirmed by numerical simulation of the viscous flow around the considered body configuration. The application of the proposed control to reducing loads and scour of a bridge pier is discussed.

Keywords: Computational Fluid Dynamics, standing vortex model, flow topology, bridge pier

1. Introduction

Maintaining the stability of bridges during their operation has always been a big challenge for engineers and builders due to the forced interaction between the structure and natural river flow. Scour of bridge piers is known to be one of the main causes of bridge failures. The use of flow altering countermeasures allows mitigate the scour effect by weakening the hydraulic loads in the area located immediately in front of the pier. In this study, we propose to install two symmetrical ledges on the upstream side of the bridge pier to achieve a favourable flow pattern here. This passive scheme of control is expected to divert the flow away from the pier. To understand the flow pattern around the bridge pier with frontal ledges, the cross-section of this structure is considered. We use the dynamic model of a standing vortex [1] to obtain optimal characteristics of the control device. It is based on the critical-point theory, which is able to predict the behaviour of the flow in the configuration under consideration. To confirm the conclusions of the reduced model, 2D numerical simulation of the viscous flow in the region is performed. It allows to derive large-scale flow patterns and dynamic loads in the system.

In practice, the control strategy proposed consists in producing two symmetrical recirculation zones between the ledges and the front side of the body. Theoretically, it is aimed at creating the desired flow field topology, which means changing the location and type of critical points of the flow in accordance with the objectives of the control. In the dynamic model, the recirculation zone is replaced by a point vortex, which must be immovable and prevent flow separation at the leading edge of the body. The viscous flow in the region is modelled by the hybrid vortex method based on the velocity-vorticity form of the Navier-Stokes equations. This approach has been applied to justify a similar control strategy for a square prism [2]. The stabilization of the wake past the prism with attached frontal plates and a significant reduction of its dynamic loads were recorded.

2. Problem statement and results

In this study, a rectangular prism with an aspect ratio of 3:1 is considered as a bridge pier prototype. The effect of two small symmetrical ledges, which are plates in a horizontal section, attached to the front side of the prism is investigated. The side view and transverse view, as well as the input parameters and coordinate axes are depicted in Fig. 1. Note that all variables in this study are normalized to the width of the rectangle a and uniform flow velocity U_∞ .

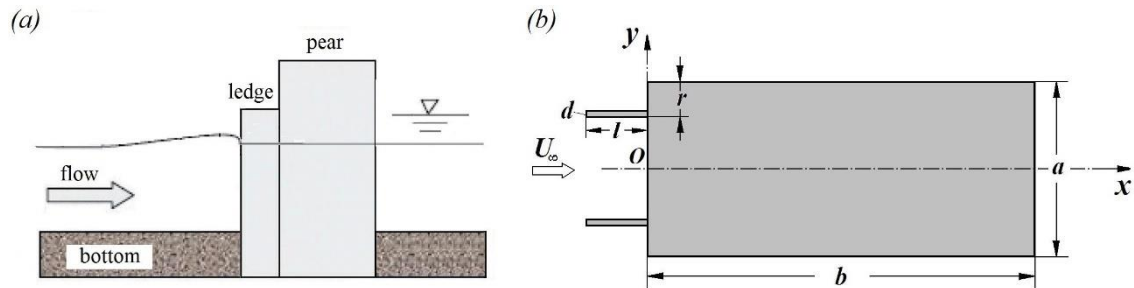


Figure 1. Bridge pier with frontal ledges: (a) – side view, (b) – top view

The problem is considered in the horizontal plane Oxy . The control scheme will be effective if the recirculation zone formed in the corner between the attached plate and the prism is stable and closed. In the dynamic model, the zone is replaced by a point vortex, which must be immovable and prevent the flow separation in the prism leading edge. This is a standing vortex lying at the critical point of the flow. The problem is reduced to the PDE system relatively coordinates and circulation of the standing vortex as well as the plate length l and distance r . The reduced model lets us to calculate the dependency $r(l)$ provided that the standing vortex is located in the critical point, which is a stable focus. The points lying on this curve ensure a set of optimal geometric parameters of the control device

Then numerical modeling of the viscous flow around the original rectangular prism and the prism with attached frontal plates was carried out at $Re = 10^3$. The parameters of the plates were selected based on the data of the dynamic model. It follows from the simulation that frontal plates with optimal parameters contribute to enhancing the stability of the wake behind the body, which leads to a decrease in its instantaneous drag and lift. The mean drag coefficient of the modified rectangular prism calculated on temporal data is equal to about 0.85, which is 30% less than this value for the original prism (≈ 1.4). The effect of the plates on the amplitude of the lift coefficient is even more pronounced. In the presence of control plates, it drops by 3 times compared to the original rectangular prism, which indicates stabilization of the structure. An analysis of the longitudinal velocity field before the structure showed that the energy-consuming horseshoe vortex would move upstream if a pier with frontal ledges was used.

It was also obtained in this numerical experiment that an arbitrary choice of parameters of the control device can worsen the vortex situation around the structure and its dynamic characteristics not only in comparison with the optimal case, but also with the original rectangular. This fact demonstrates the importance of preliminary estimation of control scheme parameters using either numerical or physical experiment. It should be also noted that involving a simplified standing vortex model for the analysis allows reducing the settlement time for energy-consuming numerical simulation of the flow under consideration.

References

- [1] Gorban V and Gorban I 1998 *AGARD Report* vol 827 p 15
- [2] Gorban I and Khomenko O 2016 *Advances in Dynamical Systems and Control. Studies in Systems and Control* vol 69, ed V Sadovnichiy and M Zgurovsky p 327

Improvement of the aerodynamic performance using the developed method of energy-efficient flow control

N Yurchenko¹, P Vynogradskyy¹, R Pavlovskyy

¹Institute of Hydromechanics, National Academy of Sciences of Ukraine, Laboratory for Advanced Aerodynamics and Interdisciplinary Research, M.Kapnist St. 8/4, 03068 Kyiv, Ukraine

E-mail: nina.yurchenko@gmail.com

Abstract. Flow control is studied here using the developed strategy of near-wall flow structure generation with a given space scale. The proposed method of active flow control is based on the application of spanwise arrays of mechanical or thermal disturbers including plasma discharges. Aerodynamic coefficients are found for the 12.5% supercritical airfoil model controlled by the multi-discharge system. Measurements showed growth of a maximal lift coefficient by 8% and the stall angle by 2° accompanied by drag reduction.

Keywords: Aerodynamics, Experimental Fluid Mechanics, Interdisciplinary Research, Biological Prototyping, Flow Restructuring, Lift and Drag Coefficients.

1. Introduction

The idea of energy-efficient flow control was conceived from the studies of high-speed marine animals with their skin features thoroughly selected and polished by evolution [1]. Relevant engineering realizations were designed in the form of spanwise arrays of pointlike mechanical or thermal generators including plasma discharges. The multidisciplinary approach to investigations connecting biology with engineering and fluid dynamics with plasma physics showed itself very promising. It resulted in the development of new instruments for active flow control which appeared to be logical and energy-efficient [2, 3]. Its impact on aerodynamic performance was studied numerically and experimentally taking into account the correlation between basic flow and control parameters. Aerodynamic coefficients and pressure fields were measured for a number of models controlled by thermal grids and multi-discharge arrays of disturbers. Here measured lift and drag coefficients are discussed for models controlled by embedded spanwise-regular thermal grids and by arrays of pointlike plasma discharges generated over the model surface with varying electromagnetic parameters for various Reynolds numbers.

2. Spanwise-regular vortex-generators

Evolution-optimized features of living systems, e.g. the regular pattern of shark scale (Fig. 1, a), have long ago become attractive for engineers in terms of their copying and applications in technology. Skin-flow interaction of high-speed marine creatures is one of the points of interest that was used to develop riblet coatings (Fig. 1, b) which are proven to improve aerodynamic performance. Our development of this idea was implemented as arrays of mechanical vortex-generators (Fig. 1, c), the so-called “thermal

riblets”, a flush-mounted grid of longitudinal resistively heated elements [2] (Fig. 1, d), and further as the “virtual thermal riblets”, heated wakes downstream of the plasma array near a surface (Fig. 1, e).

Application of thermal riblets turned passive flow control by mechanical riblets into active control

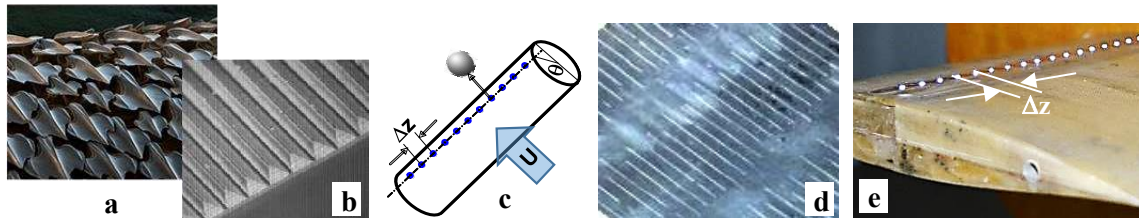


Figure 1. Spanwise-regular structure of the surface properties: shark scale (a), mechanical riblets (b), arrays of mechanical disturbers (c), embedded heated strips (d), and plasma discharges (e)

due to the possibility to vary spanwise temperature gradient in a process of system (d) operation and due to variation of electromagnetic parameters (intensity, frequency, duty cycle) in the (e) system. Measured lift and drag coefficients of a model revealed a possibility to improve the aerodynamic performance before the stall, i.e. for near-critical angles of attack for the (d) system [2].

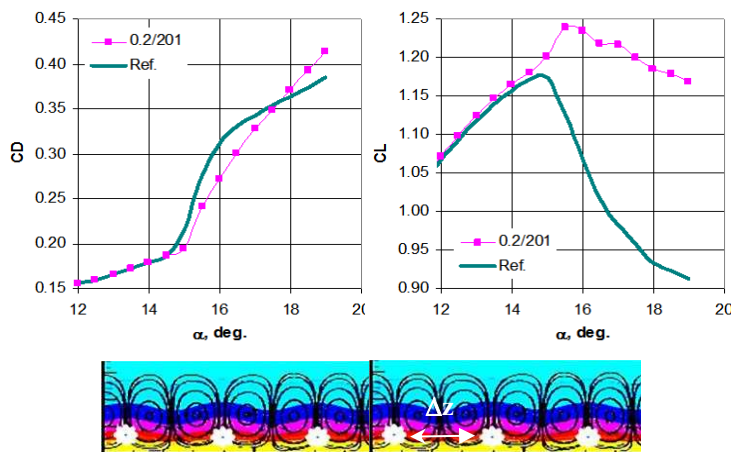


Figure 2. Drag and lift coefficients of an airfoil model controlled by pulsating plasma discharges with $\Delta z=10$ mm, red lines: $Re_x = 5 \times 10^5$; $F=200$ Hz; $\tau=150$ μ s.

Application of plasma discharges gives a possibility to reach a greater favorable impact [3, 4], Fig 2. This approach is also advantageous because

- it enables active and remote flow control depending on a way of energy deposition to plasma actuators;
- the control factor is applied directly to the flow maintaining the surface smooth;
- it is more flexible and versatile due to pulsating operation modes with several control parameters.

An adequate flow response to the scale of introduced disturbances supposes certain sustainability of the organized structure and its impact on

integral flow characteristics. The measure of plasma impact on the flow is found from the variation of the aerodynamic performance, lift and drag coefficients (Fig. 2). The conclusions are verified using analysis of the pressure field redistribution around a model as well as due to the numerical analysis of flow fields over the controlled models.

References

[1] N. Yurchenko, From Marine Animals to Plasma Aerodynamics, (*Invited lecture, AIAA SciTech 2016, 4–8 January 2016, San Diego*), 2016, *AIAA Paper 2016-1819, 8 pp.*
 [2] N. Yurchenko, Research strategy for active flow control based on distributed thermal fields. 2010, *Int. J. of Fluid Mechanics Research*, v. 57, No. 5, pages 470-489.
 [3] N. Yurchenko, P. Vynogradskyy, N Rozumnyuk, Parametric control of separated flows, 2013, *AIAA Paper-2013-0100.*
 [4] Nina F. Yurchenko, Conceptual approach to energy-efficient separation control. 2021, *Academia Letters*, 3 pp. <https://doi.org/10.12989/aas.2013.1.1.000>.

Experimental Methods

Integrated Approaches in Microfluidic Design for Enhanced Droplet Manipulation and Biological Insights

P M Korczyk¹, T Kurniawan¹, S Błoński¹, B Kupikowska-Stobba¹

¹Institute of Fundamental Technological Research, Polish Academy of Sciences, ul. Pawińskiego 5B, 02-106 Warszawa, Poland

E-mail: piotr.korczyk@ippt.pan.pl

Abstract. The Institute of Fundamental Technological Research's Microfluidic Laboratory is focused on enhancing the accuracy and practical use of microfluidic methods for chemical and biological studies, as well as creating tailored microfluidic instruments to address specific biological research needs. In this document, we present a few of our latest projects.

Keywords: Micro-, Nano- and Bio-flows, Multi-phase Flows, Droplets

1. Introduction

Microfluidics has rapidly evolved from its inception, becoming a vital interdisciplinary field that spans fluid mechanics at microscales and has myriad uses in biology, chemistry, and diagnostics [1]. Its allure lies in the ability to precisely control and manipulate fluid flows, achieved through the tiny dimensions of microchannels, the smooth, laminar flow characteristics [2], and the significant influence of surface tension in flows involving different phases [3]. Our research focuses on both single and multiphase flows.

2. Droplet microfluidics

Using more than one immiscible phase allows for the controlled formation [4] and manipulation of droplets in microfluidic channels. Each droplet can be a miniature reactor containing samples, reagents, or biological components.

Our research delves into the basic principles of two-phase flows within microchannels [4,5]. Utilizing the insights gained, we craft innovative microfluidic designs, such as for the passive handling of droplets [6,7] and sequential logic devices for meticulous droplet management [7,8]. These advancements allow for the execution of complex procedures intricately encoded within the layout of our microfluidic systems.

Additionally, we employ digital algorithms to precisely adjust concentrations by selectively merging and equally dividing droplets, enhancing our processes' accuracy, repeatability, and adaptability [9].

3. Applications in biomedical research

Confined geometry of microfluidic chambers and superior flow control renders this technology suitable for mimicking physiological conditions for culturing cells [10]. One of our lab's primary objectives is to tailor microfluidic devices to meet specific biological research needs. A notable achievement is developing a microfluidic system that precisely controls the generation of tension gradients through the deformation of epithelial layers, enabling a detailed study of tissue mechanics, including strain and curvature effects on epithelial responses.

In collaboration with the University Grenoble Alpes in France, this system's application has provided insights into how curvature influences the propagation of calcium waves caused by folding on short timescales and affects gene expression spatially over more extended periods [11]. Our findings reveal that gradients in cell shape and the mechanical stresses they induce lead to distinct biochemical responses across the tissue layer, offering new perspectives on cell differentiation mechanisms during tissue development.

Another example is a device developed in collaboration with the University of Oxford, designed to study erythrocytes' oxygen release rate [12]. Our microfluidic system with the medium exchange chamber was applied for an experimental method to monitor the oxygen flow in individual red blood cells, combining ultrarapid solution switching to manipulate gas tension with single-cell O₂ saturation fluorescence microscopy.

Recently, this approach has been used to investigate human kidneys perfused with stored blood during transplantation; the respiratory rate of the organ was measured [13]. The study challenges the conventional definition of oxygen delivery based on blood flow and oxygen content, highlighting its inadequate representation of blood efficiency in tissue oxygenation. However, the research uncovered a robust correlation between monitored kidney respiration and erythrocytes' oxygen release rate.

References

- [1] G.M. Whitesides, The origins and the future of microfluidics, *Nature* 442 (2006) 368–373.
- [2] K.W. Oh, K. Lee, B. Ahn, E.P. Furlani, Design of pressure-driven microfluidic networks using electric circuit analogy, *Lab Chip* 12 (2012) 515–545. <https://doi.org/10.1039/C2LC20799K>.
- [3] C.N. Baroud, F. Gallaire, R. Danga, Dynamics of microfluidic droplets, *Lab Chip* 10 (2010) 2032–2045.
- [4] P.M. Korczyk, V. van Steijn, S. Blonski, D. Zaremba, D.A. Beattie, P. Garstecki, Accounting for corner flow unifies the understanding of droplet formation in microfluidic channels, *Nature Communications* 10 (2019) 2528.
- [5] T. Kurniawan, M. Sahebdivani, D. Zaremba, S. Blonski, P. Garstecki, V. van Steijn, P.M. Korczyk, Formation of droplets in microfluidic cross-junctions at small capillary numbers: Breakdown of the classical squeezing regime, *Chemical Engineering Journal* 474 (2023) 145601. <https://doi.org/10.1016/j.cej.2023.145601>.
- [6] P.M. Korczyk, L. Derzsi, S. Jakiela, P. Garstecki, Microfluidic traps for hard-wired operations on droplets, *Lab Chip* 13 (2013) 4096–4102. <https://doi.org/10.1039/C3LC50347J>.
- [7] D. Zaremba, S. Blonski, M. Jachimek, M.J. Marijnissen, S. Jakiela, P.M. Korczyk, Investigations of modular microfluidic geometries for passive manipulations on droplets, *Bull. Pol. Acad. Sci.-Tech. Sci.* 66 (2018) 139–149.
- [8] D. Zaremba, S. Błonski, P.M. Korczyk, Integration of capillary–hydrodynamic logic circuitries for built-in control over multiple droplets in microfluidic networks, *Lab Chip* 21 (2021) 1771–1778. <https://doi.org/10.1039/D0LC00900H>.
- [9] D. Zaremba, S. Blonski, P.M. Korczyk, Concentration on demand – A microfluidic system for precise adjustment of the content of single droplets, *Chemical Engineering Journal* 430 (2022) 132935.
- [10] D.N. Breslauer, P.J. Lee, L.P. Lee, Microfluidics-based systems biology, *Mol. BioSyst.* 2 (2006) 97–112.
- [11] S. Blonski, J. Aureille, S. Badawi, D. Zaremba, L. Pernet, A. Grichine, S. Fraboulet, P.M. Korczyk, P. Recho, C. Guilluy, M.E. Dolega, Direction of epithelial folding defines impact of mechanical forces on epithelial state, *Developmental Cell* 56 (2021) 3222–3234.e6. <https://doi.org/10.1016/j.devcel.2021.11.008>.
- [12] J. Rabcuka, S. Blonski, A. Meli, S. Sowemimo-Coker, D. Zaremba, D. Stephenson, M. Dzieciatkowska, D. Nerguizian, R. Cardigan, P.M. Korczyk, P.A. Smethurst, A. D'Alessandro, P. Swietach, Metabolic reprogramming under hypoxic storage preserves faster oxygen unloading from stored red blood cells, *Blood Advances* 6 (2022) 5415–5428. <https://doi.org/10.1182/bloodadvances.2022007774>.
- [13] R. Dumbill, J. Rabcuka, J. Fallon, S. Knight, J. Hunter, D. Joyce, J. Barrett, M. Ellen, A. Weissenbacher, T. Kurniawan, S. Blonski, P.M. Korczyk, R. Ploeg, C. Coussios, P. Friend, P. Swietach, Impaired O₂ unloading from stored blood results in diffusion-limited O₂ release at tissues: evidence from human kidneys, *Blood* 143 (2024) 721–733. <https://doi.org/10.1182/blood.2023022385>.

Influence of micro- and mesoscale on the permeability characteristics of 3D printed porous objects

K Bukowski¹ and L Klotz¹

¹ Warsaw University of Technology, Faculty of Power and Aeronautical Engineering, ul. Nowowiejska 24, 00-665 Warszawa, Poland

E-mail: karol.bukowski.stud@pw.edu.pl

Abstract.

The study aims to deepen the understanding of fluid behaviour within porous media by examining the influence of different porosity structures on permeability and exploring the relationship between pressure gradients and flow efficiency. Hybrid structures combining micro- and mesoscales were created to assess their combined impact on fluid flow. Experimental data derived from measuring pressure gradients and flow velocities were used to calculate permeability coefficients according to the Darcy-Forchheimer law. The study introduces dimensionless flow efficiency coefficients, linking geometric characteristics of porous objects with their flow impact, revealing that hybrid structures exhibit superior flow efficiency. These findings contribute significantly to the field of porous media analysis, offering insights into optimizing industrial applications through an improved understanding of fluid flow dynamics.

Keywords: Experimental Fluid Mechanics, Darcy-Forchheimer Law, Micro- and Mesoscale Porosity, 3D Printing, Permeability Characteristics

1. Geometry models

The elementary cell used to create the microscale structure is the framework of a single truncated octahedron. This work conducted an analysis on only one microscale structure. The mesoscale porosity structure was created based on a fully filled sphere of a given diameter. The hybrid porosity structure was created based on a porous sphere, which was formed using the previously defined microscale and mesoscale structures. This study conducted an analysis of four different sphere diameters for both variants, namely with the spheres fully filled and with the presence of microscale porosity. The analysis of porous objects in this study is based on macro cubes created using the previously described porosity structures.

2. Permeability measurements

The experimental setup used in this research is detailed in the publication [1]. Figure 2 shows the measurement points, illustrating the relationship between the pressure gradient $\frac{\Delta p}{L}$ and the average velocity in the channel U , with polynomial approximations applied. Different colors and markers on the chart represent data for cubes with different porosity structures, as described in the legend. A division of curves into three groups was observed, corresponding to the different porosity structures applied. The highest pressure gradients were observed for the cube with

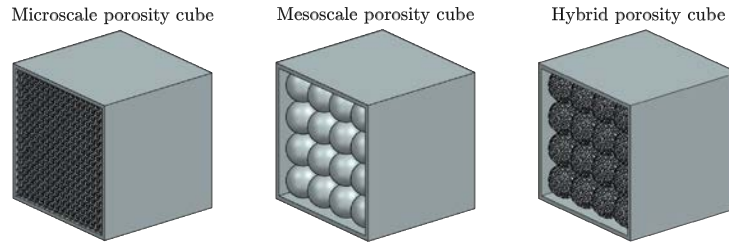


Figure 1. Porous objects used in the study. Example models for cubes with fully filled and porous spheres. The models of porous cubes were printed using DLP 3D printing technology.

microscale porosity structure, then for the cubes with full spheres, and the lowest for the cubes with porous spheres. In the case of cubes with full spheres, a dependency of the pressure gradient on the sphere diameter was noticeable – higher pressure gradients were observed for cubes with smaller spheres. However, no such dependency was observed for cubes with porous spheres.

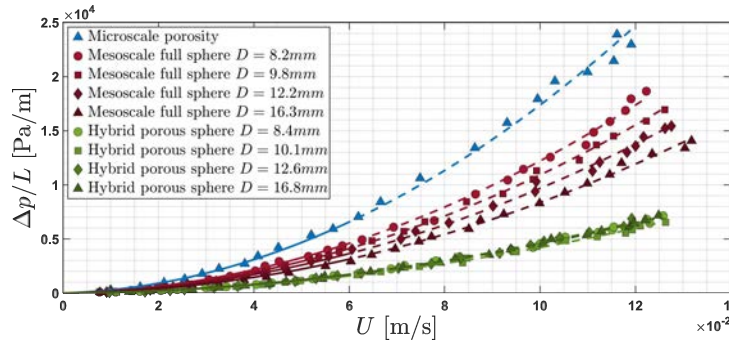


Figure 2. Measurement points of pressure gradient as a function of average velocity in the channel, for different porosity structures and sphere diameters.

3. Flow efficiency coefficients

The analysis of the presented permeability coefficients and geometric parameters enables the definition of dimensionless coefficients that link the geometric characteristics of the porous object and its impact on flow. These coefficients have been identified as combinations of the normalized surface area $\alpha[\frac{1}{m}]$ and the specific surface area $\sigma[\frac{1}{m}]$ with the permeability coefficients $\sqrt{k_1}[m]$ for the viscous component and $k_2[m]$ for the inertial component.

The flow efficiency coefficients provide insights into how effectively a porous object can interact with the fluid flowing through it, taking into account both its surface characteristics and flow dynamics. These coefficients are thoroughly explained in the work [2]. Cubes with hybrid porosity structure, combining features of porous and microscale structures, exhibit the highest values of the newly defined coefficients. The hybrid structure has high geometric parameter values, typical of the microscale structure, while maintaining low, or even lower than in the mesoscale structure, flow resistances.

References

- [1] W. Regulski et al. "Pressure drop in flow across ceramic foams — A numerical and experimental study". Chemical Engineering Science 137 (2015), p. 320–337.
- [2] K. Bukowski "Influence of micro- and mesoscale on the permeability characteristics of 3D printed porous objects". Bachelor Thesis under the supervision of L. Klotz at Warsaw University of Technology (2024) in Polish language

PIV measurement of model nuclear fuel rod bundle

D Duda¹, V Yanovych^{1,2} and V Uruba^{1,3}

¹ University of West Bohemia in Pilsen, Faculty of Mechanical Engineering,
ul. Univerzitní 22, 306 14 Pilsen, Czech Republic

² Výzkumný a zkušební ústav Plzeň s.r.o.,
ul. Tylova 1581/46, 301 00 Pilsen, Czech Republic

³ Czech Academy of Sciences, Institute of Thermomechanics,
ul. Dolejškova 1402/5, 182 00 Prague, Czech Republic

E-mail: dudad@fst.zcu.cz

Abstract. Particle Image Velocimetry (PIV) method is used to map the flow inside a model of nuclear fuel rod bundle of hexagonal symmetry. Four planes perpendicular to the flow are studied in distances $x = 1D, 2D, 3D$ and $5D$ past the mixing grid, here D is the fuel rod diameter. Reynolds number is $7.8 \cdot 10^4$ (which is still $3.3\times$ lower than the values in real reactor). Novel are the parabolic mixing vanes deflecting the fast flow from main channel (between 3 rods) into narrower part (between 2 rods).

Keywords: Experimental Fluid Mechanics, Nuclear reactor, Mixing grid, Particle Image Velocimetry, Wind Tunnel

1. Introduction

The fuel rods are organized in nuclear reactor of European and Russian types in regular hexagonal symmetry. A *spacer grid* keeps the rods in their positions; this grid is sometimes connected with *mixing grid*, which mixes the fluid between fuel rods in order to enhance the heat transfer and thus the reliability and effectiveness of the entire power plant. One of its possible configurations are the *mixing vanes*[3], which divert the flow from the main channel (between 3 rods) to its narrower part (between 2 rods), possibly even into the neighboring channel. The technical details of grids used in real nuclear power plants are top secret. Therefore, we designed and manufactured our own mixing grid in order to test the measuring methodology and to be able to share the interesting results with scientific community; a similar step has been done by Matozinhos et al.[2] but for rod bundle with square symmetry.

2. Experiment

Our mixing grid is scaled to the sizes of wind tunnel [4] of University of West Bohemia in Pilsen. The geometry is larger than the real one, the rods are not heated. Rod diameter $D = 50$ mm (in real nuclear reactor $D_R = 9.1$ mm), the rod spacing is $R_E = 67.1$ mm ($R_R = 12.2$ mm). Additionally, there are parabolic mixing vanes with deflection f growing with stream-wise distance x as $f(x) = f_m \cdot (x/h_l)^2$ where f_m is maximum deflection and h_l is the vane height. Vane orientation alters between diverging, orbiting and intermediate cell types; see the grid in Fig. 1(a). The fuel rods are modeled as empty sever tubes with black-colored ends to avoid

laser reflections. Working fluid is ambient air with high viscosity, therefore the Reynolds number reached in our model is only $Re_E \approx 7.8 \cdot 10^4$, while the real nuclear reactor VVER-440 reaches $Re_R \approx 2.6 \cdot 10^5$ due to low values of kinematic viscosity of pressurized warm water.

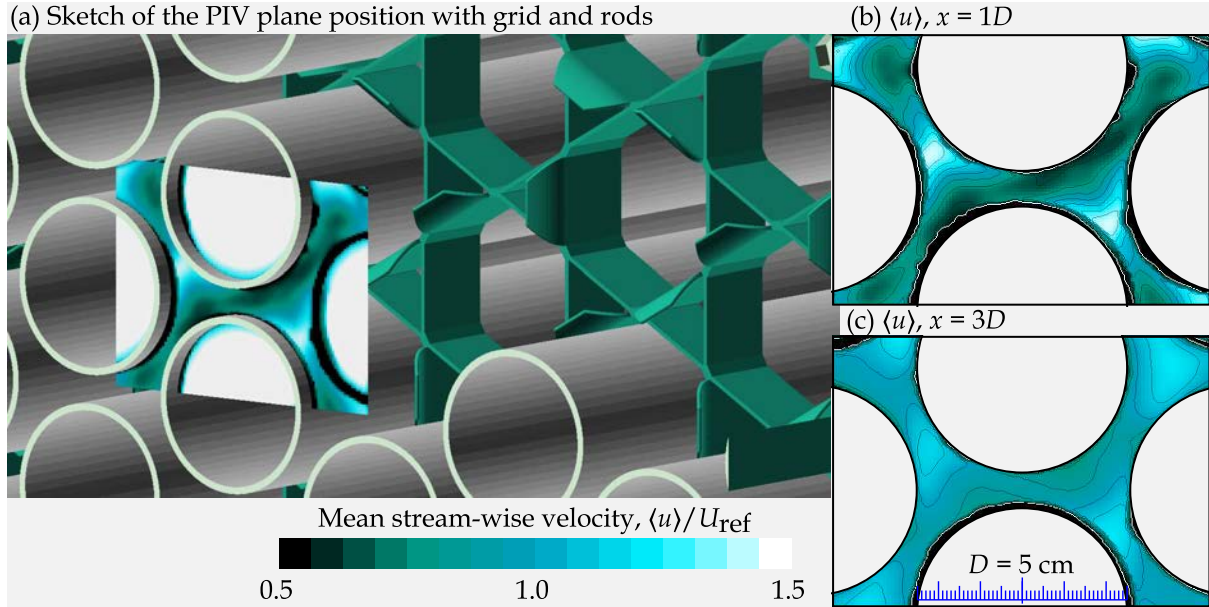


Figure 1. Sketch of the position of PIV measuring plane in respect to the mixing grid and model fuel rods – some of them are not plotted for sake of clarity. Panels (b, c) show example of ensemble-averaged stream-wise velocity component (perpendicular to the measured plane) in two distances past the grid. Velocity of the air $U_{ref} = 24\text{ m/s}$.

A flow field is measured in a plane 1 mm behind the end of the fuel rods normal to the flow by using the Stereo Particle Image Velocimetry (SPIV) method.

The mean field displays effective deflection of the faster flow into the narrower part of the channel, which remains in that location even in larger distances (see Fig. 1(b, c)). Turbulence decays [1] relatively fast and therefore one may expect uneven cooling of the fuel rods in dependence on distance from the mixing grid. The turbulence produced by boundary layers does not seem to enhance that in the main channel. Fluctuations are strongly anisotropic dominated by stream-wise component.

Acknowledgments

We acknowledge the project CANUT II of TAČR no. TN02000012.

References

- [1] D. Duda, V. Yanovych, and V. Uruba. An experimental study of turbulent mixing in channel flow past a grid. *Processes*, 8(11):1–17, 2020.
- [2] Camila F. Matozinhos, Gabriel C.Q. Tomaz, Thien Nguyen, André A.C. dos Santos, and Yassin Hassan. Experimental measurements of turbulent flows in a rod bundle with a 3-d printed channel-type spacer grid. *International Journal of Heat and Fluid Flow*, 85:108674, 2020.
- [3] Gergely Imre Orosz, Boglárka Magyar, Dániel Szerbák, Dániel Kacz, and Attila Aszódi. Allegro gas cooled fast reactor rod bundle investigations with cfd and piv method. *Nuclear Engineering and Design*, 400:112062, 2022.
- [4] V. Yanovych, D. Duda, V. Horáček, and V. Uruba. Research of a wind tunnel parameters by means of cross-section analysis of air flow profiles. *AIP Conference Proceedings*, 2189(020024), 2019.

Experimental Challenges of Nano and Microfluidics

T Kowalewski¹

¹Institute of Fundamental Technological Research, Polish Academy of Sciences, Department of Biosystems and Soft Matter, Pawinskiego 5B, PL 02-106 Warsaw, Poland

E-mail: tkowale@ippt.pan.pl

Abstract. The landscape of contemporary fluid mechanics experiments has evolved, increasingly focusing on micro- to nanoscale phenomena. This shift aims to elucidate the underlying mechanisms of living nature. At such scales, visualization methods have embraced novel and exciting approaches, some nearing the molecular limits where the traditional assumptions of continuity and determinism are challenged. Particularly at short time and length scales, diffusion governed by Brownian motion emerges as a predominant transport mechanism. While the analysis of ideal spherical objects in this context remains straightforward, comprehending the complex behaviour of elongated, deformable objects is considerably more intricate.

This abstract highlights experimental techniques that enable the monitoring and manipulation of individual microscale objects in flow. Utilizing a commercial Atomic Force Microscope (AFM) integrated with a confocal microscope, our system is enhanced by the addition of three lasers, beam shaping, and steering optics, forming the basis for optical tweezing. This setup not only facilitates the manipulation of small dielectric objects within fluids but also allows for precise displacement and force measurements with unprecedented resolution and accuracy within the same AFM scanning zone. This advancement significantly improves the force resolution capability of a standalone AFM and introduces a methodology to conduct experiments employing a hybrid double probe technique. This method holds considerable potential for applications in nanomechanics, molecular manipulation, and biological studies. We demonstrate the preparation of hydrogel nanofilaments via co-axial electrospinning, yielding highly flexible structures with defined mechanical properties. These nanofilaments' shape deformations and cross-stream migration in microchannel flow are observed to mirror those of long DNA strands, suggesting a novel experimental model for exploring the hydrodynamic behaviour of long biological molecules in fluid suspensions Nakielski et al. [1]. Through precise optical measurements and evaluation of hydrodynamic mobility, our model offers a microscale experimental framework that allows for the detailed investigation of mechanical properties of elastic hydrogel nanofilaments. These properties are assessed by analysing dynamic bending in shear flow and deformations induced by thermal fluctuations, with findings corroborated by AFM nanoindentation measurements Zembrzycki et al [2].

Keyword: Micro fluidics

References

- [1] Nakielski P, Pawłowska S, Pierini F, Liwinska V, Hejduk P, Zembrzycki KE, Zabost E. and Kowalewski, T.A. 2015, PLOS ONE 5, 10(6).
- [2] Zembrzycki K., Pawłowska S., Pierini F., Kowalewski T.A. 2023 *Polymers* 15 (3), 787-1-13.

Mapping the efficiency of a novel rotating arc-wall inline mixer

M. Kiwan¹, E. Younes², C. Castelain¹, T. Burghelca¹

¹ Nantes Université, CNRS, Laboratoire de thermique et énergie de Nantes, LTeN, UMR6607, F-44000 Nantes, France

² Okinawa Institute of Science and Technology, Japan

E-mail: mosbah.kiwan@univ-nantes.fr - eliane.younes94@outlook.com -
cathy.castelain@univ-nantes.fr - teodor.Burghelca@univ-nantes.fr

Abstract. This study investigates the application of laminar chaotic advection to improve mixing and heat transfer within an inline mixer–heat exchanger using viscous fluids. Employing different analysis methods on experimental data systematically allowed the analysis of the interplay between the degree of chaos and mixing. The results presented in this abstract contribute to a deeper understanding of the mixer’s efficiency and how chaotic advection can be manipulated and thus quantified.

Keywords: Experimental Fluid Mechanics, Measurement Techniques, Interdisciplinary Areas in Heat and Fluid Flow, Laminar Chaotic Advection, Viscous Fluids, Particle Image Velocimetry, Laser-Induced Fluorescence, Mixing Efficiency.

1. Introduction

Controlling the transport phenomena in fluids is a topic of increasing interest. The natural way of transport between fluids is through molecular diffusion, which may be inefficient due to the significant time required for the process. Alternative methods of transport employ additional mechanisms to enhance efficiency, such as generating turbulent flows. However, using turbulence for highly viscous fluids often results in substantial energy expenses [1]. Another way is by using chaotic advection, which is considered an effective method for mixing these fluids. Numerous chaotic advection mixers have been proposed [2], promoting both modes of transfer. A new inline mixer previously proposed in ref. [3] has been tested numerically for its efficiency spanning a wide range of control parameters in terms of the frequency of the perturbations versus the characteristic time of advection (Strouhal number, St) and the amplitude of rotation (k). Following that work, an experimental setup (see figure 1) has been built and tested using Newtonian viscous fluids in ref. [4] and provided some insights on the experimental validation of the efficiency map in ref. [3]. The complete validation of the efficiency map is yet to be done in the case of Newtonian and non-Newtonian fluids.

2. Present Work

The objective of the study is to quantify experimentally the degree of chaos and mixing properties for a large range of controlling flow parameters (Reynolds number (Re), Strouhal number (St),

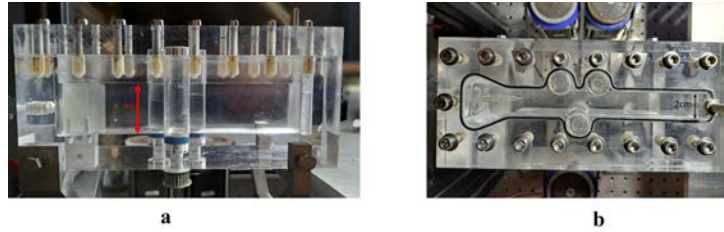


Figure 1. Representation of the mixer from (a) side view, (b) top view

amplitude of rotation (k). This allows us to understand the evolution of these two properties about each other, and to generate a map of these properties versus the different parameters. The new inline mixer "Rotating Arc-Wall mixer (RAW mixer)" is composed of a rectangular cross-section channel with an active mixing zone consisting of three rotating cylinders. These cylinders are positioned vertically, perpendicular to the direction of the flow. Velocity field measurements, obtained by the particle image velocimetry (PIV) method show different flow topologies (figure 2). Fluid trajectories computed with experimental velocity fields have allowed to evaluation of the residence time distributions, and finite-size Lyapunov exponents. The mixing of two fluids is quantified using mixing patterns obtained by the laser-induced fluorescence (LIF) technique. Some numerical preliminary results have shown that there exists an optimal combination between Re , St , and k to achieve the highest efficiency for mixing as indicated in the theoretical model in ref.[3]. Lagrangian and Eulerian experimental analysis results, such as the Finite-time Lyapunov exponent, residence time distributions, and space-time concentration distribution maps will be compared to the previous theoretical and numerical studies, and will allow to correlate the degree of chaos with the mixing properties.

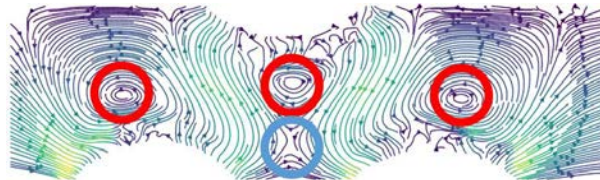


Figure 2. Flow streamlines at $t/T = 1.75$ for $St=0.4$ and $k=10$ showing elliptical points (red circles) and hyperbolic points (blue circle)

Acknowledgments

The authors would like to acknowledge Nantes University for funding Mosbah Kiwan's doctoral contract.

References

- [1] F. Raynal and J.-N. Gence, "Energy saving in chaotic laminar mixing," *International Journal of Heat and Mass Transfer*, vol. 40, no. 14, pp. 3267–3273, 1997.
- [2] H. Aref, J. R. Blake, M. Budišić, S. S. Cardoso, J. H. Cartwright, H. J. Clercx, K. El Omari, U. Feudel, R. Golestanian, E. Guillard, *et al.*, "Frontiers of chaotic advection," *Reviews of Modern Physics*, vol. 89, no. 2, p. 025007, 2017.
- [3] K. El Omari, E. Younes, T. Burghelea, C. Castelain, Y. Moguen, and Y. Le Guer, "Active chaotic mixing in a channel with rotating arc-walls," *Physical Review Fluids*, vol. 6, no. 2, p. 024502, 2021.
- [4] E. Younes, Y. Moguen, K. El Omari, T. Burghelea, Y. Le Guer, and C. Castelain, "Experimental study of chaotic flow and mixing of newtonian fluid in a rotating arc-wall mixer," *International Journal of Heat and Mass Transfer*, vol. 187, p. 122459, 2022.

Flow Control and Optimization

LES of flow dynamics downstream of new type bluff bodies

L Caban¹, A Wawrzak¹, A Tyliczszak¹ and D Thévenin²

¹ Czestochowa University of Technology, Faculty of Mechanical Engineering and Computer Science, al. Armii Krajowej 21, 42-201 Czestochowa, Poland

² Otto von Guericke University Magdeburg, The Laboratory of Fluid Dynamics and Technical Flows, Universitätsplatz 2, 39106 Magdeburg, Germany

E-mail: lena.caban@pcz.pl

Abstract.

This study focuses on flow dynamics downstream of cylindrical and star-shaped bluff bodies with flat, convex, and concave surfaces. The star-shaped geometry alters the formation of large vortical structures observed behind typical cylindrical bluff bodies. It induces the appearance of tiny vortices, which intensify the mixing process. We analyze to what extent this shape combined with an inclination of the upper bluff body surface modifies the flow behavior in its closest vicinity and how it affects the size and position of the recirculation zone formed downstream.

Keywords: Computational Fluid Dynamics, Flow Control, Mixing Enhancement

1. Introduction

Passive flow control methods, although lacking the dynamic adjustability of active methods, offer distinct advantages in optimizing flow dynamics within specific regimes. They demonstrate cost-effectiveness and energy efficiency by employing passive control elements or shaping of flow domains. These benefits are particularly desirable in combustion applications, where improved aerodynamics contributes to the reduction of pollutant emissions. A prominent example of passive control relies on embedding specially designed bluff bodies in injector systems of combustion chambers. The bluff body serves as the flame holder, ensuring stable combustion by creating a recirculation zone behind it. The bluff body shape significantly impacts the dynamics of the flame, its size, position, and maximum temperature [1]. For typical cylindrical geometries, the periodic occurrence of toroidal vortices intensifies the mixing processes while widening the flame. The acute parts added to the geometry produce small-scale flow phenomena that enhance mixing in the shear layer formed between the recirculation zone and the oxidizer stream.

In the present study, the impact of bluff body shape on the flow dynamics is investigated based on a bluff body burner set-up similar to the one used in [2]. We modify the basic shape as shown in Fig. 1 and consider the original cylindrical geometry and star-shaped bluff body [1] with concave and convex surfaces. The aim of this research is to analyze whether the inclination of the bluff body surface changes the size and position of the recirculation zone and to what extent such a modification affects the mixing process influencing the NO_x generation. The computations

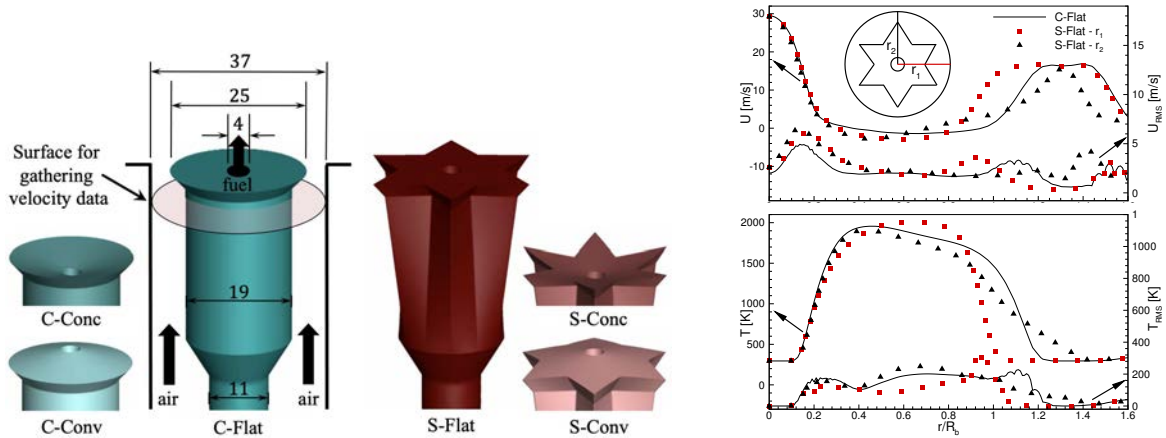


Figure 1. Bluff body geometries (left). Profiles of mean and RMS axial velocity (U , U_{RMS}) and temperature (T , T_{RMS}) along radii r_1 and r_2 at location $y/D_b = 0.5$ (right).

are performed applying the Large Eddy Simulation method involving ANSYS Fluent and an in-house high-order code SAILOR [3]. In the first stage, the ANSYS Fluent is used to model the flow around complex bluff body shapes and to generate a time-varying velocity signal slightly below the oxidizer channel exit (transparent surface in Fig. 1). The stored velocity signal is used as the boundary condition imposed on the inlet plane of the Cartesian computational domain for the second stage of the computations carried out with the help of the SAILOR code.

2. Results

The differences in velocity and temperature distributions downstream of cylindrical and star-shaped bluff bodies with flat surfaces are depicted in Fig. 1. It is evident that for the S-Flat configuration, in the region $r/R_b > 0.3$, the low-velocity region is narrowed, and the minimum velocity is smaller compared to the C-Flat case. Above the oxidizer duct ($r/R_b > 1$), although the maximum velocities are similar, significant differences are observed in the velocity distribution. Depending on the radius along which the results are presented, the velocity profile varies, being either flat or narrow with local maximum. Substantial differences are also noted in velocity fluctuations. In the case of the S-Flat bluff body, distinctly higher U_{RMS} values are observed. Regarding temperature profiles, elevated temperatures for the S-Flat configuration are found in the region $0.6 < r/R_b < 0.9$. Along the radius r_1 , the maximum temperature is approximately 200 K higher. Additionally, T_{RMS} values near $r/R_b = 1.0$ are higher than in the C-Flat case. This may lead to high thermal stresses damaging the bluff body. We investigate to what extent the inclining of its surface prevents contact with a flammable mixture.

Acknowledgments

This work was supported by the National Science Center in Poland (Grant No. 2020/39/B/ST8/02802). The computations were carried out using the PL-Grid Infrastructure and the Poznan Supercomputing and Network Center.

References

- [1] Wawrzak A, Caban L, Tyliczszak A and Mastorakos E 2023 *Appl. En.*, submitted.
- [2] Kypraiou A, Giusti A, Allison P M and Mastorakos E 2018 *Exp. Therm. Fluid Sci.* **95** 81–87.
- [3] Tyliczszak A 2016 *Comput. Fluids* **127** 131–145.

Machine learning-supported CFD optimization of heat transfer in a pipe with a corrugated wall shape

P Kamiński¹, Y Li², K Wawrzak¹, A Tyliczszak¹ and BR Noack^{2,3}

¹ Department of Thermal Machinery, Częstochowa University of Technology, al. Armii Krajowej 21, 42-201 Częstochowa, Poland

² Chair of Artificial Intelligence and Aerodynamics, School of Mechanical Engineering and Automation, Harbin Institute of Technology, 518055 Shenzhen, P.R. China

³ Guangdong Provincial Key Laboratory of Intelligent Morphing Mechanisms and Adaptive Robotics, Harbin Institute of Technology, 518055 Shenzhen, P.R. China

E-mail: piotr.kaminski@pocz.p1

Abstract. This paper focuses on identifying the optimal wall corrugation of a heated pipe to maximize heat transfer while minimizing pressure losses. The corrugation is characterized by a multi-parameter function, enabling extensive variations in wall shape. The optimization process utilizes an innovative topology-assisted method, iteratively working alongside a high-order numerical code. The immersed boundary method is employed to simulate the wall on a structured mesh. Initial findings reveal substantial variations in both the pressure drop coefficient and temperature distribution, depending on the type of corrugation employed.

Keywords: Computational Fluid Dynamics, Machine Learning, Heat Transfer, Optimization

1. Introduction

Studying the flow and heat transfer within a pipe is essential for optimizing heating or cooling processes in injection devices, heat exchangers and heat pipes [1]. Various techniques can be employed to augment heat transfer, among them the alteration of a wall surface through waviness is often used [2]. This particular form of wall corrugation proves effective in enhancing the mixing process, which intensifies heat exchange. In existing literature, the most prevalent and extensively researched type of wavy walls is the regular sinusoidal shape, primarily due to its ease of production. However, recent advancements in 3D printing and manufacturing processes allow for the consideration of significantly more complex configurations. In this study, we propose a novel irregular corrugation type that involves sharpening the waviness and tilting them in either the streamwise or counter-streamwise direction.

2. Problem statement

The objective of the research is to optimize the shape of the corrugated pipe walls (see Fig. 1) to obtain the maximum heat transfer at a minimum pressure drop. The corrugation is defined using an iterative formula given as:

$$r^0(x) = A_{1,2}(n) \times \sin\left(x \frac{2\pi N}{L_w}\right), \quad r^{i+1}(x) = A_{1,2}(n) \times \sin\left(x \frac{2\pi N}{L_w} + \frac{r^i}{s}\right) \quad (1)$$

where $A_1(n)$ and $A_2(n)$ represent the corrugation amplitudes for radii $r(x) > 0$ and $r(x) < 0$, N stands for the number of periods along L_w , n denotes the period index, s is a parameter defining the tilt, and I denotes the number of iterations ($i = 0, 1, 2, \dots, I$). The corrugated wall becomes less smooth when I increases.

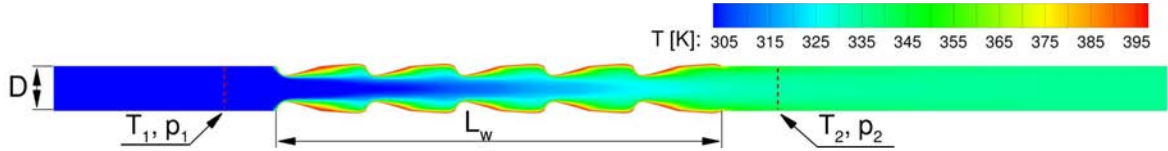


Figure 1. Temperature distribution in the pipe. The central section (L_w) is heated.

3. Results

The simulations are conducted for Reynolds numbers $Re = U_{in}D/\nu = 650 - 4000$, where U_{in} represents the inlet velocity, D denotes the inlet pipe diameter, and ν is the kinematic viscosity. The inlet temperature is fixed at $T_{inlet} = 300$ K, while the corrugated walls maintain a temperature of $T_{wavy} = 400$ K. Downstream, the walls are treated as adiabatic. The optimization process will be performed by employing a topology-assisted method [3] working in a loop with a high-order SAILOR [4] code. The heated wall segment is embedded into the computational domain via the immersed boundary method.

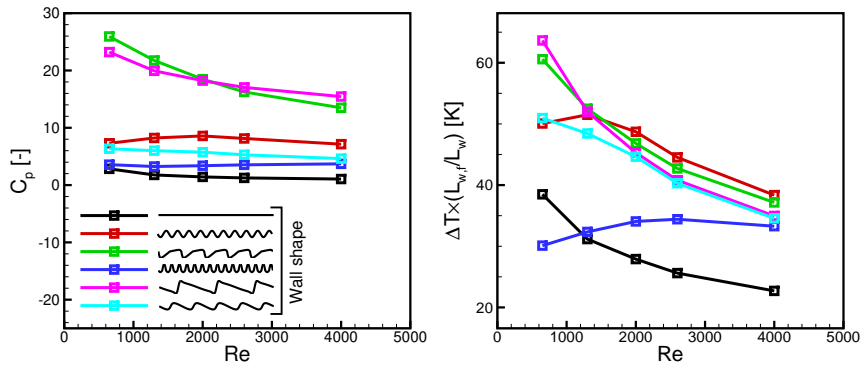


Figure 2. Pressure drop coefficient (left) and downstream temperature increase $\Delta T L_{w,f}/L_w$.

The preliminary results are presented in Fig. 2. They show the pressure drop coefficient $C_p = |p_2 - p_1|/0.5\rho U_{in}^2$ and $\Delta T = T_{2,ave} - T_{1,ave}$, normalized by a ratio of the flat wall and corrugation lengths ($L_{w,f}/L_w$). A strong dependence on the wall shape and Re is evident, particularly for low Re values. Both ΔT and C_p display nonlinear changes with Re that complicates the optimization procedure. The number of control parameters equals 5 (see Eq. 1). The optimization entails their adjusting assuming the cost function based on C_p and ΔT .

Acknowledgments

This work is supported by the National Science Center in Poland (Grant 2020/39/B/ST8/01449).

References

- [1] Mameli M et al. 2014 *International Journal of Thermal Sciences* **75** pp. 140-152.
- [2] Bazdar H et al. 2020 *Journal of Thermal Analysis and Calorimetry* **139** pp. 2365-2380.
- [3] Wang T et al. 2023 *Physics of Fluids* **35** no. 5.
- [4] Tyliczszak A 2014 *Journal of Computational Physics* **276** pp. 438-467.

Airfoil design in separated ultra-low Reynolds flows using a shear stress-based inverse design method

Z Drafsh¹, M Nili-Ahmadabadi^{1*} and MY Ha^{2*}

¹ Isfahan University of Technology, Department of Mechanical Engineering, Isfahan, Iran

² Pusan National University, School of Mechanical Engineering, Busan, South Korea

E-mail: m.nili@iut.ac.ir, myha@pusan.ac.kr

Abstract. Pressure-based inverse design (ID) methods encounter convergence challenges in separated flow regimes. In this research, a shear stress-based ID method was developed for airfoil design at $Re = 1000$ including separation. NACA 4404 airfoil was considered as the initial geometry and its wall shear stress distribution was modified with three distinct approaches at optimum and stall angles of attack. The resulting geometries obtained through ID exhibited drastic changes, leading to a significant enhancement in aerodynamic performance. As a result, the lift-to-drag ratio increased by 16%.

Keywords: Aerodynamics, Shear stress-based inverse design, Ultra-low Reynolds, Airfoil

1. Introduction

Pressure-based ID methods determine the geometry corresponding to a target wall pressure distribution. Safari et al. [1] innovated the Elastic Surface Algorithm (ESA) for the ID of airfoils, in which the airfoil wall is modeled as an elastic bent beam. The difference between the target and current pressure distribution causes the geometry to deform until reaching its final shape when the difference becomes zero [1]. Pressure-based ID methods in separated flows often become unstable in convergence [2]. Noorsalehi et al. [2] developed the ESA for airfoil ID at high-Reynolds external flows with separation, incorporating a linear combination of pressure and shear stress as the target flow parameter. In ultra-low Reynolds flows, separation persists even at the optimal angle of attack, posing a significant challenge for ID in this flow regime. Therefore, this research upgrades the ESA by exclusively utilizing the wall shear stress distribution for airfoil ID in ultra-low Reynolds flows ($Re = 1000$) at $AOA = 7^\circ$ and 11° .

2. Shear stress-based ESA method

In the shear-stress-based ESA method, the difference between the current and target Shear Stress Distributions (SSD) is utilized instead of the pressure difference for correcting the flexible airfoil wall (elastic beam), as illustrated in Fig. 1(a). The geometry correction process, outlined in the flowchart in Fig. 1(b), continues until the convergence criterion for the shear stress difference is met. The deflection of the beams is calculated by solving the finite-element equations of the Timoshenko beam. Subsequently, the wall shear stress distributions for the corrected geometries are computed using Fluent 2022R2.

3. Results and Discussion

Figure 2 displays three designed airfoils and the NACA4404, along with corresponding wall shear stresses on the upper and lower sides. Designs 1 and 2 were executed at $AOA = 7^\circ$, while Design 3 was conducted at $AOA = 11^\circ$, all with separation. In Design 1, modifications were applied only to the upper side, whereas in Designs 2 and 3, both sides underwent modifications. The visual representation highlights that even minor alterations in shear stress resulted in significant changes in geometry, indicating a considerable design space when shear stress is employed for corrections. Figure 3 compares the performance characteristics of the three designed airfoils and the NACA4404. Despite Design 3 being optimized for $AOA = 11^\circ$, its performance showed improvements across all angles of attack.

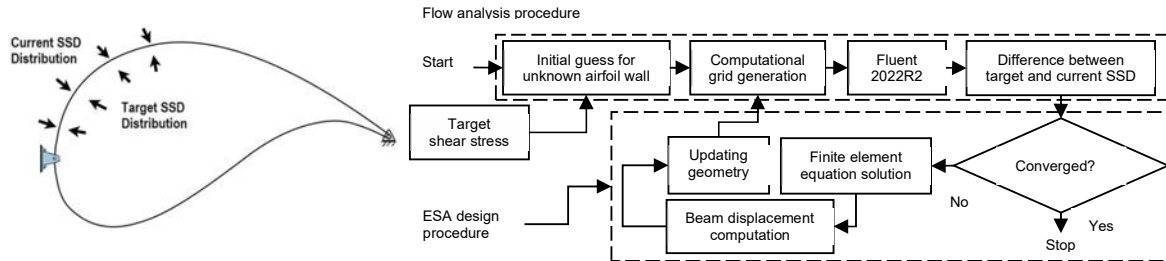


Figure 1. (a) Schematic of the beam used for the airfoil, (b) Flowchart of the shear stress-based ESA ID.

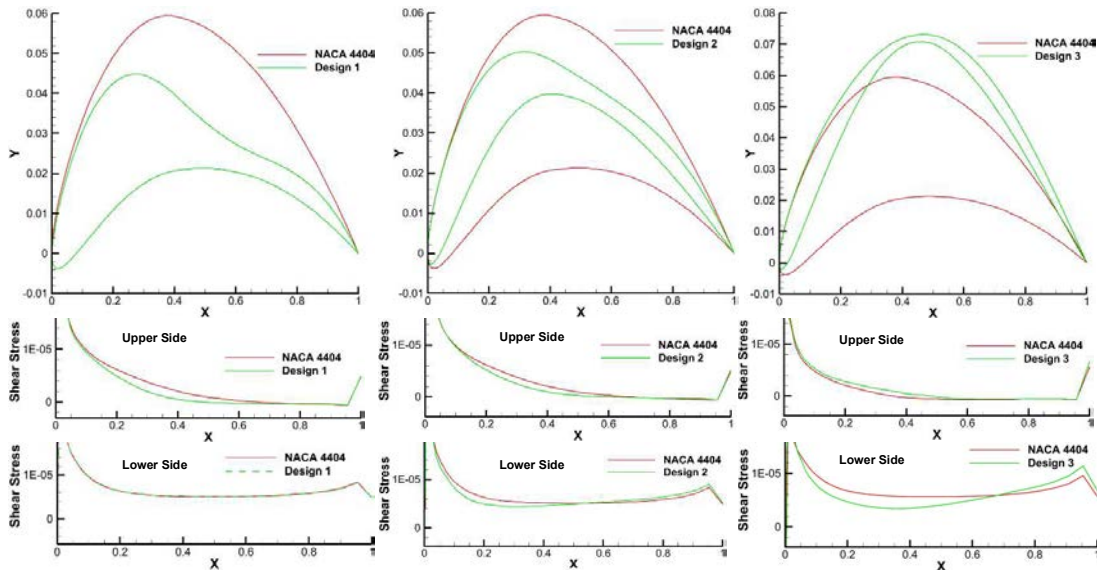


Figure 2. Three designs and NACA4404 with corresponding wall shear stresses on the upper and lower sides.

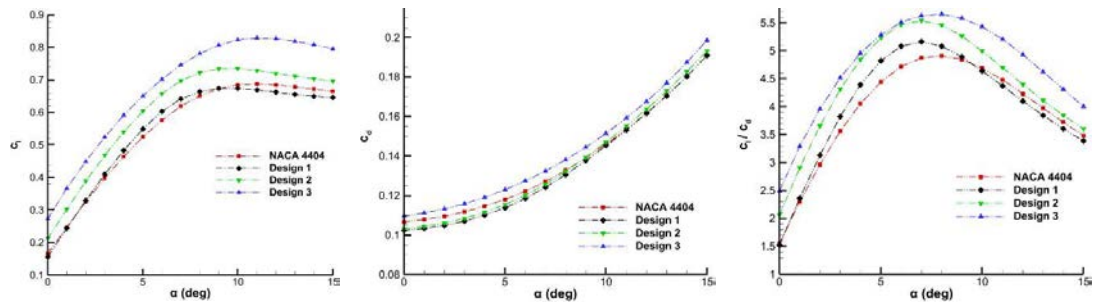


Figure 3. Comparison of performance characteristics of three designed airfoils and NACA4404.

Acknowledgements

This research was supported by the Brain Pool program funded by the Ministry of Science and ICT through the National Research Foundation of Korea (No. NRF-022H1D3A2A02063642).

References

[1] Safari M., Nili-Ahmadabadi, M., Ghaei, A., and Shirani, E., "Inverse design in subsonic and transonic external flow regimes using Elastic Surface Algorithm", *Computers & Fluids*, vol.102, pp. 41-51, 2014.
 [2] Noorsalehi M.H., Nili-Ahmadabadi M., and Kim K. C., "Inverse shape design method based on pressure and shear stress for separated flow via Elastic Surface Algorithm", *Inverse Problems in Science and Engineering*, vol.29, pp. 2357-2400, 2021.

Box-spline parameterisation of motion kinematics in aerodynamic optimisation of flapping motion

M Rutkowski¹ and Ł Łaniewski-WoŃk¹

¹ Warsaw University of Technology, Faculty of Power and Aeronautical Engineering, ul. Nowowiejska 24, 00-665 Warszawa, Poland

E-mail: mariusz.rutkowski@pw.edu.pl

Abstract. Purpose of the research was to propose simple yet efficient way of imposing the limitations of derivatives in motion optimisation for flapping flight. That was also made to explore ability to control the derivatives without creating additional penalty functions.

In previous work, the results of which are compared to proposed method, authors choose to represent the motion with B-spline. Optimising densely distributed B-spline nodes without a constraint on the values of their neighbours can yield unrealistic results.

The results of the optimisation and the comparison with the previous work showed that it was possible to increase the control over the derivatives of the solution. This makes it possible to increase the number of optimisation nodes and therefore manipulate the trajectory of the wing in places previously inaccessible. The work presented here holds the promise of solving the problem at relatively low cost.

Keywords: Computational Fluid Dynamics, Lattice-Boltzmann Method, Optimisation, Biomimetic flight

1. Introduction

In the current work, authors wanted to focus on parameterisation of motion kinematics. This is the next step in an attempt to create the efficient tools for study phenomena of biomimetic flight and develop optimal aerodynamic performance for such propulsion.

In the literature, concerning flutter motion, we can distinguish several approaches to the parameterisation of motion. The first and the most commonly selected is the description of the motion using finite Fourier series [1, 2, 3]. By appropriately choosing the number of terms of the series, it is possible to reproduce the complex motion. The disadvantage of this approach is high sensitivity to high gradients and the occurrence of the Gibbs effect [4]. Another way is to create the kinematics of motion using an interpolating function [5, 6]. In this case, the interpolation nodes are parameters of the motion. In this method, the authors of the experimental work [4] hit the problem of possible high gradients between points in the optimization process. Next type of parameterisation of flapping motion worth mentioning is the modal reconstruction based on proper orthogonal modal decomposition (POD) of many previously known trajectories [4].

In authors' previous work [6], flapping motion was represented by B-spline interpolation. That approach gave, smooth, high order, trajectory of wing motion. However, with B-spline, one is limited with density of nodes. The small number of nodes makes it so that a single value determines a large portion of the trajectory. On the other hand, optimisation of a large number

of parameters could give unrealistic values. Result will be optimal but it will not be reproducible in reality [4].

In the present work, the authors propose to use Box-Spline interpolation [7, 8, 9].

2. Method and results

One way of constructing box-spline interpolation is based on the idea of convolutions:

$$Z(t) = (f_1 * f_2 * \dots * f_n)(t) * g(t), \quad (1)$$

where $Z(t)$ is n degree spline, $f_i(t)$ are rectangular step functions with integral equal to 1.0 and $g(t)$ is set of interpolation nodes with constant separation α . It can be noted that, when all rectangle functions, $f(x)$, in equation (1) have the same width α , it is simply description of univariate, cardinal B-splines, used in authors' previous work.

This type of interpolation has important properties that meet the requirements set:

- Convolution cannot exceed over limits of smoothed function.
- Assuming the most extreme case, when there is a function $g(t)$ that $g[t + \frac{\alpha}{2}] = \max(g)$ and $g[t - \frac{\alpha}{2}] = \min(g)$, convolution prevents derivative from exceeding over certain limits. The user is able to impose design constraints related to subsequent motion derivatives, such as instantaneous maximum power.

To summarise, with this approach it is possible to impose design constraints related to motion and subsequent motion derivatives, such as instantaneous maximum power.

Results of proposed methodology are compared with B-spline approach. The impact of the introduction of constraints on the optimised trajectories is noticeable.

Acknowledgments

This research was supported in part by PLGrid Infrastructure [grant number clb2023].

References

- [1] van Schroyen Lantman, M. P., Fidkowski K. (2013) *21st AIAA Computational Fluid Dynamics Conference*, AIAA 2013-2848.
- [2] Corban, B., Bauerheim, M., Jardin, T., (2023) *Journal of Fluid Mechanics* vol 974
- [3] So, H. K., Jo, T. H., Lee, Y. H., Kim, J. S., Han, J. H., Koo, B. C., Lee, D. H. (2016), *Journal of computational fluids engineering* Korea Society for Computational Fluids Engineering.
- [4] Busch, C., Gehrke, A., Mulleners, K. (2022) *Experiments in fluids*, vol 63, p 10.
- [5] Gehrke, A. and Mulleners, K. (2021) *Bioinspir. Biomim.* 16 026016
- [6] Rutkowski, M., Gryglas, W., Szumbariski, J., Leonardi, C., Laniewski-WoHk, L. (2020). [?] 79.
- [7] Arge, E., Dæhlen, M., Tveito, A., (1992) *Journal of Computational and Applied Mathematics* vol 44, issue 3
- [8] de Boor, C., Höllig, K., Riemenschneider, S.(1993) *Springer-Verlag* New York
- [9] Entezari, A., Nilchian, M., Unser, M., *IEEE Transactions on Medical Imaging* vol. 31, no. 8, pp. 1532-1541

Multiphase Flows and Complex Fluids

Collision efficiency of cloud droplets considering electrostatic and hydrodynamic interactions

A Michel^{1,2}, B Rosa^{2,3} and A Ababaei²

¹ Laboratoire de Modelisation et de Simulation à l'échelle Système (LMSF), CEA de Saclay, 91191 Gif-sur-Yvette, France

² Institute of Meteorology and Water Management – National Research Institute, Podleśna 61, 01-673 Warsaw, Poland

³ Department of Applied Mathematics, Warsaw University of Life Sciences (SGGW), Nowoursynowska 166, 02-776 Warsaw, Poland

E-mail: antoine.michel@cea.fr

Abstract. Gravitational collision efficiency of two droplets falling in viscous air has been computed accounting for electrostatic interaction. Different levels of realism were considered, from the simplest, i.e. Coulomb's forces only, to the more accurate one based on an analytical solution for two charged dielectric spheres of finite sizes. The study is conducted for three radii of the larger droplet (collector: $a_1 = 10, 20, 30 \mu\text{m}$) relevant to cloud physics, and for radius ratios $0 < a_2/a_1 < 1$. The results have been compared with the case where only aerodynamic interaction are included. Electrostatic interaction is found to strongly impact the collision efficiency for smaller collector droplets when polarization effects are accounted for and droplets carry opposite sign electric charges.

Keywords: Multi-phase Flows, Collision efficiency, Electrostatics, Aerodynamic interaction.

1. Introduction

Droplet growth by collision-coalescence is a key process leading to drizzle onset and rainfall initiation in warm clouds [1]. In a quiescent environment, the collision rate is mainly driven by the differential settling velocity between droplets. Thus, this mechanism favors collisions between droplets of different sizes. The development of reliable numerical weather prediction models and parametrizations usable for mesoscale simulations however requires an accurate description of the small-scale processes leading to precipitation formation.

The rise of computational power has brought significant insight into the underlying microphysical processes of clouds. These processes depend on the droplet inertia, and are additionally affected by the velocity perturbation induced by their relative motion, i.e. aerodynamic interactions, and by electrostatic forces for charged droplets. All these effects modify the trajectories of nearby droplets and consequently change the collision rate. In the present study, Lagrangian point-particle simulations are conducted to investigate the influence of these interactions on the collisions of small droplets settling in a quiescent viscous fluid. The relative contribution of these two interactions and their influence on the collision efficiency is analyzed.

2. Results and discussion

Fig. 1 presents the values computed for collision efficiency of settling droplets. This quantity is the ratio of the collision rate relative to the reference case of non-interacting droplets (i.e. no electrostatic force or aerodynamic interaction). The reference case, marked by “LUB”, only accounts for aerodynamic interaction force considering *lubrication effects* [2]. The other three cases additionally account for the electrostatic interaction, which are valid for widely separated point particles (Coulomb’s law), for conducting finite-size particles (e.g. metal) and for dielectric particles (e.g. water) and include short-range polarization effects [3, 4]. No significant change in the collision efficiency is visible when Coulomb’s law is employed, except at $a_2/a_1 > 0.95$, indicating a minor influence of the electrostatic interaction. In contrast, the collision efficiency increases when polarization effects are accounted for, especially when the droplets carry different-signed charges. The enhancement is more pronounced for small collector droplets of 10 and 20 μm and occurs for a wide range of radius ratios. These results highlight the influence of the attractive force induced by polarization effects on charged particles to promote collisions and enhance spectral broadening in clouds.

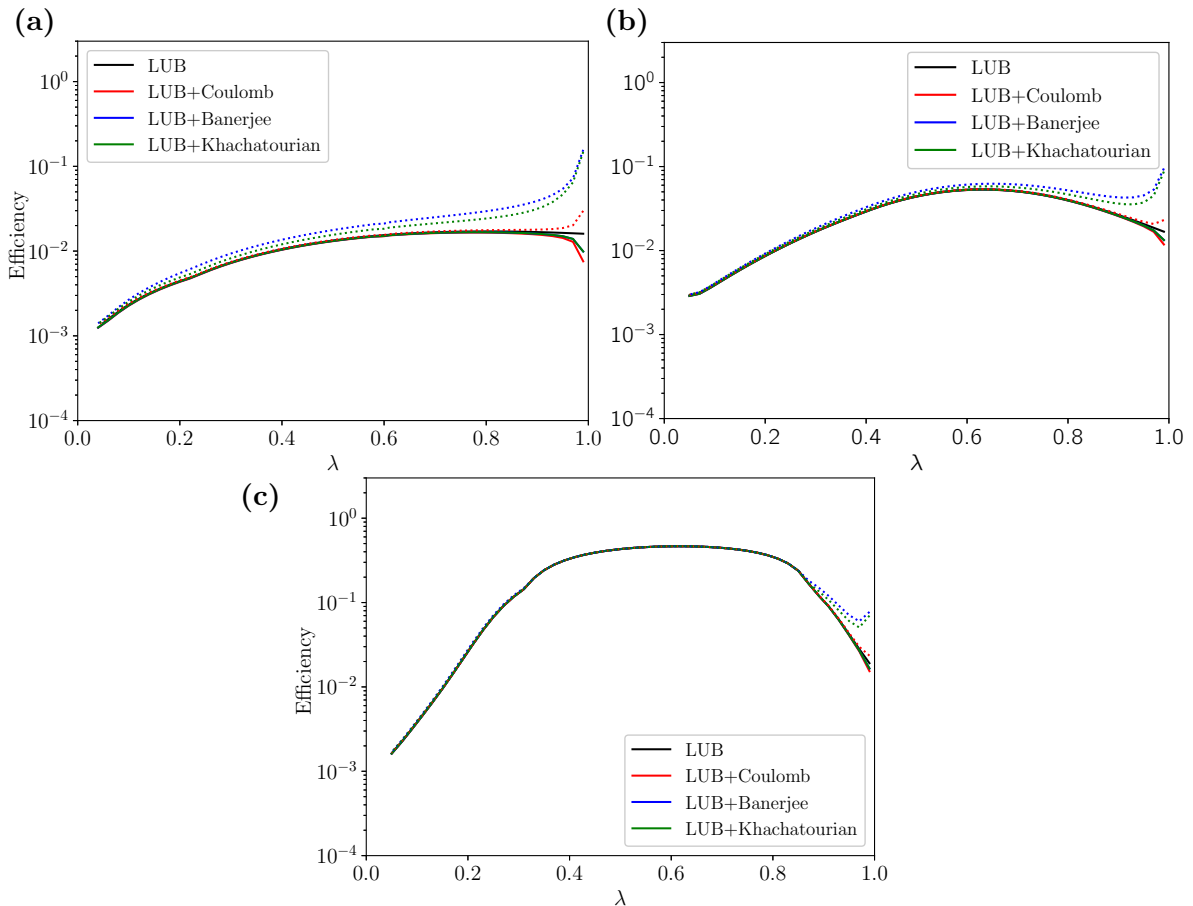


Figure 1. Collision efficiency as a function of $\lambda = a_2/a_1$ for water droplets falling in air. Collector droplet of radii (a) 10 μm , (b) 20 μm , and (c) 30 μm having same-sign (solid lines) as well as opposite-sign (dotted lines) charges - computed using Twomey’s formula [5].

References

- [1] Grabowski W W and Wang L P 2013 *Annu. Rev. Fluid Mech.* **45** 293–324.
- [2] Jeffrey D J and Onishi Y 1984 *J. Fluid Mech.* **139** 261–290.
- [3] Banerjee S, Peters T, Brown N and Song Y 2021 *Proc. R. Soc. A.* **477** 20200866.
- [4] Khachatourian A, Chan H K, Stace A J and Bichoutskaia E 2014 *J. Chem. Phys.* **140** 074107.
- [5] Twomey S 1956 *Tellus* **8** 445–452.

Enhancing numerical resolution of statistical phase-field method

T Waclawczyk

Warsaw University of Technology, Faculty of Power and Aeronautical Engineering,
ul. Nowowiejska 24, 00-665 Warszawa, Poland

E-mail: tomasz.waclawczyk@pw.edu.pl

Abstract. This work concerns modification of the conservative phase-field method equations based on the statistical model of interphase region (SMIR). In spite of the interphase region model formulation, adopting the best features of the sharp and diffuse interface models, it contains one cumbersome property. Namely, a problem with representation of tails of the cumulative distribution function (c.d.f.). We show this is caused by the finite precision of the computers. To overcome the aforementioned difficulty and extend a domain where the statistical phase-field method can offer predictions, this problem is outlined and its solution is proposed.

Keywords: Multi-phase Flows, Computational Fluid Dynamics, Numerical Methods

1. Introduction

To model dynamics of two-phase separated flow additional equation(s) governing the evolution of the interphase/interface region are solved [1, 2]. For this task, the sharp interface methods use the discontinuous phase indicator function $0 \leq H(\mathbf{x}, t) \leq 1$ and/or the signed distance function $-\infty \leq \psi(\mathbf{x}, t) \leq \infty$ where $|\nabla\psi| \equiv 1$. $\psi(\mathbf{x}, t)$ is used to localize regularized phase indicator function $0 \leq \tilde{H}(\psi) \leq 1$ that is changing its value from zero to one on two or four grid cells [2]. In [3, 4] inspired by the experiment [5], the present author put forward the statistical model of the interphase region (SMIR) enabling clarification and expansion of the applicability of the sharp interface models [6]. For example, [3] shows that the sharp interface models can be derived as the case of the SMIR diffuse interface model where the local width of the interphase region $\epsilon_h \rightarrow 0$. The key to these results is statistical interpretation of order parameters

$$\alpha_1(\psi_1) = \frac{1}{1 + \exp(-\psi_1/\epsilon_h)} \quad \text{or} \quad \alpha_2(\psi_2) = \frac{1}{1 + \exp(-\psi_2/\epsilon_h)}, \quad \psi_1 = -\psi_2 \quad (1)$$

obtained as the analytical solution to the stationary re-initialization equation(s), where $\epsilon_h \sim \Delta x$ and $\psi_1(\alpha_1) = \epsilon_h \ln[\alpha_1/(1 - \alpha_1)]$ is the signed distance function. In [3, 4] it is recognized that $\alpha_1(\psi_1)$ is c.d.f. and $\psi_1(\alpha_1)$ is quantile of the logistic distribution. From the mathematical definition of c.d.f. we know: $0 < \alpha_1 < 1$ for all real numbers and $\lim_{\psi_1 \rightarrow -\infty} \alpha_1 = 0$, $\lim_{\psi_1 \rightarrow \infty} \alpha_1 = 1$.

2. The problem description

To guarantee a correct implementation of SMIR, the mapping between $\alpha_1(\psi_1) - \psi_1(\alpha_1)$ has to work in the whole domain. However, the term $(1 - \alpha_1)$ is present in the mapping function to

obtain ψ_1 and the term $\alpha_1(1-\alpha_1)$ is in the re-initialization equation [3]. Figure 1 explains, that the numerical representation of α_1 does not satisfy the mathematical definition of c.d.f. The error occurs when falsely $\alpha_1=1$ at the distance $\psi_1 > 64\Delta x$ due to insufficient number of digits in double precision representation of variable used to store α_1 field, this impairs $\alpha_1(1-\alpha_1)$, too.

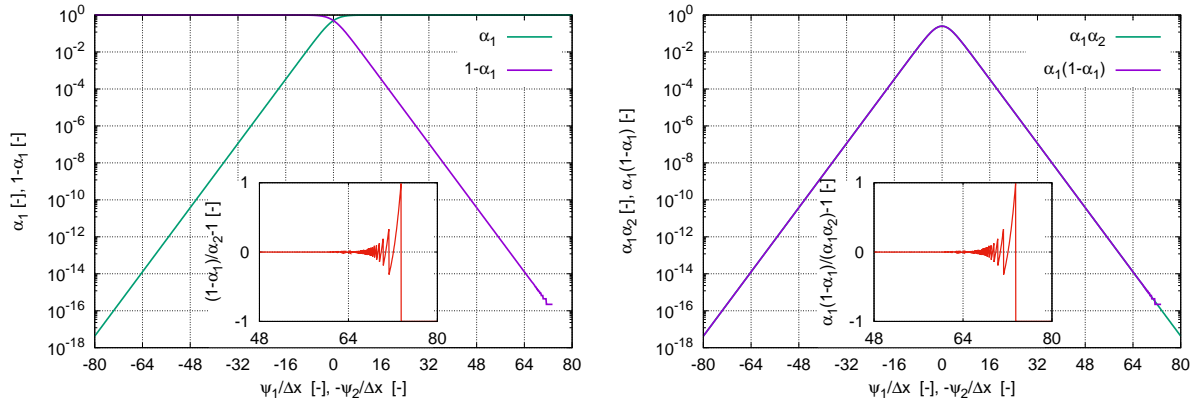


Figure 1. In the whole domain: $\alpha_1 + (1-\alpha_1)$ should be equal 1 (left), $\alpha_1\alpha_2$ and $\alpha_1(1-\alpha_1)$ should be the same, too (right). Due to errors in numerical representation of α_1 , they are not.

3. Modification of SMIR equations

As it is depicted in Figure 1 and explained in the previous section, the main task when improving the formulation of the transport and re-initialization equations of SMIR using the c.d.f. α_1 is to remove from the equations terms containing the difference $(1-\alpha_1)$. This can be done only by introduction of the new transport and re-initialization equations for α_2 leading to the set of equations equivalent to the original formulation. To resolve above issue, we propose to solve two advection and two re-initialization equations for α_1 and α_2 in the form

$$\frac{\partial \alpha_1}{\partial t} + \nabla \cdot (\mathbf{u}\alpha_1) = 0, \quad \frac{\partial \alpha_2}{\partial t} + \nabla \cdot (\mathbf{u}\alpha_2) = 0, \quad (2)$$

$$\frac{\partial \alpha_i}{\partial \tau} = \nabla \cdot [\alpha_i \alpha_j (|\nabla \psi_i| - 1) \mathbf{n}_i], \quad i, j = 1, 2 \quad i \neq j \quad (3)$$

where \mathbf{u} is known velocity field, t , τ denote, respectively, physical and fictitious re-initialization time, the signed function(s) is/are computed from the mapping $\psi_i = \epsilon_h \ln(\alpha_i/\alpha_j)$ and the normal vector $\mathbf{n}_i = \nabla \psi_i / |\nabla \psi_i| = -\mathbf{n}_j$ where $i, j = 1, 2$ and $i \neq j$. Such formulation of the transport and re-initialization equations avoids numerical error coming from the finite number (in double precision 16) significant decimal digits used to store the variables representing α_1, α_2 fields. Presented herein modification of the statistical phase-field method equations, provides the possibility to solve the problem of advection and re-initialization of the order parameter(s) $\alpha_i(\psi_i)$ up to the round-off precision. Detailed analysis of numerical solutions to Eqs. (2) and (3) in the case of (non-)equilibrium two-phase flow is the new contribution of the submitted work.

References

- [1] Tryggvason G and Scardovelli R and Zaleski S 2011 *Direct Numerical Simulations of Gas-Liquid Multiphase Flows* (Cambridge University Press)
- [2] Osher S and Fedkiw R 2003 *Level Set Methods and Dynamics Implicit Surfaces* (Springer Verlag, NewYork)
- [3] Waclawczyk T 2017 *Int. J. Multiphase Flow* **90** p 60.
- [4] Waclawczyk T 2020 *Int. J. Multiphase Flow* **134** 103459.
- [5] Aarts L and Schmidt M and Lekkerkerker W 2004 *Science* **304** 5672.
- [6] Waclawczyk T 2022 *Act. Mech. Sin.* **38** 722045

Interaction of liquid droplets with microstructured and nanostructured surfaces

N Kizilova¹

¹ Warsaw University of Technology, Faculty of Power and Aeronautical Engineering, ul. Nowowiejska 24, 00-665 Warszawa, Poland

E-mail: nataliya.kizilova@pw.edu.pl

Abstract. Micro/nanostructured solid surfaces are promising for modern and future technologies but there is no a unique solution for their mechanical design and optimization due to enormous number of materials, surface geometries and their combinations. The nature-inspired approach is very helpful due to high efficiency of the double-scale micro- and nano- structured surfaces with unique physical properties in plants and animals. In this study a detailed review of the natural and engineered surfaces and their properties based on both experimental and theoretical data is given. A novel approach to quantitative estimation of surface energy of the non-uniform surfaces with double roughness based on the Gibbs energy minimization and the grand potential are presented. The generalized Young and Young-Laplace laws for the non-uniform non-smooth surfaces are derived.

Keywords: Interdisciplinary Areas in Heat and Fluid Flow, Liquid Droplet, Contact Angle.

1. Introduction

Interaction of liquid droplets with solid surfaces is determined by their surface energy γ that is defined as the excess energy per unit area of the interface between the solid and liquid phases [1]. Recently the engineered surfaces with double micro- and nano roughness have been intensively studied due to their unique physical properties as superhydrophobicity, icephobicity, heat insulation and strength [2,3]. Since the combined micro- and nano-structured surfaces are abounding in nature, their geometry is widely used in the nanotechnologies as a nature-inspired biomimetic design but its efficiency must be substantiated by the nanoscale solid mechanics, fluid dynamics and thermodynamics that is an interdisciplinary approach [1]. The surface energy γ of the solid material is defined by the contact angle θ at the solid-liquid and gas interface, while the definition of γ was introduced for smooth uniform surfaces only but for non-uniform rough surfaces its determination is still discussed. In this study a detailed literature review on the biomimetic double-scale micro/nanostructured surfaces taken from animals, fish, insects and plants is presented, and the physical mechanisms underlying their unique mechanical properties are analyzed.

2. Materials and method

The dataset of θ measured on the solid surfaces (metal alloys, polydimethylsiloxane, silicone, etc.) with different types of roughness was analysed and systematized [2,3].

Thermodynamic characterization of the surfaces with micro/nano roughness based on minimization of the free Gibbs energy G of the surface

$$G = \sum_{i,j} \gamma_{ij} A_{ij} + \sum_{i,j,k} \kappa_{ijk} L_{ijk} + C, \quad (1)$$

where γ_{ij} , A_{ij} are the surface energy and surface area of the interface between the i -th and j -th phases, L_{ijk} is the length of the three-phase contact line (CL) and κ_{ijk} is the line tension introduced by Gibbs, C is the surface- and line independent part; the approach corresponds to the physical state characterized by given temperature, pressure and the number of particles $\{T, P, N\}$.

Another approach based on the grand potential $\Psi = \sum_i p^i V^i + G$ [1] minimization was used and compared to the Gibbs energy theory (1). Direct computations of G and Ψ on the surfaces of known double-scale design (Fig.1) with 120 different geometries were carried out.

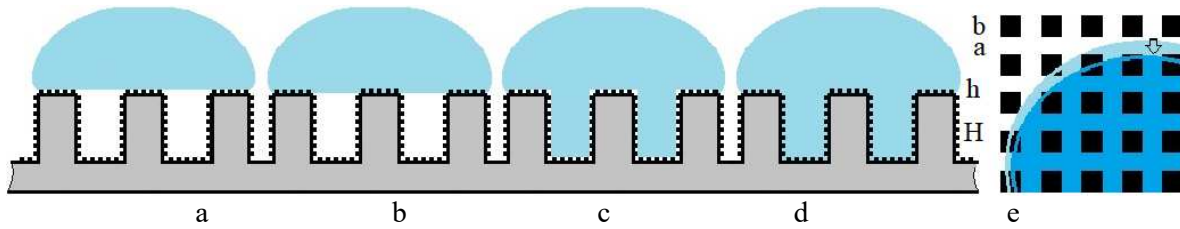


Figure 1. A liquid droplet on the surfaces with double roughness in the micro/nano-Cassie (a), micro-Cassie/nano-Wenzel (b), micro-Wenzel/nano-Cassie (c) and micro/nano-Wenzel (d) states, and the top view of the surface (e).

3. Results and conclusion

The Gibbs approach (1) gives a generalized expression of the classic Young's law $\cos \theta = (\gamma_{sg} - \gamma_{sl}) / \gamma_{lg}$, where the subscripts $\{s,l,g\}$ relate to the solid, liquid and gas phases, to the non-uniform rough surfaces in the form $\cos \tilde{\theta} = f(\theta, A_{sl}, A_{gl}, L_{sgl})$, where $\tilde{\theta}$ is the mean contact angle along the CL. Depending on the materials and $\{a,b\}$ values for the microscale (Fig.1e) and nanoscale roughness, the value G could be lower for different states (Fig.1a-d). Therefore, the droplet in the initial metastable state (Fig.1a) could move into the microscale (Fig.1c), nanoscale (Fig.1b) or both (Fig.1d) roughness. The obtained generalized expression for the Young's law allows direct consideration of the design optimization problem by minimization of the Gibbs energy $G(a,b) \rightarrow \min$.

In a similar way, the grand potential based approach gives a generalized Young-Laplace law

$$\frac{p^l - p^g}{\gamma_{gl}} = \frac{1 + \kappa(1 - \psi)}{H(1 - \varepsilon(1 - \psi))} F(\theta, \gamma_{sl}), \quad (2)$$

where $\varepsilon = h/H$, $\psi = A_{sl}/A$ is the surface porosity, κ is the surface roughness.

Numerical computations on (2) for the materials and geometries studied in the experiments [2,3] demonstrated a very good correspondence. It is shown, the surface energy of the rough surface with double roughness can be very low (the contact angles $\tilde{\theta} > 155^\circ$ at $\theta \sim 100-120^\circ$) when a proper geometry $\{a,b,h,H\}$ is used. The developed theory will be very useful for design optimization of the water repelling, anti-icing and heat insulating coatings.

References

- [1] Bedeaux D, Kjelstrup S and Schnell S 2024 *Nanothermodynamics. Theory and Applications* (Singapore: World Scientific)
- [2] Atthi N, et al. 2020 *Microelectronic Engin* 224 111255
- [3] Atthi N, et al. 2011 *J Nanosci Nanotechnol* 11 8967

Impact of pipe inclination on fill height for partially filled pipes used in a custom slurry transport rig

A Bose¹, D J Borman², T N Hunter³, J T Spencer⁴ and C J Cunliffe⁵

¹ CDT Fluid Dynamics, School of Computing, University of Leeds, Woodhouse Lane, Leeds, LS29JT, UK

² School of Civil Engineering, University of Leeds, Woodhouse Lane, Leeds, LS29JT, UK

³ School of Chemical & Process Engineering, University of Leeds, Woodhouse Lane, Leeds, LS29JT, UK

⁴ National Nuclear Laboratory, Chadwick House, Birchwood Business Park, Warrington, Cheshire, WA3 6AE, UK

⁵ National Nuclear Laboratory, Havelock Rd, Workington, Cumbria, CA14 3YQ, UK

E-mail: scabo@leeds.ac.uk

Abstract. Fill-height is a crucial factor for partially filled pipes transporting solid particles where the depth of the water influences solid particle transport. This study investigates the impact of pipe inclination on the fill-height ratio over a range of Reynolds numbers through the use of unsteady VOF-RANS simulations performed in OpenFOAM. The fill-height ratio vs. Re curves for a range of pipe inclinations are compared to experimental observations as well as those predicted from the Manning equation. It is shown that the fill-height ratio vs. Re curve agree well with experiments.

Keywords: Multi-phase flows, CFD, VOF model, Partially filled pipe flows, Fill-height ratio, Pipe inclination, Manning equation, OpenFOAM

1. Introduction

Air-liquid two-phase flows have applications in many areas of industry, including chemical processing, drainage systems, mining operations and pipeline facilities where water or other liquids are transported in partially filled pipes. The presence of the air phase changes the dynamics of the system compared to filled pipes, mainly because of induced secondary currents¹. Previous works on two-phase partially filled pipe flows have focused on air pocket effects on pressure surges and other air-water interactions during rapid filling^{2,3}, heat transfer in rotating pipes⁴ and the influence of wall roughness on velocity distribution⁵. Despite the notable work, there are limited studies that consider CFD modelling to investigate the impact of pipe inclination on the fill-height (d) in industrial settings. Fill height (d) is particularly important in industrial cases where partially filled pipes transport liquids with suspended solid particles and where the depth of the water influences solid particle transport⁶.

The objective of this study is two-fold, firstly to investigate the air-water two-phase flow in a custom industrial pipe that is part of a slurry transport rig used by the National Nuclear Laboratory⁶, and secondly, to determine the effectiveness of an unsteady RANS CFD Volume of Fluid (VOF) approach to predict fill-height at different pipe inclinations for a range of flow rates and associated hydraulic Reynolds numbers (Re)⁶.

2. Methodology

The multiphase solver *interFoam* in OpenFOAM is utilized to conduct unsteady RANS turbulent two-phase air-water flow simulations using the k - ϵ RNG turbulence model. Water enters into a 12 m pipe system of diameter, $D = 0.0762$ m. The pipe has an initial vertical drop of 0.5 m from the inlet and then moves through an approximate right angle to the gently inclined region as shown in Figure 1(a). Mass flow rates ranging between $\dot{m} = 0.5$ kg/s to 2.5 kg/s and pipe inclinations ranging between 1% and 5% are simulated. The predicted results (taken at 9m along the pipe) are compared with the experimental results of those from Cunliffe et al.⁶ along with those predicted by the Manning equation⁶ for a smooth pipe ($n=0.009$).

3. Results

The flow reaches a steady state after around 25 s. The flow approximately reaches a fully-developed state in the working section of the pipe, with small undulations along the length of the free surface. By nine meters along

the pipe, the amplitude of the undulations is mostly negligible. Fill-heights in the study are observed between 32.13% and 67.37% for 1% slope. Figure 1(a) shows the 3D isosurface of the water-free surface colored by velocity magnitude at 50 s for mass flow rate of 0.8 kg/s and 1% slope. The working section of the pipe is broken into two parts, 1) initial 1.2 m and 2) last 1 m for results presentation. Figure 1(b) shows the volume fraction of water (in red) and air (in blue) on a 2D plane sliced through the middle of the 3D pipe along its length. The effect of pipe inclination on fill-height ratio (d/D) with Hydraulic Reynolds number can be seen in Figure 1(c). Here the CFD results are compared to the Cunliffe et al.⁶, where for the increasing pipe inclinations it is observed the expected reduction in fill-height. The CFD results are in good agreement with the experimental results and the Manning equation.

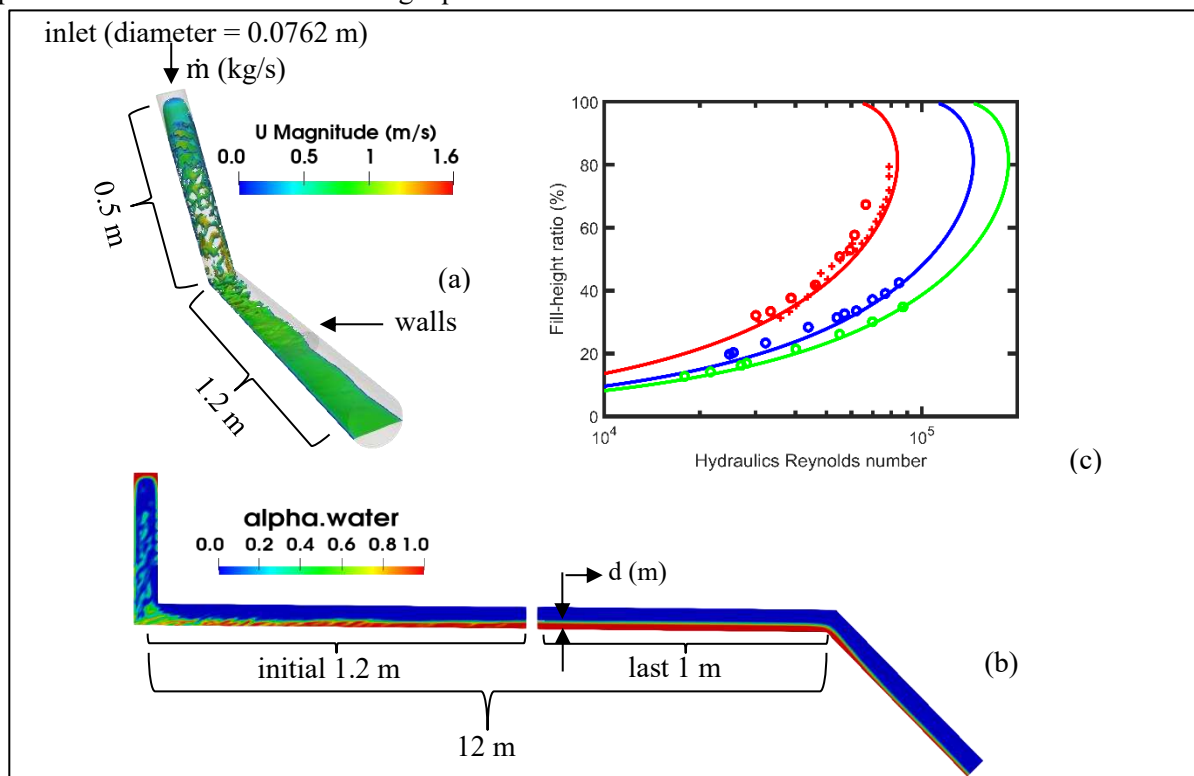


Figure 1. a) Isometric view of pipe arrangement showing 3D isosurface coloured by velocity magnitude at 50 s, b) water level (in red) on a 2D pipe cross section for mass flow rate of 0.8 kg/s and inclination of 1% at 50 s, c) predicted fill height ratio (%) vs hydraulic Reynolds number for pipe inclinations of 1%, 3% and 5% alongside experimental results⁶. (red = 1%, blue = 3%, green = 5%). Circles represent CFD predictions, pluses represent experimental results and solid lines are Manning equation⁶ ($n=0.009$).

3. Conclusion

The VOF CFD results agree well with both the experimental results and are in line with those predicted by the Manning equation for a smooth pipe. These results will be useful for informing the next phase of our work where particle-laden flow transport will be included in the CFD analysis inside the same geometry.

4. Acknowledgements

We gratefully acknowledge the use of the HPC facilities of the University of Leeds and the EPSRC and the National Nuclear Laboratory, UK for their support.

References

- [1] Liu Y, Stoesser T and Fang H 2022 *Journal of Fluid Mechanics* v 938 p A16
- [2] Zhou L, Liu D and Ou C 2011 *Engineering Applications of Computational Fluid Mechanics* v 5 p (127-140)
- [3] Huang B, Fan M, Liu J and Zhu D 2021 *World Environmental and Water Resources Congress* p (495-507)
- [4] Chatterjee S, Sugilal G and Prabhu S 2018 *International Journal of Heat and Mass Transfer* v 123 p (867-878)
- [5] Alihosseini M and Thamsen P 2019 *Technische Mechanik-European Journal of Engineering Mechanics* v 39 p (113-124)
- [6] Cunliffe C J, Dodds J M and Dennis D J.C. 2021 *Chemical Engineering Science* v 235 p 116465

Droplet surfing on a boundary layer - origin of droplet shape oscillation

M Klamka¹ and T Bobinski¹

¹ Warsaw University of Technology, Faculty of Power and Aeronautical Engineering, ul. Nowowiejska 24, 00-665 Warszawa, Poland

E-mail: michal.klamka@pw.edu.pl

Abstract. Droplets interacting with air boundary layer produced by moving solid surfaces may levitate due to pressure distribution beneath the droplet. In certain range of flow velocity the shape of the droplet starts to be time-dependant. We perform numerical simulations of a laminar regime flow to analyze the resulting aerodynamic forces rendered by the interaction of a droplet with a boundary layer and investigate the flow field with Particle Image Velocimetry to reveal the origin of droplet shape oscillations.

Keywords: Experimental Fluid Mechanics, Computational Fluid Dynamics, Multi-phase Flows, Micro-flows

1. Introduction

Droplet contact with a surface is essential to many industrial applications in which liquid is applied on a surface as a spray, e.g. painting, cooling, or washing. Non-wettable properties can be observed for surfaces when heat exchange is introduced to such a system, as presented in [1], where vapour cushion generated beneath the droplet prevents direct contact with the surface (Leidenfrost phenomenon). At ambient temperatures, altering the system's dynamics can provide a similar effect [2, 3]. Moving a surface immersed in a fluid generates a boundary layer that may prevent contact between the droplet and a surface. Such levitation can be obtained in low- and high-velocity regimes (Fig.1a,b). In a specific velocity range, the droplet levitation becomes unsteady, and oscillation of droplet shape (Fig.1c) is observed [4]. The origin of this phenomenon remains unexplored.

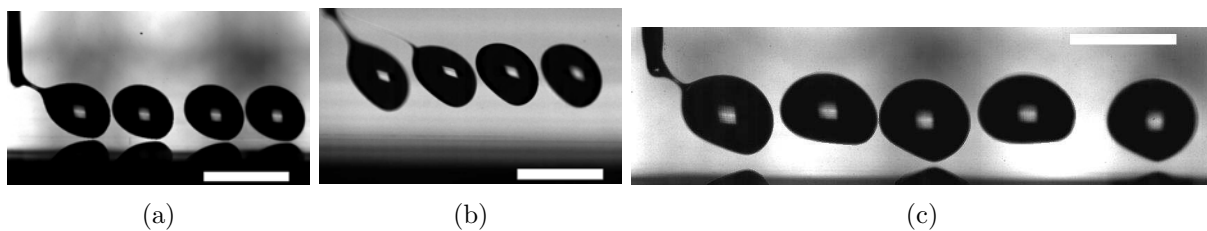


Figure 1: Droplet shape during levitation in: (a) laminar regime, (b) turbulent regime, (c) oscillatory droplet levitation in laminar boundary layer with spiral vortices [4].

2. Goals

In this research, we focus on describing the flow around a droplet. We explore the interaction between the base flow of the rotating disk and a droplet levitating over the disk surface. We explore base flow modifications due to droplet presence and the consequences on the resulting aerodynamic force acting on a droplet. In particular, we explain the origin of the droplet's shape oscillations during levitation. We analyse flow instabilities and their consequences on the pressure distribution acting on a droplet.

2.1. Numerical simulations

In the computational fluid dynamics approach, we solve fully developed flow over a rotating surface in a wide range of rotation speeds. We consider a low-velocity regime where the boundary layer remains laminar. The droplet is introduced as a rigid body model into the base flow. The droplet's shape is derived based on high-speed camera footage taken during experimental work [4]. We employ the finite volume method implemented in ANSYS Fluent environment to solve the governing set of equations.

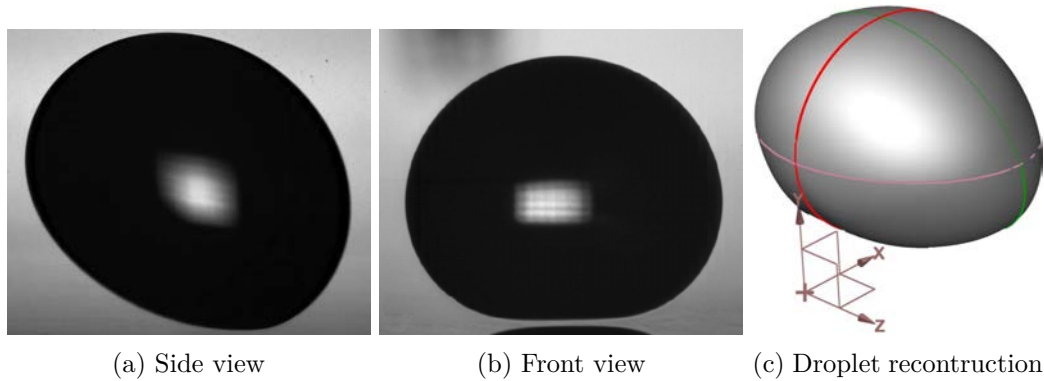


Figure 2: Rigid-body model of a droplet based on front and side photographs

2.2. Experiments

In the experimental approach, we investigate the velocity field in the wake behind a silicone oil droplet levitating on a boundary layer above a rotating disk with Particle Image Velocimetry. We employ a Photron SA-5 high-speed camera and an Nd-YAG high-power pulse laser. We introduce seeding in the form of tiny oil droplets $O(10\mu\text{m})$. We derive the velocity field in the horizontal and vertical plane in the wake behind the droplet. We analyze the outcome of the interaction between the droplet and base flow above the disk.

Acknowledgments

Research was funded by the Warsaw University of Technology within the Excellence Initiative: Research University (IDUB) programme. TB was supported by the Foundation for Polish Science (FNP) and Polish Ministry of Science and Higher Education.

References

- [1] D. Quéré, “Leidenfrost dynamics,” *Annual Review of Fluid Mechanics*, vol. 45, no. 1, pp. 197–215, 2013.
- [2] A. Gauthier, J. C. Bird, C. Clanet, and D. Quéré, “Aerodynamic Leidenfrost effect,” *Phys. Rev. Fluids*, vol. 1, p. 084002, Dec. 2016.
- [3] H. Lhuissier, Y. Tagawa, T. Tran, and C. Sun, “Levitation of a drop over a moving surface,” *J. Fluid Mech.*, vol. 733, p. R4, Oct. 2013.
- [4] M. Klamka, M. Remer, and T. Bobinski, “Beyond laminar regime – droplet interaction with air boundary layer,” *International Journal of Heat and Mass Transfer*, vol. 133, pp. 542 – 547, 2019.

Forces acting on a pendant drop on a small pillar

M Arogeti¹ and A Vinod² and M Tadmor¹

¹ Mechanical Engineering Department, Shamoon College of Engineering, 8410802, Israel

² Mechanical Engineering Department, Ben Gurion University, 8443944, Israel

E-mail: meravar@sce.ac.il

Abstract. In this study, we explored the force necessary to detach a pendant drop from a small, circular pillar. The pillar dimensions dictate the magnitude of the solid-liquid contact area. We established a linear correlation between the force needed for the drop to split and the drop volume by applying normal force to different drop volumes. Our findings indicate a decrease in the force needed for detachment with increasing drop volume, while it rises with the increase of the solid-liquid contact line.

Keywords: Experimental Fluid Mechanics, Hydromechanics, Pendant drop, force balance, Edge effect

1. Introduction

In the current work we studied forces required to remove a pendant drop from a small round pillar. Tate's law $mg = \sigma\pi D$ describes the force balance involved in this phenomenon, the weight mg and the capillary force, where σ is the surface tension of the liquid, πD is the drop perimeter. This equilibrium determines the maximal volume that the surface can hold before the drop falls and is therefore used to measure experimentally the surface tension [1] However, this balance does not consider the remaining volume and requires corrections [2]. In our study, we applied external normal force by using the Centrifugal Adhesion Balance (CAB) apparatus in addition to the drop weight as the detachment force. This device can apply a one-directional force to the drop in the normal or tangential direction [3]. By using CAB we could study different drop volumes, not only the maximal volume for the given pillar. In this study, we focus on drops placed on small pillars with edges that limit the drop spread and create an edge effect that determines the solid-liquid contact area and increases the apparent contact angle [4]. We explore the relationship between the applied force at the moment of detachment and the influence of the edge effect.

2. Experimental setup

We measure the normal force applied on a water drop placed on round cylindrical pillars. The pillar diameters are 2mm, 2.5mm, and 3mm. The experimental apparatus used to generate the normal force is the CAB (Centrifugal Adhesion Balance) system. This system can isolate force applied on a drop in one direction by neutralizing the effect of other forces from different directions by using centrifugal force and adjusting the drop contact plane with the surface [3]. We set the system to apply only normal force on the drop and measured the force until the drop pulled off and split.

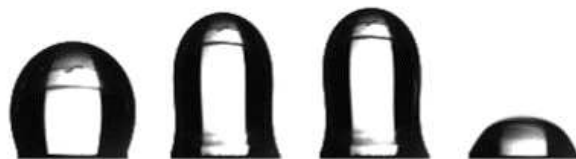


Figure 1. Drop in volume of $23\mu\text{l}$ is placed on 3 mm pillar, under normal force before and after the drop split

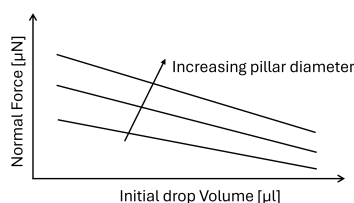


Figure 2. Normal force to split the drop for different initial volumes for examined diameters

2.1. Results and discussion

During the experiment, a normal force was applied to the surface of a drop, denoted by F_{\perp} . The force caused the drop to elongate, develop a narrow neck, and eventually split. The main portion of the drop detached, leaving less than 30% of the original volume on the surface. The experiment showed that the adhesion generated by the edge effect at the solid-liquid contact line was stronger than the normal force applied, leading to the drop splitting without any change in the contact line, as shown in Figure 1.

The normal force of drop pull-off from each pillar was measured for varying drop volumes, indicating a linear relationship for each pillar. A descending straight-line equation describes the relationship.

$$F_{\perp} = -aV + b \quad (1)$$

The drop's initial volume is denoted by V , and the constants a and b depend on the pillar diameter. The required force to split a drop decreases as the volume increases. This is because the stability of the drop reduces as it grows. The contact area, determined by the pillar diameter, enhances the stability of the drop. As a result, the required force to split the drop increases, as shown in Figure 2.

Acknowledgments

We acknowledge Prof. Rafael Tadmor- Ben Gurion University, Israel, for the permission to use the CAB apparatus in our experiments.

References

- [1] Adamson Arthur W. and Gast Alice P., *Physical Chemistry of Surface*. Wiely, 1997.
- [2] B. B. Lee, P. Ravindra, and E. S. Chan, "A critical review: Surface and interfacial tension measurement by the drop weight method," 8 2008.
- [3] R. Tadmor, R. Das, S. Gulec, J. Liu, H. E. N'guessan, M. Shah, P. S Wasnik, and S. B. Yadav, "Solid-Liquid Work of Adhesion," *Langmuir*, vol. 33, pp. 3594–3600, 4 2017.
- [4] G. Fang and A. Amirfazli, "Understanding the edge effect in wetting: A thermodynamic approach," *Langmuir*, vol. 28, pp. 9421–9430, 6 2012.

Particle clustering and velocity statistics in large-eddy simulations of isotropic turbulence

M Rajek¹ and J Pozorski¹

¹Institute of Fluid-Flow Machinery, Polish Academy of Sciences, Fiszera 14, 80-231 Gdańsk

E-mail: jp@imp.gda.pl

Abstract. As a generic turbulent flow case, already complex enough to study the dynamics of heavy inertial particles, we consider forced homogeneous isotropic turbulence in a periodic box. The Lagrangian particle tracking is coupled to a state-of-the-art pseudospectral code for the carrier phase. The large-eddy simulations are run to check whether an effect of inertial-scale particle clustering can be observed at achievable resolutions, similarly to the one recently reported in fully resolved simulations. Another issue to be discussed is the impact of the spectral viscosity and possible subfilter particle dispersion modelling on particle velocity statistics and the clustering phenomenon at smaller flow scales.

Keywords: Multiphase flow, turbulence, large-eddy simulation, inertial particles, clustering

The large-eddy simulations (LES) have become a convenient computational tool for diverse turbulent flows, including those with the dispersed phase. Here, we consider small heavy particles of finite inertia, treated as material points but their density is considerably larger than that of the carrier phase. Among open issue in particle-laden LES is the impact of non-resolved flow scales and possibilities to account for them, often referred to as subfilter particle dispersion, see [1] and references therein. Actually, the subfilter flow scales affect not only the non-uniform distribution in space, or clustering, but also particle velocity statistics. Both are important for a correct prediction of particle collisions/break-up, wall deposition etc. Applications include cloud droplets, particle separators, agglomerators, and spray combustion.

Recently, thanks to direct numerical simulations (DNS) achievable on 4096^3 grid points, a larger-scale clustering has been reported [2], in addition to the well-known, small-scale phenomenon characterized by a size being typically a few Kolmogorov length scales. The latter is affected by LES filtering, and it has been an incentive for development of so-called structural models of particle dispersion. As discussed in the present contribution, none of the models proposed so far have been fully successful. Also, applying a novel, efficient and accurate pseudo-spectral flow solver [3], we attempt to clarify whether the larger-scale clustering (identified in the inertial range) can also be observed in the LES and, if so, what would be its consequences for other particle statistics such as relative pair velocity or mean settling.

References

- [1] Pozorski J 2017 *Particles in Wall-Bounded Flows*, pp. 97-150, Springer.
- [2] Matsuda K, Yoshimatsu K and Schneider K 2022 *12th Int. TSFP Symposium*, Osaka, Japan, July 19-22
- [3] Rajek M 2024 *IFFM Trans.* **239** (in print)

Estimation of Droplet size using Pressure Oscillation-based approach in Microfluidics by Simulations

Babajan Bakhtar Khan^{1*}, Sunil Kumar Thamida², Anil B. Vir³

Department of Chemical Engineering, Indian Institute of Technology Tirupati,
Yerpedu – 517619, India.

¹E-mail: babjan2999@gmail.com, ²E-mail: sunil76@iittp.ac.in, ³E-mail: anilvir@iittp.ac.in

Abstract The present study describes a new pressure oscillation-based approach for counting and measuring the droplet size in the microfluidic system. Numerical simulations were performed in a co-flow microchannel, and the details of pressure fluctuations on the wall at a point were measured as the droplet passes towards the exit. The Droplet formation frequency (DFF) was determined by applying the Fast Fourier transform (FFT) to the recorded pressure signal and time series. The dispersed phase flow rate and DFF can be used to compute the droplet size.

Keywords: Microfluidics, Droplet formation, Two-phase flow, Fast Fourier transform.

1. Introduction

Traditionally, image analysis of video captured with a high-speed camera coupled to a microscope is used for cytometry or estimating droplet formation frequency (DFF)¹. The droplet production rate was determined by analyzing laser-scattered signals for size, shape, and frequency at the detection site².

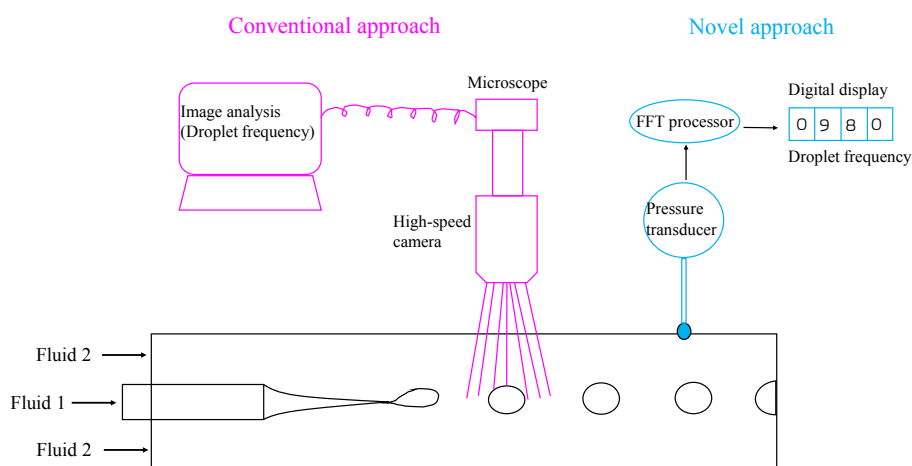


Figure 1. Schematics of conventional and novel methods for measuring droplet formation frequency. In the present study, a computer simulation was performed for droplet production using two immiscible fluids in a co-flow microfluidic channel through 2D axisymmetric geometry using COMSOL Multiphysics software combined with MATLAB. Figure 1 illustrates the brief procedure of measuring DFF in conventional and the present method. This research will aid in the precise and regulated generation of droplets in microfluidics systems at a relatively inexpensive cost compared to traditional method, particularly in emulsion-based applications and droplet-based targeted dosage in drug delivery treatments.

2. Governing equations and mathematics

The flow characteristics of the continuous and dispersed fluid can mathematically be governed by mass continuity as in Eq. (1) and momentum equation as in Eq. (2) as follows.

$$\nabla \cdot \underline{u} = 0 \quad (1)$$

$$\rho(\phi) \left[\frac{\partial \underline{u}}{\partial t} + (\underline{u} \cdot \nabla) \underline{u} \right] = -\nabla p + \nabla \cdot \underline{\tau} + \underline{F}_\sigma + \underline{F}_g \quad (2)$$

Where \underline{u} is the velocity vector, $\rho(\phi)$ is density, t is the time, p is the pressure, $\underline{\tau}$ is the shear stress, \underline{F}_σ is the interfacial tension force and \underline{F}_g is the gravity force.

3. Preliminary Results and Discussions

A particular point was considered on the wall at a distance of 600 μm from the inlet and 200 μm from exit. The pressure developed at that point for various input pressures of dispersed and continuous phases is shown in Figure 2(a).

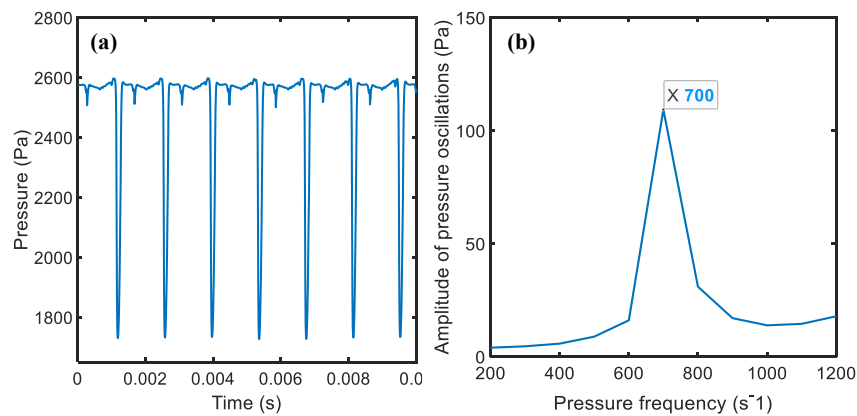


Figure 2. (a) Pressure oscillations and (b) FFT analysis of pressure signal for continuous phase pressure inlet of 14000 Pa and dispersed phase inlet pressure $P_d=17000$ Pa.

In Figure 2(a), the number of oscillations in 0.01 seconds are 7, which was equal to the 700 droplets in a second shown in Figure 2(b). After calculating the DFF, the droplet size can be calculated without visualization.

Conflict of interest statement

The authors have no conflicts to disclose.

References

- ¹ H.R. Safford, and H.N. Bischel, “Flow cytometry applications in water treatment, distribution, and reuse: A review,” *Water Res.* **151**, 110–133 (2019).
- ² X. Chen, A.P. O’Mahony, “The characterization of particle number and distribution inside in-flight 3D printed droplets using a high speed droplet imaging system,” *J. Appl. Phys.* **130**(4), (2021).

Utilizing a pressure-based CFD solver for modelling wet steam flow in low-pressure turbine stages: a predictive approach to assessing flow losses

S Shabani¹, M Majkut¹, S Dykas¹, K Smółka¹

¹ Silesian University of Technology, Department of Power Engineering and Turbomachinery, 44-100 Gliwice, Poland

E-mail: sima.shabani@polsl.pl

Abstract. This research focuses on addressing a critical challenge in steam turbine operation, specifically condensation losses within the Low-Pressure (LP) section. Such losses have a significant impact on energy efficiency and operational costs in industries like power generation and manufacturing. The objective of this research is to predict condensation losses in the LP part of steam turbines and propose mitigation methods. The search for the most efficient CFD tool has concluded. We commenced with our proprietary in-house code (a density-based approach), progressed through ANSYS Fluent, and ultimately opted for the utilization of ANSYS CFX.

Keywords: Multi-phase Flows, Steam turbine efficiency, Condensation losses, Geometry modification

1. Introduction

Steam turbines are pivotal components in diverse industrial sectors, playing a crucial role in power generation and manufacturing processes. However, a significant challenge faced in steam turbine performance, particularly in the Low-Pressure (LP) section, is the occurrence of condensation losses. These losses result in diminished energy efficiency and increased operational expenses, posing a considerable obstacle to the overall effectiveness of steam turbine systems. Researchers have identified that these losses arise from the transition of steam to water as it passes through the turbine blades, leading to decreased energy output. Studies by [1-2] emphasized the importance of accurate prediction models for condensation losses, highlighting the need for a comprehensive understanding of the thermodynamic processes within the turbine. Additionally, Studies by [3-6] explored the impact of blade geometry on condensation losses, underscoring the potential for improvements through optimized blade shapes. While existing literature has made valuable contributions to understanding condensation losses, there remains a gap in the implementation of practical solutions. This study seeks to bridge this gap by integrating predictive models with tangible modifications to the steam turbine blades, with a specific focus on the LP section. The objective is to enhance energy efficiency, reduce operational costs, and contribute to the overall sustainability of steam turbine systems in diverse industrial applications.

2. Methodology

Numerical modelling of the wet steam flow has been carried out in ANSYS CFX. Wet steam is a two-phase mixture. Water vapour makes up the carrier phase, which is treated as a continuous fluid. Condensed water droplets make up the liquid phase in a dispersed form. The governing equations including RANS equations (mass and momentum and energy conservation equations) were applied for a steady state 2D compressible flow. Transport equations have been used to predict the liquid phase quantity. The $k-\omega$ SST turbulence model has been employed to consider the turbulence flow effects. For estimating liquid and vapor thermodynamic properties, IAPWS-IF97 formulations [7] are used, which are tabular data to estimate various fluids properties. The technique of pressure-based approach was employed, and the coupling of pressure and velocity was ensured through the high-quality Rhie-Chow scheme. A high-resolution technique was used to discretize the convective part of the Navier-Stokes equations. The convergence criterion for all parameters involved in the equations is supposed to be 10^{-6} . The study focuses on examining the geometry of the fixed blade (stator) and the moving blade (rotor) associated with the final stage of a 200 MW steam turbine (Fig. 1). A simulation is conducted to analyze the flow of wet steam around these components, with subsequent calculations determining the extent of condensation losses.

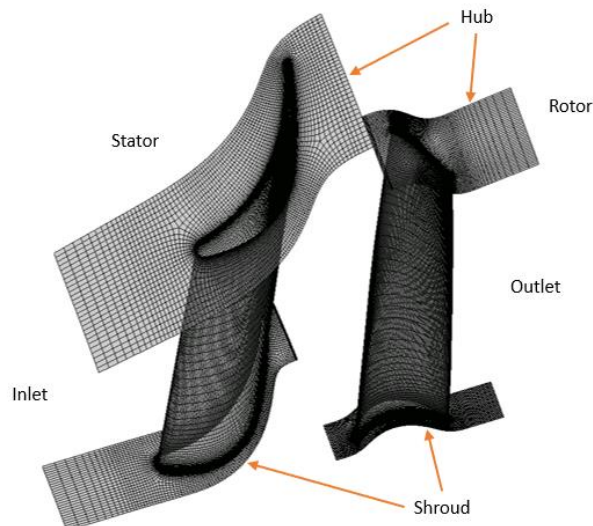


Figure 1. The view of the final stage of a 200 MW steam turbine

Acknowledgments

Research reported in this publication was supported by the National Science Centre under number 2020/37/B/ST8/02369, and by statutory research funds for young scientists.

References

- [1] X. Yu, Zh. Xiao, D. Xie, Ch. Wang, C. Wang 2015, *Int. J. Heat and Mass Transfer* **84** 642–652.
- [2] Ch. Wen, Y. Yang, H. Ding, Ch. Sun, Y. Yan 2021, *Applied Thermal Engineering* **189** 116748.
- [3] S.M.A. Noori Rahim Abadi, A. Ahmadvour, S.M.N.R. Abadi, J.P. Meyer 2017, *Applied Thermal Engineering* **112** 1575–1589.
- [4] M. Ansari, V. Esfahanian, M.J. Izadi, H. Bashi, A. Tavakoli, M. Kordi 2024, *Int. J. Heat and Mass Transfer* **220** 124964.
- [5] H. Miyazawa, A. Uemura, T. Furusawa, S. Yamamoto, K. Yonezawa, Sh. Umezawa, Sh. Ohmori, T. Suzuki 2020, *Proceedings of ASME Turbo Expo*.
- [6] M.R. Aghdasi, A.R. Teymourtash, E. Lakzian 2022, *Applied Thermal Engineering* **211** 118445
- [7] ANSYS CFX-solver theory guide, release 15 November 2013.

Numerical simulation of the oil-water flow in a horizontal pipe in a stratified flow regime

D Asendrych

Częstochowa University of Technology, Faculty of Mechanical Engineering and Computer Science, al. Armii Krajowej 21, 42-201 Częstochowa, Poland

E-mail: dariusz.asendrych@pcz.pl

Abstract. The paper presents a numerical study of a 2-phase oil-water flow in a horizontal pipeline in a stratified flow regime. Flow velocity, oil volume fraction as well as ambient temperature were varied during the simulations. The parametric calculations allowed us to show how the flow parameters influence the pressure drop and to indicate how the hydraulic transport costs could be optimised in the oil extraction industry.

Keywords: Multi-phase Flows, Oil Extraction, Pipe Flow, Temperature-dependent Viscosity, Computational Fluid Dynamics, Volume of Fluid (VOF)

1. Introduction

Multiphase flows are widely encountered in industrial applications, just to mention chemical and process industries, food and pharmaceutical processing, and hydraulic and pneumatic transport. Among various multiphase flow configurations, 2-phase oil-water flow with two immiscible liquids plays a quite important role in reflecting the oil extraction technology. Stratified and fully dispersed flow regimes are of the most importance, as they are commonly encountered in extraction installations. A variety of parameters like flow structure, flow velocity, mixture composition and material properties make the prediction of pressure drop difficult and consequently lead to an uncertain estimation of energy demand. That is why extraction installations are usually oversized as they are based on empirical formulas derived for a limited range of operating conditions and physical properties.

2. Numerical approach

In the present paper, the oil-water flow in a horizontal pipe of diameter 110mm in a stratified flow regime is investigated with the use of computational fluid dynamics (CFD). The flow was simulated using the Ansys Workbench commercial software package with the use of a 3-dimensional Eulerian approach combined with a Volume of Fluid (VOF) method allowing for a reconstruction of an oil-water interface in a stratified regime. Surface tension was included in the momentum equation as a source term. Water and paraffin oil were used as working fluids. Oil viscosity used in calculations followed the work of Santos et al. [1] and its variation upon ambient temperature was simulated using the experimental data given in [2]. For the temperatures considered in the paper, the oil viscosity varied in a quite wide range, i.e. 15-45mPas.

3. Simulation results

The model was verified by conducting a series of simulations following the flow conditions of the experimental-numerical work presented in a reference paper [1] devoted to the 2-phase oil-water flow. The predicted pressure drops in test simulations showed very good agreement with reference data [1], proving the relevance of the applied numerical approach. The verified model was employed to carry out a parametric study for a stratified flow regime, with the following ranges of operating parameters: flow velocity 0.3-1.0m/s, oil volume fraction 0.06-0.6 and temperature 5-45°C. The results of the calculations allowed us to collect a database and show how oil volume fraction, flow velocity and temperature influence flow resistance. The predicted pressure drops turned out to vary in a quite wide range with its minimum value around 20Pa/m and exceeding 200Pa/m for the worst conditions (high velocity, low temperature, high oil volume fraction). It shows how important the choice of operating conditions can be to optimise energy consumption. The collected data allowed us to propose a functional dependence of pressure drop on 3 independent variables investigated in the present research. The proposed correlation, although limited to paraffin oil and pipe diameter, can be effectively used in managing oil transport in pipeline systems.

Acknowledgements

The present research work was supported by statutory research funds of the Częstochowa University of Technology under grant BS/PB-1-100-301/2023/P. The PL-Grid Infrastructure is gratefully acknowledged for providing its computational resources.

References

- [1] Santos D, Faia P, Garcia F, Rasteiro M 2019 *J. of Petroleum Science and Engineering* **174** 1179
- [2] Dai Q, Khonsari M, Shen C, Huang W, Wang X 2016 *Langmuir* **32** 7485

Liquid-gas flow modelling in horizontal pipe

**M. Jaszczur¹, P. Marczak¹, R. Hanus², A. Golijanek-Jędrzejczyk³,
A. Andruszkiewicz⁴, M. Zych⁵**

¹ AGH University of Krakow, Faculty of Energy and Fuels, Al. Mickiewicza 30, 30-059 Kraków, Poland

² Rzeszów University of Technology, Faculty of Electrical and Computer Engineering, al. Powstańców Warszawy 12, 35-959 Rzeszów, Poland

³ Gdańsk University of Technology, Faculty of Electrical and Control Engineering, ul. G. Narutowicza 11/12, 80-233 Gdańsk, Poland

⁴ Wrocław University of Science and Technology, Faculty of Mechanical and Power Engineering, Wybrzeże Wyspiańskiego 27, 50-370 Wrocław, Poland

⁵ AGH University of Krakow, Faculty of Geology, Geophysics and Environmental Protection, Al. Mickiewicza 30, 30-059 Kraków, Poland

E-mail: jaszczur@agh.edu.pl, pmarczak@agh.edu.pl

Abstract. Liquid-gas flow modelling approach strongly depends on flow regime and available computational infrastructure. In this research study compares simulation times and accuracy between most popular models for setup, which will be in future experimentally validated are compared. The results of the analysis will improve the quality of the upcoming experiment by defining the proper setup and placement.

Keywords: : Multi-phase Flows, CFD, Volume of Fluid, Mixture model, Plug flow, Slug flow

1. Introduction

There are various ways to two-phase liquid-gas model, which differ both in complexity and computational effort. Some of those describe only selected flow types, which induces the need to switch models when fluid parameters enter into another regime. The following article focuses on the Volume of Fluid and Mixture model, since plug and slug flow will be studied. As a test case will be used a T-junction, where liquid-gas mixture will be flowing.

The objective of this paper is to determine the usage of each modeling method, as well as provide an overview of computational time and effort needed. The purpose of numerical simulation is to support the upcoming experiment related to multiphase flow measurement, similar to described by Hanus R, Zych M [1]. Since simulation needs to be prepared before the test, that information is important allowing to better allocate resources and plan all milestones, respectively. Also results from the simulation provide better understanding when flow is fully developed and stabilized, which is vital for placement of velocity measurement devices.

2. Scope of work

Article will show mesh sensitivity study and time step analysis (constant vs. adaptive). Solver stability for the VOF method and mixture for different liquid-gas (water-air in room

temperature) velocity inlets will be examined. Initial calculations are made in 2D, after achieving good stability and promising results, study in 3D will be conducted. Since it is an axisymmetric problem, the possibility of calculating half of the pipe will be checked and the results compared to the full 3D model.

2.1. Geometry, Boundary conditions and mesh

The test case consists of a 50 mm diameter, 2m long pipe with main water supply, 1 mm nozzle that injects air into the main channel (see Figure 1. for the placement of the boundary conditions).

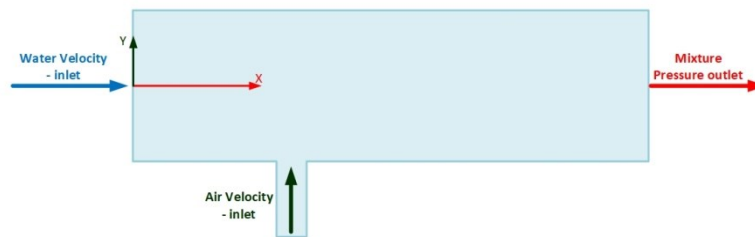


Figure 1 Overview of boundary conditions (not to scale)

3. Results

The results show that for the same boundary conditions, different void fraction shape is calculated. Figure 2 shows an air distribution after time $t=0.1s$ for three different approaches: VOF and Eulerian. All of the results were calculated with Hybrid NITA Schemes, and adaptive remeshing which reduced computational effort significantly. The main differences are bubble formation, its size and amount of secondary, small structures.

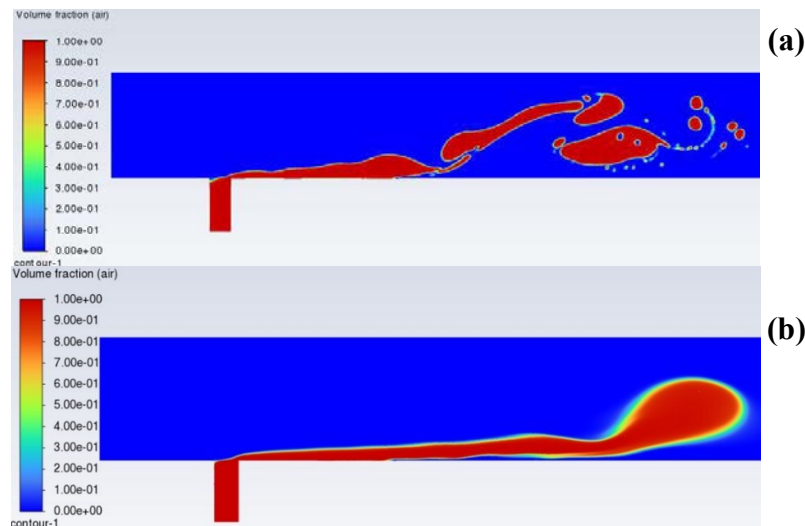


Figure 2 Void fraction after $t=0.1 s$: (a) – VOF model, (b) – Eulerian

Acknowledgements

Scientific work co-financed from the state budget under the program of the Minister of Education and Science called Polish Metrology, project no. PM/SP/0020/2021/1



References

[1] Hanus R, Zych M, Kusy M, Jaszczur M, Petryka L 2018 *Identification of liquid-gas flow regime in a pipeline using gamma-ray absorption technique and computational intelligence methods, Flow Measurement and Instrumentation* Volume 60 Pages 17-23

Time-resolved imaging of reactive transport instability during multiphase flow in porous media.

M Dzikowski and P Szymczak¹

¹University of Warsaw, Faculty of Physics, ul. Pasteura 5, 02-093, Warszawa

E-mail: mdzikowski@fuw.edu.pl

Abstract. Positive feedback between reactant transport in porous media and dissolution of porous matrix can lead to the creation of preferential flow pathways, which in turn dramatically increase the permeability of the rock, or porous media in general. We used high-speed synchrotron X-ray tomography to gather time-resolved data on the appearance and evolution of those paths during two-phase flow in porous media.

Keywords: Computed tomography, two-phase flow, porous media, reactive transport

1. Introduction

Highly localized flow paths or channels, termed wormholes, arise during the dissolution of fractured and porous media under certain flow conditions. Their growth is governed by positive feedback between the flow field and chemical reactions at pore surfaces. Those newly created channels become preferential flow paths, in which both the flow and reactant transport become spontaneously localized. Since dissolution fingers dramatically increase the permeability of the rock, or porous media in general, wormholing is important both for industrial applications and in hydrogeological studies.

The existing body of work on two-phase dissolution, both experimental [6-12] and numerical [5, 12, 13] give somewhat contradictory results: on one hand a pre-existing or injected non-reactive gas or oil phase is reported to increase wormhole growth rates by focusing flow and reducing branching [7-9, 13]; on the other hand, some researchers report that blocked flow from generated or injected CO₂ limits wormhole development [9-12]. Up to our knowledge, the only studies that offer the dynamic information on wormhole development are those of Ott and Oedai [10] and Snippe et al. [12], who captured the wormhole growth using X-Ray tomography during CO₂/carbonic acid co-injection experiments under in-situ conditions relevant for carbon capture and storage. Presence of gas in capillary flow could also increase the local reaction rate due to enhanced mixing, a phenomenon which is also observed during heat transfer in catalytic reactors and was hypothesized in unstable dissolution experiments [20].

2. Experimental results

Leveraging the capabilities of the Fast-X laboratory at NCBJ in Świerk (Poland) and the ID-19 beamline at ESRF in Grenoble (France), these in-situ experiments sought to capture high-resolution images of developing wormholes to understand their interaction with the surrounding porous matrix. During the two-phase experiments, the acid solution was injected in discrete pulses, alternating between 30 minutes of continuous flow and 30 minutes without flow. This approach mirrored the CO₂ experiments conducted by Ott. In contrast, nitrogen was supplied continuously at a constant pressure exceeding the capillary threshold, ensuring a relatively stable nitrogen flow. Though preliminary analysis did not reveal significant interaction between the growing wormhole and nitrogen, observations suggest presence of different types of two-phase regimes inside and around the growing structure, ranging from bubbly flow within the wormhole itself, to fully locked area and branches. First measurements at ID-19 and using standard tomograph confirmed that, indeed, an emerging wormhole channel can be blocked by gas ganglia or exhibit bubbly transport (Fig. 1).

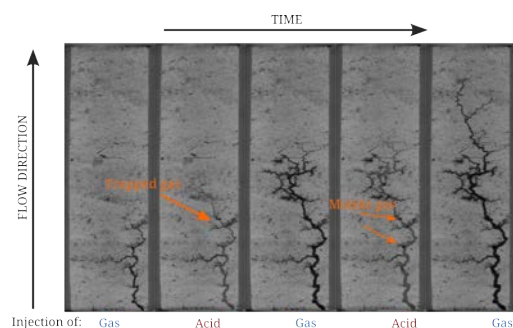


Figure 1. Time lapse of wormhole development during cycled acid/gas injection. Different gas transport and rock dissolution interaction regimes are observable.

Acknowledgements

Presented work was funded by Polish National Science Centre (NCN) under CEUS-UNISONO grant number UMO-2020/02/Y/ST3/00121. Initial 4D imaging experiment were performed in National Centre For Nuclear Research (NCBJ), we would like to thank Sławomir Wronka and Tymoteusz Kosiński for the assistance. The European Synchrotron Radiation Facility (ESRF) provisioned of synchrotron radiation facilities and we would like to thank Marta Majkut for assistance and support in using beam-line ID-19, under grant ES-1301.

References

- [1] Daccord, G., PRL 1987, 58, 479-482
- [2] Szymczak, P.; Ladd, A.J., JFM 2014, 738, 591-630
- [5] Covington, M.D., Geol Soc Am Spe. Pap 516, 2016, 113-127
- [6] Bernadiner, M.G., et al., SPE Prod Eng 1992, 7, 4, 350-356
- [7] Shukla, S., et al., SPE J., 2006, 11, 3, 273-281
- [9] Song, Wen, et al., Lab Chip 2014, 14, 22, 4382-43
- [10] Ott, H.; Oedai, S, Geophys Res Lett 2015, 42, 7, 2270-2276
- [12] Snippe, J., et al., Int J Greenh Gas Cont 2020, 94, 102901
- [13] Wei, W., et al., SPE J 2017, 22, 6, 2-067.
- [16] Zboray, R.; Trtik, P., MethodsX 2018, 5, 96-102
- [17] Cooper, M.P. et al., AGU Fall Meeting 2019, H21M-1931
- [18] Reynolds, C. A. et. al. PNAS 114, 31, 8187-92.
- [19] Li et al., JGR Sol. Earth 2019, 124, 11,055-11,073
- [20] Qiu et al., SPE, 2013, pp. SPE—164245--MS

Sponsor's Session

Dantec Dynamics systems in Macro and Micro Experimental Fluid Dynamics

K. Dörner¹






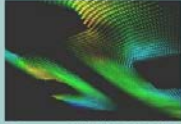
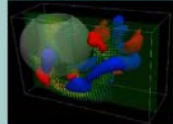



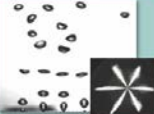
¹ Dantec Dynamics A/S, DK-2740 Skovlunde, Denmark

E-mail: kdr@dantecdynamics.com

Abstract. Scientists and Engineers in fluid dynamics and solid mechanics rely on measurements to make breakthroughs in applied research, technology development, and quality assurance. Dantec Dynamics develops and sells integrated measurement systems for diagnostics and research into fluid mechanics, solid mechanics, microfluidics, spray analysis and combustion technology. We deliver turnkey and customized solutions built on high-end laser optics, imaging, and sensor technologies. Our user-friendly software performs advanced data analysis and produces real-time results. Furthermore, we pride ourselves in providing our clients superior technical application support worldwide. You gain accurate measurement results easily and quickly which help you accelerate the pace of discovery, innovation, quality control or NDT. Our distinct competence and experience in integrating measurement methods and technologies into the right solution for you, is unique. Partnering with Dantec Dynamics helps you gain crucial knowledge from any test or measurement campaign. Dantec Dynamics – Turn Measurements into Knowledge.

Keywords: Aerodynamics, Atmospheric Science, Combustion, Experimental Fluid Mechanics, Flow Machinery, General Fluid Dynamics, Hydromechanics, Interdisciplinary Areas in Heat and Fluid Flow, Measurement Techniques, Microflows, Multi-phase Flows, Turbulence

1. Complete solutions for your experimental fluid mechanics

<p>Point techniques:</p> <ul style="list-style-type: none"> > velocity > temperature > size > concentration 	 <p>CTA/CCA (3D V, T)</p>	 <p>ComfortSense (V, T)</p>	 <p>LDA (3D V)</p>	 <p>PDA (3D V, D)</p>
<p>Imaging techniques:</p> <ul style="list-style-type: none"> > velocities (planar & volume) 	 <p>2D PIV (2D2C V)</p>	 <p>StereoPIV (2D3C V)</p>	 <p>Vol PIV (3D3C V)</p>	
<p>Imaging techniques:</p> <ul style="list-style-type: none"> > shape, velocities > size > temperature > concentration 	 <p>LIF (T, c, pH)</p>	 <p>CLIF (flame front)</p>	 <p>Rayleigh (T)</p>	 <p>Shadow (D, 2.5D V)</p>

2. Sample results from Poland

Probably first in the world shown results of 2D3C PIV obtained from 3D-printed micro-channel – carotid artery in this case (Figure 1).

Results of 3D3C TR-PIV measured in wind-tunnel with pressure distribution and Q-criterion shown on Figure 2.

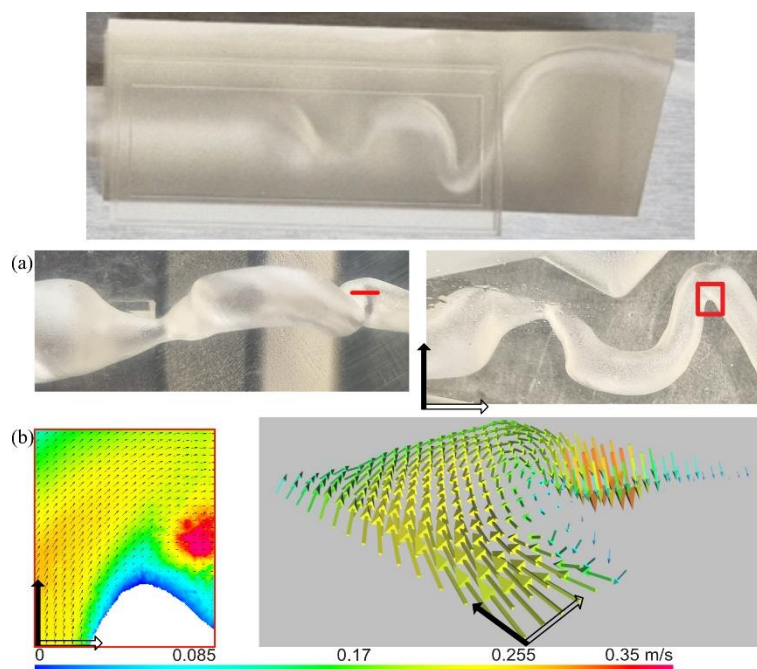


Figure 1.ⁱ Stereo μ PIV from 3D-printed model of a human carotid artery. top – phantom view; (a) – imaging area locations; (b) – velocity and vector maps.

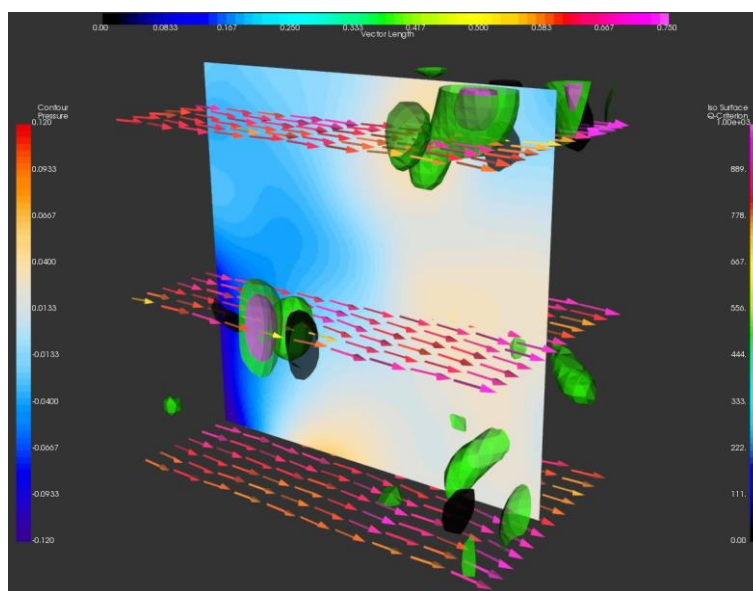


Figure 2.ⁱⁱ Volumetric time-resolved PIV (3D3C) in aviation application.

ⁱ Arkadiusz M. Antonowicz “Non-invasive methods for measuring the flow field in 3D printed circulatory system phantoms”, PhD thesis (in preparation).

ⁱⁱ Dantec Dynamics Volumetric time-resolved PIV results. Measurements by Arkadiusz M. Antonowicz (Eurotek International)

Turbulence and Transition

Turbulent cascades in the Atmospheric Boundary Layers

M Waclawczyk¹, J L Nowak¹, J C Vassilicos², S Król¹ and S P Malinowski¹

¹ University of Warsaw, Faculty of Physics, Pasteura 5, 02-093 Warsaw, Poland

² Univ. Lille, CNRS, ONERA, Arts et Metiers Institute of Technology, Centrale Lille, UMR 9014 – LMFL – Laboratoire de Mécanique des Fluides de Lille – Kampé de Fériet, F-59000 Lille, France

E-mail: marta.waclawczyk@fuw.edu.pl

Abstract. We investigated scale-by-scale budget of turbulence kinetic energy in atmospheric boundary layers using airborne measurements performed in shallow trade-wind regime over ocean by the ATR aircraft during EUREC4A experiment. We calculated the buoyancy forcing term, the third-order velocity structure functions and estimated the transport in physical space. We found that the contributions of buoyancy and transport are significant in the large-scale part of the inertial range.

Keywords: Atmospheric Science, Experimental Fluid Mechanics, General Fluid Dynamics

1. Introduction

The Kolmogorov 4/5 law is a cornerstone of turbulence theory. It describes relation between the longitudinal third-order structure function $\overline{\delta u^3}$, dissipation rate ϵ and the distance between points r . The 4/5 law is valid only under assumptions of local homogeneity and isotropy and at restricted range of scales, which are not affected either by viscosity or by forcing. The third-order structure function is related to the rate of energy transfer between eddies of different sizes. If it is negative the energy flows across the scales from large to small ones. The energy transfer rate can change within the inertial range, if contributions of forcing and transport in physical space are non-negligible.

In this work we perform a study of the energy budget in the space of scales by analysing data from airborne EUREC4A experiment held in Jan-Feb 2020 in the western tropical Atlantic off the coast of Barbados, cf. Ref. [3]. We study contribution of different terms and estimate the rate of energy transfer.

2. Methods and results

In our work we follow the approach presented in Refs. [1, 2] and consider the Kármán–Howarth–Monin–Hill equation for the second order structure functions. We assume stationarity and horizontal homogeneity and further circumvent the issue of anisotropy by integrating all terms in the equation over a sphere of radius r . In this way we obtain the transport equation written

symbolically in the following form

$$4\epsilon = W(r, z) - S_3(r, z)r^{-1} - T(r, z), \quad (1)$$

where $W(r, z)$ is the rate of energy production due to buoyancy at scales smaller or equal to r , $-S_3$ is the third-order structure function, which represents the rate of energy transfer to scales of size $\leq r$, $-T(z, r)$ denotes vertical transport in physical space, z is the vertical coordinate.

The four terms estimated from available measurement data are presented in Figure 1. At the altitude of 64 m the buoyancy forcing W is the major source of turbulence kinetic energy. Part of this energy is transported towards smaller scales in the direct energy cascade, with the transfer rate $-S_3 > 0$. Another part of the energy is transported in the physical space upwards ($-T < 0$ at large scales). In the top-subcloud region (595 m) the transport $-T > 0$ is the major source of turbulence kinetic energy. The buoyancy forcing W is small and becomes negative at large scales, due to stable stratification of the environment.

The present analysis provides an insight into processes in the atmospheric boundary layers. It suggests that significant departures from the Kolmogorov equilibrium are present. In particular, the third order structure function deviates from its inertial-range predictions due to non-negligible contribution of the buoyancy forcing and transport in the physical space. We intend to present further results during the XXVI Fluid Mechanics Conference.

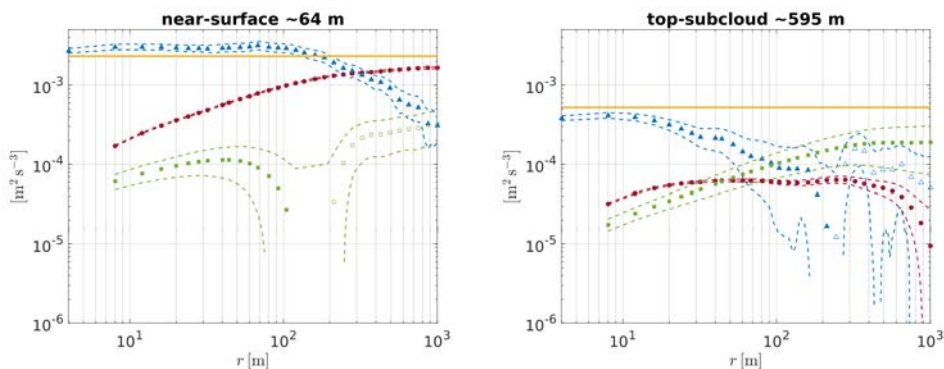


Figure 1. Scale-by-scale budget of turbulence kinetic energy in convective atmospheric boundary layer, cf. Eq. (1). Negative values are denoted by empty symbols.

Acknowledgments

The research idea was developed during Lille Turbulence Programme 2023. MW, JN, SPM acknowledge the European Union’s Horizon 2020 research and innovation programme under Grant Agreement 101003470, project Next Generation Earth Modelling Systems (NextGEMS). MW acknowledges the support of the National Science Centre, Poland, Project 2020/37/B/ST10/03695. JN was supported by the Foundation for Polish Science.

References

- [1] Valente P C and Vassilicos J C. 2015 *Physics of Fluids* **27** 1070
- [2] Apostolidis A, Laval J P and Vassilicos J C 2023 *J. Fluid Mech.* **967** A22.
- [3] Stevens B et al 2021 *Earth System Science Data* **13** 4067

Atmospheric turbulence: anisotropic, nonstationary and intermittent. What can we do?

S Malinowski¹, M Waławczyk¹, J Nowak¹, S Król¹ and R Grosz¹

¹ University of Warsaw, Faculty of Physics, ul. Pasteura 5, 02-093 Warszawa, Poland

E-mail: szymon.malinowski@uw.edu.pl

Abstract. In general, atmospheric flows are nonstationary, intermittent and anisotropic. In this presentation we will discuss new tools developed to analyze airborne measurements of turbulent atmosphere beyond standard techniques and approaches applicable to Kolmogorov type turbulence.

Keywords: Atmospheric Science, Turbulence, Airborne Measurements

There is no general theory of turbulence. While we investigate atmospheric turbulence, we usually use theoretical tools developed after Kolmogorov in mid 20th century under the assumption of isotropic, stationary and homogeneous turbulence, despite the fact that we know that the atmospheric turbulence we study does not fulfill these assumptions. In high-resolution numerical simulations we can, at least, diagnose some properties of turbulence from evolving in time 3-D fields of velocity components and thermodynamic variables. However, to analyze in-situ data on atmospheric turbulence collected by research aircraft, consisting of time series of velocity components, temperature, humidity and other variables, collected along the 1-D complicated trajectory, such diagnostics was, so far, hardly available.

In this talk we present new approaches and tools, which allow to diagnose and describe anisotropy, nonstationarity and intermittency of turbulence from such measurements. We focus on the measurements collected inside and around clouds as well as within the atmospheric boundary layer and cloud fields.

The main conclusion is that what we describe by term “turbulence” is in fact a variety of transient states of atmospheric flows. Properties of these states (anisotropy, nonstationarity, and intermittency) can be quantitatively characterized from the measurement data, allowing to distinguish between different “turbulences”. Such a distinction paves the road to improved understanding of atmospheric turbulence, turbulent transport, entrainment, mixing in clouds and atmospheric boundary layer.

Acknowledgments

This research was supported by the European Union's Horizon 2020 research and innovation programme under Grant Agreement 101003470, project Next Generation Earth Modelling Systems (NextGEMS)

References

- [1] Waławczyk M, Ma Y-F, Kopec JM and Malinowski SP 2017 *Atmos. Meas. Tech.* **10** 4573-4585
- [2] Akinlabi EO, Waławczyk M, Mellado JP and Malinowski SP 2019 *J.Atmos.Sci.* **76** 1471–1488
- [3] Waławczyk M Gozingan A Nzotungishaka J Mohammadi M Malinowski SP 2020 *Atmosphere* **11** art.199
- [4] Waławczyk M, Nowak JL, Siebert H and Malinowski SP 2022 *J.Atmos.Sci.* **79** J 2757-2772
- [5] Król S, Blyth A, Böing S, Denby L, Lachlan-Cope TA and Malinowski SP 2024, *Geophys. Res. Lett.*, to appear

Influence of porous material on the flow behind backward-facing step - experimental study

K. Bukowski¹, K. Gumowski¹, and L. Klotz¹

¹ Warsaw University of Technology, Faculty of Power and Aeronautical Engineering, ul. Nowowiejska 24, 00-665 Warszawa, Poland

E-mail: lukasz.klotz@pw.edu.pl

Abstract.

We investigate effect of porous insert located upstream of the separation edge of backward-facing step (BFS) in early transitional regime as a function of Reynolds number. This is an example of hydrodynamic system that is a combination of separated shear flow with large amplification potential and porous materials known for efficient flow destabilisation. Spectral analysis reveals that dynamics of backward facing step is dominated by spectral modes that remain globally coherent along the streamwise direction. We detect two branches of characteristic frequencies in the flow and with Hilbert transform we characterise their spatial support. For low Reynolds numbers, the dynamics of the flow is dominated by lower frequency, whereas for high enough Reynolds numbers cross-over to higher frequencies is observed. Increasing permeability of the porous insert results in decrease in Reynolds number value, at which frequency cross-over occurs. By comparing normalized frequencies on each branch with local stability analysis, we attribute Kelvin-Helmholtz and Tollmien-Schlichting instabilities to upper and lower frequency branches, respectively. Finally, our results show that porous inserts enhance Kelvin-Helmholtz instability and promote transition to oscillator-type dynamics. Specifically, we observe that amplitude of vortical (BFS) structures associated with higher frequency branch follows Landau model prediction for all investigated porous inserts.

Keywords: Experimental Fluid Mechanics, Hydrodynamics, Backward-Facing Step, Porous Materials, Vortical Coherent Structures

1. Experimental measurements of the flow behind a backward-facing step (BFS)

We investigate vortical BFS structures that are generated behind the sudden expansion of the geometry, i.e. backward-facing step (BFS) as shown in Fig. 1. We measure the velocity with Particle Image Velocimetry to quantitatively characterise these structures. An example of the spatial distribution of the measured wall-normal velocity component is shown in Fig. 1 as an alternating street of positive (in red) and negative (in blue) velocity fluctuations. We characterise these BFS structures using spectral analysis in analogy to the methodology described elsewhere [1]. Specifically, we observe a narrow-band spectrum with a characteristic frequency that corresponds to shedded vortices. In addition, we determine the dependence of the characteristic frequency and their amplitude on the Reynolds number. Our analysis is concentrated on the first instabilities of the laminar flow that occur at low Reynolds numbers.

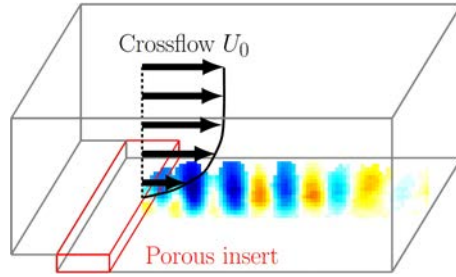


Figure 1. Geometrical configuration of backward-facing step under investigation. Black profile represents the shear flow directly upstream of the boundary layer separation at the top step corner characterised by free stream velocity U_0 . Red volume represents the location, at which the replaceable porous insert is placed. Blue and red contours illustrate the spatial distribution of wall-normal velocity component that represents the BFS structures formed downstream of the separation edge.

2. Quantitative characterisation of the flow structures formed downstream of a separation edge

We estimate the critical Reynolds number, above which the BFS coherent structures emerge. Spectral analysis reveals that the dynamics of backward facing step is dominated by spectral modes that remain globally coherent along the streamwise direction. We detect two branches of characteristic frequencies in the flow and with Hilbert transform we characterise their spatial support. By comparing normalized frequencies on each branch with local stability analysis, we attribute physical mechanisms for both observed frequencies. Finally, our results show that porous inserts enhance the amplitude of one of the characteristic branches and promote transition to oscillator-type dynamics.

3. Effect of porous material on the flow structures formed downstream the separation edge

Another parameter under consideration in our study is the permeability of porous inserts located directly upstream of the separation edge. We consider three different inserts along with a reference case with impermeable walls. Using a second independent experimental installation we characterise the permeability of each of three porous inserts under investigation. The effect of porous medium on coherent BFS structures is evaluated, which includes the determination of characteristic frequency and amplitude of shedded vortices. We observe that the permeability of the fluid-solid interface can be an effective method for passive control of the flow behind a backward-facing step.

Acknowledgments

Presented work is currently under consideration for publication in Journal of Fluid Mechanics [2]. This research was funded in fraction by National Science Center (Poland) within OPUS-21 project (2021/41/B/ST8/03142).

References

- [1] "Experiments on a jet in a crossflow in the low-velocity-ratio regime", L. Klotz, K. Gumowski and J.E. Wesfreid, Journal of Fluid Mechanics, 2019, pp. 386-406, vol. 863
- [2] "Influence of porous material on the flow behind backward-facing step - experimental study", L. Klotz, K. Bukowski and K. Gumowski, under consideration for publication in Journal of Fluid Mechanics

Replicating environmental flows with an active grid

P Baj¹, P Czubak¹, B Załęcki¹ and A Czaplńska¹

¹ Warsaw University of Technology, Faculty of Power and Aeronautical Engineering, ul. Nowowiejska 24, 00-665 Warszawa, Poland

E-mail: pawel.baj@pw.edu.pl

Abstract. Preliminary results from the newly constructed active grid (AG) are presented, demonstrating its capability to manipulate mean velocity and turbulence intensity profiles. Unlike passive methods, which lack flexibility, the AG allows for real-time control of flow conditions by independently adjusting the axes with dedicated motors. This approach offers promising potential for precise flow control in aerodynamic studies.

Keywords: Active Grid, Turbulence, Flow control, Experimental Fluid Mechanics.

1. Introduction

Experimental investigations of aerodynamic loads acting on urban structures or pedestrian wind comfort studies require faithful replication of the atmospheric boundary layer (ABL) flow in a suitable laboratory facility. The detailed characteristics of the flow are defined by relevant technical standards (e.g., Polish Standard PN-EN-1991-1-4-2008). Passive solutions are typically used to accomplish those requirements. Such approaches rely on disturbing the flow along its development with obstacles (e.g. spires, fences, roughness elements) with different characteristic length scales. Although the passive methods can be effective (see [1]), their downside is the lack of flexibility. A single setup of the obstacles yields a single flow condition. An investigation including several flow conditions requires time-consuming reconfiguration of obstacles. Additionally, passive methods require a considerable length of the wind tunnel upstream of the test section to develop the desired flow conditions.

An alternative method of adjusting a wind tunnel flow utilizes a so-called active grid (AG, [2, 3]). AG is a device composed of several axes forming a sparse grid, which disturbs the flow. The axes can spin independently and are controlled by dedicated motors. Several thin blades are attached to each axis. Depending on the angular position, the blades can constitute a negligible or significant local blockage of the flow (respectively, if set parallel or normal to the flow). Different flow conditions can be achieved by varying the motors' control approaches.

The present work provides preliminary results of controlling the wind tunnel flow profiles (mean velocity and TI) by means of the newly constructed AG. To the authors' knowledge, this is the first AG used in a Polish wind tunnel facility and also one of a few such devices worldwide (according to [3], roughly 30 such facilities were constructed before 2019).

2. The active grid design

The active grid was designed to fit the Environment Wind Tunnel facility of the Division of Aeronautics at the Faculty of Power and Aeronautical Engineering, Warsaw University of

Technology. The wind tunnel has the cross-section of $1 \times 1 \text{ m}^2$ and maximum attainable flow velocity of 25 m s^{-1} . The AG consists of 8 vertical and 8 horizontal axes (see fig. 1a). Each axis comprises 9 blades assembled into chains with short, rod-shaped links. This design, known as the low-blockage design [4] (see fig. 1b), ensures the lowest possible minimum blockage of the grid (i.e. the blockage exerted when blades are set parallel to the flow), which in this case is 9.5%. This contrasts with classic designs (e.g., [2], see fig. 1c), where the rods span the entire cross-section.

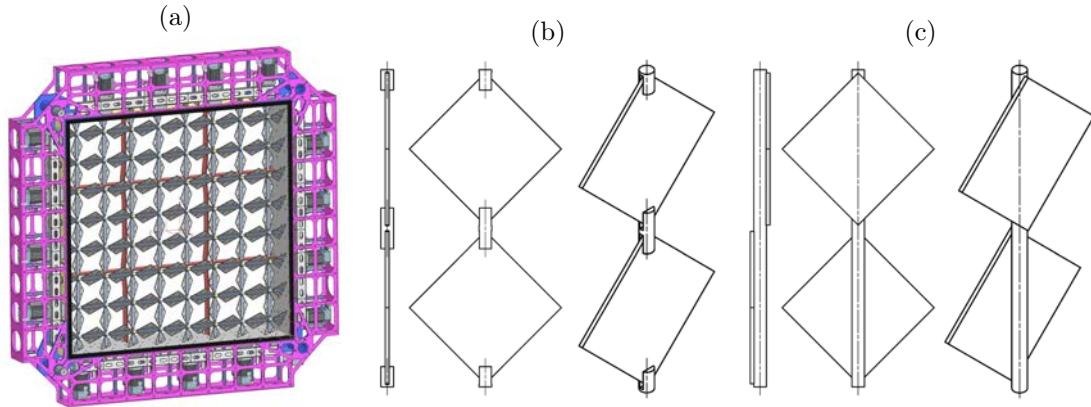


Figure 1: From left to right: a visualization of the AG, low-blockage design, classic axis design.

Each axis is driven by a dedicated stepper motor that delivers 3 Nm of torque and operates in a closed feedback loop. The trajectory of the n -th motor, $\varphi_n(t)$, is parameterized by eq. (1) (where $[\varphi_{0,n}, \Omega_n, A_n, f_n, \theta_n]$ is the set of parameters). The control system communicates consecutive target positions to all the motors at a rate of 100 Hz. In order to stabilize the load of the wind tunnel fan, the overall blockage of the AG is maintained at a constant level. Towards that goal, the axes are split into master and slave groups. Master axes are actively controlled, while the slaves compensate for the blockage change due to the motion of masters.

$$\varphi_n(t) = \varphi_{0,n} + \Omega_n t + A_n \sin(2\pi f_n t + \theta_n) \quad (1)$$

3. Anticipated Results

An experimental campaign is scheduled to identify the potential for tuning the wind tunnel flow with the AG. In particular, the effect of the parameters of the trajectories on the mean velocity and turbulence intensity (TI) profiles will be tested. It is expected that both profiles can be adjusted simultaneously, where the time-averaged value of $\varphi_n(t)$ would primarily affect the mean velocity behind the n -th axis, while the variance would dictate the local TI. The ultimate goal is to establish a mapping that evaluates suitable control parameters for any arbitrary flow profile.

Acknowledgments

Research was funded by Warsaw University of Technology within the Excellence Initiative: Research University (IDUB) programme.

References

- [1] Irwin H 1981 *Journal of Wind Engineering and Industrial Aerodynamics*, 7(3), pg. 361–366.
- [2] Makita H 1991 *Fluid Dynamics Research*, vol 8, 1-4, pg. 53.
- [3] Hearst J R 2019, *Progress in Turbulence VIII*.
- [4] Reinke N, Homeyer T, Hölling M and Peinke J 2017. *arXiv preprint arXiv:1703.00721*.

A shear flow in counter-rotating Taylor-Couette configuration

E Tuliszka-Sznitko

Poznan University of Technology, Institute of Thermal Energy, ul. Piotrowo 3, 60-965 Poznan, Poland

E-mail: ewa.tuliszka-sznitko@put.poznan.pl

Abstract. The transitional and turbulent flows between the short coaxial counter-rotating cylinders are investigated numerically (DNS) for Reynolds number up to $Re_1 = \Omega_1 R_1 (R_2 - R_1) = 3000$. To check the influence of the curvature of the cylinder walls on the turbulence, the computations are performed for different radius ratios $\eta = R_1/R_2 = 0.5-0.9$.

Keywords: Turbulence, Shear flows, Rotating flows, Taylor-Couette flows, DNS

1. Introduction

The fluid flow between two independently rotating coaxial cylinders (Taylor-Couette flow) for decades has been used to study the influence of rotation on the turbulent flow. This flow is ruled by two Reynolds numbers of the inner and outer cylinders $Re_1 = R_1(R_2 - R_1)\Omega_1/\nu$, $Re_2 = R_2(R_2 - R_1)\Omega_2/\nu$ (respectively), aspect ratio $\Gamma = H/(R_2 - R_1)$ and radius ratio $\eta = R_1/R_2$, where Ω_1 , Ω_2 are angular velocities of the inner and outer cylinders, R_1 , R_2 are radiuses of the cylinders, H is the configuration height and ν is the kinematic viscosity. The combination of two Reynolds numbers and radius ratio η creates two new parameters which perfectly capture the features of key processes occurring in such configuration, i.e. shear Reynolds number $Re = 2|\eta Re_2 - Re_1|/(1+\eta)$ and rotational number $R_\Omega = (1-\eta)(Re_1 + Re_2)/(\eta Re_2 - Re_1)$. The laminar-turbulent transition processes are divided into two main groups. In the first group, named supercritical, the transition process begins with a gradual linear increase of disturbances followed by a series of subsequent bifurcations, ultimately leading to turbulence. The second group, named subcritical, is observed in the counter-rotating configuration (mostly for $R_\Omega > 0$) if the distance between cylinders is small enough and η is close to 0.9.

The bifurcation processes and the characteristic features of turbulent flows observed in the Taylor-Couette configurations strongly depend on all above-mentioned parameters, and on the axial end-wall boundary conditions. The influence of these factors on the Taylor-Couette flow dynamics has been studied by many authors, [1-5] for example. The current research is also in this mainstream.

2. Results and discussion

The present 3D computations (DNS) are performed in a short counter-rotating cavity of $\Gamma = 4.7$ for η from 0.5 to 0.9 (the end-walls are attached to the inner cylinder). Reynolds number of the inner cylinder

Re_1 is increased along the $Re_1=Re_2\eta/\alpha$ lines (see [1]) up to $Re_1=3000$. The values of rotational rate $\alpha=\Omega_2/\Omega_1$ are taken from the range $[-0.92, -0.5]$. The presented results are performed mostly for $R_\Omega \geq 0$, although, for comparative purposes, some flow examples with slightly negative R_Ω are also presented. To better characterize the processes observed for turbulent Reynolds numbers the radial profiles of the azimuthal velocity component $\langle v \rangle_{t, A(R)}$, Reynolds stress tensor components $(\langle v'v' \rangle_{t, A(R)})^{0.5}$, $\langle u'v' \rangle_{t, A(R)}$, and production $\langle P^+ \rangle_{t, A(R)}$ are presented (all these parameters are averaged in time, in the axial and azimuthal directions).

The obtained results are discussed in the light of the data published in [1-5]. In [1] the authors have studied numerically and experimentally the subcritical laminar-turbulent transition in the counter-rotating Taylor-Couette configuration of axial aspect ratio $\Gamma = 5.26$ and radius ratio of $\eta=0.905$ (with the end-walls attached to the outer cylinder). With the gradual, small increase of Re_1 the authors have observed the transient interpenetrating spirals whose roles in the Taylor-Couette flow dynamics they compare to the role played by Tollmien-Schlichting waves in channels, [1]. In [2] the influence of the cylinders curvatures on the transition scenarios has been investigated (DNS) by computing the laminar-turbulent processes for different radius ratios η . The authors showed that for η close to 1 the Taylor-Couette solution approximates well the rotating plane Couette flow.

The DNS code used in the present investigations is based on a pseudo-spectral Chebyshev-Fourier approximation. The governing equations are approximated in time by using the second-order semi-implicit scheme i.e. an implicit scheme for the diffusive terms is used and an explicit Adams-Bashforth scheme is used for the non-linear convective term [3, 6]. The λ_2 method is used to visualize flow.

Figure 1 shows the example 3D flow structure obtained using the DNS method in the radial middle section of cavity, $Re_1=448$, $\alpha=-0.8$, $\eta=0.8$, $R_\Omega=0.0$.

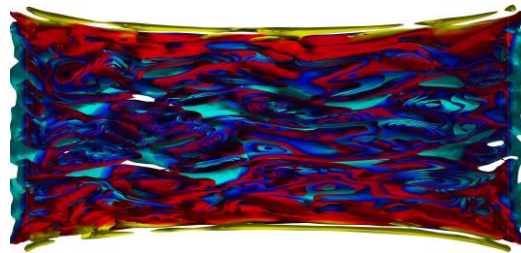


Figure 1. The perspective view of the 3D flow obtained for $Re_1=448$, $\alpha=-0.8$, $\eta=0.8$, $R_\Omega=0.0$ in the middle radial section of cavity. The λ_2 iso-surfaces are used to visualize the flow.

Acknowledgements

The DNS computations have been performed in Poznan Supercomputing and Networking Center, which is gratefully acknowledged.

References

- [1] Crowley C, Krygier M, Borrero-Echeverry D, Grogoriev R and Schatz M 2020 *J. Fluid Mechanics* **892** A12
- [2] Brauckmann H, Salewski M and Eckhardt B 2016 *J. Fluid Mechanics* **790** p 419
- [3] Tuliszkza-Sznitko E 2024 "Meccanica" Springer **1** **59** p 107
- [4] Feldmann D, Borrero-Echeverry D, Burin M, Avila K and Avila M 2023 *Philosophical transactions of the Royal Society A* **381** p 2246
- [5] Berghout P, Dingemans R, Zhu X, Verzicco R, Stevens R, Saarloos W and Loshe D 2020 *J. Fluid Mechanics* **887** A18-1
- [6] Peyret R 2002 Spectral Methods for Incompressible Viscous Flow, *Applied Mathematical Sciences*, Springer **148**

Large Eddy Simulation of turbulent flow at the entrance to an annular pipe section

Piotr Prusiński¹ and Sławomir Kubacki²

¹National Centre for Nuclear Research (NCBJ), Department of Complex Systems, Division of Nuclear Energy and Environmental Studies, Andrzeja Sołtana 7, 05-400 Otwock, Poland

²Warsaw University of Technology, Faculty of Power and Aeronautical Engineering, Institute of Aeronautics and Applied Mechanics, Nowowiejska 24, 00-665 Warszawa, Poland

E-mail: piotr.prusinski@ncbj.gov.pl

Abstract. The turbulent flow characteristics at the sudden contraction from the circular to the annular pipe section are studied by means of Large Eddy Simulation (LES). The inner flat front of the rod (25% blockage ratio) accelerates flow up to Reynolds number 40530 in the annular section. The separation bubble, with a weak anisotropy of the turbulent normal stresses, forms on a side surface of the rod. A secondary separation bubble is observed inside the primary one. The significance of circumferential velocity fluctuation in annular space is indicated by formation of large-scale helical stripes as well as lateral tilting of axially-oriented turbulent streaks.

Keywords: nuclear fuel rods, Computational Fluid Dynamics, Large Eddy Simulation (LES), detached boundary layer, separation bubble, helical oblique stripes

1. Motivation

The cylindrical surfaces within the heat exchangers of nuclear reactors are exposed to severe flow unsteadiness. The small amplitude vibrations in fuel bundles may lead to collisions between cylindrical components and support structures. Consequently, this may cause fretting wear, fatigue, and ultimately structural cracking, resulting in system failure. Fretting wear is predominantly accountable for the majority of fuel leaks detected in water-cooled nuclear reactors [1]. Hence, it is crucial to investigate the intricate flow dynamics using high-fidelity numerical tools.

The benchmark fully-developed pipe and annular flows have been extensively studied in the past by means of experiments, Direct Numerical Simulation (DNS) or LES. However, there is a lack of high-quality data for a developing annular pipe flow. For the first time, through this study, the flow characteristics at the entrance to the annular section are analyzed using LES. The aim of the work is twofold. The first aim is to study complex flow physics. The second objective is providing data for closure or improvement of the classic turbulence models.

2. Results

The turbulent flow simulation through a circular pipe followed by an annular section was performed with an application of the dynamic Smagorinsky model. The annular section was

established between an inner surface of a circular pipe and outer surface of a coaxially aligned rod. The rod's front surface was shifted by 2 hydraulic diameters with respect to the inlet section of the circular pipe. The grid of 120 million cells was employed. The grid quality was verified by analyzing the ratio of the local grid size, Δ , to the Kolmogorov length scale, $\eta = (\nu^3/\varepsilon)^{1/4}$ (where ν is the kinematic viscosity and ε is the dissipation of the turbulent kinetic energy). The ratio was under 15 for the majority of the separated shear layer and under 5 outside the separated boundary layer. Pope suggests that scales sized, Δ/η , between 8 and 60 are responsible for the bulk of dissipation. Hence, this ensures good quality of the present numerical results.

Within the research several interesting flow features has been observed and partially quantified, including dual counter-rotating separation bubbles. The standing toroidal vortices were formed in front part of the primary separation bubble. After formation, they were trapped in the low-velocity zone of the separated boundary layer. Occasionally, the vortices became perturbed by the freestream flow unsteadiness and underwent the vortex pairing process. The flow in the rear part of the separated boundary layer was characterized by highly turbulent motion. The axially-oriented streaks were observed in this region. They were later tilted in the circumferential direction. The development of large-scale alternating helical oblique stripes was observed in the developing annular section. They influenced the turbulent flow dynamics in the developing annular flow. This is the first time the helical stripes are observed at the medium-high Reynolds number studied here. Fig. 1 a) presents helical oblique stripes pattern visualized by iso-surfaces of circumferential velocity fluctuation: red: clockwise direction, light blue: counterclockwise direction. Fig. 1 b) shows variation of turbulent length scales along wall-normal (radial) direction at three axial distances L4 ($L_z/D_h=0.3$), L5 ($L_z/D_h=0.6$) and L6 ($L_z/D_h=1$). Good agreement was reported between computations and theory ('log-law') in terms of the turbulent length scale variation along the radial direction after the boundary layer reattachment line (L6 in fig. 1b). A weak anisotropy of the Reynolds normal stresses was reported inside the separated boundary layer. The peak value of the circumferential stress was closer to the rod surface than the axial and radial stresses. This was caused by strong vortex tilting in the rear part of the separated flow.

The complexity of the turbulent flow dynamics makes this test case challenging for predictions using the Reynolds-averaged Navier-Stokes (RANS) techniques. So the outcomes of this work are also relevant for refinement of the classic turbulence models.

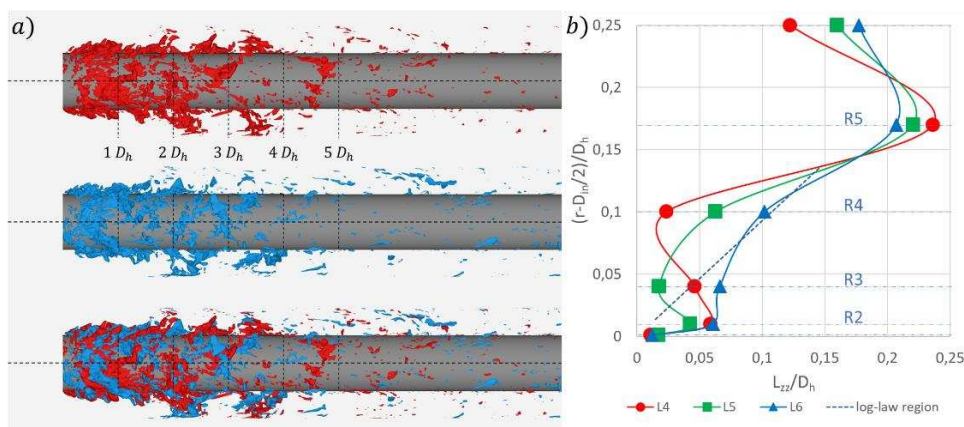


Figure 1. a) Helical oblique stripes pattern, b) variation of turbulent length scales.

Reference

- [1] Cioncolini A, Silva-Leon J, Cooper D, Quinn MK, Iacovides H 2018 *Nuclear Engineering and Design* 338, pp. 102–118.

Anisotropic turbulence in marine cumulus clouds

Stanisław Król¹, Szymon Malinowski¹

¹ Insititute of Geophysics, Faculty of Physics, University of Warsaw, ul. Pasteura 5, 02-093
Warszawa, Poland

E-mail: skrol@fuw.edu.pl

Abstract. Clouds are such objects in the atmospheric flow, where different physical processes influence the flow at various scales. This motivates the studies of deviations from Kolmogorovs theory of homogeneous and isotropic turbulence. In this work, time series obtained from marine cloud penetrations are studied with the usage of anisotropy invariant maps. Preliminary results suggest that the turbulence in clouds is anisotropic.

Keywords: Atmospheric Science, Turbulence, Multi-phase Flows, Anisotropy, Nonlinear analysis

1. Introduction

Clouds are manifestations of turbulent flow in the atmosphere. Different physical processes and effects such as radiation, entrainment, microphysical interactions, non-zero vertical gradients of temperature and wind speed, influence the flow at different scales.

When analysing turbulence characteristics in clouds, one often assumes homogeneity, isotropy, and equilibrium. Those assumptions simplify the problem, but might not capture the whole picture. For such complicated systems as clouds, in which many thermodynamical and microphysical processes take place, these assumptions might fall short. In this work, we make a case study of clouds in terms of anisotropic turbulence. The data comes from EUREC⁴A campaign [1], as well as MAGPIE-SHIMMER campaign, where Twin-Otter aircraft performed penetrations of marine cumulus clouds near Barbados. An analysis of wind speed time series is performed with the usage of anisotropy invariant maps.

2. A taste of the results

Preliminary results suggest that the turbulence in clouds is to some degree anisotropic. This manifests in non-zero values of invariants of the Reynolds stress anisotropy tensor [2]:

$$a_{ij} = \frac{\overline{u'_i u'_j}}{2k} - \frac{\delta_{ij}}{3}, \quad (1)$$

namely:

$$II = \lambda_1^2 + \lambda_1 \lambda_2 + \lambda_2^2, \quad (2)$$

$$III = -\lambda_1 \lambda_2 (\lambda_1 + \lambda_2), \quad (3)$$

where λ_i are the eigenvalues of the tensor described by equation 1. By employing a simple transformation $(\eta^2, \xi^3) = (II/3, III/2)$, one obtains a new coordinate system, where all of the possible values are bounded by a geometrical figure called Lumley's triangle. Typically for isotropic turbulence II and III are equal to 0.

Figure 1 shows the values of η and ξ for different time instances during cloud penetration:

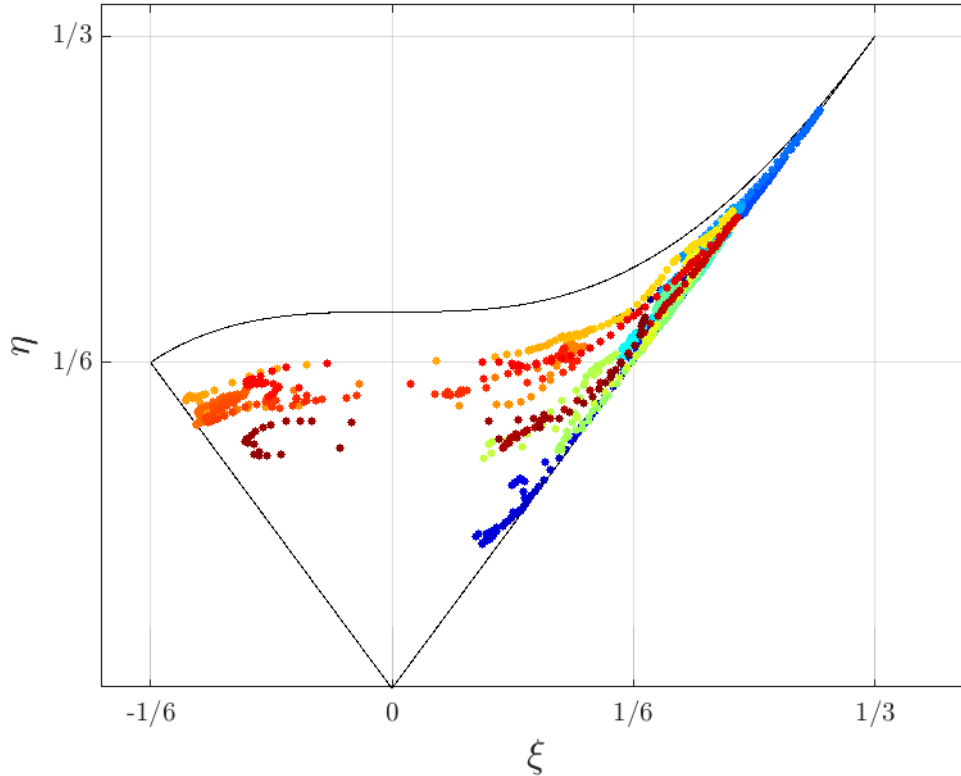


Figure 1. Lumley's triangle for cloud penetration. Colour indicates different time instance in the series.

Most of the values align on a line connecting points $(0, 0)$ and $(1/3, 1/3)$, which means that the turbulence is expanded along one direction. The discussion of the results will include more study cases, the physical interpretation of the Lumley's triangle, as well as the implications together. The time series will be analysed and divided, based on the recurrence quantification analysis [3]. The division will include cloudy air, turbulent air around cloud and environmental undisturbed air.

References

- [1] Stevens, B., Bony, S., Farrell, D., Ament, F., Blyth, A., Fairall, C., . . . Zöger, M. (2021). *EUREC4A*. Earth System Science Data, 13 (8), 4067–4119. doi:10.5194/essd-13-4067-2021
- [2] Emory, M., Iaccarino, G. (2014). *Visualizing turbulence anisotropy in the spatial domain with componentality contours* Center for Turbulence Research Annual Research Briefs
- [3] Król, S., Blyth, A., Boeing, S., Denby, L., Lachlan-Cope, Tom., Malinowski, S. P. (2024). *Can recurrence quantification analysis be useful in the interpretation of airborne turbulence measurements?* Geophysical Research Letters, accepted: 14.02.2024

Tracking invariant solutions of the Navier-Stokes equations within spectral element framework

S Gepner¹ and G Kawahara²

¹ Warsaw University of Technology, Faculty of Power and Aeronautical Engineering, ul. Nowowiejska 24, 00-665 Warszawa, Poland

² Graduate School of Engineering Science, Osaka University, 1-3 Machikaneyama, Toyonaka, Osaka 560-8531, Japan

E-mail: stanislaw.gepner@pw.edu.pl

Abstract. This work presents an approach for tracking invariant solutions of the Navier-Stokes equations, which leverages the flexibility and efficiency of the spectral element method (SEM) and offers an advantageous alternative to existing case-specific solvers. Traditional methods usually rely on global discretizations, tailored for specific geometries and are often limited to particular polynomial bases, which limits their applicability beyond most basic geometrical configurations. In contrast, our method leverages the flexibility and efficiency of the spectral element method (SEM), enabling seamless handling of complex geometries and diverse boundary conditions.

Keywords: Turbulence, Computational Fluid Dynamics, General Fluid Dynamics.

1. Introduction

In the realm of turbulence, invariant solutions of the Navier-Stokes equations hold significant importance. Taking on the form of travelling waves, periodic or relative periodic orbits, these solutions represent specific flow states that remain invariant under the evolution of the Navier-Stokes system. Due to their low-codimension stable manifold, invariant solutions act by attracting the flow state, which remains trapped in their proximity for significant amounts of time, only to eventually repeal it towards other such solutions along one of their few unstable directions. Consequently, stable manifolds of a number of invariant solutions populating the state space, weave a web that forms the turbulent attractor [1]. At the same time, invariant solutions manifest the statistical view of turbulence as coherent structures [2], leading to the intriguing degree of organisation that often transpires in well-defined secondary flows.

Due to the role of invariant solutions, their proper identification, understanding and characterisation offers valuable insights into the character of turbulent flow. Invariant solutions may serve as reference points for studying turbulence dynamics and provide a much deeper understanding of the transition phenomena, especially since the laminar-turbulent boundary may be a codimension-one stable manifold of a particular invariant solution - the so-called edge state. At the same time, invariant solutions can be crucial for developing new turbulence models and serve as benchmarks to validate their accuracy in engineering simulations. Additionally, knowledge of invariant solutions and their relations can help design efficient strategies for controlling and manipulating turbulent flows across various technologies.

2. Tracking invariant solutions

Tracking invariant solutions of the Navier-Stokes equations, as well as evaluating their stability, is a challenging task. Several methods have been applied to this problem so far. On the one hand, homotopy continuation methods are based on applying a parameter-controlled perturbation to the system to force its transition in the proximity of the desired solution, followed by a continuous variation of the parameter, decreasing the perturbation magnitude until the desired solution is obtained. On the other hand, edge-tracking or bisection methods exploit the fact that invariant solutions often lie on a laminar-turbulent edge, along which they act as relative attractors and might be reached by continuously refining initial perturbation along a selected direction that intersects with the desired solution's stable manifold. Consequently, as the bisection process progresses, consecutive approximations fall closer to the stable manifold, and eventually, the desired solution may be approached. Finally, with a sufficiently good initial approximation of the invariant solution, Newton-Krylov methods become extremely efficient, offering rapid convergence, provided that the consecutive linear system approximations are sufficiently well-behaved. Once an invariant solution is known, evaluation of its character and stability is a task that requires the solution of a large system eigenvalue problem. This part is usually handled using a time-stepping method and an Arnoldi iteration process.

Tracking and stability evaluation methods are often constructed around purpose-specific solvers that utilise high-order discretization methods 'global' over the entire domain. By global, we mean methods that apply a non-compact support base that spans the entire domain to interpolate flow variables. Consequently, such solutions are efficient in tracking invariant solutions for specific problems but, at the same time, remain inflexible and limited only to a narrow range of simple geometrical configurations, significantly limiting their applicability to more complex flow geometries and boundary conditions.

3. Implementation within SEM framework

In this work, we present an approach for tracking invariant solutions of the Navier-Stokes equations constructed around a general-purpose spectral element h/p library Nektar++ [3] that leverages SEM's flexibility and high fidelity. To the best of our knowledge, this marks the first attempt at utilising SEM to track invariant solutions of the Navier-Stokes equations. Incorporating SEM as the base of the invariant solution tracking framework offers several advantages. Firstly, our approach features geometric flexibility, allowing for studying flows through complex geometries and overcoming the limitations of the more traditional methods. Secondly, the approach allows for versatility in the application of boundary conditions. Finally, the application of a general-purpose solver allows the process to benefit from ready-to-use parallelisation and computational efficiency during repeated direct numerical solutions (DNS) of the turbulent flow problem.

Acknowledgments

The authors would like to acknowledge the financial support of the Japan Society for the Promotion of Science (JSPS) in the form of the FY2020 JSPS Postdoctoral Fellowship for Research in Japan (Short-term) no. PE20715 and the National Science Centre, Poland, in the form of a Sonata-15 (2019/35/D/ST8/00090) grant.

References

- [1] Hof, B., Van Doorne, C. WH, Westerweel, J., Nieuwstadt, F. TM, Faisst, H., Eckhardt, B., Wedin, H., Kerswell, R. and Waleffe, F. 2004 Experimental observation of nonlinear traveling waves in turbulent pipe flow. *Science*, 305 (5690), 1594–1598.
- [2] Kawahara, G., Uhlmann, M. and van Veen, L. (2012). The significance of simple invariant solutions in turbulent flows. *Annual Review of Fluid Mechanics*, 44, 203–225.
- [3] Cantwell, C.D., Moxey, D., Comerford, A., Bolis, A., Rocco, G., Mengaldo, G., De Grazia, D., Yakovlev, S., Lombard, J.-E., Ekelschot, D., Jordi, B., Xu, H., Mohamied, Y., Eskilsson, C., Nelson, B., Vos, P., Biotto, C., Kirby, R. M. and Sherwin, S. J. 2015 Nektar++: An open-source spectral/ element framework. *Computer Physics Communications* 192, 205 – 219.

Global instabilities on ROTEX-T cone-flare model in hypersonic flow at high altitude cruise conditions

K Dylewicz¹ and V Theofilis²

¹ University of Liverpool, School of Engineering, L69 3GH, Liverpool, United Kingdom

² Technion, Faculty of Aeronautics and Space Engineering, 32000, Haifa, Israel

E-mail: sgkdylew@liverpool.ac.uk

Abstract. Viscous laminar Mach 6 flow over a cone-flare geometry is investigated numerically to determine the critical Reynolds number past which self-excited instabilities inside the boundary layer naturally lead flow to laminar-turbulent transition. To this end, direct numerical simulations (DNS) are performed to converge the unsteady axisymmetric equations of motion to steady-state solutions. Subsequently, global linear modal and non-modal stability analyses are performed, taking the azimuthal direction to be homogeneous, to unravel the leading unstable three-dimensional (non-axisymmetric) perturbations. Finally, results are verified in full DNS which follows the linear evolution of the perturbations up to the early nonlinear breakdown.

Keywords: Aerodynamics, Computational Fluid Dynamics, Linear Stability Analysis, Transition to Turbulence

1. Introduction

The present work investigates the cone-flare ROTEX-T [1] configuration with respect to its linear, modal and non-modal, perturbations that lead axisymmetric flow to laminar-turbulent transition. These small-amplitude disturbances are associated with shock wave/boundary layer interactions (SBLIs), as well as amplified and self-excited perturbations of the laminar separation bubble (LSB) formed at the cone-flare. Herein, the flow conditions corresponding to a vehicle cruising at altitude of $50km$ according to U. S. Standard Atmosphere, with free-stream Mach number $M_\infty = 6.0$, were selected in order to maintain laminar and steady flow over the geometry while achieving the size of the model that is of practical relevance. Additionally, such choice of flow conditions ensures that the second Mack mode [2], which develops inside the boundary layer prior to the flare, is convectively stable, which permits neglecting interaction of boundary layer instabilities with those developing in the flare region on account of SBLI.

2. Ongoing work

Our recent work at high unit Reynolds numbers [3] provided evidence of global instability of the axisymmetric flow. Consequently, here we focus on the identification of conditions at which the laminar flow is truly steady and axisymmetric on the cone preceding the flare, and compute this flow in a time-accurate manner until a true steady-state has been reached. One of the objectives of the present investigation is the identification of a critical Reynolds number at which the flow becomes globally unstable on account of modal linear perturbations.

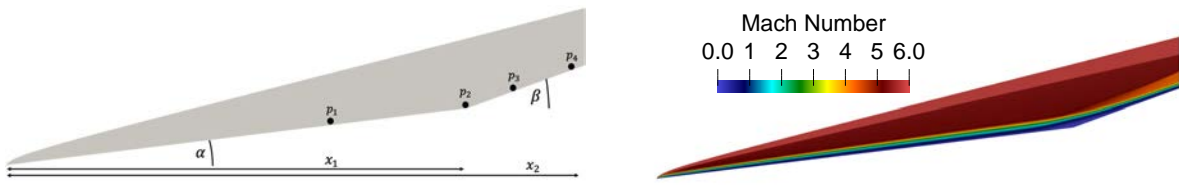


Figure 1: Geometry outline with chosen parameters and probes' locations indicated (left) and Mach number flow field for a converged steady-state at $Re_\xi = \rho_\infty u_\infty x_1 / (\mu_\infty \cos \alpha) = 5.0 \times 10^4$.

To this end, a steady-state is obtained by means of a direct numerical simulations over the ROTEX-T geometry shown in figure 1 (left) where $x_1 = 0.4377m$, $x_2 = 0.55m$, $\alpha = 7^\circ$, $\beta = 20^\circ$ and $Re_\xi = \rho_\infty u_\infty x_1 / (\mu_\infty \cos \alpha) = 5.0 \times 10^4$. Here, an open-source *rhoCentralFoam* code [4] has been used with second-order temporal scheme and CFL number maintained below 0.75 throughout the simulation. Time-accurate convergence of the flow towards the steady-state has been verified using residuals computed within the boundary layer using probes; for their approximate locations see p_1 , p_2 , p_3 and p_4 in figure 1 (left). The steady-state solution is shown, using Mach number field, in figure 1 (right). Residuals convergence proves that the flow remains globally stable in the axisymmetric sense. However, previous experience on this geometry [3] might suggests that the onset of the global instability happens on account of three-dimensional perturbations, sustained within the separated shear layer, with high periodicity along the azimuthal direction. Therefore, presently computed steady-state is a good candidate to begin systematic investigations of modal and non-modal three-dimensional linear perturbations to eventually determine critical flow conditions past which self-excited instabilities inside the boundary layer naturally lead flow to laminar-turbulent transition.

3. Future work

Future work includes mesh independence study of the steady-state solution at present Reynolds number of 5.0×10^4 followed by modal and non-modal global stability analysis using extensively validated BiGlobal stability code [5].

Acknowledgments

This work is supported by the AFOSR under award number FA8655-23-1-7031 with Dr. Douglas Smith as PO. Computational time provided by UKTC and EPSRC on the UK supercomputing facility ARCHER2 via projects EP/R029326/1 and EP/X035484/1 is gratefully acknowledged.

References

- [1] A. Güllhan, T. Thiele, F. Siebe, F. Klingenberg, R. Kronen, A. Stamminger, F. Scheuerpflug, A. Kallenbach, and W. Jung, "Main Achievements of the Rocket Technology Flight Experiment ROTEX-T." 21st AIAA International Space Planes and Hypersonics Technologies Conference, 2017.
- [2] L. M. Mack, "Boundary-layer linear stability theory," tech. rep., California Inst of Tech Pasadena Jet Propulsion Lab, 1984.
- [3] J. Davami, T. J. Juliano, A. Scholten, P. Paredes, E. K. Benitez, C. L. Running, K. Dylewicz, V. Pezlar, V. Theofilis, T. Thiele, *et al.*, "Separation and Transition on the ROTEX-T Cone-Flare," in *AIAA SCITECH 2024 Forum*, p. 0499, 2024.
- [4] C. J. Greenshields, H. G. Weller, L. Gasparini, and J. M. Reese, "Implementation of semi-discrete, non-staggered central schemes in a colocated, polyhedral, finite volume framework, for high-speed viscous flows," *International journal for numerical methods in fluids*, vol. 63, no. 1, pp. 1–21, 2010.
- [5] H. Quintanilha, P. Paredes, A. Hanifi, and V. Theofilis, "Transient growth analysis of hypersonic flow over an elliptic cone," *Journal of Fluid Mechanics*, vol. 935, p. A40, 2022.

URANS numerical analysis of turbulence intensity influence on laminar separation bubble in the case of the NACA0018 airfoil

J Michna¹ and K Rogowski¹

¹Warsaw University of Technology, Institute of Aeronautics and Applied Mechanics, ul. Nowowiejska 24, 00-665 Warszawa, Poland

E-mail: jan.michna.dokt@pw.edu.pl

Abstract. This work investigates the effect of turbulence intensity on laminar separation bubble characteristics using the URANS approach. The ANSYS Fluent software was used with Transition SST model turbulence to simulate flow over the boundary layer of the NACA0018 airfoil. The low-Reynolds number (80,000 and 125,000) conditions were chosen to reach airfoil performance similar to a small Darrieus-type wind turbine with moderate tip speed ratios. The result was compared with the PIV experiment [2].

Keywords: Turbulence, Separation Bubble, Laminar-to-turbulent transition, RANS modeling, Vertical Axis Wind Turbines

1. Introduction

Darrieus-type wind turbines, as a subgroup of Vertical Axis Wind Turbines (VAWT), convert wind energy based mainly on the lift force phenomenon. These devices are built of straight or curved vertical airfoil-shaped blades. The wind flow over the turbine's rotor produces a torque that can be converted to e.g., electrical power. Correct aerodynamic forces calculation significantly influences accurate wind turbine power estimation. Due to varying flow conditions, occurrence of dynamic stall, and steady changes in the angle of attack during rotation, CFD (computational fluid dynamics) methods are the most accurate. Various input settings, such as Reynolds number and turbulence intensity, noticeably affect final power results. As has been observed [1], this is induced by the occurrence of the laminar-to-turbulent transition in the boundary layer of the airfoil.

2. Methodology

To study this influence more deeply, this work investigates the effect of turbulence intensity on laminar separation bubble (LSB) characteristics using the URANS approach (Unsteady Reynolds-Averaged Navier Stokes equations). The ANSYS Fluent 22.1 software was used with Transition SST model turbulence to obtain velocity distribution in the boundary layer and pressure values on NACA 0018 airfoil. The turbulence model is a correlation-based transition model and is formulated of 4 transport equations. Two of them are as in the k-omega SST model, and two are transport equations for intermittency and momentum thickness Reynolds number

prepared on semi-empirical correlations. A structural 2-dimensional mesh with 633 thousand quadrilateral elements was prepared.

The size, position, and thickness of LSB were examined for two Reynolds numbers $Re=80000$ and $Re=125000$. Freestream turbulence intensities from the range of 0.06% to 0.53% were chosen. All cases are performed only for an angle of attack of 4 degrees.

3. Results and Conclusions

As has been observed, the LSB occurs on the suction side of the NACA0018 airfoil for all cases. The size (around 25%-30% of the chord) and position (around 30% of the chord) of the laminar bubble are similar for all numerical results. The thickness of the bubble varies from 1% to 0.5% of the chord. For the lower Reynolds number, the bubble is larger and thinner. If turbulence intensity lowers, then the bubble size becomes larger.

These CFD results are compared to the Particle Image Velocimetry experiment [2]. The difference is noticeable, especially for larger turbulence intensity values. For turbulence intensity equal to around 0.06% and $Re = 80,000$, the LSB size and position are very similar, as shown in Figure 1.

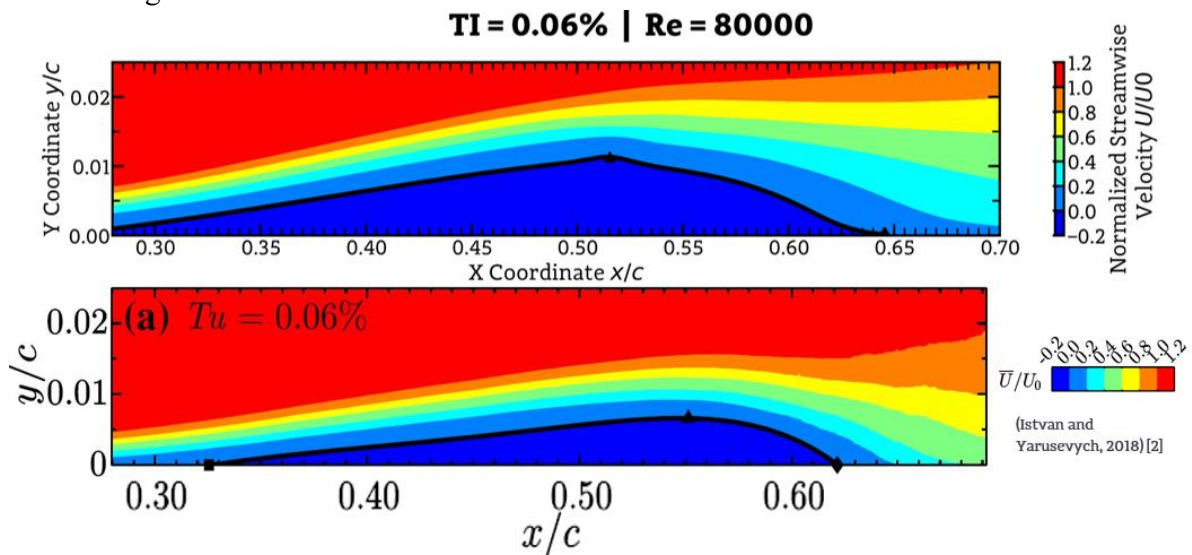


Figure 1. Streamwise velocity in the boundary layer on the suction side of NACA0018 from URANS calculations (up) compared to experimental PIV results [2] (bottom)

Funding

This research was carried out with the support of the Interdisciplinary Centre for Mathematical and Computational Modelling at the University of Warsaw (ICM UW) under computational allocation no GB83-33. The research was funded by POB Energy of Warsaw University of Technology within the Excellence Initiative: Research University (IDUB) programme. Grant No. 1820/355/Z01/POB7/2021.

References

- [1] Michna, J., Rogowski, K., 2022. *Numerical Study of the Effect of the Reynolds Number and the Turbulence Intensity on the Performance of the NACA 0018 Airfoil at the Low Reynolds Number Regime*. Processes 10, 1004. <https://doi.org/10.3390/pr10051004>
- [2] Istvan, M.S., Yarusevych, S., 2018. *Effects of free-stream turbulence intensity on transition in a laminar separation bubble formed over an airfoil*. Exp Fluids 59, 52. <https://doi.org/10.1007/s00348-018-2511-6>

Young Researchers
Prof. J.W. Elsner's Competition

Turbulent Coherent Structures in Thermal Vortex Rings

P. Jędrejko¹, Y-I. Yano² and M. Waławczyk¹

¹ University of Warsaw, Faculty of Physics, Institute of Geophysics Pasteura 5, 02-093 Warszawa, Poland

² CNRM UMR3589 (CNRS), Météo-France, 31057 Toulouse Cedex, France

E-mail: p.jedrejko@uw.edu.pl

Abstract. A thermal vortex ring is generated from an isolated buoyancy anomaly. This study simulates this formation process by the vortex-blob method. The vortex sheet initially generated at the boundary induces a Kelvin-Helmholtz instability. Further, the wave number of the growing perturbation is then sequentially halved. This cascade process induces a turbulent flow, which leads to coherencies associated with the formation of the ring.

Keywords: Turbulence, vortex, ring, sheet, Kelvin-Helmholtz, instability, interface, buoyancy, convection, thermal

1. Background and Motivation

It has been recognized for many years that coherencies are ubiquitous in turbulent flows. Yet, we still lack of satisfactory understanding of this process. In this study, we attempt to under it by adopting a prototype system - a formation process of a thermal vortex ring.

2. Formulation of the Problem

The formation of a vortex ring from an initial spherical buoyancy anomaly is considered under the Boussinesq approximation. The anomaly is homogenous with a discontinuity at the boundary. The system is assumed to remain axisymmetric, and all diffusivities are neglected. Under these assumptions, the evolution of the system is determined solely in terms of the anomaly interface, which corresponds to a vortex sheet. The velocity field by which it is advected is consistently determined from a given vorticity distribution.

Under this formulation, the problem can be solved numerically in the following manner:

- (i) Lagrangian approach used in a description of vortex-sheet evolution[1]
- (ii) Fast multipole method, for the velocity-computation acceleration[2]
- (iii) Contour surgery, to optimize the local resolution[3]

3. Results

As the buoyancy anomaly rises upwards, it experiences a collapse at the bottom which transforms it into a ring. During this process, the vortex sheet at the sides is subjected to Kelvin-Helmholtz instability in a wavenumber determined by its thickness. The resulting “cat eyes” increase the

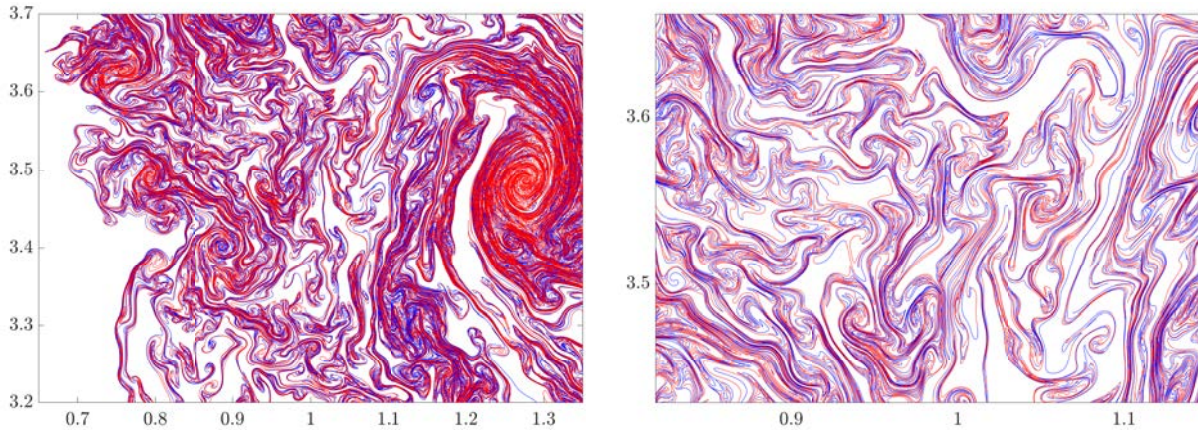


Figure 1: Interfacial vortex sheet forming the turbulent structures. Intervals with positive vorticity are marked red and with negative - blue.

effective thickness, halving the unstable wavenumber. The process continues sequentially in the form of an inverse cascade. It iteratively applies Smale’s horseshoe map at different scales resulting in chaotic mixing and exponential growth of the interface’s length. Older and smaller vortices are stretched and winded onto new foci of instability. As the length scales involved in the process approach the radius of the anomaly, a few large, coherent vortices dominate the ring dynamics. At that time, the vortex sheet tightly fills the “interior” of the ring, reproducing the fine structure of turbulence (Figure 1). This representation is further used to analyze the fractal dimension of the turbulent patterns.

The described multiscale Kelvin-Helmholtz instability clearly executes energy transfer toward large scales. This is further quantified by the kinetic-energy spectrum. Such inverse energy cascade is characteristic of two-dimensional turbulence and here is driven by pure advection, without any diffusive processes. However, assigning the sheet some finite thickness dumps the smallest scales. This results in a finite effective Reynolds number which is estimated and compared to grid-based simulations.

Acknowledgments

Financial support of the National Science Centre, Poland, Project 2020/37/B/ST10/03695 is gratefully acknowledged.

References

- [1] R. Krasny (1985) *Desingularization of Periodic Vortex Sheet Roll-up*, J. Comput. Phys.
- [2] L. Greengard and V. Rokhlin (1987) *A fast algorithm for particle simulations*, J. Comput. Phys.
- [3] D. G. Dritschel (1987) *Contour Surgery: A Topological Reconnection Scheme for Extended integrations Using Contour Dynamics*, J. Comput. Phys.

Control of turbulent boundary layer separation using a sinusoidal-type wavy-wall

P Kamiński¹ and A Tyliszczak¹

¹Department of Thermal Machinery, Częstochowa University of Technology, al. Armii Krajowej 21, 42-201 Częstochowa, Poland

E-mail: piotr.kaminski@pcz.pl

Abstract.

This paper focuses on optimizing wall corrugation parameters (waviness type and amplitude) to efficiently control the wall-shear stress (τ_w) and delay turbulent separation. The research employs the Large Eddy Simulation method. The results obtained for a regular sine wave are compared to a novel, tilted shape of waviness. It is demonstrated that the suitably selected shape of the corrugated wall significantly affects the flow field by enhancing turbulent kinetic energy, increasing τ_w , and leading to the postponement of the separation.

Keywords: Computational Fluid Dynamics, Turbulent Separation, Wavy-Wall

1. Introduction

The turbulent boundary layer (TBL) exposed to adverse pressure gradient (APG) conditions often undergoes separation, resulting in significant energy loss. To prevent this, various flow control methods are being developed, of which passive methods are currently attracting the most interest as they do not require additional external input. It is well known that surface roughness plays a significant role in TBL control, however, such a method has been effective only for laminar or transitional flows, as noted by McMasters and Henderson [1]. Interesting findings, in turn, are provided by Drózdź et al. [2], who demonstrated the possibility of effective control of APG TBL using streamwise waviness. They reported a significant increase in τ_w and a postponement of separation. They also showed that the mechanisms governing the increase in τ_w caused by wavy-wall are similar to amplitude modulation of small scales by the large scales. Recently, Kamiński et al. [3] pointed out the importance of the sinusoidal wavy-wall parameters such as amplitude ($A(x)$), a number periods (N_λ) and the effective slope. In the present paper, we extend this study by including leftward or rightward wave shapes with varying degrees of tilt. We compare the performance of these asymmetric walls with the regular ones (sinusoidal) and the flat plate case.

2. Problem statement

The research objective is to identify a wavy-wall shape that maximizes the growth in the wall-shear τ_w to achieve a significant delay in TBL separation. The computational domain is depicted in Fig. 1, which also includes the formulas defining both regular and tilted waviness.

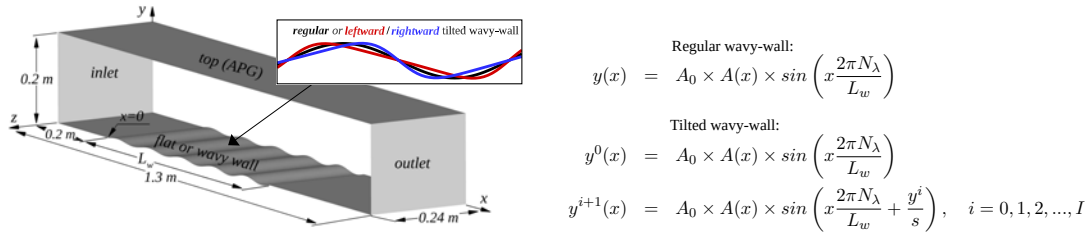


Figure 1. Computational domain and formulas defining regular and tilted wall shapes.

3. Results

The simulations are conducted for the Reynolds number based on friction velocity u_τ and boundary layer thickness δ equal to $Re_\tau = \delta u_\tau / \nu = 2500$, where ν is the kinematic viscosity. The choice of such a relatively low Re_τ was dictated by the need for performing a parametric LES study at reasonable computational costs. The analysis is carried out for $0 \leq A_0 \leq 2.0$ and $1 \leq N_\lambda \leq 7$, which, at a fixed waviness length (L_w), constitutes a variable period length $\lambda = L_w / N$. For the fundamental amplitude $A(x)$, which slightly grows with x [2], A_0 equals to 1. For the combination of $A_0 = 1.2$ and N_λ providing a maximal τ_w enhancement, a modification of the waviness by tilting it to the left was introduced. This modification is defined in the right subfigure of Fig. 1. It relies on an iterative process (I denotes the number of iterations) in which the parameter s controls the degree of inclination, influencing the strength of the waviness tilting.

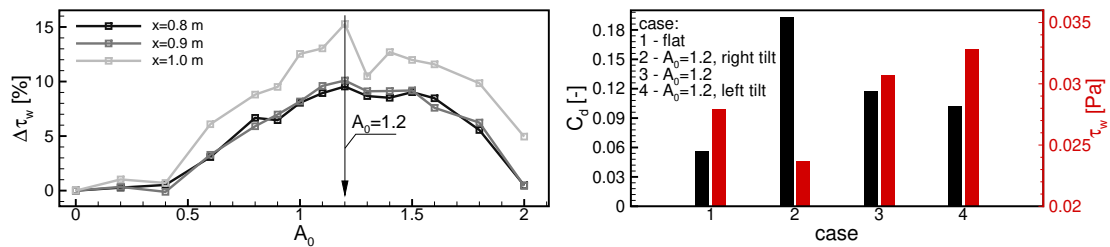


Figure 2. Profiles of $\Delta\tau_w$ at different x -distances (left), τ_w as well as C_d for $A_0 = 1.2$, tilted waves and flat wall (right).

The results obtained so far are presented in Fig. 2. They show the increase in wall-shear stresses expressed as $\Delta\tau_w$ as the function of A_0 (left) as well as $\tau_w(x)$ and total drag coefficient C_d for tilted sine waves compared to regular waviness and flat wall. It can be observed that τ_w strongly depends on A_0 and for the regular sine waviness, $A_0 = 1.2$ and $N_\lambda = 5$ lead to the highest increase in the wall-shear stress. However, it turns out that τ_w can be enhanced even more by only a tiny leftward tilting of the waviness (case 3). Interestingly, it is found that leftward tilt also provides a reduction in C_d in contrast to a regular wave. Consequently, an opposite is observed by utilizing rightward tilt. We will analyze whether adjusting s and/or I can provide further benefits and try to explain why this happens.

Acknowledgments

This work is supported by the National Science Center in Poland (Grant 2020/39/B/ST8/01449).

References

- [1] McMasters JH and Henderson ML 1979 *The Sci. and Technol. of Low Speed and Motorless Flight* **Pt. 1**.
- [2] Drózd A et al. 2021 *Experimental Thermal and Fluid Science* **121** 110291.
- [3] Kamiński P et al. 2023 *Applied Mathematical Modelling* (under review)

Impact of flashing conditions on impinging-jet sprays

B Kaźmierski¹ and ŁJ Kapusta¹

¹ Warsaw University of Technology, Faculty of Power and Aeronautical Engineering,
Institute of Heat Engineering, Poland

E-mail: bartosz.kazmierski.dokt@pw.edu.pl,
lukasz.kapusta@pw.edu.pl

Abstract. The study presents a comparative analysis of the spray size and shape formed by the collision of two water jets under subcooled and flash-boiling conditions. The flashing effects were attained by increasing the water temperature prior to the injection. Synchronised two-camera imaging was used to observe the sprays from two perpendicular directions. The results showed a significant increase in spray size under flash-boiling conditions. Additionally, the predominant propagation direction of spray was perpendicular to the jets' plane, despite their disintegration before the collision.

Keywords: Experimental Fluid Mechanics, Multi-phase Flows, Impinging jets, Flash Boiling

1. Introduction

Impingement of liquid streams at a common point produces droplets if the developed instabilities are sufficient to disintegrate the emerging liquid structure. This atomisation method enables mixing of injected liquids and control over the droplet size. Therefore, it has been widely used in rocket engine injectors [1]. In space, the initial injection of fuel and oxidiser occurs in near-vacuum conditions, which may cause rapid vaporisation of liquid streams. Gas bubbles, which nucleate, expand and burst, become a dominant breakup factor, increasing the radial-to-axial momentum ratio and widening the spreading angles of the streams.

The interactions between jets under flashing conditions have been studied for injectors with diverging nozzle axes, indicating possible spray collapse [2-6]. The collapse results from the self-entraining of overlapping sprays and vapour, forming a single, integrated spray plume. Therefore, it is not a direct consequence of flash vaporisation, but its secondary effect [4]. In contrast to diverging-axes injectors, the implications of flash boiling on self-impinging jets have not been sufficiently investigated. Hence, this research aims to fill this gap by analysing the overall shape of the spray from two symmetrical impinging water jets under flashing conditions.

2. Methods

Sprays were analysed using images from two synchronised sCMOS cameras with global illumination. The observation directions were parallel and perpendicular to the plane of liquid jets. The images were captured at a 20-Hz frequency. The spray angle and width were measured at the geometrical intersection point of the nozzles' axes. The averaging was performed for three measurement series and within 8.5-9.5 seconds after the start of an injection. This delay limited the analysis results to the period when temperature and spray shape stability were reached.

The injector was equipped with two 0.7-mm nozzles with an impinging angle of 30° and a collision distance of 12 mm. The deionised water was injected under pressure of approximately 7.1 bar (gauge) into ambient air at 1 bar and $\sim 20^\circ\text{C}$. The flash-boiling injection was attained by increasing the water temperature before the injection over the boiling point in the ambient air. Two cases were considered: 40°C and 140°C water temperature. Water temperature was controlled within all main elements of the test rig using electric heaters and silicon oil circulation.

3. Results and conclusions

The spray formed as a result of self-impinging water jets under subcooled and flash-boiling conditions indicated that:

- In the superheated case, the collisions of two liquid columns changed into the interactions of sprays and vapour streams due to the jets' breakup and vapour generation before the collision,
- The intensity was considerably raised in the superheated case (Fig. 1) due to an increased amount of condensing vapour and finer droplets (compared with a subcooled case), caused by abrupt water evaporation and bursting of gaseous bubbles.
- The spray width and angles under flashing conditions were significantly increased.
- Momentum was effectively exchanged between jets under flashing conditions since two cores of vapour and fine droplets propagated in the right direction to the jets' plane (Fig. 1C), while a single plume was maintained when observed from the other direction (Fig. 1D).

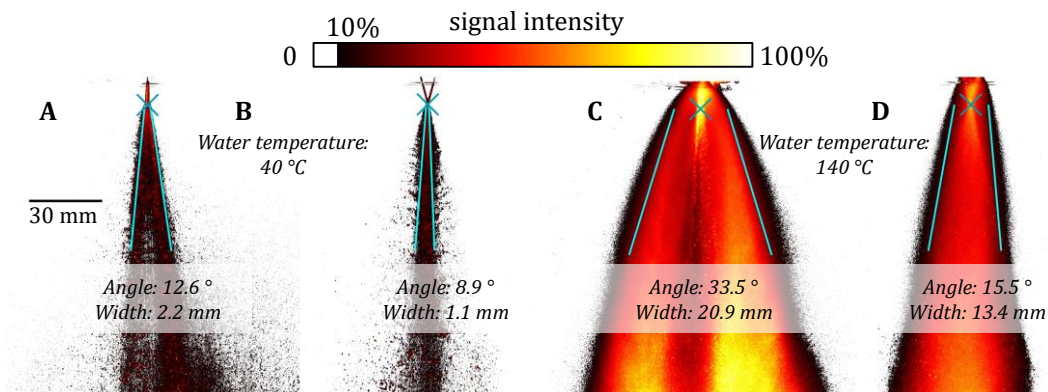


Figure 1. The instantaneous signal intensity from the globally illuminated sprays captured ~ 9.5 s after the start of the injection; A, C – view parallel to the jets' plane; B, D – view perpendicular to the jets' plane; geometrical impingement point and sides of the spray angles were marked with a cyan colour

Acknowledgements

This research was funded in whole or in part by the National Science Centre, Poland, within the framework of the SONATA programme, grant number: 2020/39/D/ST8/00947. For the purpose of Open Access, the author has applied a CC-BY public copyright licence to any Author Accepted Manuscript (AAM) version arising from this submission.

References

- [1] Casiano M, Hulka J, Yang V 2009 *J. Propuls. Power* **26**
- [2] Jiang C, Parker MC, et al. 2019 *Appl. Energy* **254** p 113735
- [3] Kang Z, Bai Y, et al. 2024 *Case Stud. Therm. Eng.* **55** p 104141
- [4] Kapusta ŁJ 2022 *Energy* **247** p 123388
- [5] Xu Q, Pan H, et al. 2019 *Int. J. Heat Mass Transf.* **138** p 608
- [6] Zeng W, Xu M, et al. 2012 *Fuel* **95** p 287

Numerical investigation of local aerosol deposition in a real scale T-junction of a ventilation network

R Ploix^{1,2}, J Malet¹, E Gehin²

¹ Institut de Radioprotection et de Sûreté Nucléaire (IRSN), PSN-RES/SCA/LEMAC, F-91400, Saclay, France

² Univ Paris-Est Créteil, CERTES, F-94010 Créteil, France

E-mail: remy.ploix-upec@irsn.fr

Abstract. In this study, numerical simulations of local aerosol deposition in a T-junction of a ventilation network are compared with experimental results obtained on a real scale facility. An analysis of the numerical flow at global and small scale is proposed to assess the validity of the simulation. The experimental and numerical results show the same aerosol deposition tendency on the outer branch of the T-junction.

Keywords: Computational Fluid Dynamics, multi-phase Flows, turbulence, deposition, singularity, T-junction

1. Introduction

Aerosol deposition in ventilation ducts plays an important role in particulate pollution transfers in industrial facilities. The lack of specific model for aerosol deposition in singularities like T-junction is a problem to estimate the deposition in a whole ventilation facility. CFD simulation is a good way to develop new correlations and need to be validated. This work focuses on the comparison between experimental and numerical results of aerosol deposition inside an horizontal T-junction with two inlets and one outlet.

2. Experimental procedure

The experimental results come from our facility, a sixty meters long industrial size venting system, with rectangular section ($a = 600$ mm and $b = 400$ mm) and many singularities (bends, T-junction and converging channel) presented in [1]. A protocol for local deposition measurement [2], has been used to get local deposition at different points upstream, downstream and inside T-junctions [3]. This paper presents the results associated to different parameters: four flow ratios, three shapes of T-junctions with sharp and smooth angles and three particle diameters were experimentally investigated and are used for simulation validation.

3. Numerical procedure

The simulation domain is the whole experimental facility. One geometry of each singularity has been chosen as reference for flow validation. Three meshes have been considered, with the same wall refinement ($y^+ \approx 1$) but different bulk elements size (0.1, 0.075 and $0.05 \times D_h$). The simulations were

conducted on ANSYS Fluent 2022R1 using two RANS models, the $k-\omega$ SST and the RSM (ϵ -based). For the particle simulations, the lagrangian tracking method is used, with stochastic eddy interaction model [4].

3.1. Mesh validation

Based on RSM flow calculations, the mean flow field at different distances downstream the T-junction have been compared between the three meshes. No differences were observed. When looking at turbulent kinetic energy profiles and Reynolds stresses [5], some differences appeared on the location of maximum values. The intermediate mesh was chosen for the continuation of the study, to get a convenient computational time. Another comparison, in a straight duct of the facility, was done between numerical and experimental results on nondimensional near wall Reynolds stress component $U_i'U_i'^+$ and streamwise velocity U_i^+ , that is shown in Figure 1. On the Reynolds stress graph, the experimental peak in the buffer layer is lower than the numerical one. This is an effect of hot-wire filtering due to the probe size (the non-dimensional size of the wire l^+ is just below 30) [6]. The second peak is not visible on numerical data which can be a limitation of standard RSM model. Considering the experimental uncertainties and the proximity of a singularity, the experimental and numerical near-wall non-dimensional streamwise velocity profiles are in good agreement and are not so far from the classical boundary layer profile [7].

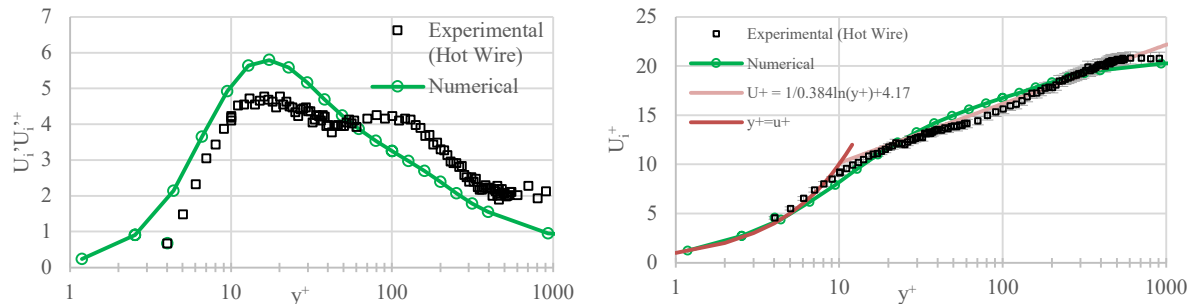


Figure 1 : Experimental and numerical horizontal near wall profiles of $U_i'U_i'^+$ (left) and U_i^+ (right), $7 D_h$ downstream a horizontal bend and at $0.6b$

3.2. T-junction flow analysis

Five experimental cases were simulated and compared. Turbulent kinetic energy, streamwise, spanwise and wall-normal velocity profiles downstream of the T-junction were compared and showed that sharp angle of a T-junction is a parameter that has much more impact on downstream flow than a high flow ratio in a smooth angles T-junction. Increasing the flow with a constant flow ratio increases the turbulent kinetic energy peak, but this effect is extremely local compared to the effect of the sharp angle. These results agreed with pressure losses study on sharp and smooth angle bends [8].

4. Results and discussion

All the cases were simulated and compared to experimental data. To do so, experimental deposited masses (m_{zone}) are adimensionalized as local deposited mass fraction: $y_D^S = m_{zone}/m_{ref}$. The same thing is done for numerical number of particles (nb_{zone}): $y_D^S = nb_{zone}/nb_{ref}$. Both experimental and numerical results show a tendency to increase the deposition downstream the T-junction on the opposite side of the secondary inlet.

References

- [1] Malet J 2024 Proc. XXVI Fluid Mechnaics Conference, (Warszaw, Poland)
- [2] Costa D et al. 2022 *Measurement Science and Technology* vol. 33
- [3] Ploix R et al. 2023 *European Aerosol Conference*, (Paris, France)
- [4] Graham and James 1996 *Int. J. Multiphase Flow* vol. 22
- [5] Lee and Moser 2015 *J. Fluid Mech* vol 774
- [6] Ghanadi F and Djenidi L 2021 *Experiments in Fluids* vol. 62
- [7] Österlund et al 2000 *Physics of Fluids* vol 12
- [8] Modi PP and Jayanti S 2004 *Chemical Engineering Research and Design* vol. 82

Evaluation of hot-wire measurement accuracy in turbulent boundary layers under strong adverse pressure gradient conditions

M Romańczyk¹, A Drózdź¹ and W Elsner¹

¹Czestochowa University of Technology, Department of Thermal Machinery, Aleja Armii Krajowej 21, 42-200 Czestochowa, Poland

E-mail: mathias.romanczyk@pcz.pl

Abstract. The paper discusses problems arising when measuring velocity fluctuation profiles in a turbulent boundary layer with hot-wire probes. The study highlighted the problem of spatial resolution, which is essential when measuring small-scale turbulence in wall-bounded flows. The attention was paid to the inconsistency in streamwise fluctuation measurements using single- and cross-wire probes. To explain this problem, the energy premultiplied streamwise velocity spectra using wavelet transformation were calculated. The analysis was performed for five cases, where the friction Reynolds number was in the range of $Re\tau = 2700-4000$.

Keywords: Experimental Fluid Mechanics, Turbulent Boundary Layer, Hot-Wire Measurements, Spatial Resolution

1. Introduction

Hot-wire anemometry is still one of the most common techniques used for turbulent boundary layer measurements. and its application is a major challenge especially in non-canonical flows, including those with a strong adverse pressure gradient (APG) present. Insufficient spatial resolution of hot-wire probes causes attenuation of energy in the measurement of small-scale turbulence, especially in high Reynolds number flows. A well-known source of experimental error in hot-wire anemometry measurements of turbulence is the spatial filtering of velocity fluctuations, which occurs when the sensing length of the probe – l , is larger than the smallest turbulence length scale, the Kolmogorov length [1]. The effect of spatial averaging weakens with the increasing of Rotta-Clauser β parameter. In order to quantify this effect for different pressure conditions a comparative study of the turbulence statistics was conducted for signals recorded with single- and cross-wire probes.

2. Methodology and experimental setup

The experimental study was performed in an open-circuit wind tunnel under APG conditions using single (Dantec Dynamics 55P31) and cross-wire (Dantec Dynamics 55P61) probes. The turbulent boundary layer was developed on a 5035 mm long flat plate at the end of which the friction Reynolds number amounted between $Re\tau = 2700-4000$ and the free-stream turbulence

intensity was at the level of 0.7%. Measurements were taken in a test section where a strong adverse pressure gradient was forced. The directional calibration of X-wire was used to obtain map of velocity vector modulus and angles. A more detailed description of the experimental measurement facility can be found in our previous works [2].

3. Results and discussion

In the current research, measurements of five different cases were analyzed, for two different freestream velocities of 15 m/s (two velocity profiles – $\beta = 13.1$ and $\beta = 35.9$) of 24 m/s (three velocity profiles – $\beta = 9.9$, $\beta = 18.5$ and $\beta = 30.7$). Measurements were performed using a single and cross-wire probe under the same flow conditions, which allowed for a thorough comparative analysis. One case from this extensive analysis is presented in this abstract, i.e. the case for 15 m/s and $\beta = 13.1$. A more detailed analysis containing all measured cases will be presented during the conference. Figure 1a shows the effect of spatial averaging on the measured streamwise Reynolds normal stress for strong adverse pressure gradient, while Figure 1b presents the isocontours of premultiplied viscous scaled streamwise energy spectra for moderate adverse pressure gradient. The results shows that near the wall the wall-normal V component is equal to almost zero even for strong APG, while the impact of non-zero V component in the outer part of TBL on turbulent scales is minor as the energy of that component is very low. Elevated energy levels for the V component are observed only near the outer edge of the boundary layer in the small-scale range, as shown by the red dashed line in Figure 1b. Thus, it can be concluded that even for high β single wire measurements gives a proper estimation of streamwise mean and fluctuation components.

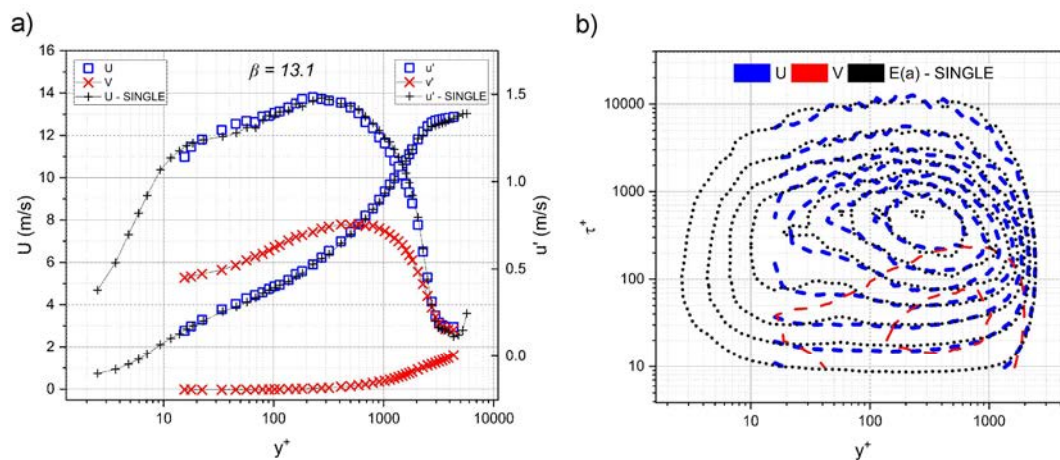


Figure 1. Velocity statistics – mean U, V and rms u', v' components – a), Isocontours of premultiplied viscous scaled streamwise energy spectra – b). Blue and red colour describes cross-wire measurements – black colour describes single-probe measurements.

Acknowledgements

The investigation was supported by the Polish National Science Centre under grant no. UMO-2020/39/B/ST8/01449.

References

- [1] A. Ashok, S. C. C. Bailey, M. Hultmark, A. J. Smits. Hot-wire spatial resolution effects in measurements of grid-generated turbulence. *Exp Fluids* 2012; 53:1713–1722.
- [2] Drózdź A, Niegodajew P, Romańczyk M, Elsner W. Effect of Reynolds number on turbulent boundary layer approaching separation. *Exp Therm Fluid Sci* 2021;125:110377.

Aeroacoustic analysis of propeller rotor noise using the porous FW–H acoustic analogy

T Suresh¹, O Szulc¹, P Flaszynski¹

¹Institute of Fluid-Flow Machinery, Polish Academy of Sciences, Fiszera 14, 80-231 Gdansk

E-mail: thanu@imp.gda.pl

Abstract. Permeable surface extension of the Ffowcs-Williams and Hawkins acoustic analogy is implemented on an in-house aeroacoustic code. A thorough validation of the implementation for elementary acoustic sources against analytical solutions is presented. Investigation of the noise emitted by a propeller rotor using the validated code is conducted.

Keywords: Aerodynamics, Computational aeroacoustics, FW–H analogy.

1. Introduction

Sound emission is one of the major concerns for various industries – aerospace, wind turbines, urban air mobility, etc. To reduce noise levels without compromising performance and efficiencies, a thorough understanding of the physics and mechanisms involved in sound generation and propagation is necessary. Computational Aeroacoustics (CAA), an hybrid approach of utilizing the Ffowcs-Williams and Hawkins acoustic analogy (FW–H) [1] to predict far-field acoustics is utilized. An in-house aeroacoustic code based on the solid surface FW–H analogy has been implemented and validated thoroughly [2]. It is a general post-processing tool based on the integral solution (Farassat’s Formulations [3]) to the FW–H analogy for bodies in subsonic motion. An extension to the code i.e porous/permeable surface FW–H formulation that allows to include volumetric noise sources is presented in the current paper. This formulation will take into account flow non-linearities, thereby increasing the range of applications and operating conditions for which acoustic predictions can be made. Thus, aiding design and optimization of novel noise mitigation strategies. An extensive validation of this code extension is presented for the thickness and loading noise mechanisms using the analytical solutions [4] of elementary acoustic sources (stationary/rotating monopole and dipoles). The validated code is utilized for the investigation of sound emitted by a propeller. A comparison between the solid and permeable surface formulations is anticipated.

2. Theoretical background

The porous surface formulation proposed by Farassat [3] are given by Equations 1 and 2.

$$4\pi p_T(x, t) = \int_{f=0} \left[\frac{\rho_0(\dot{U}_n + U_{\dot{n}})}{r(1 - M_r)^2} \right]_{ret} dS + \int_{f=0} \left[\frac{\rho_0 U_n (r\dot{M}_r + c_0(M_r - M^2))}{r^2(1 - M_r)^3} \right]_{ret} dS \quad (1)$$

$$\begin{aligned}
 4\pi p_L(x, t) = & \frac{1}{c_0} \int_{f=0} \left[\frac{\dot{L}_r}{r(1-M_r)^2} \right]_{ret} dS + \int_{f=0} \left[\frac{L_r - L_M}{r^2(1-M_r)^2} \right]_{ret} dS \\
 & + \frac{1}{c_0} \int_{f=0} \left[\frac{L_r (r\dot{M}_r + c(M_r - M^2))}{r^2(1-M_r)^3} \right]_{ret} dS.
 \end{aligned} \tag{2}$$

where p_T , f , \hat{r}_i , M_i , dS , p_L , $\cos\theta$, v_n , $u_n(x, t)$, ρ_0 , \vec{r} , M_r , \vec{M} , \vec{M} , p' , c_0 and τ represent the thickness noise term, moving surface, unit radiation vector, unit Mach vector components, elemental area, loading term, the local angle between normal to the surface and radiation vector at emission time, local normal velocity of the panel, flow normal velocity, observer time-space, density, radiation vector, Mach number in the the direction of the observer, source time derivative of the Mach vector, Mach vector, acoustic pressure, speed of sound and source time respectively.

3. Validation Case 1: Fluctuating source of mass (monopole)

The porous surface implementation is validated for thickness noise mechanism using a monopole against analytical solution [4]. A monopole is defined as a time derivative of elementary mass source, accounting for the displacement effect of the fluid produced by the body movement. The stationary monopole is modelled as a sphere with fluctuating volumetric mass flux. This sphere has a mass flux $Q = A \sin(\omega t)$ of maximum amplitude $A = 0.1$ kg/s, pulsating with a frequency (f) of 100 Hz. The far-field stationary observer is located at a distance of 8 m in the source plane. Preliminary comparison of the predicted signal from the aeroacoustic code against the analytical solution is presented in Figure 1. The FW-H code prediction is in good agreement with the analytical solution in the time domain.

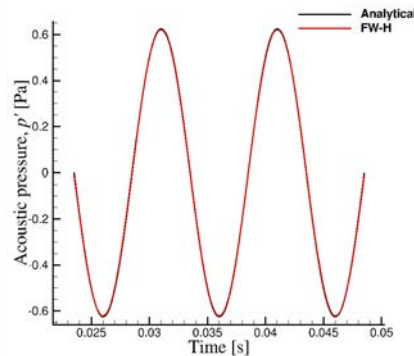


Figure 1. Total acoustic pressure (p') for a stationary monopole in time domain.

Acknowledgments

This research was supported by the National Science Centre, Poland's funding scheme Preludium under project No. 2022/45/N/ST8/01425.

References

- [1] Ffowcs-Williams J E and Hawkings D L 1969 *Phil. trans. of the Roy. Soc. of London Series A* **264**, p 321–342.
- [2] Suresh T and Szulc O and Flaszynski P 2022 *Arch. Mech.* **74**, 2–3, p 201–246.
- [3] Farassat F 2007 *NASA Tech. Rep.* **214853** p 1–25.
- [4] Rienstra S W and Hirschberg A 2019 *Tech. Rep. Eindhoven: Technische Universiteit* **0103**.

Rectangular waveguide cavities as cloaks for cylindrical obstacles

D Żyła¹ and T Bobinski¹

¹ Warsaw University of Technology, Faculty of Power and Aeronautical Engineering, ul. Nowowiejska 24, 00-665 Warszawa, Poland

E-mail: daria.zyla.dokt@pw.edu.pl

Abstract. We present a new type of cloaking device making a waveguide defect, being a circular cylinder, invisible to the incident waves. We analyse the problem by considering surface water waves in the linear regime. As such the applicability of our results extends to electromagnetism and acoustics. The wave scattering characteristics of a waveguide with cylinder can be examined through reflection R and transmission T coefficients (reflected and transmitted portion of the incident wave). The cloaking effect is achieved when the R coefficient is minimized. We demonstrate that achieving cloaking is not only feasible in numerical simulations, but also in an experimental counterpart.

Keywords: Experimental Fluid Mechanics, Surface Water Waves, Cloaking

1. Introduction

A new class of materials, the so-called metamaterials developed at the beginning of 21st century, allow to achieve phenomena that cannot be achieved by means of natural materials. New functionality of these materials is obtained thanks to its subwavelength structure. One of the most exciting application of metamaterials is making an object invisible. This phenomenon is known as cloaking, and in recent years, it has been subject to intensive investigation in many areas of wave physics [1].

In the context of surface water waves, cloaking can be achieved in several ways [2]. The first is to design proper bathymetry around an object to be hidden. The second option is to surround the object with an array of surface piercing pillars or by means of an elastic membrane mounted to an object. In our work we propose a new type of a cloak. This study focuses on achieving invisibility by optimizing the waveguide geometry in the vicinity of the cylindrical defect. By locally varying the width of a waveguide we are able to substantially reduce scattering produced by a defect. We present the properties of a cloaking device both numerically and experimentally.

2. Design of a cloaking device

Cloaking device should be able to minimize scattering in a broad range of frequencies. To design the cloak for the surface-piercing cylinder, placed inside a waveguide, the following objective function has been formulated, considering linear water waves.

$$X = \frac{\psi}{\psi_0} = \frac{\int_k |R|^2 dk}{\psi_0} \quad (1)$$

With ψ_0 representing the respective coefficient for the reference case (cylinder in a waveguide with straight walls). The coefficient R denotes reflection coefficient for a given frequency and k stands for frequency range. The propagation of linear water waves is modelled using Helmholtz's equation. The cloak geometry is obtained within an optimization process employing Surrogate Optimization solver. Shape of the cloak is defined through Fourier series. The optimization procedure sets the optimal number of Fourier terms and corresponding amplitudes of the terms.

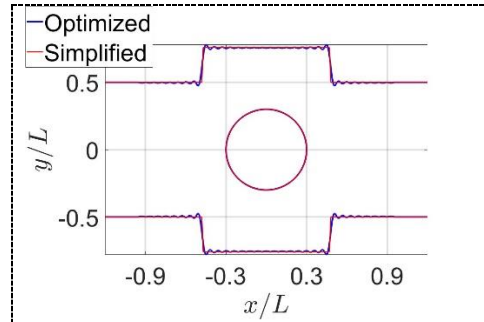


Figure 1. Top view of optimized geometry. L denotes channel width.

3. The results of numerical simulations and description of experimental studies.

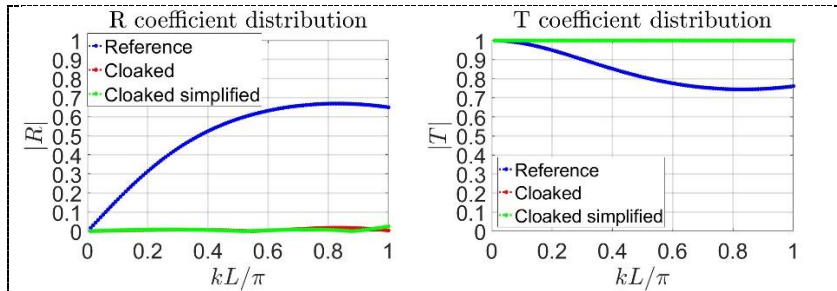


Figure 2. Scattering properties of a cloaking device with respect to a reference case (cylinder in the straight waveguide).

To investigate the propagation of surface water waves in the optimized waveguide geometry, numerical simulations of selected cloak were conducted along with experimental studies. The results of numerical simulations were conducted in the MATLAB PDE Toolbox using the finite element method. Figure 2 illustrates a comparison of the

global distribution of the reflection coefficient R and the transmission coefficient T between the reference case and case with a cloaking device, considering both the simplified geometry and the optimized geometry.

In the experimental counterpart, measurements were conducted using a combination of two methods: the Optical Flow technique [3] and the Synthetic Schlieren technique [4]. The Optical Flow method enables the extraction of displacements from a reference image (e.g., dots), while the Synthetic Schlieren method transforms these displacements into deformations of the water surface. Based on the obtained deformation of the water surface we extract coefficients R and T .

4. Conclusions

We show new type of a cloaking device for a defect within a straight waveguide. The device is designed by altering locally waveguide width around a defect. Our studies demonstrate the fact that the optimized geometry (along with its simplification) almost perfectly cloaks the cylinder. The numerical results are very promising, with values of $X = 5.555e - 05$ for the optimized geometry and $X = 1.9477 - 04$ for the simplified geometry, respectively. This means the defect is cloaked in a broadband manner within a considered frequency range.

Acknowledgements

This research was funded by National Science Centre, Poland under agreement UMO-2020/39/D/ST8/01.

References

- [1] Pendry, J. B., Schurig, D., & Smith, D. R., *Controlling electromagnetic fields* (Science, 2006) 1780-1782).
- [2] Porter, Richard. *Cloaking in water waves. Handbook of Metamaterials Properties 2* (2017).
- [3] Farneback G., *Two-Frame Motion Estimation Based on Polynomial Expansion* (Halmstad: Image Analysis: 13th Scandinavian Conference, SCIA 2003)
- [4] Moisy, Frédéric, Marc Rabaud, and Kévin Salsac., *A synthetic Schlieren method for the measurement of the topography of a liquid interface* (Experiments in Fluids 2009), 1021-1036

Posters

Preliminary wind tunnel testing of a racing motorcycle using a scale model

K Balcerzak¹ and B Potęga¹

¹ Warsaw University of Technology, Faculty of Power and Aeronautical Engineering, ul. Nowowiejska 24, 00-665 Warszawa, Poland

E-mail: bartosz.potega.stud@pw.edu.pl

Abstract. The main goal of this study is to investigate the influence of the Reynolds number on the aerodynamic coefficients of a racing motorcycle using a scale model. The obtained results are compared with CFD results of the equivalent geometry at full scale. The experimental test cases include several different Reynolds numbers and variable yaw angle of the motorcycle. This paper aims to determine the scale of the wind tunnel model.

Keywords: Aerodynamics, Motorcycle Aerodynamics, Aerodynamics Performance, Wind Tunnel Tests, Scale Models.

1. Introduction

Nowadays, aerodynamics is one of the critical aspects of the vehicle design process. The latest motorbike designs in the top racing series differ significantly from the earlier concepts. While the focus was on minimizing drag coefficient in the past, new aerodynamic devices are recently being added to increase downforce. Hence, research into motorbike aerodynamics is a very topical subject again. Numerical methods are becoming increasingly popular when studying the external aerodynamics of vehicles. However, wind tunnel testing is still the analysis that gives the closest results to reality.

This paper presents the use of a scale model to describe the effect of the Reynolds number on the aerodynamic coefficients of a racing motorcycle. This research provided a better understanding of the airflow around the motorbike and aimed to help correctly determine the scale of the model for future tests. In addition, the results obtained were compared with a detailed CFD analysis [1] of a motorbike with the same but more detailed geometry.

2. Model

An electric racing motorcycle developed by the Student Association for Vehicle Aerodynamics (of which the authors are members) is the vehicle of interest for the wind tunnel tests. It was necessary to simplify the very detailed geometry of the motorbike to manufacture such a model using the additive manufacturing apparatus available. The changes mainly occurred in the thickness of the fairing and the internal components of the motorbike. The wheels on the test model were stationary and did not rotate.

Contrary to cars, the aerodynamic characteristics of a motorbike are very much influenced not only by the shape of the vehicle, but also by the shape of the rider, as the motorbike fairing does not entirely cover them. Therefore, to increase the accuracy of wind tunnel testing, it is crucial to represent the rider's appearance as accurately as possible. For this purpose, a 3D scan of the motorcyclist was made to obtain a natural human model.

Due to the limitations of the size of the wind tunnel and the velocities it can generate in the test section, it was necessary to scale the model. Considering the limitations of employed additive manufacturing methods, it was decided to make the model in the scale 1/4, to meet all the described requirements.

The **Figure 1** shows the described model geometry.

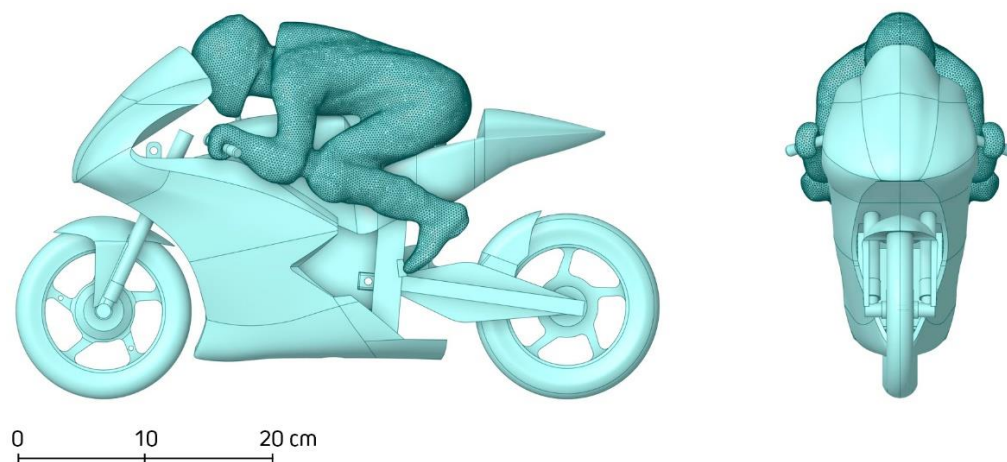


Figure 1. Geometry of the tested model

3. Research methodology

The measurements took place in one of the wind tunnels located at the Faculty of Power and Aeronautical Engineering of the Warsaw University of Technology. The facility is designed to test aeronautical models and has a closed return circuit layout with an open test section. The maximum wind speed is 50 m/s, which corresponds to a Reynolds number of one million for the tested model. The blockage ratio of the model is about 4%, which is less than the recommended 5% [2]. The forces acting on the model are measured using a six-component balance located near its center of gravity. The balance was connected to the NI DAQ and LabView environment.

In order to validate the results, a reference Ahmed's body model was made and then aerodynamic coefficients were tested on it. At first, aerodynamic characteristics of the motorcycle model were tested for different Reynolds numbers and yaw angles. Basic wool tufts and surface oil flow were used to visualize the flow. Measured aerodynamic coefficients were compared with the CFD simulations in the real scale using velocity that corresponds to Reynolds number of two million.

References

- [1] Wiński, K.; Piechna, A. *Comprehensive CFD Aerodynamic Simulation of a Sport Motorcycle*. *Energies* 2022, 15, 5920.
- [2] Barlow, JB; Rae, WH; Pope A. *Low-Speed Wind Tunnel Testing*. 3rd ed. Wiley; 1999.

Fluid Dynamics of Flow around Various Cylinders Geometries

R Gnatowska¹, K Gumowski², P Niegodajew¹ and K Gajewska¹

¹ Czestochowa University of Technology, Faculty of Mechanical Engineering and Computer Science, Armii Krajowej 21 42-200, Czestochowa, Poland

² Warsaw University of Technology, Faculty of Power and Aeronautical Engineering, Nowowiejska 24, 00-665 Warszawa, Poland

E-mail: renata.gnatowska@pcz.pl

Abstract. The study includes measurements conducted for single square and single various triangular cylinders to show how the object geometries modifies the flow field. Particular attention was devoted to examining the effect of the cylinder shape on the dynamics of flow structure. The major conclusion that the wake behind research objects is consistently wider for the square case compared to triangular cylinders, resulting in a significantly different vorticity field compared to a circular or square cylinder.

Keywords: Experimental Fluid Mechanics, Cylinder Shapes, PIV Measurement

1. Introduction and methodology

The flow around bluff bodies (BBs) has been extensively studied for many decades, both experimentally and numerically. Existing research are limited to the flow study around circular or square cylinder [1-3], and less often around triangular cylinder [4-6], where the flow field has been studied. Current literature highlights the need for comprehensive investigations into the flow characteristics of triangular cylinders to understand their aerodynamic behavior better.

A diverse-shaped cylinder ($D = 0.02$ m) was positioned in the center of the wind tunnel measurement section (see Fig. 1). In the study, various shapes and their orientations with respect to the incoming flow were analyzed. The experiment was conducted using the TR PIV system, and a single value of the Reynolds number was examined $Re = 10 \cdot 10^3$.

2. Results

The flow structure around objects is exemplified by the evolution of instantaneous vorticity contour maps over time (with the time interval of 0.005 s), presented for selected cases: S, T30, and T60 in Fig. 2. The cross-sectional shape of the objects plays an important role in modifying the flow. The wake downstream of the S case generates a significantly wider pattern with numerous small structures, than the triangular cylinder. This effect can be attributed to the flat front edge of the square cylinder. The most significant change in the vorticity field is observed for T30 (Fig. 2b), where large and well-arranged vortices shed alternately. In contrast, the vortices shed alternately from the triangle T60 (Fig. 2b) are much less organized than for case of T30.

Consequently, the streamwise length of the wake behind the square and circular cylinders are less than for the triangular cylinders. Regarding TKE, higher production is observed in the wake of a square cylinder.

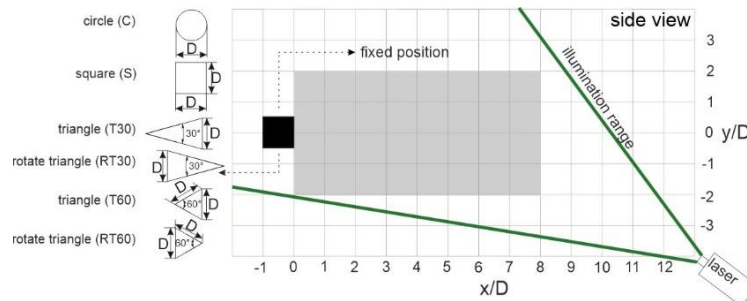


Figure 1. Sketch of the experimental setup.

In summary, based on the average velocity fields, instantaneous vorticity fields, and the vortex shedding frequency, the research offers a systematic understanding of the impact of the cylinder shape on the fluid dynamics of flow around various cylinders geometries.

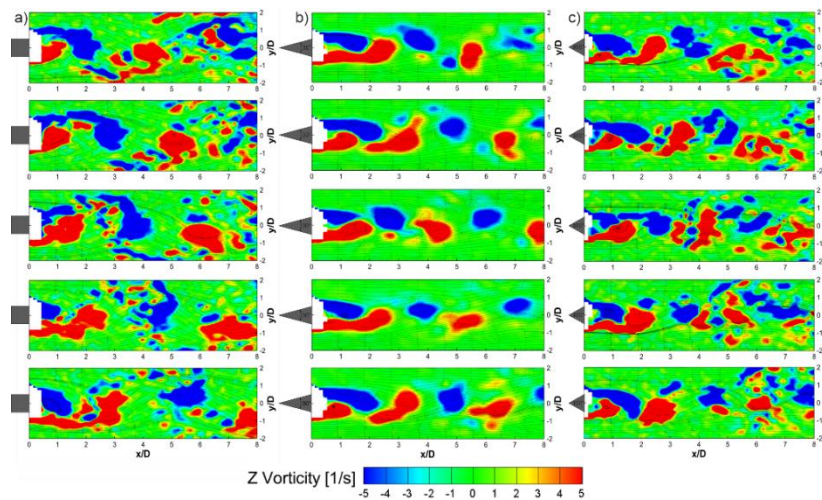


Figure 2. Evolution of instantaneous vorticity for cases: a) square (S), b) triangle T30 and c) triangle T60.

Acknowledgements

The investigation was supported by the statutory funds BS/PB-1-100-3016/2023/P.

References

- [1] Uruba V Procházka P 2020 *MATEC Web Conf.* vol 328 pp 05–06
- [2] Gnatowska R 2011 *Int. J. Turbo Jet-Engines* vol 28 pp 21–29
- [3] Niegodajew P Gajewska K Elsner W Gnatowska R 2024 *J Fluids Struct* **124** 104045
- [4] Agrawal N Subhash M 2021a *Mater. Today: Proc.* **46** 10718–10724
- [5] Farhadi M Sedighi K Korayem, A M 2010 *Int. J. Therm. Sci.* **49** (6) 1010–1018
- [6] Çelik, Z Altaç Z 2023 *Ocean Eng.* **269** 113468

Multiphase flow analysis in horizontal pipe - numerical issues

P. Marczak, M. Jaszczur

AGH University of Krakow, Faculty of Energy and Fuels, Al. Mickiewicza 30, 30-059
Kraków, Poland

E-mail: jaszczur@agh.edu.pl, pmarczak@agh.edu.pl

Abstract. Air-water mixtures can be numerically modelled using various techniques. The aim of this study was to investigate the sensitivities of Volume of Fluid method. The synthetic case was designed to capture the change in volume fraction of each phase, the change in velocity profiles, and shape of the structures. The study has shown that the results are strongly correlated with time step size and mesh resolution. Numerical schemes and adaptive meshing also contribute to the change in the aforementioned results. This indicates that even similarly set-up cases with VOF models could vary in results.

Keywords: Multiphase Flows, CFD, Volume of Fluid, Plug flow

1. Introduction

Volume of Fluid (VOF) method provides a vast number of settings related to the numerical solution to the problem. Some of them are crucial to achieving convergence itself, when the purpose of rest is to provide better quality results. Typically results of the experiment are hardly replicable in great detail due to slight changes in temperature, pressure and parameters of the fluid, we expect results of correctly set-up numerical simulation should be always the same, no matter the machine which was used for calculation and numerical way the equations were solved. The key objective of this article is to determine whether it's possible to obtain for identical boundary conditions single numerical solution or there is an infinite number of possible solutions. This will be checked by an analysis of two-phase air-water flow in a 2D T-junction.

In order to check solution dependencies, following changes to calculation were made:

- numerical analysis with Iterative Time-Advancement (ITA) and Hybrid-NITA (Non-Iterative Time-Advancement) schemes,
- different workstation architecture was used calculations,
- different number of domain decompositions used for calculation,
- global mesh refinement and adaptive mesh refinement were compared
- adaptive time-step size and fixed time step size were used for calculation.

The parameters selected for comparison were pressure drop, velocity profiles, shape of the fluid-air interface, and void fraction. These were identified in the literature as the most important for the potentially matching the experimental data [1,2].

The test case used for the investigation was purely synthetic, as its purpose was to demonstrate the difference in results between runs.

2. Geometry and boundary conditions

The geometry used for the analysis was a T-junction, where to channel with running water air was injected from the bottom.



Figure 11. Geometry used for calculations and its dimensions

The case was calculated in 2D, with fixed water speed ($v_{H_2O} = 1.0$ m/s) and air speed ($v_{air} = 1.25$ m/s). The chosen criteria resulted in plug flow, which, due to its structure, should be accurately described by VOF method. The physical placement of each boundary condition is illustrated in Figure 2. A transient analysis was performed with duration of 0.04 s, during which time, the bubble formed by the air injected was transported by 4.5 mm. All calculations were carried out using ANSYS Fluent 2023R2.

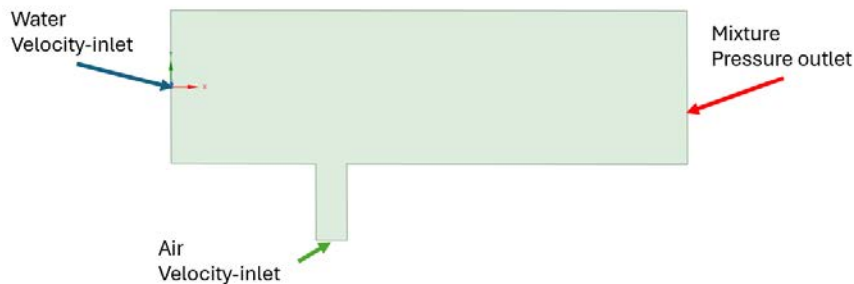


Figure 22. Boundary Conditions Diagram

3. Results

A mesh sensitivity study has been conducted, revealing a high dependence on mesh resolution, as depicted in Figure 3, in terms of changes in void fraction and average speed. Furthermore, the coarser case with adaptive remeshing was tested, resulting in a significant reduction in computational effort.

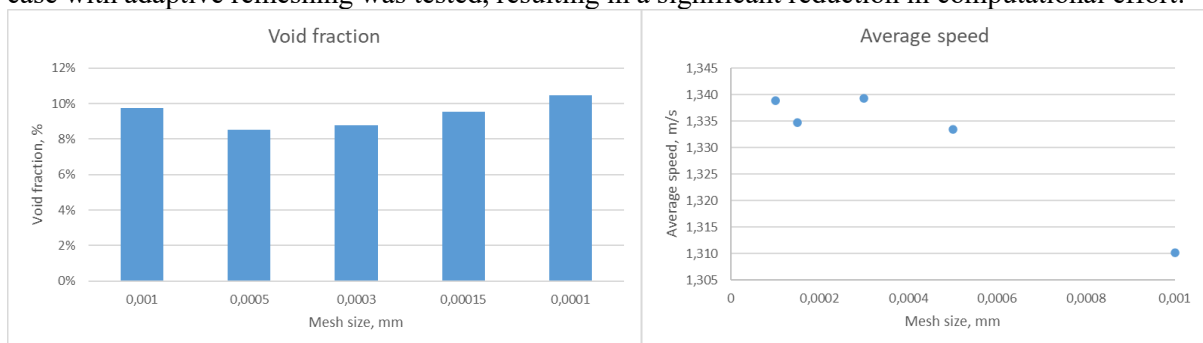


Figure 33. Void fraction and average speed at the averaging plane

References

- [1] Raj K, Ramadan A and Saeed S 2020 *Chemical Engineering Research and Design* Volume 153 (Elsevier), p 201-211
- [2] Akhlaghi M, Mohammadi V, Nouri N M, Taherkhani M and Karimi M 2019 *Chemical Engineering Research and Design* Volume 152 (Elsevier) p 48-59

Experimental analysis of fractal distributors

A Merdjani¹ and N Kizilova¹

¹ Warsaw University of Technology, Faculty of Power and Aeronautical Engineering, ul. Nowowiejska 24, 00-665 Warszawa, Poland

E-mail: abdelhakim.merdjani.dokt@pw.edu.pl

Abstract. Fractal distributors represent a significant advancement in the design and efficiency of fluid distribution systems promising to enhance their performance in wide range of industrial applications as fuel cells. There the fractal system can be used as a flow field plate for uniform delivery of the gas fuels, this experimental study aims to analyse fluid distribution uniformity of fractal 5-generation (16 outlets) design to validate numerical simulation.

Keywords: Experimental Fluid Mechanics, Fractal Distributor, Fuel Cell.

Introduction

Fractal distributors are increasingly gaining attention for their potential to enhance process efficiency in various sectors, including chemical processing, pharmaceutical manufacturing, and environmental management. These distributors are designed based on fractal geometry, offering unique advantages such as improved mixing quality and higher surface area-to-volume ratios compared to traditional distribution systems. Despite their growing application, the experimental analysis of fractal distributors remains an area ripe for further exploration. Current research predominantly focuses on theoretical models and simulation studies, with a noticeable gap in empirical data that validates these models under varied operational conditions.

1. Analysis of flow uniformity distribution

To study the uniformity of flow distribution within fractal geometries, the dimensionless parameters are presented as: the first parameter is the standard flow rate deviation (D_g) or as known in some studies as maldistribution factor which is related to the number of outlets and the flow rate of each one, as expressed in equation 1.

$$D_g = \sqrt{\frac{1}{N-1} \sum_{i=1}^N \left(\frac{v_i}{v_{ave}} - 1 \right)^2} \quad (1)$$

where N stands for number of the open outlets, v_i is the flow rate through each outlet, v_{ave} is the average flow rate.

The second parameter is the maximal flow rate ratio θ which represents the ratio of the maximum to the minimum flow rates as expressed in equation 2.

$$\theta = \frac{v_{max}}{v_{min}}. \quad (2)$$

2. Experimental setup

the experimental study for flow rate from fractal distributors has been conducted, the proposed prototype fabricated of Plexiglas of 2 mm by laser engraving machine, the prototype tested by conducting a colorant fluid to check sealing between layers as it shown in figure 1a. The inlet flow rate operated during the test are :7ml/s, 18ml/s,30ml/s and 43ml/s.

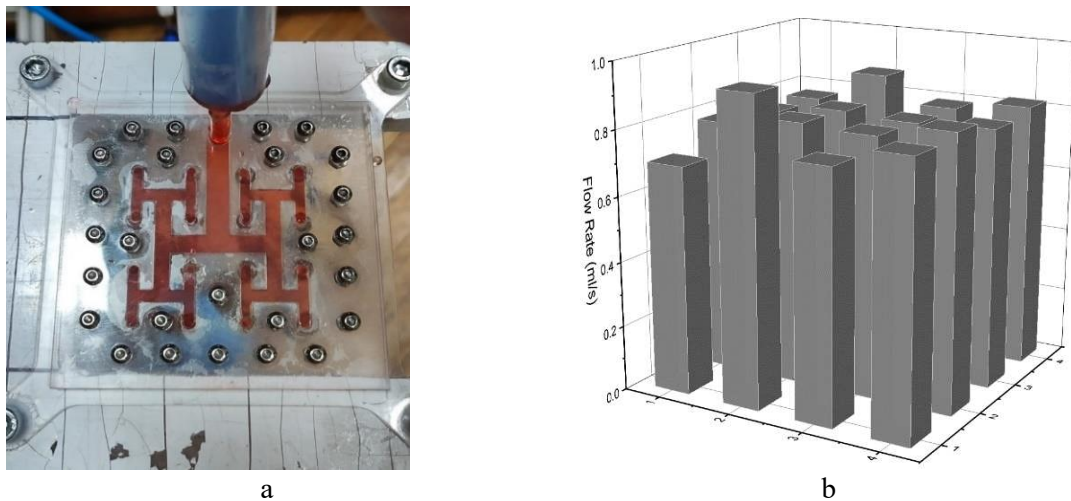


Figure 1. fractal prototype (a) and flow rate distributions in the outlets (b).

3. Results and conclusions

The results presenting the flow rate of fractal (16 outlets) distributor of inlet mass flow :43ml/s in figure 1b. The fractal prototype showed experimentally acceptable uniformity where the maximal flow rate ration was between 1.12 and 1.20, the obtained results was compared to the 3D numerical results, the deviation between CFD and experiment is from 14% to 22%. The more uniform flow distribution can be achieved with N=64 or N=128 outlets. This needs a more sophisticated manufacture procedure and will be a topic for future experiments.

Acknowledgments The participation in the XXVI Fluid Mechanics Conference is supported by the Aerodynamics Department of Warsaw University of Technology.

References

- [1] Kizilova, Natalya, et al. "Fractal-like flow-fields with minimum entropy production for polymer electrolyte membrane fuel cells." *Entropy* 22.2 (2020): 176.
- [2] He, Gongqiang. *Applications of CFD Simulations on Fractal Fluid Distributor*. Louisiana State University and Agricultural & Mechanical College, 2015.

Extending Channelflow: Incorporating Temperature Effects in Poiseuille and Couette Flows

K Michałowski¹ and S Gepner¹

¹ Warsaw University of Technology, Faculty of Power and Aeronautical Engineering, ul. Nowowiejska 24, 00-665 Warszawa, Poland

E-mail: krzysztof.michalowski.stud@pw.edu.pl

Abstract. This study extends the well-established Channelflow library to include temperature effects in Poiseuille and Couette flows. Leveraging the Boussinesq approximation, it enables efficient modelling of thermal variations' impact on hydrodynamic stability. The framework facilitates the exploration of thermally driven phenomena, crucial for diverse fields from fluid dynamics to engineering.

Keywords: Computational Fluid Dynamics, Thermal-fluid problems, Boussinesq Approximation, Channelflow.

1. Introduction

This work introduces a significant extension to the Channelflow library [1], enabling the incorporation of temperature effects in Poiseuille and Couette flows. The study addresses the critical need to understand the impact of thermal variations on hydrodynamic stability and turbulence onset in such flow configurations. Our approach centres around leveraging the Boussinesq approximation and aims at the development of a computational framework allowing for the efficient numerical exploration of thermally driven phenomena, bridging the gap between classical isothermal flow simulations and real-world scenarios where temperature variations play a crucial role.

2. Methodology

The Channelflow library, developed by Gibson [1], has been a powerful tool for studying incompressible Navier-Stokes flow in simple channel geometries. However, its current capabilities are limited to isothermal conditions, overlooking the significant influence of temperature on flow dynamics in various natural and industrial settings. Our effort aims to fill this gap by extending the library's capabilities to handle coupled fluid-scalar field problems, paving the way for a deeper understanding of complex flow phenomena.

The implementation involves the addition of a scalar field representing temperature coupled with the flow velocity field through the Boussinesq approximation. This extension entails the incorporation of appropriate Advection-Diffusion transport equations for the scalar quantity, modification of boundary conditions, and the introduction of mechanisms coupling scalar distribution to the velocity field to accommodate thermal variations.

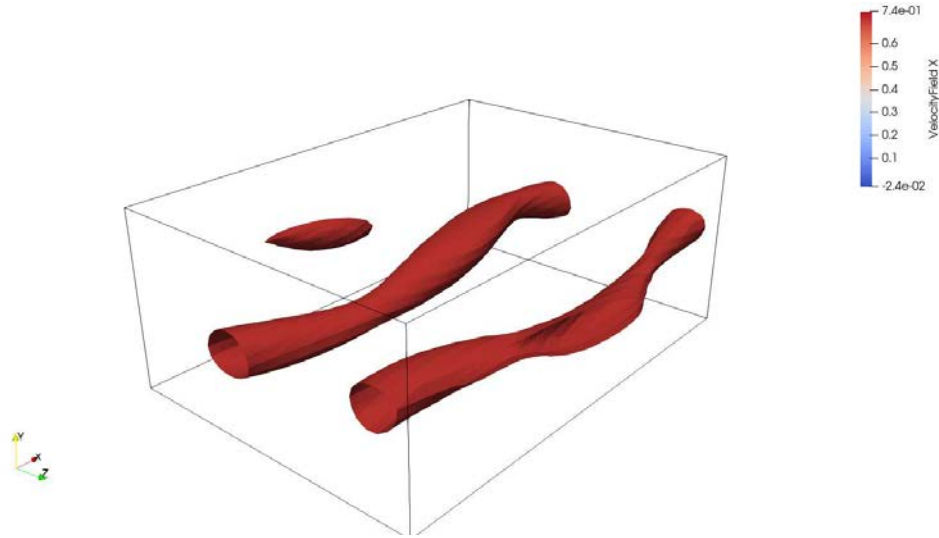


Figure 1. Constant streamwise velocity iso-contour at $u = 0.8$ illustrating the meandering motion past the onset of the secondary, travelling wave instability.

Utilising the Boussinesq approximation, density variations caused by temperature changes are efficiently modelled by supplementing the governing equations with an additional volume forcing term (buoyancy), which considers variations in the temperature distribution. By extending the Channelflow framework to handle thermal effects, we hope to explore a wider range of flow regimes, including Rayleigh-Bénard-Poiseuille (RBP) flow, where pressure-driven flow and thermally driven convection occur.

3. Preliminary results

In the case of the flow through a channel, considering the effects of heating, the effects of buoyancy forces result in the well-known Raileigh-Benard convection, which manifests in mushroom-like plumes, moving the fluid in the direction perpendicular to the thermally active walls. We consider this to be the primary instability. With the heating pattern applied to either Couette or the Poiseuille flow, the fluid motion resulting from this primary RB instability leads to the spanwise modulation of the streamwise velocity distribution and, consequently, to a secondary form of instability [2]. This secondary instability manifests in the form of a wave travelling down stream and, when amplified to the nonlinear regime, leads to the time -dependant, meandering motion of the flow, which is shown in figure 1. With the implemented extension to the Channelflow library, we aim to study thermally driven, hydrodynamic instabilities resulting from the application of spatially modulated heating. Spatial modulation of heating allows for more control over the resulting flow dynamics. Our preliminary results show that for a range of heating configurations, patterned heating leads to a decrease in the critical conditions necessary for the onset of the travelling wave instability.

In conclusion, extending the Channelflow library to include temperature effects offers an efficient tool for exploring the complex interplay between fluid dynamics and thermal variations, with applications spanning from fundamental research to industrial processes.

References

- [1] Gibson, J. F. (2012). Channelflow: A spectral Navier-Stokes simulator in C++. New Hampshire, 900.
- [2] Clever, R. M. and Busse, F. H. (1991). Instabilities of longitudinal rolls in the presence of Poiseuille flow. *Journal of Fluid Mechanics*, 229, 517-529.

Fractal-Type Structures for Heat Exchangers: A CFD Investigation of Tube Geometry Influence

Abdulmuttalib A. MUHSEN¹, Natalya KIZILOVA¹ and Bashar Hassan ATTIYA²

¹ Warsaw University of Technology, Faculty of Power and Aeronautical Engineering, ul. Nowowiejska 24, 00-665 Warszawa, Poland

²Imam Ja'afar Al-Sadiq University, Kirkuk, Iraq

E-mail: abdulmuttalib.muhsen.dokt@pw.edu.pl

Abstract. A heat exchanger is a device used for efficient heat transfer from one medium to another. The optimization of heat transfer rates is of utmost importance in a wide range of industrial applications, leading to ongoing endeavors aimed at improving the efficiency of heat transfer processes. In the present context, researchers have shown considerable interest in the application of fractal-type structures. In contrast to conventional pipelines, fractal-type structures have exhibited enhanced heat transfer performance despite their larger surface area. The present study investigates the cooling efficiency of various fractal-type structures and performs a comparative analysis utilizing Computational Fluid Dynamics (CFD) techniques. The temperature data obtained from the output of the computational fluid dynamics (CFD) analysis is then utilized in the governing equations for heat transfer to assess the thermal and hydraulic resistance. This research makes a valuable contribution to the current investigation of heat transfer techniques, providing insights into the potential of fractal-type structures for enhancing heat transfer processes.

Keywords: Fractal-type structures, computational fluid dynamics (CFD), thermal resistance, heat exchanger performance

1. Introduction

The design and optimization of heat exchangers play a crucial role in various engineering applications, ranging from refrigeration systems to power plants. The use of innovative heat exchanger configurations, such as fractal-type structures, has gained significant attention due to their potential to enhance heat transfer efficiency. In this study, we investigate the influence of tube geometry on the performance of fractal-type heat exchangers using computational fluid dynamics (CFD) simulations. By analyzing the flow and heat transfer characteristics of different tube configurations, we aim to provide insights into the potential benefits of utilizing fractal-type structures in heat exchanger design. This research is significant as it contributes to the ongoing efforts to improve the efficiency and sustainability of thermal systems.

2. Tube Geometry

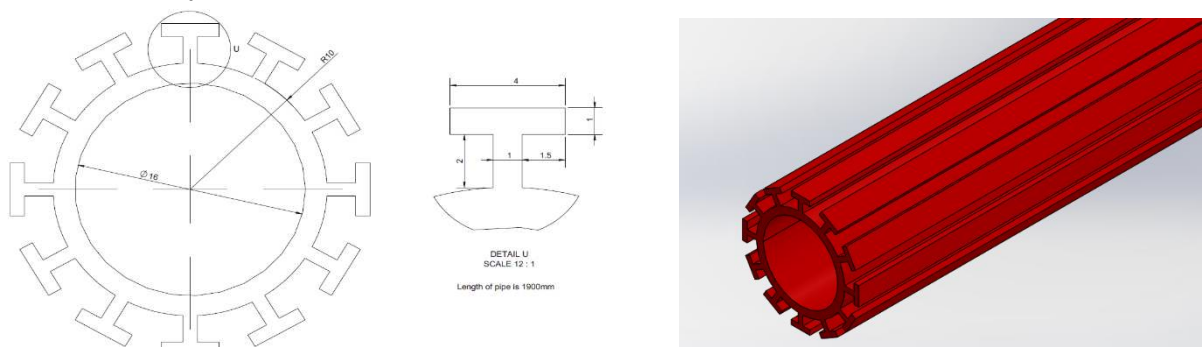


Figure 2-1. T-shaped fractal pipe cross section

Numerical Investigation of Gas Injection into the Crossflow for High Reynolds Number

Sahrish B. Naqvi¹ and Maciej Matyka¹

¹ University of Wrocław, Institute of Theoretical Physics, Pl. Maxa Borna 9, 50-204 Wrocław, Poland

E-mail: naqvi.sehrish@yahoo.com

Abstract. We study numerically unsteady fluid flow around a group of cylinders with gas injection, revealing mixing and transitions from laminar to turbulent for sufficiently high Reynolds flows. We observe that high injection velocities affect vortex interactions, flow symmetry, and mixing efficiency of the injected gas into the crossflow. We find that momentum increases with the secondary fluid injection velocity rate. To understand energy distribution in the system, we suggest measuring the participation number, which quantifies energy localization in the flow.

Keywords: Computational Fluid Dynamics, High Reynolds Crossflow, Gas Injection, Energy Localization, Flow Asymmetry.

1. Introduction

Fluid emissions and mixing, particularly of gases, present critical risks in underground coal mining operations. For instance, Methane-air mixtures resulting from these processes are a leading cause of explosions within mines [1]. Moreover, the study of gas dispersion and mixing is essential across diverse applications, including geophysical flows, chemical reactors, and transpiration cooling, highlighting the significance of investigating velocity fields and impact of gas injection and dispersion on transported quantities, [2, 3]. The technique of injecting gases into the cross flow, alters the boundary layer, concentration, or velocity fields and is crucial for designing and controlling various structures, such as ships and airplanes [4]. However, despite extensive study on simple configurations at low Reynolds numbers, research needs more complex cylinder arrangements at high Reynolds numbers, a gap that overlooks potential flow interactions of the injected gas and crossflow dynamics.

We performed two-dimensional simulations to explore interactions of vortical structures, flow symmetry breakage, and energy localization of gas injection into two-dimensional crossflow over the regularly arranged cylinders. This problem offers insight into the complex mixing process for relatively high Reynolds number flows. However, the two-dimensional simulation approach for transient gas dispersion in cross-flow lacks the ability to capture essential 3D flow dynamics, transitions from laminar to turbulent flow, and detailed scalar mixing effects, which can result in inaccuracies when predicting real-world dispersion patterns. Despite these limitations, it provides a simplified and computationally efficient way to gain initial insights into gas dispersion, providing a qualitative understanding of the underlying flow and mixing mechanisms.

2. Model, Preliminary Results

We combined the Navier-Stokes Eq. 1 for two-dimensional, unsteady, and incompressible crossflow with the advection-diffusion equation Eq. 2 to simulate gas concentration in rectangular domains (Fig. 1) with uniformly arranged cylinders. The distance between the inlet and the first column of cylinders is $5D$. The system of equations (1-2) are expressed as:

$$\nabla \cdot \mathbf{u} = 0, \quad \frac{\partial \mathbf{u}}{\partial t} + (\mathbf{u} \cdot \nabla) \mathbf{u} = -\frac{1}{\rho} \nabla p + \nu \nabla^2 \mathbf{u}, \quad (1)$$

$$\frac{\partial C}{\partial t} + (\mathbf{u} \cdot \nabla) C = D_0 \nabla^2 C. \quad (2)$$

Here, \mathbf{u} , p , t , ρ , ν , C , and D_0 , represents the velocity field, pressure, time, fluid density, fluid kinematic viscosity, scalar mass concentration, and tracer diffusion coefficient respectively.

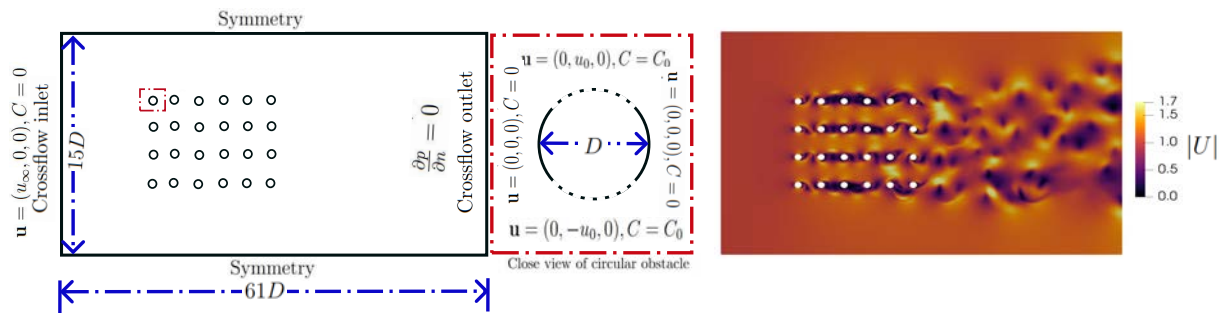


Figure 1. Flow domain (left frame) with zoom view of cylinder (middle frame). Velocity magnitude at $Re = \rho u_\infty D / \mu = 500$ for no gas injection $\epsilon = 0$ case (right frame). The parameter ϵ is dimensionless velocity from free-stream velocity (u_∞) to the gas injected velocity (u_0).

We modified the pimpleFoam solver in OpenFOAM-v 2212 to include an additional scalar equation 2 alongside the Navier-Stokes equations 1, using the finite volume method for a comprehensive solution. This extension incorporates a one-way coupling to integrate the scalar equation, facilitating the simulation of gas concentration dynamics within the flow domain. For domain discretization, we have utilized the standard tool blockMesh and generated hexahedral mesh in the entire domain with additional mesh refinement. The proof of concept results presented in Fig. 1 (right side) illustrate the fluid flow and emerging vortices for $\epsilon = 0$. Our study will explore the impact of continuous gas injection into crossflow for $\epsilon > 0$, focusing on energy localization, symmetry disruption, and the shift from laminar to turbulent flow regimes.

Acknowledgments

Funded by the National Science Centre, Poland, under the OPUS call in the Weave program 2021/43/I/ST3/00228. This research was funded in whole or in part by the National Science Centre (2021/43/I/ST3/00228). For the purpose of Open Access, the author has applied a CC-BY public copyright license to any Author Accepted Manuscript (AAM) version arising from this submission.

- [1] M. Li, H. Wang, D. Wang, Z. Shao, S. He, Risk assessment of gas explosion in coal mines based on fuzzy ahp and bayesian network, *Process Safety and Environmental Protection* 135 (2020) 207–218.
- [2] J. C. Kurnia, A. P. Sasmito, A. S. Mujumdar, Cfd simulation of methane dispersion and innovative methane management in underground mining faces, *Applied Mathematical Modelling* 38 (14) (2014) 3467–3484.
- [3] J. R. Baron, The binary mixture boundary layer associated with mass transfer cooling at high speeds, *Techn. Rep. 160*, Mass. Inst. Technology, Naval Supersonic Laboratory, Cambridge Massachusetts (1956).
- [4] C. Norberg, Fluctuating lift on a circular cylinder: review and new measurements, *Journal of Fluids and Structures* 17 (1) (2003) 57–96.

Time dependence of similarity functions in the atmospheric boundary layer

Jackson Nzotungishaka¹, Marta Waclawczyk¹ and Jun-Ichi Yano²

¹ University of Warsaw, Faculty of Physics, Institute of Geophysics, ul. Pasteura 5, 02-093 Warszawa, Poland

² UMR3589 (CNRS), Meteo-France, Toulouse, France

E-mail: j.nzotungish@student.uw.edu.pl

Abstract. In this work, the validity of the Monin-Obukhov similarity theory (MOST) is investigated in the case of strong stratification. The results show that a possible source of deviations from the predictions of Monin and Obukhov are non-stationary states of mean momentum and temperature. We attempt to parametrize these non-stationarities using symmetry invariant solutions defined under the Lie-group theory.

Keywords: Atmospheric Science, General Fluid Dynamics.

1. Introduction

The atmospheric boundary layer (ABL) is the thin layer of the atmosphere of the depth less than one kilometer above the surface of the Earth. The ABL plays a crucial role in numerous natural and anthropogenic processes, influencing weather patterns, air quality, and the dispersion of pollutants.

The MOST (cf. Ref. [1]) generalizes the mixing length theory in non-neutral conditions. MOST describes the non-dimensionalized mean flow and mean temperature in the surface layer as functions of the dimensionless height parameter z/L , where L is the characteristic length scale of the surface layer turbulence called the Obukhov length. It characterizes the relative contribution to turbulent kinetic energy from buoyant production and shear production. L is defined as

$$L = -\frac{u_*^3 \langle \theta_v \rangle}{\kappa g \langle w' \theta_v' \rangle}, \quad (1)$$

where $u_* = \sqrt{-\langle u'w' \rangle}$ is the friction velocity, θ_v is the virtual potential temperature, κ is the von Karman constant, g is the gravity acceleration, primes are the fluctuating components about the mean and $\langle \rangle$ is a time/space averaging operator. The Obukhov length acts also as a criterion for static stability of surface layer: when the Obukhov length is negative, the surface layer is statically unstable, if L is positive, the surface layer is stable.

This work concerns the stably stratified surface layer, with $L > 0$. In such case MOST predicts that the universal non-dimensional stability functions are expressed as

$$\psi_m = \frac{\kappa z}{u_*} \frac{d\langle U \rangle}{dz} = 1 + \beta \frac{z}{L}, \quad \psi_h = \frac{\kappa z}{\theta_*} \frac{d\langle \theta \rangle}{dz} = 1 + \beta \frac{z}{L}, \quad (2)$$

where $\beta = 5$ is a constant and $\theta_* = -\langle w'\theta' \rangle / u_*$ is the temperature scale.

2. Methods and results

The universal stability functions ψ_m and ψ_h estimated from the SHEBA database (cf. [2]) are presented in Fig. 1. It is seen that, as the stratification increases, they increasingly deviate from the predictions of MOST. The deviations are caused by intermittent structure of the very stable ABL, where turbulence may locally re-laminarise, which also leads to strong non-stationarities of the flow. To parametrize these deviations we use similarity solutions derived based on the symmetry transformations. In this method we look for such transformations of dependent and independent variables which leave the underlying system of equations unchanged. Both the logarithmic solution for the mean velocity and temperature in the neutral ABL and the linear solutions for strong stratification can be derived as symmetry invariant solutions, cf. [3]. Further analysis (cf. [4]) suggests that in case of non-stationarity, ψ_m and ψ_h depend not only on the non-dimensional height z/L , but also on the non-dimensional ratio $\langle w'^2 \rangle / \langle u'w' \rangle$. Hopefully, derived invariant functions will improve parametrizations of the stable atmospheric boundary layer and provide the basis for turbulence closures which account for the intermittent structure of ABL.

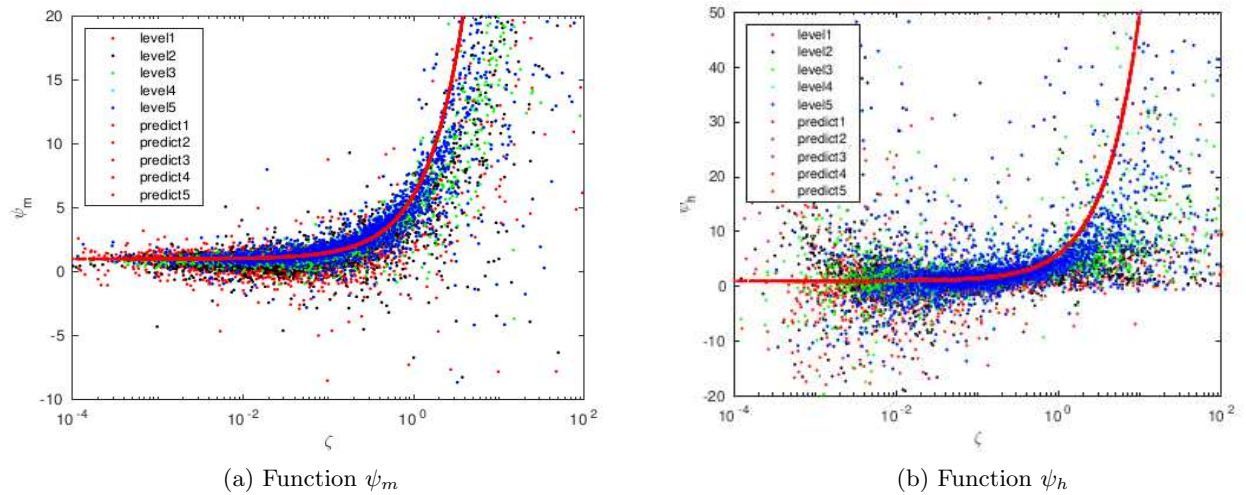


Figure 1: Functions ψ_m and ψ_h estimated from SHEBA database (scatter points) at five levels above the ground compared to the Monin-Obukhov predictions (lines).

Acknowledgments

We acknowledge the support of the National Science Centre, Poland, Project 2020/37/B/ST10/03695.

References

- [1] Monin AS and Obukhov AM 1954 *Tr. Nauk SSSR Geophys. Inst.* **24** 163.
- [2] Grachev A A et al. 2007 *Boundary-Layer Meteorology* **124** 315.
- [3] Yano J-I and Waclawczyk M 2024 *Journal of the Atmospheric Sciences* **81** 263.
- [4] Waclawczyk M et al 2024 *submitted to Boundary-Layer Meteorology*.

Surrogate model of missile's flight control surface aerodynamics

B Olszański¹

¹ Warsaw University of Technology, Faculty of Power and Aeronautical Engineering,
ul. Nowowiejska 24, 00-665 Warszawa, Poland

E-mail: bartosz.olszanski@pw.edu.pl

Abstract. This study concerns aerodynamic characteristics (static) identification and subsequent construction of the approximation-based surrogate model for guided missile's flight control surface (FCS). The identification was performed through RANS simulations and wind tunnel tests in supersonic (\sim Mach 1.9) flow conditions. The obtained results were compared to analytical and semi-empirical models. It is shown that canard vortices have a major influence over the rolling (adverse behavior) and the pitching moment through interference effects.

Keywords: Aerodynamics, CFD, Missile, Flight Control Surface, Wind Tunnel, Surrogate Model

1. Introduction

For the aerodynamically controlled tactical missile, the geometry and size of flight control surfaces (FCS) significantly impact its maneuverability and stability [1]. Regardless of the control law selected or the autopilot architecture, airframe aerodynamics and rigid-body dynamics properties are primary input variables for the controller's tuning process. Despite the tremendous progress achieved in the field of control techniques, the reliable source of aerodynamic characteristics (ADC) is still the biggest source of uncertainty. Vast look-up tables from a wind tunnel or flight tests covering the entire flight envelope of the missile are usually unavailable (cost, infrastructure), especially during conceptual or preliminary design phases. Modernizing existing systems in line may also be challenging since their complex mathematical model may not exist or is out of access. In that case, the approximation-based, simulation-driven, wind tunnel-corrected metamodel with the strict algebraic formulation of aerodynamic loads may be an attractive alternative when dealing with ADC identification and subsequent control algorithm tuning. The current study focuses on the former, taking legacy, canard-controlled, surface-to-air missile as a test object. The main scientific goal is to examine and quantify the interference effects induced by FCS on the rolling (C_l) and pitching moment (C_m).

2. Problem specification

Surrogate models are commonly used inside optimization frameworks, offering an efficient pathway for swift, cheap-to-evaluate, accurate evaluation of ADC [2]. Due to the military application, the available data for the missile examined is too scarce to construct an elaborate metamodel based solely on literature [3]. As a countermeasure, high-fidelity data was generated through a series of free-stream, compressible RANS simulations performed in ANSYS Fluent solver. Moreover, the access to the missile's FCS hardware introduced wind tunnel tests (using the 6-component external load cell,

Ma ≈ 1.9) to validate CFD simulation results. Response Surface Methodology (RSM) utilizing multivariate polynomial regression leads to the resulting approximation model of FCS’s aerodynamics (including interference effects) between input (Mach, α, δ) and output (C_N, C_m, C_i) variables.

The core idea of Response Surface Equations (RSE) that should fit the data elegantly and quantify the interference effects in a component build-up way originates from the canonical Pitts et al. paper [4]:

$$C_{NBCT} = C_{NB} + C_{NC(B)} + C_{NB(C)} + C_{NT(B)} + C_{NB(T)} + C_{NT(C)} \quad (1)$$

$$C_{NC(B)} + C_{NB(C)} + C_{NT(C)} = [(K_C + K_B)\alpha_c + (k_C + k_B)\delta]_C \frac{\partial C_{NC}}{\partial \alpha} + \left(1 + \frac{k_B}{k_C}\right)_T \Delta\alpha_V \frac{\partial C_{NT}}{\partial \alpha} \quad (2)$$

The method distinguishes the influence of α and δ through separate Morikawa’s carryover factors (K and k) that mimic the scale of increment load due to the interference between canard and body. The last term in Eq. (2) incorporates canard-tail interference through an average upwash angle (Δα_V). In its original form, the factors are assessed through Slender Body Theory (SBT) and apply only to small α without any Ma influence. In the current study, SBT is substituted for RANS CFD, which provides insight into the nonlinearities, including the wing-only derivatives at high α and δ.

3. Results and conclusions

Fig. 1 compares results (α-sweeps, Ma = 1.9) for selected linear analytical, semi-empirical models and CFD for isolated FCS flow. This preliminary study proves that linear SWP in the case of C_{NC} gives a reasonable estimate, but only a more sophisticated MDC method can follow the nonlinear trend of FCS hinge load (C_{m_c}). Wind tunnel tests proved the movement of the FCS centre of pressure with α.

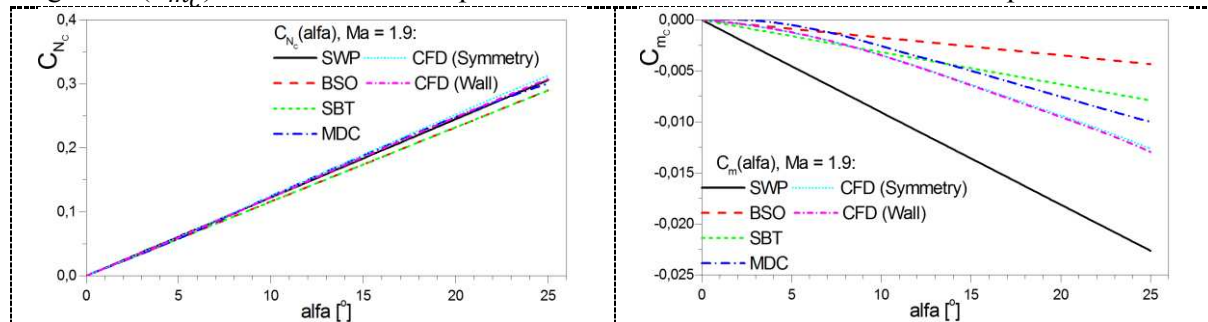


Figure 1. Comparison of analytical and CFD results for missile’s FCS, Mach ≈ 1.9.

SWP – Slender Wing Potential Theory, BSO – Busemann’s Second Order, SBT – Sweepback Theory, MDC – Missile DATCOM: C_N(α) (left side), C_m(α) (right side).

Significant nonlinearities of ADC associated with aerodynamic interferences induced by canard tip and inboard vortices were captured. Flow perturbations travel along the body length, hit the tailfin set, and cause adverse rolling moment (C_i) in favorable conditions (oe. cruciform configuration), usually for low α cases. That mechanism is relatively well-known in the literature [5]. The surrogate model indicates that despite C_i relaxation by allowing the tailfins to rotate freely, there are segments of tail assembly angular positions relative to the fixed canard plane where lift generated on rear aerodynamic surfaces is influenced negatively by canard and body vortices. It has the potential to reduce further the longitudinal static margin, which is not so high already as the missile requires high control authority.

References

- [1] Fleeman EL 2001 *Tactical Missile Design* (Reston, VA: AIAA)
- [2] Yoo S, Jeong S, Jung J and You K 2023 *Optim. Eng.* In press
- [3] Murman SM and Aftosis MJ 2003 *Proc. 21st AIAA Applied Aerodynamics Conf. (Orlando, FL)* vol 1 (Reston, VA: AIAA) p 1-13
- [4] Pitts WC, Nielsen JN, Kaattari, GE 1957 *NACA-TR-1307*
- [5] McDaniel M and Evans C 2010 *Proc. 28th AIAA Applied Aerodynamics Conf. (Chicago, IL)* vol 1 (Reston, VA: AIAA) p 1-17

Composition tracking of CO₂-rich streams in large-scale pipeline networks under steady-state conditions

A Osiadacz, Ł Kotyński, F Uilhoorn, T Bleschke, M Kwestarz and M Chaczykowski¹

¹Warsaw University of Technology, Department of District Heating and Gas Systems, ul. Nowowiejska 20, 00-653 Warszawa, Poland

E-mail: maciej.chaczykowski@pw.edu.pl

Abstract. In this paper we are conducting simulations for large-scale CO₂ network transporting CO₂ streams such as those for Carbon Capture and Storage. Simulation results of the tree-type as well as looped network structures are presented. Composition tracking, using nodal mixing rules, is presented. The development of the GIS graphical user interface for incorporating spacial data on the topology of the network is presented. A case study is conducted for conceptual Polish country-wide CO₂ transport infrastructure showing the functionality of the computational code.

Keywords: General Fluid Dynamics, Numerical Simulation, CCS, Large Scale Network, Hydraulic Modelling, GIS Applications

Extended Abstract

Carbon capture and sequestration (CCS) will play a major role in eradicating the contributions of industrialised countries to climate change and reaching the 2050 net zero commitments. CCS clusters, in which several industrial facilities create a network of emitters and share CO₂ transport and storage infrastructure, can provide strategic benefits for developing technologies such as CCS.

This work contributes to the assessment of CO₂ transport infrastructure in terms of hydraulic modelling capabilities of pipeline networks. In particular, the objective of this simulation-based study was to facilitate identification of the technical characteristics of pipeline networks for power and industrial decarbonisation projects.

To this end, a steady-state analysis was used to assess the flowrates, pressures and temperatures in the network, while composition tracking analysis provided results for identification of the CO₂ stream impurities in network nodes. The steady-state network simulation approach was developed for the analysis of pipeline networks of arbitrary size and structure.

We consider a network with N nodes, M pipes, IU units (pumps/compressors/pressure or flow regulators.) There are N nodal flow balancing equations (I Kirchhoff's circuit law). There are M pressure drop equations expressed by nodal pressures. Nodal balance equations are rewritten in matrix form by means of $N \times M$ node-branch incidence matrix. The network simulation begins with an initial estimate of flows in each pipe that may not necessarily satisfy flow continuity. At each iteration new nodal pressures are found by solving the system of nonlinear equations. Each right hand side term consists of the net flow imbalance at a node. After new pressures are computed by solving above equations, new flows are found from pressure drop equations. The system of equations must be solved using a sparse

matrix methods based on node re-ordering. Re-ordering of the nodes allows us to minimize the amount of fill-in for Jacobian matrix. Furthermore, a symbolic factorization is carried out so that only the non-zero elements of the Jacobian matrix need to be stored and operated on in memory. Equations describing non-pipe elements are solved simultaneously.

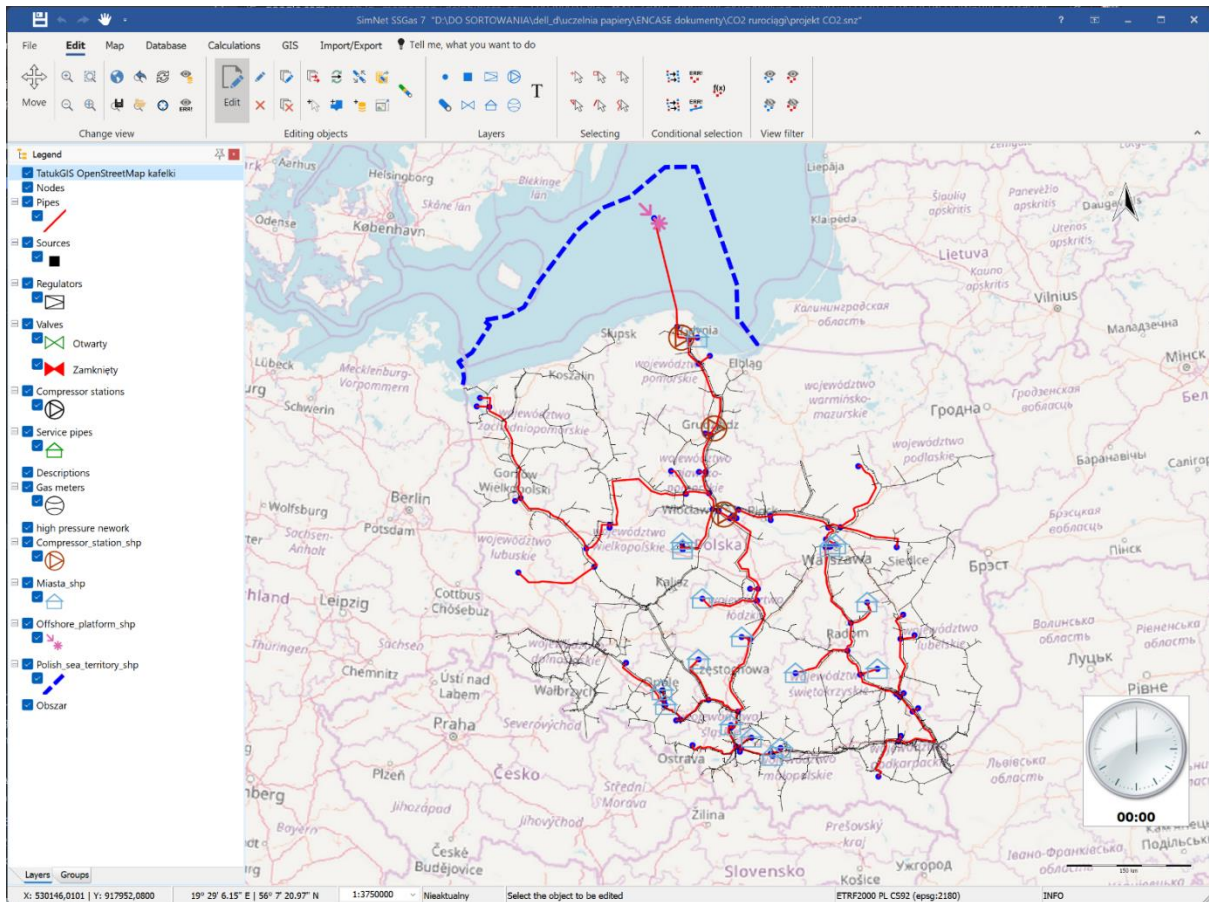
The presence of non-pipe units introduces extra unknown variables and hence additional IU equations are needed for the solution with coefficients whose values depend on the controlling constraint of the non-pipe unit.

Once a distribution of the flows in a network has been calculated, the composition of the streams at the nodes and the branches is to be calculated. Gas composition tracking is described by the following procedure:

- 1) give all the nodes an initial stream composition,
- 2) calculate the nodal pressures and pipe flow rates in the network,
- 3) repeat:
 - recalculate the composition at each node,
 - recalculate the pressures and flow rates in the network,
 until the change in composition is negligible.

If there are branches with zero flow, the solvability of the system of composition equations needs to be maintained.

A case study is conducted for conceptual Polish country-wide CO₂ transport infrastructure showing the functionality of the computational code. Implementation of the composition tracking model under steady-state conditions for arbitrary network structure (including GERG 2008 equation of state) will be presented.



Optimisation of the design of Formula SAE car aerodynamics

T Polski¹, M Żyto¹, M Płatek¹, Ł Rybakowski¹, M Bartoszek¹, G Spruch¹, R Szulejko¹, E Podlewski¹

¹ Warsaw University of Technology, Faculty of Power and Aeronautical Engineering, WUT Racing Team, ul. Nowowiejska 24, 00-665 Warszawa, Poland

E-mail: tomasz.polski@wutracing.pl

Abstract. This study details an innovative workflow by the WUT Racing Students Association for improving a Formula Student vehicle's aerodynamics, emphasising efficient design evolution and computational resource optimisation. Utilising a collaborative sprint method and model reduction techniques, it achieves a balance between simulation accuracy and resource efficiency, offering a novel approach to aerodynamic design in competitive automotive engineering

Keywords: Aerodynamics, Computational Fluid Dynamics, Workflow, WUT Racing, Formula SAE

1. Introduction

The optimisation study presents an analysis of the integration of a novel workflow within the WUT Racing Students Association aimed at the development of the aerodynamic package for a Formula Student vehicle. The primary objective was to establish a systematic approach to facilitate the synergistic interaction of individual aerodynamic components to enhance downforce generation and improve flow quality across elements such as front wing, sidepods, rear wing, engine cover, wing mount, floor and brake ducts [1,2]. The strategy involved devising an optimal workflow to unify the project's objectives and establish precise reference points for subsequent advancements. Additionally, a critical parameter was the optimisation of the use of computational resources, necessitated by their limited availability to the team members.

The innovative workflow for the forthcoming season aimed to enhance the management of design progression and facilitate potential modifications prior to the commencement of the project's production phase. The structure is such that each critical component of the design is assigned to a different team member, thereby maximizing the scope for iterative enhancements. Following a period referred to as a "sprint," the outcomes from individual contributions are to be consolidated and scrutinized to gauge the collective design advancement and establish benchmarks for future iterations. This workflow model inherently anticipates an extension of the initial sprints' durations to allow team members to acclimate to the project demands imposed by their colleagues, with the expectation that these durations will diminish as the project advances, culminating in a standardized design timeline per sprint. It also assumes differences in design approaches of different members and impossibility to make a detailed design of the entire aerodynamic package upfront. Each sprint fixed problems introduced in previous iteration while presenting new smaller ones, ultimately converging into an optimal design solution.

2. Further Development and Results

Another means of resource management is the model reduction in the driving direction as an approach to optimise the simulation process by reducing the size of the computational grid, which directly influences the reduction of hardware and time requirements.

At the beginning of each sprint, a velocity profile, turbulence kinetic energy, and energy dissipation rate calculated for the entire domain were exported, and then this profile was set as the velocity-inlet condition on the inlet of the shortened domain [3]. It was crucial to import the velocity profile at the same coordinates from which it was exported. Such a procedure allowed for the minimization of error after the cutting process, so the integrity of the flow dynamics around these key components was preserved. The analysis of the aerodynamic properties of the car was conducted, allowing for the identification of areas where shortening will not negatively impact the quality and reliability of the simulations. Potential challenges associated with the shortening of the model include impacts on the boundary conditions of the simulation and possible unexpected changes in the behaviour of the fluid flow. All modifications were made at an appropriate distance behind the cutting plane so as to not negatively affect the quality of the flow representation. This method was used in the design of the rear wing, the rear wing mounting, and the engine cover.

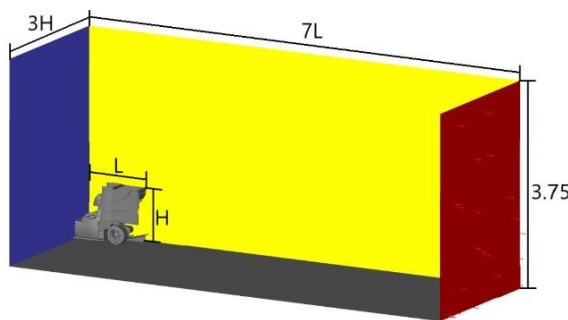


Figure 1. Shortened domain

	REAR WING DOWNFORCE [N]		
	SPRINT RESULTS	INDIVIDUAL RESULTS	DIFFERENCE [%]
Sprint v1	76,00	79	3,95%
Sprint v2	102,52	95,15	7,19%
Sprint v3	110,85	110,3	0,50%
Sprint v4	109,10	109,84	0,68%
Sprint v5	118,25	116,09	1,83%

Figure 2. Rear wing downforce comparison between each sprint

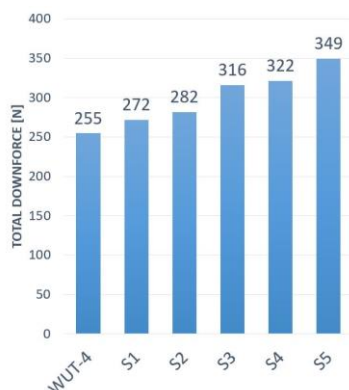


Figure 3. Total downforce on half of the aerodynamic package after each sprint

3. Summary

The main novelty of the presented work is that it deals with the problem of lacking computational resources and strictly limited time for completing the designing phase of the aerodynamic package. The adopted work scheme allowed for regular verification of the results and flexibility in adjusting the project to the changing nature of the flow. In summary, the obtained results demonstrate the validity of the applied methodology, which contributed to a satisfactory improvement in the flow characteristics around the vehicle throughout the design process and within the resource constraints.

References

- [1] J. Catz, '6.7, 6.10, 7.2' in Automotive Aerodynamics, 2016
- [2] J. Piechna, '3.4, 4.2, 4.3 4.4, 8.1, 8.2, 8.7' in Aerodynamika pojazdów, 2000
- [3] F.R. Menter / R. Lechner, Ansys Germany GmbH A. Matyushenko, NTS, St. Petersburg, Russia, '3.3, 9.2.1, 9.3.1' in Best Practice: RANS Turbulence Modeling in Ansys CFD



Warsaw University of Technology builds upon the traditions of Polish technical universities that used to function in Warsaw - the Polytechnic Institute founded in 1826 thanks to the efforts of Stanisław Staszic and the School of Hipolit Wawelberg and Stanisław Rotwand established in 1895.

Warsaw University of Technology started on its own in 1915 thanks to the efforts of the Association for Scientific Courses and the Citizens' Committee of the City of Warsaw. Working uninterruptedly, the University has been producing generations of graduates and has had an increasing number of scientific and technical achievements.

At Warsaw University of Technology, over 160 student research groups, organisations and associations are active, and the educational offer includes many fields of study.



ISBN: 978-83-943935-1-9

